5-2012

NANOPILLAR BASED ELECTROCHEMICAL BIOSENSOR FOR MONITORING MICROFLUIDIC BASED CELL CULTURE

Rajan Gangadharan
Clemson University, rgangad@g.clemson.edu

NANOPILLAR BASED ELECTROCHEMICAL BIOSENSOR FOR MONITORING MICROFLUIDIC BASED CELL CULTURE

A Dissertation
Presented to
the Graduate School of
Clemson University

In Partial Fulfillment
of the Requirements for the Degree
Doctor of Philosophy
Bioengineering

---

by
Rajan Gangadharan
May 2012

Accepted by:
Dr. Guigen Zhang, Committee Chair
Dr. Stephen Creager
Dr. Zhi Gao
Dr. Ken Webb

ABSTRACT

In-vitro assays using cultured cells have been widely performed for studying many aspects of cell biology and cell physiology. These assays also form the basis of cell based sensing. Presently, analysis procedures on cell cultures are done using techniques that are not integrated with the cell culture system. This approach makes continuous and real-time *in-vitro* measurements difficult. It is well known that the availability of continuous online measurements for extended periods of time will help provide a better understanding and will give better insight into cell physiological events.

With this motivation we developed a highly sensitive, selective and stable microfluidic electrochemical glucose biosensor to make continuous glucose measurements in cell culture media. The performance of the microfluidic biosensor was enhanced by adding 3D nanopillars to the electrode surfaces. The microfluidic glucose biosensor consisted of three electrodes - Enzyme electrode, Working electrode, and Counter electrode. All these electrodes were enhanced with nanopillars and were optimized in their respective own ways to obtain an effective and stable biosensing device in cell culture media. For example, the 'Enzyme electrode' was optimized for enzyme immobilization via either a polypyrrole-based or a self-assembled-monolayer-based immobilization method, and the 'Working electrode' was modified with Prussian Blue or electropolymerized Neutral Red to reduce the working potential and also the interference from other interacting electro-active species. The complete microfluidic

biosensor was tested for its ability to monitor glucose concentration changes in cell culture media.

The significance of this work is multifold. First, the developed device may find applications in continuous and real-time measurements of glucose concentrations in *in-vitro* cell cultures. Second, the development of a microfluidic biosensor will bring technical know-how toward constructing continuous glucose monitoring devices. Third, the methods used to develop 3D electrodes incorporated with nanopillars can be used for other applications such as neural probes, fuel cells, solar cells etc., and finally, the knowledge obtained from the immobilization of enzymes onto nanostructures sheds some new insight into nanomaterial/biomolecule interactions.

DEDICATION

This work is dedicated to two of the most wonderful women in my life, my mother Grace Gangadharan and my wife Annamalar Jeyasehar. I thank them for providing me with the support and encouragement to accomplish this goal.

ACKNOWLEDGMENTS

First and foremost I like to express my sincere gratitude to my advisor and mentor Dr.Guigen Zhang, for his guidance and support during the past six years. I thank him for his understanding, encouragement and personal guidance he has provided me throughout my time in his lab. I thank him for several of the brainstorming sessions which helped me develop critical and outside the box thinking. His mantra of a balanced life and passion for perfection has taught me valuable lessons for pursuing my future dreams. I am finally very grateful for his patience in correcting all my documents and publications.

I like to thank my committee members Dr. Stephen Creager, Dr.Bruce Gao and Dr. Ken Webb their guidance and advise. I like to thank Dr,Stephan Creager for clarifying some of my electrochemical questions. I like to specially thank Dr.Bruce Gao for allowing me to use his cleanroom facility. I am grateful to Dr. Ken Webb for guiding me in my cell culture work.

I would also like to acknowledge other faculties who have helped me accomplish many of project goals. I like to thank Dr. Jim Harriss for training me with photolithographic and deposition procedures. I like to thank Dr. Jason Locklin of University of Georgia for letting me use their cleanroom facility. I like to thank Cassie Gregory for helping me with the cell culture experiments. I also like to thank Dr. Taghi Darroudi for helping me with the SEM and TEM images

I like to thanks all my lab members past and present for helping me with most my research and day to day lab activities. Mainly I would like to thank Dr.Venkataramani Anandan from whom I inherited this work. Without his inputs this project would have not been possible. I also like to thank Dr. Yeshwant Rao and Dr. Xiaoling Yang for helping me start this work. I like to thank Gareth Sheppard from University of Georgia for providing me the necessary help in the cleanroom. I also like to acknowledge the present members Nrutya Madduri, Johnie Hodge and Sam Bearden for their support. I like to thank the help I got from Andrew Zhang in conducting my experiments. I like to thank members of Dr. Ken Webb's lab, mainly Atanu Sen and Jeremy Zhang for providing me with the cells. I also like to thank members of Dr. Frank Alexis lab for helping me with the nanoparticle synthesis.

I am indebted to all the staff in the Department of Bioengineering and the Institute of Biological Interfaces of Engineering at Clemson University, and the staff in the Biological and Agricultural Engineering Department at University of Georgia for making my PhD student experience a pleasant one.

I am also grateful to the financial support from the Faculty of Engineering at the University of Georgia, the Institute for Biological Interfaces of Engineering at Clemson University, and the Grand Challenge Explorations grant from the Bill and Melinda Gates Foundation.

TABLE OF CONTENTS

Page

Table of Contents (Continued)

Page

Table of Contents (Continued)

Page

Table of Contents (Continued)

Page

LIST OF TABLES

LIST OF FIGURES

List of Figures (Continued)

Figure Page

List of Figures (Continued)

Figure Page

List of Figures (Continued)

Figure Page

List of Figures (Continued)

Figure Page

List of Figures (Continued)

Figure Page

List of Figures (Continued)

Figure Page

List of Figures (Continued)

Figure Page

CHAPTER 1

INTRODUCTION

Real time in vitro analysis of cell culture is important in various studies of cell physiology, cell based therapeutics and cell biology [1]. These types of studies require the monitoring of activities of ion channels in cell membrane and of signaling analytes and metabolites such as oxygen, nitric oxide (NO), glucose, glutamate, ascorbate, dopamine, and so on. In therapeutic research it is crucial to study high-resolution, real-time measurement of biochemistry in living cells when exposed to pharmaceuticals, drugs, and biotoxins. In cell biological studies, it will be possible to investigate how cells act in concert and also how populations of cells communicate with each other, by analyzing the chemicals released from the cultured cells spatially and temporally.

The main impediment for real time analysis of cell cultures is the lack of technologies that can be used to observe the analytes continuously from live cell cultures. The foremost problem is the choice of an appropriate detection method that can be integrated with cell culture system. The most used methods are optical and fluorescent based detection methods. Present optical methods need bulkier detection devices and alignment of the detectors, even though some progress has been made in integrating them with micro-fluidic systems. They need potential labeling of molecules or cells as in the case of fluorescence methods. Certain cell functions like membrane potentials cannot easily be studied with optical techniques. This is where the electrochemical techniques can be very

effective. Integration of electrodes onto cell cultures will provide information that will be complementary to that generated by fluorescent detection methods [2].

Other advantages of electrochemical techniques for cell analysis are [3]

- Compared with optical methods, they are most convenient for recording and processing;
- Easy to integrate into devices and for miniaturization (suitable for microfluidic devices);
- Alignment of detector and object of interest is not necessary;
- Some activities of ion channels and neurons which are electrical in nature can be easily obtained;
- They generally don't need any labeling of bio-molecules or cells;
- Non-destructive measurements possible on cells unlike patch clamp studies.

In the future, the combination of optical probes and electro-analytical methods could present a great potential for the development of multi-analyte detection systems to monitor cellular dynamics.

Until now electrochemical studies in cell cultures is limited to potentiometric electrodes like pH electrodes and oxygen sensors. Even though electrochemical amperometry is a very powerful tool for continuous *in-vitro* studies, it is limited by specificity and detection limit problems. These problems should be addressed to get reliable and accurate measurements using amperometry. So below are listed some of the advantages and essential features of a good amperometric biosensor.

Advantages of amperometric biosensor include: 1) rapid, 2) easy integration, 3) non-interfering with the cells, 4) simple operation, 5) cost effective, and 6) good for continuous measurements. Essential criteria for a good amperometric biosensor include [4]: 1) high sensitivity, 2) good selectivity, 3) long shelf life, 4) no interference, 5) large linear range, and 6) low detection limit.

All of the above criteria have to be met for developing an amperometric biosensor system that can be effectively used for cell culture monitoring. But amperometric biosensors presently found in literature lack many of these essential features and cannot be readily used for continuous monitoring. There was not any biosensor system reported in literature that has been prepared to withstand the cell culture media conditions. This motivated us to develop an enzymatic amperometric biosensor system with all the essential criteria and especially suited for cell culture media solutions.

A microfluidic biosensor platform was chosen in our study because it will allow us to perform continuous measurements and obtain measurements at very low analyte volumes. In such a biosensor, electrodes should also be made small enough to fit into the microfluidic channels. This will limit the surface area of the electrodes and therefore reduce the sensitivity of the biosensor. In this work we overcame these challenges by developing 3D electrodes incorporated with nanopillars. Due to a lack of information in the literature on the development of microfluidic biosensors integrated with 3D nanostructures, several studies were performed to optimize many existing methods for constructing amperometric biosensors whose electrodes were made of 3D nanopillars. With the information obtained from these studies, an effective biosensor with superior

performances was realized for cell culture monitoring. This dissertation presents the details of these relevant studies performed for the development of a microfluidic biosensor for monitoring glucose in a cell culture environment.

1.1 Outline of the dissertation

1) Chapter 2 contains the background literature information mainly on the cell culture monitoring, electrochemical methods for cell culture monitoring and finally nanomaterials used for improvement of electrochemical glucose biosensor
2) Chapter 3 discusses about the proposed ideas and the five objectives of this work
3) The rest of chapters have been categorized into five sections based on the five objectives. The chapters under each section talks about the studies performed and their corresponding results to accomplish each of objectives.

   SECTION I: Development of 3D nanopillars (1 Chapter)

   SECTION II: Development of the enzyme electrode (4 chapters)

   SECTION III: Microfluidic glucose biosensor (2 chapters)

   SECTION IV: Modifications of the working electrode (2 Chapters)

   SECTION V: Cell culture monitoring (1 Chapter)

When there is more than 1 chapter in a Section, the last chapter of that Section has a summary of the best results from the multiple studies done (under the title – “Highlights of ……..studies”).

CHAPTER 2

BACKGROUND INFORMATION

2.1 Introduction

Mammalian cell culture grown in laboratory settings have become essential in understanding the dynamics of the complex cellular system and the whole functioning of the human body. The in vitro cell culture models have been essential in advances in cell biology mainly in investigating cell-cell interactions, cell-extracellular matrix interactions, and transport phenomena. The cell cultures also are elementary to studies involving tissue culture and engineering. Apart from the basic cell biological research they are also fundamental tools in drug development, clinical diagnostics, therapy, environmental monitoring and manufacturing of various important biochemicals such as vaccines, enzymes, hormones and antibodies [1].

Cells are complex and dynamic nanostructured microsystems that contain functional subunits located in compartments and connected by an intricate signaling network. The cells functions and properties are also continuously changed by the biochemical responses to the numerous chemical and mechanical stimuli. A weak stimulus is amplified by the signaling network and results in the appropriate cell function. Defects in the sensing, transduction or cellular response have been found to be the underlying cause of various diseases like cancers, immune disorders, cardiac hypertrophy, genetic malformations, and neuropathies [2].

In *in-vitro* cell culture the in-vivo cell-cell and cell- environment interactions are mimicked and studied, to understand the fundamental aspects of these interactions. Even though *in-vitro* culture is used extensively in conventional experiments, there are questions whether the system mimics the in-vivo conditions satisfactorily. To improve on these drawbacks, 3D cell growth has been introduced to create models equivalent to the animal and human models. Recent advances in micro and nanotechnologies have also contributed extensively to improve cell culture environments as cells in-vivo are the best example of nano- micro- macro integration. [6]. One such solution is using microfluidic systems for cell culture, also called as Lab-on-chip. Lab-on-chip systems are capable to conducting high through put cell based assays and they also mimic the *in-vivo* microenvironment more accurately [7]. In these systems there can be control of the cell interactions and control of the distribution of biomolecules. There are also additional advantages of short diffusion lengths, laminar flow with low Reynolds numbers, high surface to volume ratio, and need of small amount of reagents [8]. More sophisticated microfluidic devices have used three-dimensional microstructures and polymer scaffolds to mimic the in vivo environment even better.

These microfluidic based devices have advanced rapidly in recent times that they can perform various tasks such as cell sorting, cell viability, sampling and handling [9,10]. The ultimate goal is to achieve a fully integrated lab-on-chip that can perform repeated cell growth, reagent introduction and real time cell based analysis [1]. One of the most important issues that need to be addressed to achieve this goal is the development of miniaturized multi-property detection systems with high sensitivities, high signal to noise

ratio and fast response time. So in this literature review we will concentrate on the analysis systems that can to be integrated with the microfluidic based cell culture. Development of rapid, cheap, specific and sensitive methods for biochemical assays that can be integrated with the microfluidic cell culture has been the focus of research activities in recent years. Numerous studies have used detections schemes that can be categorized as optical detectors, electrochemical detectors, mass spectrometric detectors and nuclear magnetic resonance (NMR) detectors according to the different detection principles. Among the various detectors, optical and electrochemical based biosensors are the most used detection schemes. Optical detection method is a versatile and effective method to visualize cells and the sub-cellular structures. Conventional optical detectors can be easily interfaced with the microfluidic system without any requirement of interconnections between the detector and microfluidic device. As they involve only photons for detection they involve minimum disturbance to the reaction system observed. [11]. Fluorescene based methods have been successful in detecting proteins by observing the expressed recombinant fluorescent protein, such as green fluorescent protein, in live cells. But the major problems with optical detection methods are that they are less suited for long term monitoring of cultured cells due to the toxic properties of many of the dyes used. It is not easy to integrate the light sources and detectors into small portable lab-on-chip devices. Furthermore, there is no apt optical method available for cell adhesion studies and monitoring metabolic and electrical activities [2].

Electrochemical biosensors are attractive for micro-fluidic based assay because of the inherent portability, simplicity, bio-compatibility and ease of fabrication of micro-

electrodes. The instrumentation cost for electrochemical detection method is also the lowest. Integration of electrochemistry in lab on chip is a convenient way to realize multi-analytical functions in a single miniaturized device. Electrodes integrated with the microfluidic systems are not only used as the conducting elements for detecting electrochemical species [12], but also for manipulating materials using electrophoretic principle [13] and also as surface layers for biomolecular immobilization and hybridization [14]. The most commonly used electrochemical techniques for detection in cell culture based assays are potentiometry, amperometry/voltammetry and electrochemical impedance spectroscopy (EIS). These detection schemes can be readily used for monitoring extracellular metabolites such as oxygen, carbon dioxide, and glucose and even pH. Various ionic species such as Na^{+}, K^{+}, Ca^{+}, and NH^{3+} can also be detected using this technology. Inherently electro-active species such as ascorbate, dopamine, and nitric oxide can also be detected at the electrode surface. Most importantly other analytes such as glucose, lactate, glutamate, choline, acetyl choline and ATP that are not electro-active can be measured using enzyme based electrodes. Recent advances have also led to the detection of various species like amino acids, peptides and DNA. But electrochemical methods are plagued by important issues like lesser sensitivity at the smaller microelectrodes, interference from other electro-active species, and loss of activity of the biomolecules used for detection.

The first part of the review presents the advances in electrochemical biosensing technology that can be integrated with a cell culture in a microfluidic environment. Examples of different electrochemical techniques applied to cell culture assays found in

literature will also be presented. In the second part of the review, the drawbacks of the electrochemical techniques and ways to improve the performance of the electrochemical biosensor using nanomaterials will be discussed in detail. Electrochemical glucose biosensor is chosen as the model system to discuss the electrode modifications with nanomaterials.

2.2 Overview of parameters to be monitored in cell culture

Before we go into the details of electrochemical biosensing technologies, we will briefly review on the parameters that can be monitored in cell culture.

2.2.1 Metabolic activity in cells

Chemical energy in the cells is exclusively derived from the ATP molecules in the cells. Any metabolic pathway involved in the making of ATP is a catabolic pathway. Any metabolic pathway for assembling complex molecules like DNA, RNA, proteins and fatty acid is an anabolic pathway. The catabolic pathway is simply the transfer of energy stored in glucose bonds to phosphate bonds. For this glucose first undergoes glycolysis to form pyruvate, releasing some ATP molecules and reducing nictoniamide adenine dinucleotide (NAD) to NADH. Pyruvate enters the Krebs cycle and more NADH and $FADH_2$ are produced. The Krebs cycle converts some ADP molecules to ATP and also completes the conversion of glucose to carbon dioxide. NADH and $FADH_2$ release the energy to create a proton gradient which in turn produces more ATP molecules. Many of the amino acids needed by cells to assemble proteins can be made from molecules such as Acetyl CoA taken from Krebs cycle reactions. By-products of glycolysis are also used to prepare RNA and DNA. So the sum of these catabolic and anabolic pathways makes

up the cell metabolic activity. So observing any of the biochemicals involved in the pathways will provide vital information of the metabolic activity of the cells.

Below is the list of some of these metabolites and parameters that can be sensed and the information they provide [15]:

Extracellular Oxygen: indicates respiration rate

Extracellular Carbon Dioxide: reflects efficiency of the Krebs cycle and the viability of the cell

Extracellular Glucose: indicates the capacity of the cell to perform anabolic activity

Intracellular ATP: fuel availability in the cell

Intracellular NADH and FADH: reflects the proper completion of glycolysis

Intracellular pH: across the mitochondrial membrane indicates the proton gradient

Extracellular pH: mostly changed due to amount of CO_2 present

So biosensors used detect these changes can give us wealth of information about the basic metabolic activity of the cell.

2.2.2 Enzyme activity

Enzymes play an important role in sustaining most of the biological processes happening in the cell. Assay and regulation of enzymes is important tool now in clinical diagnosis and therapy. Microdevice with cell lysis and optical biosensors has been used to detect the enzyme like lysozyme.[16].

2.2.3 Cell signaling

Intercellular signaling takes place in nerve, immune and endocrine systems using the first messengers such as neurotransmitters, cytokines, and hormones respectively. These

molecules bind either to ion-channel, kinase or G protein-coupled membrane receptor proteins, and trigger the respective down-stream intracellular signaling. Sometimes oxygen and nitric oxide can also act as cellular signaling messengers. These are called redox signaling molecules, which includes free radicals, reactive oxygen species (ROS) and other electro-active species. The electro-active property of these molecules helps in directly measuring the molecules using metal electrodes. Some signaling molecules such as adenosine, ATP and acetylcholine that are not electro-active can be measured using enzyme/multi-enzyme based electrochemical biosensors.

Biosensors are also critical in understanding various neuro-transmitters that mediate communication between neurons and non-neuronal cells such as glia and muscles cells. Faulty neurotransmission has been linked to various conditions like depression, schizophrenia and other degenerative diseases. Some of neurotransmitters such as catecholamines (dopamine, epinephrine, and norepinephrine), 5-hydroxytryptamine (5-HT or serotonin), histamine and peptides containing a tryptophan or tyrosine residue are also electroactive and can be measured using micro-electrodes [17]. Most of these neurotransmitters and hormones are secreted in discrete packets in a process called quantal exocytosis. Measurement of quantal release is important as it provide information about the mechanism and regulation of exocytosis and also evidence that the release is from exocytosis and not cell lysis. Electrochemical detectors have been used in this case to detect the spike in current resulting from oxidation of the quanta of the transmitter [18]. Other techniques such as liquid chromatography (LC), capillary electrophoresis

(CE) separations with fluorescent techniques, and mass spectrometry (MS) have also been used to monitor the neurotransmitters in in-vivo and in-vitro conditions [19].

2.2.4 Cell adhesion and morphology

Cell adhesion studies are important in cancer cell research. Cancer cell metastasis and invasion trough adhesion and penetration can be studied using electrochemical impedance biosensors or peizo/acoustic wave biosensors [20]. Changes in cell adhesion and morphology give information about the viability of the cell.

2.2.5 Electrophysiological measurements

One of the most important studies in electrophysiology is ion channel studies. Ion channel are trans-membrane proteins that allow passage of ions through pores across a non-permeable lipid layer. Studies of Ca^{2+}, K^{+}, Na^{+} ion channels have shown their importance in homeostasis and other pathological processes. Defective ion channels due to acquired or hereditary reasons are responsible for various diseases. Micro-electrodes and patch clamp experiments are useful in understanding the ion channels and electro-physiology of the cells. Multi-site analysis of activity patterns of network of neuronal and muscle cells are important in finding the origin of action potential

2.3 Electrochemical biosensors for cell culture monitoring

Before we get into the details of electrochemical biosensor Table 1 gives an overview of different method that can be used for monitoring cell culture. The advantages and disadvantages of each method are also presented.

Methods	*Applications*	*Advantages*	*Disadvantages*
Biosensors	Metabolites	Simple to make and use	Limited by enzyme stability
			Frequent calibration
	Cytokines	Reliable results	Some sterilization issues
			Consumables costly to maintain
IR spectroscopy	Metabolites	Rapid analysis of multiple analytes	Signal overlap results in broad bands, less distinct features
		Several on-line configurations available	
NMR spectroscopy	Metabolites	Detects O_2 and cell distribution	Labelling required
			Low sensitivity
	Cytokines	Provides wealth of information	Signal to noise issues
Immunoassays (ELISA)	Cytokines	Well-established and standardized	Long assay development times
		Very sensitive	Difficulty in online implementation
		Accurate, reliable results	Cross-reactivity may occur
HPLC	Metabolites	Highly accurate and reliable	Long sample analysis time
			Mostly applied as off-line method
Flow cytometry	Cells	Quantifies cell numbers and characterise populations	Labour-intensive sample preparation
		Able to analyse at high rates	On-line applications not practical
In-situ microscopy	Cells	Good stability and system performance	Limitations in differentiating cell types
		Capable of automatic control and image analysis	
Raman	Cells	Non-invasive	Low sensitivity
		Simple sample preparation	Degradation by laser beam exposure possible

Table 1.1: Summary of monitoring techniques (adapted from Mayasari at al. [21])

2.3.1 Biosensors Definition and Classification

As we have seen from the Table 1.1 all methods have disadvantages related to online integration with cell cultures and it gets even more complicated with a microfluidic environment. Alternatively biosensor technology is an attractive method for cell culture studies since it can be easily integrated for online studies. IUPAC definition of a biosensor is that it is a "integrated receptor-transducer device, which is capable of providing selective quantitative or semi-quantitative analytical information and which uses a biological recognition element (bio-receptor) and a transducer in direct spatial contact" [4]. The use of the biological recognition element distinguishes the biosensor from chemical sensor. Biosensor can also be differentiated from a bio-analytical system by not needing pretreatment methods and addition of external reagents.

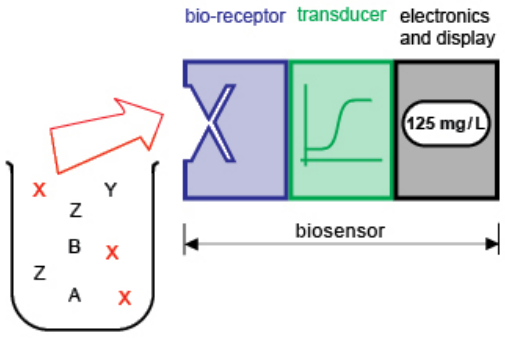

Figure 2.1: Principle of a biosensor [22]

Figure 2.1 describes the principle of the biosensor. The first step in a biosensor is the recognition of the specific analyte using a biological recognition element. Then the bio-recognition event is converted to detectable signals using a transducer and finally, the transducer signal is processed. Biosensors may be classified according to the type of

biological recognition mechanism employed or by the type of transducer used. An ideal biosensor should be small, easy to use, reagentless, fast and reversible responses with high sample throughput, and exhibit storage and operational stability [23]. To obtain these properties the biosensor should have the meet the following requirements

1) The bio-recognition element should be highly specific and stable at working conditions and upon storage.
2) Transducing element should not interfere with the analyte and cause false signals.
3) Accurate results should be obtained with minimum or no pretreatment procedure.
4) Signal response should be fast, reproducible, and linear to the concentration of analyte.
5) Should have very high signal to noise ratio.
6) Should be biocompatible and probe miniaturization should be possible.

2.3.2 Electrochemical biosensors

The main transducers in biosensing applications have been electrochemical, optical and acoustic/piezoelectric transducers. In this review we will mainly look at the electrochemical transducers techniques. The operation principles, examples, advantages and disadvantages of the electrochemical transducers used in microfluidic channels based cell cultures is covered in this section.

Electrochemistry is limited to detecting those substances that can be oxidized or reduced in a range of voltage of –400 to +1450 mV. Higher potentials at the electrode surface in the positive and negative directions cause oxygen and hydrogen evolution respectively. Within this range, a large number of biological substances can be

theoretically analysed by electrochemistry including certain neurotransmitters such as biological amines (adrenaline, noradrenaline, dopamine, histamine and serotonin), some peptides, ascorbic and uric acids and some of the metabolic products derived from these substances [3].

Main advantage of using electrochemical detection for cell analysis:

- Compared to optical methods they are most convenient for recording and processing
- Easy to integrate into devices and for miniaturization
- Alignment of detector and object of interest is not necessary
- Some activities of ion channels and neurons which are electrical in nature can be easily obtained.
- They generally don't need any labeling of biomolecules or cells.
- Can be integrated onto microfluidic system easily
- Non-destructive measurements of cell possible
- Electrochemical amperometry is a very powerful tool for the *in vitro* study of the mechanisms underlying secretion from single cells or tissues and it is relatively simple and inexpensive to use [3].

Electrochemistry allows monitoring dynamic biochemical events occurring at the cell surface and intact tissues. Some processes like real-time communication between neurons and fundamental processes involving oxidative metabolism can be easily monitored using electrochemistry. The micro/nano electrodes have allowed us to probe microdomains of cells systems efficiently [24]. Electrochemical methods do not depend on reaction

volume and very small sample volumes can be used for measurement. This property is important for performing measurements in microfluidic channels. Electrochemical methods can achieve very low detection limits (atto and zeptomoles) in immunoassay with little sample preparation. Electrochemical measurements also can be done in colored and turbid samples such as whole blood since there is no interference from light interfering sample components like fat globules, RBCs and hemoglobin.

Electrochemical techniques can be categorized as measurements of current (Voltammetry/amperometry), potential (potentiometry) and Impedance. Focus will be on these three techniques are they are the most commonly used techniques.

2.3.2.1 Criteria for a good electrochemical biosensor

a) Sensitivity

Sensitivity can be defined as the output change obtained from a standardized input. In the case of biosensors it is the amount of signal change generated by a standardized amount of analyte. It is calculated from the sensor calibration curves. The sensor calibration curves are obtained by adding a standard amount of the analyte and ploting the steady state responses (R_{ss}) against the analyte concentration, C.

In case of amperometric biosensor, the magnitude of current flow (I) is detected response signal. The generalized equation for the amount of current flow at an electrode surface in amperometric conditions is (5)

$$I = n \cdot F \cdot A \cdot D \cdot \frac{\partial C}{\partial x}_{x=0}$$

Where, F- Faraday's constant, A is area of electrode, D – diffusion coefficient of the analyte species and is the concentration gradient at the electrode surface.

So increase in area of the electrode (A) will help in achieving more current output. Nanostructure based electrodes is seen as an effective solution to increase the surface area of the electrode.

b) Selectivity and interference

Selectivity is the term used to define if the signal obtained is from the analyte of interest alone. If other species in the sample of interest also contributes to the signal, the biosensor has lower selectivity. In case of electrochemical biosensors the selectivity for the analyte is improved using a biological element such as enzymes, antibodies, whole cells etc.

Nanomaterials have also been explored to increase the selectivity of glucose biosensors. For example, nanomaterials with a higher catalytic efficiency and lower overpotential for hydrogen peroxide reduction can help lower the operating potential of the glucose biosensors (6), thus minimizing the interferences from nonspecific species. Use of polymeric materials in nanocomposites as permselective filter can also help reduce interferences (7, 8).

c) Shelf Life

Enzymes and other biomolecules have limited shelf life. So the life of a biosensor is limited by the activity of the biomolecule. Nanomaterials can prolong the stability and lifespan of enzyme-based biosensors by providing a better microenvironment for the enzymes. For example, nanoparticles and nanoporous cavities are found to stabilize the enzymes by reducing the unfolding of the enzyme proteins (9).

d) Linearity

It is a range of analyte concentration in which the response of the biosensor has a linear response. When using enzymes the linearity is governed by Michealis Menton kinetics. But using diffusion barriers like porous polymeric membranes, we can make the reactions diffusion dependent. This will help in increasing the linear range but with some loss of signal.

e) Detection limit

The detection limit is mainly affected by the signal to noise ratio. So a reduction in noise and increase in signal will always improve the detection limit. Micro-electrodes with radial diffusion characteristics have helped in increasing the signal to the noise ratio. Nanoelectrodes with radial diffusion will be ideal since it would give a larger signal change than microelectrodes of the same surface area.

2.3.3 Voltammetry/amperometry

(All basic principles of electrochemistry are from ref: [25])

Voltammetric and amperometric techniques involve the measurement of current to an applied potential in reference to a reference electrode. This includes application of constant potential and various other potential wave forms. The basis for all these controlled current experiments is that the current response if related to concentration of the target analyte. This is done by observing the electron transfer happening during the redox process of the analyte

$$Ox + ne^{-} \rightleftharpoons \mathrm{Re}$$

Where Ox is the oxidized form of the analyte and Re is the reduced form of the analyte. If the system is in a thermodynamic equilibrium then the potential of the electrode can be

used to control the concentration of the oxidized species C_{OX} and reduction species C_R, governed by the Nernst equation:

$$E = E^o + \frac{nF}{RT} \ln \frac{C_{ox}}{C_R}$$

where E^0 is the standard potential, F faraday constant, R universal gas constant and T temperature in Kelvin. The amount of current generated by the oxidation of the species is called Faradaic current, and it directly related to the rate of the reaction.

Two of the common used amperometric measurements are chronoamperometry and cyclic voltammetry. In chronoamperometry the potential is raised from a value where there is no faradaic reaction to a potential where the surface concentration of electro-active species at the electrode surface become zero. The current-time graph is reflection of the concentration gradient at the electrode surface. A typical chronoamperometric current response curve is given in the Figure 2.2.

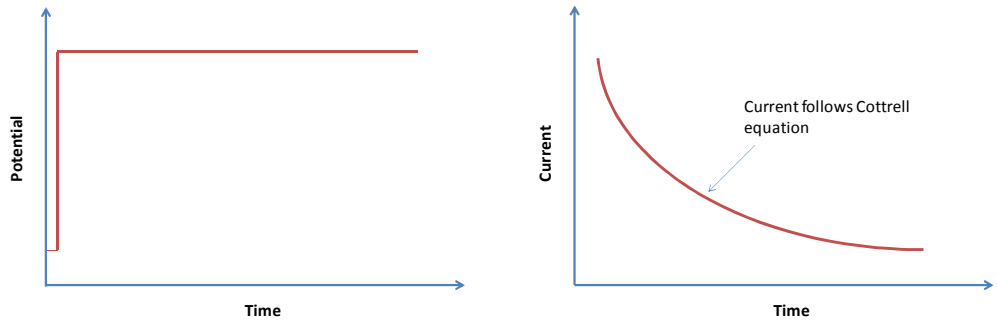

Figure 2.2: Applied potential and chronoamperometric current response curve

Current in the electrode decays with time and is governed by the Cottrell equation:

$$i(t) = \frac{nFACD^{1/2}}{\Pi^{1/2} t^{1/2}}$$

where *A* is the electrode area, *C* the bulk concentration of the electroactive species, and *D* its diffusion coefficient. Chronoamperometry is one of the simplest techniques, but still finds application in biosensors. Advantages of this method include negligible charging current or lower background signal since it is operated at a fixed potential. The amperometric signal can also be significantly improved by enhancing the mass transport using rotating electrodes or flow conditions.

Cyclic voltammetry is a technique in which the potential is cycled from an initial value to a predetermined value and then the scan is reversed as shown in the Figure 2.3. So the excitation potential has a triangular wave form and the experiment is done in an unstirred solution. This can give information about the kinetics of the reaction and also the qualitative information about homogenous reactions happening at the electrode. A typical cyclic voltammogram (CV) displays the current changes with the potential change as shown in the Figure 2.3.

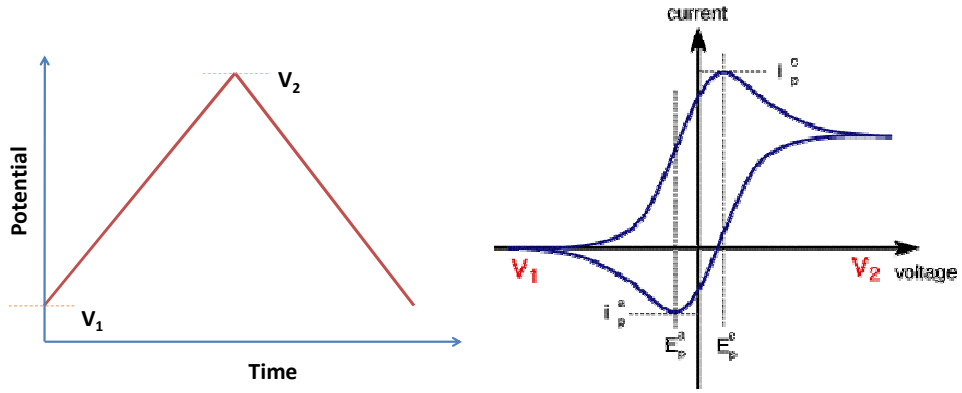

Figure 2.3: Input potential and cyclic voltammogram

The important information in the CV curves is the magnitude of the peak current and the corresponding potentials. In a completely reversible reaction the peak separation is

$$\Delta E = E_p^a - E_p^c = \frac{59}{n} mV$$

The position of the peak voltage does not change with scan rate and the peak currents are proportional to the square root of scan rate, defined by the Randle-Sevcik equation:

$$i_p = (2.69 \times 10^5) n^{3/2} A D^{1/2} C \nu^{1/2}$$

Where i_p is the peak current, □ is the scan rate (V/s). One of the most important uses of cyclic voltammetry is when a homogenous chemical reaction is followed by a heterogenous electron- transfer reaction. This kind of situation is faced by enzymatic biosensors where mediators are used for electron transfer.

2.3.3.1 Electrochemical setup for amperometry

Most all the electrochemical sensors consist of a two or three electrode setup. In a three electrode setup there is a working electrode made of conducting materials such as platinum, gold, or carbon; a reference electrode (Ag/AgCl); and a platinum or gold auxiliary electrode (Fig 2.4). The reference electrode is employed to maintain a stable potential between the working and the reference electrode. The half cell potential of the reference is stable as negligible current flows through it and most of the current flows through the counter electrode. The two electrode system has only the working and reference electrode. If the current flow is low (<μA cm^{-2}) then there is no adverse change in the reference electrode. Both configurations have been used in the electrochemical biosensor setup. Electrodes of micrometer and nanometer sizes have also been demonstrated.

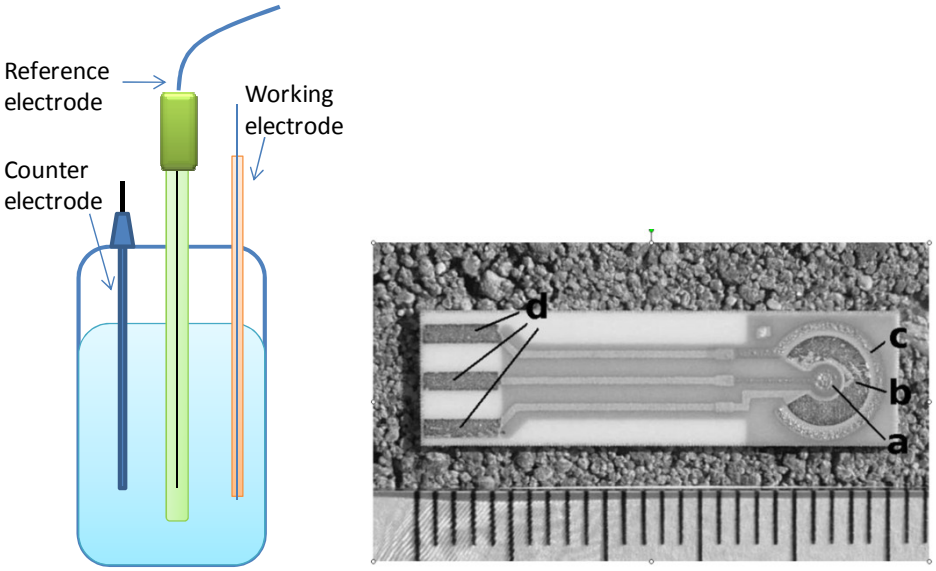

Figure 2.4: (A) Schematic of general electrochemical setup (B) Example of screen printed electrochemical biosensor ((a)-gold working electrode, (b)-Ag/AgCl reference electrode, (c)-gold auxiliary electrode (c)) [26]

Another important setup in electrochemical biosensors is the interdigitated array (IDA) setup. The IDA's consist of two pairs of working electrode in an interdigitated manner and separated by an insulating material between them. This setup causes a redox cycling of the reversible redox species (e.g redox mediators) as shown in Figure 2.5 when different potentials are applied to the electrodes. This electrode configuration enhances the signal and lowers the detection limit in biosensors.

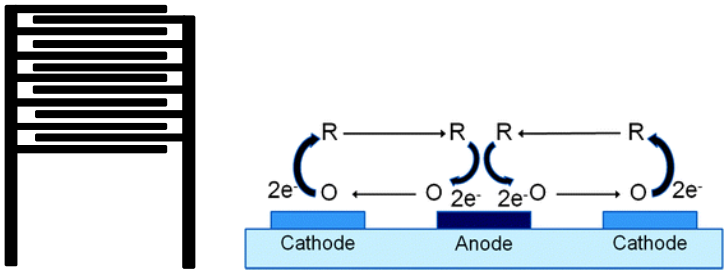

Figure 2.5: Intedigitated electrodes and their working principle (Courtesy [27])

2.3.3.2 Characteristics and limitations with amperometric methods:

Sensitivity of the electrodes gets reduced when the electrode size is reduced to fit microfluidic devices. The current response is proportional to the area of the electrode in amperometric measurements. To overcome this problem nanomaterials have been incorporated at the electrode surface to increase the effective electrochemical area [28]. The upper limit of detection of the amperometric biosensor is limited by the biocatalytic activity of the enzymes. Most of the enzyme based biosensor follows the Michaelis-Menton kinetics and therefore have non-linear behavior at higher concentrations. Michaelis Menton equation (defining the rate of substrate consumption) for a simple an enzymatic reaction $E + S \underset{k_{-1}}{\overset{k_1}{\rightleftarrows}} ES \xrightarrow{k_2} E + P$ (where, E-enzyme, S- substrate, P-product) is given by $v_o = \frac{k_2[E][S]}{K_M + [S]}$, where $K_M = \frac{k_2 + k_{-1}}{k_1}$. $V_{\max} = k_2 E$ can be replaced in the previous equation, and V_{max} gives theoretical maximal rate of reaction. In enzyme based electrodes it is desirable to have low K_M values and high V_{max} to increase the overall reaction rate and consequently the output current of the electrochemical biosensor. It is generally calculated in biosensors using a Lineweaver-Burk equation, which is obtained by taking the reciprocal form of Michaelis-Menten equation. Even though the linear range of biosensor is limited by enzyme kinetic process, control of linear range can be achieved by controlling substrate diffusion using an outer membrane [4].

One of the biggest problems with amperometric biosensors is selectivity. Selectivity is expressed as ratio of the output signal from analyte to the output signal of interferent species of the same concentration. The interference from various electro-active species

in biological fluids interfere with the main signal of the biosensor. Ascorbate, Urate and acetaminophen are common interferants in a glucose biosensor used for blood samples. Methods for reducing interference is will be discussed in Part II of the review. Some of these methods used in avoiding interference can also cause further problems. Selectively in catecholamine detection from chromaffin cells, done using coating of Nafions, blurred the spiked releases of catecholamine, by the diffusion limitation caused by the coating. Without the coating concentration spikes were observed representing the occurrence of individual vesicular release events [29]. So diffusion barrier caused by various non-interference screening materials plays an important role in transient readings.

Operational stability and shelf life of the biosensor are the other important properties of the biosensors. The operational stability depends on the external or inner diffusion of the substrate, and geometric factors of electrode and the biosensor. Shelf life is limited by enzyme stability and leaching of enzyme from the immobilized matrix [30].

2.3.4 Examples of amperometric biosensor in cell culture analysis

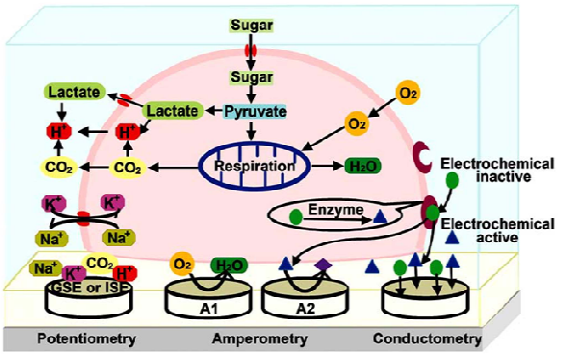

Fig. (2). Scheme of cell-based electrochemical biosensors based on cellular functions. A1: amperometric biosensor based on detection of oxygen. A2: amperometric biosensor based on detection of electroactive species produced by enzymatic reaction.

Figure 2.6: Summary of the electrochemical biosensors and their potential in monitoring the cell functions (Courtesy: [31])

i) Direct amperometry

Biosensors with no biorecognition elements have been used to detect many biomolecules that are inherently electro-active. Metabolite like oxygen is one of such candidate as the very first biosensor was the Clark oxygen sensor which amperometrically monitored the reduction of oxygen on platinum electrodes. Human cervical cancer cells (HeLa) adhering to the oxygen permeable membrane modified with amino groups was monitored for the respiratory activity [32]. Platinum electrodes as a Scanning Electrochemical Microscope (SECM) probes has also been used in detecting oxygen in Human breast cancer (MCF-7) cells [33].

Catecholamines release has also been monitored from cells as they can be directly oxidized at the electrode surface. Calcium-induced catecholamines release from PC 12 cells were monitored using a Nafion coated carbon electrode at a oxidizing potential of +0.9V [34]. Even detection of secretion from individual cells has attracted a lot of attraction recently [32]. Amperometric Detection of Quantal Catecholamine Secretion from Individual Cells using gold electrodes on Micromachined Silicon Chips has been successfully demonstrated [35]. Opening of individual exocytotic fusion pores in chromaffin cells was imaged by detecting catecholamine molecules at different electrodes in an electrochemical electrode array [36]. The other important cell signaling biomolecule that can be directly detected has been dopamine. Nanoelectrodes based capillary electrophoresis system has been applied to determine femto- molar concentration of dopamine from individual PC12 cells [37]. Amplitude and temporal aspects of dopamine release from PC12 cells was monitored using gold micro-electrode array at a potential of

0.3V. After finding out the parameters of dopamine release the effect of drugs was also studied. This study was an attempt to develop a rapid and high throughput monitoring the effect of drugs on release of dopamine [38].

The next class of electroactive substances is reactive oxygen species (ROS) and reactive nitrogen species (RNS). ROS and RNS are involved in the regulation of many biological processes such as reactivity proliferation and apoptosis. So there has been interest in developing chip based systems to study processes involving NO and O_2. NO was amperometrically detected with a carbon-ink microelectrode modified with nafion from pulmonary artery endothelial cells. The cells were immobilized onto glass substrates in PDMS microchannels coated with fibronectin for cell adhesion [39]. Reactive oxygen (ROS) and reactive nitrogen species (RNS) released by Macrophages were also detected from cell cultures on glass substrates in microchannel using platinum microelectrodes [40]. Oxidative stress in cancer prone xeroderma pigmentosum fibroblasts was monitored using Platinized carbon fiber microelectrodes. Amperometric measurements was done at +300, +450, +650and +850 mV to differentiate the potential individual ROS and RNS species got oxidized ($NO^{\bullet}$, $ONOO^{-}$, H_2O_2 and NO_2^{-}). This information was then used to calculate the original ROS and RNS species ($O_2^{\bullet -}$ and $NO^{\bullet}$) that was produced in the cell [41] .

ii) Enzyme based electrochemical sensor

Metabolites like glucose, lactate and hypoxanthine has been detected using enzyme based electrochemical biosensors. Glucose consumption in a perfusion cell culture of human amniotic epithelial cells was done using Clark type amperometric electrodes

coated with glucose oxidase. The cell viability was checked by monitoring the glucose consumption when Cu and H_2O_2 were added to the culture [42]. Platinum based glucose microsensors have been used to detect glucose gradients and mass transport within islets of Langerhans. To assess the extent of glucose gradients around and within single islets, the sensor was positioned at different distances from the islet center and the glucose concentration was recorded. These experiments were performed with islets bathed in quiescent solutions containing glucose [43]. Lactate content of single heart cells was measured using platinum microelectrodes containing lactate oxidase. When uncouplers like saponin was used to simulate ischemia like condition, the hypoxia heart cells showed to produce more lactate that the normal heart cells [44]. Hypoxanthine is another major metabolite in the degradation of adenosine nucleotide, and accumulated in heart, kidney skeletal muscles after death. Hypoxanthine has been detected using the enzyme xanthine oxidase in a myocardiac cell culture system. Using carbon fiber microelectrodes immobilized with xanthine oxidae the extracellular hypoxanthine in the myocardiac cell culture system was found to increase with ischemic tolerance [45].

Several cell signaling molecules and neurotransmitters have been detected using enzyme based sensors. Glutamate oxidase (GluOx) has been immobilized onto electrodes to sense the neurotransmitter glutamate. Glutamate plays a important role in long term changes in synaptic efficiency and increased level to glutamate has been found in disorders like as stroke, schizophrenia, Alzheimer's and Parkinson's disease. Therefore, time dependent measurements of glutamate will help in understanding neuronal disorders [46]. Several studies used electrodes coated with Osmium(Os) based gel / horseradish

peroxidase (HRP)/GluOx film for detecting glutamate from cultured rat neuronal cells [47,48]. The Os-gel/HRP was used in reducing operating potential and achieving higher conversion efficiency in enzyme based biosensors (We will see more about these electrode modifications in 'Part II' of our discussions). In an attempt to improve glutamate biosensor performance, a dual channel thin layer flow cell was used [49]. In this study, one of the channels had a carbon film electrode containing bilayer of Os-gel-HRP/ GluOx film and the other channel had a second electrode containing Os-gel-HRP film and no enzyme. The baseline noise and interference was detected with the second electrode and subtracted from the concurrent signal of the electrode containing the enzyme. This produced a highly selective data with little noise and was used to sense glutamate more accurately from a cell culture of nerve cells from the cerebral cortex of 18-day-old rat embryos. In another study the interference from ascorbic acid in the glutamate biosensor has been reduced using a pre-reactor electrode containing ascorbate oxidase before the enzyme containing electrode [50]. Glutamate release was also detected in C6-glioma cells and HN10 neuroblastoma cells simulated by potassium ion using a more efficient Osmium based redox hydrogel/HRP/GluOx based enzyme microelectrode integrated with the microtiter plate [51]. The above mentioned glutamate biosensor setup was also used along with a Ni porphyrin based electrode to detect glutamate and nitric oxide respectively in a C6-glioma cell culture [52,53].

Enzyme based electrodes have also been used to detect histamine, which is a monoamine that is known to play an important role in immune responses, gastric secretion and in neural cells. Os-gel-HRP and histamine oxidase (HAOx) coated

electrodes have been used to detect histamine [54]. Real time monitoring of histamine released from rat basophilic leukemia (RBL-2H3) cells was done using a recombinant HAOx and Os-gel-HRP. The recombinant histamine oxidase was more specific to histamine and did not show any response to diamines and polyamines, which was an improvement from histamines used in previous studies [55].

Several multi-enzyme biosensors have been used to detect biomolecules using as cascading mechanism. Important extracellular signaling biomolecules like purines (adenosine, inosine, and hypoxanthine) have been detected using a three enzyme biosensor. Amperometric biosensor for purine detection was prepared by incorporating three enzymes (xanthine oxidase, purine nucleoside phosphorylase and adenosine deaminase) on a platinum microelectrode [56]. The senor worked by successive converting adenosine to inosine, inosine to hypoxathine, and hypoxanthine to urea and hydrogen peroxide.

$$Adeno\sin e \xrightarrow[dea\min ase]{adeno\sin e} ino\sin e + NH_3$$

$$Ino\sin e + P_1 \xrightarrow[phosphorylase]{nucleoside} Hypoxanthine + Ribose$$

$$Hypoxanthine \xrightarrow[oxidase]{xanthine} Uric.acid + H_2O_2$$

This type of sensor was first used to detect purine production in the spinal cord in live fish embryos and was further improved by incorporating the same enzyme system in a platinum micro-electrode was faster response and detecting without damaging the tissues. [57]. Only adenosine detection has been done on granule cell culture using an indirect method comprising of two biosensors [58]. The first is the same biosensor as the above

for detecting all the three purines adenosine, inosine, and hypoxanthine, while the second biosensor had only enzymes nucleoside phosphorylase and xanthine oxidase to detect inosine and hypoxanthine. The difference between the 2 sensors gave the adenosine concentration. In this experiments ATP was also detected using a two enzyme ATP biosensors consisting of glycerol kinase and glycerol-3-phosphate oxidase. By including phosphocreatine kinase the signal can be amplified and also make the system sensitive to ADP [59].

iii) Electrochemical biosensors for lysed and in-vivo cells.

Microfluidic systems are readily used in cell lysis and then monitoring the contents of cells. Various enzymes, intracellular proteins and nucleic acids are detected using this method [60,61]. A microsystem integrated with electrophoretic immobilization method of micro-organisms, cell lysis and electrochemical impedance technique and amperometric method was used to detect pathogens such as Salmonella. Screen printed electrodes were used to detect the p-aminophenol released from the lysed cells thereby giving amperometric responses corresponding to the amount of cells present.[62].

The recent developments in nanoelectrodes and AFM studies have enabled electrochemical measurements to be done inside single cells (intracellular sensing). It is done using one dimension nanoprobes that can be inserted into a cell without damaging the cell membrane. One the first studies used a 42-nm polished Pt tip approached and penetrated an immobilized MCF-10A cell. This electrode was proposed for electrochemical measurements inside a living cell and to evaluate potentials, concentration profiles, and charge transfer kinetics [63]. Carbon nanotubes (CNTs) and

boron nitride nanotubes (BNNTs) and AFM based nanotips having diameters less that <30nm have been proposed as the candidates for these types of studies [64]. These studies are in its preliminary stages and there is long way to go before they can be considered under the proper definition of biosensor.

2.3.5 Electrochemical Impedance Spectroscopy

Electrochemical impedance is usually measured by applying a sinusoidal AC potential to an electrochemical cell and measuring the current through the cell. The output current generally has different amplitude and a phase shift as seen in the Figure 2.7.

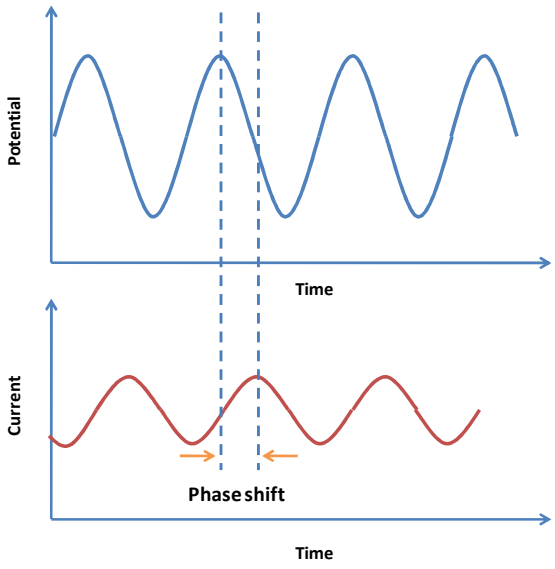

Figure 2.7: Input potential and output current in EIS measurements

This shift in behavior happens as the electrochemical interface (metal and solution meeting interface) behaves as capacitor and also there is resistive component arising from solution resistance and electron-transfer.

If the input sinusoidal signal can be denoted as $E = E_0 \sin(\omega t)$, then the output current signal can be denoted as $I = I_0 \sin(\omega t + \varphi)$,

And the impedance is

$$Z = \frac{E(t)}{I(t)} = \frac{E_0 \sin(\omega t)}{I_0 \sin(\omega t + \phi)}$$, or as complex variable, $Z = \frac{E}{I} = Z_0 e^{i\phi} = Z_0(\cos\phi + i\sin\phi)$

To get a complete data the measurements are done over a range frequency change (1 mHz- 1MHz). Equivalent circuits with capacitor and resistors are used to define the electrochemical system and this equivalent circuit model is fitted with the obtained data to get the resistor and capacitive values. In the early studies the equivalents circuits were simple (minimum number of components and single time constant) and measurement was done for only one or a few frequencies. But these assumptions still hold good if there is no electrochemical reaction happening at electrode surface.

2.3.6 Impedance spectroscopy in microfluidic cell culture system

Impedance measurements in microfluidic system have been demonstrated to be capable of cell counting and characterization of cells using cell membrane capacitance and resistance. In this study, single cells were passed through a narrow microchannel with two gold electrodes on the walls of the channel. Impedance spectra (100 Hz – 2 MHz) recorded on different cells showed significant variation in magnitude and phase angle of the output impedance [65]. A micro electrical impedance spectroscopy system (μEIS) for single cell analysis has been developed and used to differentiate ion channel activities of bovine chromaffin cells. K^+ and Ca^{2+} channels were blocked and their electrical impedances were measured over a frequency range of 100 Hz to 5.0 MHz and

compared to that of unblocked chromaffin cells. When ion channels were blocked, an increase in magnitude and decrease in phase of the measured impedances were observed [66]. Micro-electrical impedance spectroscopy (μ-EIS) system were also used to extract the pathological characteristics from the breast cancer cells separated from blood without any tagging but just the magnetic properties of red blood cells. The experimental results showed that the whole cell impedance results obtained by μ-EIS were significantly different between the normal cell lines and each of the cancer cell lines, thus allowing for cell identification and sorting based on the different pathological stages of human breast cancer cell lines [67]. Human hepatocellular carcinoma cell (HepG2) was tested for their cytotoxicity in a microfabricated chip using impedance spectroscopy by indirectly measuring the cell adhesion [68].

2.3.7 Examples of Multiparametric biosensors

All the three electrochemical techniques have also been used together on single chips to monitor cell culture. These systems not only provide multiparametric values to observe the cell better, but also demonstrate the ease of combining these techniques onto a single chip. Multiparametric silicon sensor chips mounted into biocompatible cell culture units have been used for investigations on cellular microphysiological patterns. Potentiometric, amperometric and impedimetric microsensors were combined on a common cell culture surface on the chip. Extracellular acidification rates (with pH-sensitive field effect transistors, ISFETs), cellular oxygen consumption rates (with palladium based amperometric electrode structures) and cell morphological alterations (with interdigitated electrode structures, IDES) were monitored on single chips simultaneously for up to

several days. LS174T adenocarcinoma colorectal cell line was chosen as a model for the multiparametric study and the adhesion was preferential to the palladium surfaces than to silicon surface [69] . Similar multiparametric biosensor was also used to grow colon and breast cancer cells as well as doxorubicin-sensitive and doxorubicin−resistant sarcoma cell lines. The changes in metabolic activity due to drugs like cytochalasin B and chloroacetaldehyde or doxorubicin was tested [70].

2.3.8 Electrochemical biosensors for proteins

The future of electrochemical biosensors in cell culture is not only confined to determining metabolic parameters but will also involve the ever growing protein detection methods. Protein analysis using electrochemical methods mostly uses antibodies or aptamers as the recogonition element [71]. Potentiometric, amperometric or impedimetric transducing methods have been used along with these electrochemical immunoassays. In this section we will only see examples of aptamer based electrochemical biosensors and introduce briefly some of the different methodologies used in aptamer based sensing.

Aptamers are attached mostly to gold electrodes in case of electrochemical biosensors using terminal groups like amine, thiol or biotin linked to the aptamer. Impedance spectroscopy measurements are the most used method as they shown excellent sensitivity and low detection limits. Chronoamperometry transducers are used when easier data processing and faster responses are needed [72]. Thrombin is the model protein that has been repeated tested using aptamer based electrochemical techniques. 3-D conformational changes in a ferrocene-labelled beacon aptamer to thrombin was

demonstrated as a thrombin biosensor using both chronoamperometric and impedance measurements. Lower limits upto femto molar concentration was achieved using impedance measurements [73]. Methylene blue intercalated into the aptamer has also been used to binding of thrombin using voltammetric studies [74]. The detection limit of the target thrombin in this case was 11 nM. Nanoparticles have also been used as new signal amplification strategy in electrochemical aptamer based biosensors. Platinum nanoparticles have been reported as catalytic labels in an amplified detection of thrombin. The nanoparticles catalysed reduction of hydrogen peroxide and the resulting current amplified the detection of thrombin sandwiched between the aptamer on the electrode surface and the aptamer labeled with nanoparticles [74]. There are still a lot of problem related to aptamer based electrochemical biosensing including the non-specific binding [75]. These problems and other related problems have to be overcome to realize practical biosensors in cell cultures.

2.3.9 Future of electrochemical biosensors in cell culture analysis

The future of cell culture analysis will not only depend on a single type of transducer, but will be a combination of various types of transducers depending on what they can measure more accurately. One of such future system is represented in a Figure 2.8. Electrochemical and optical transducers will definitely play a major role in these systems.

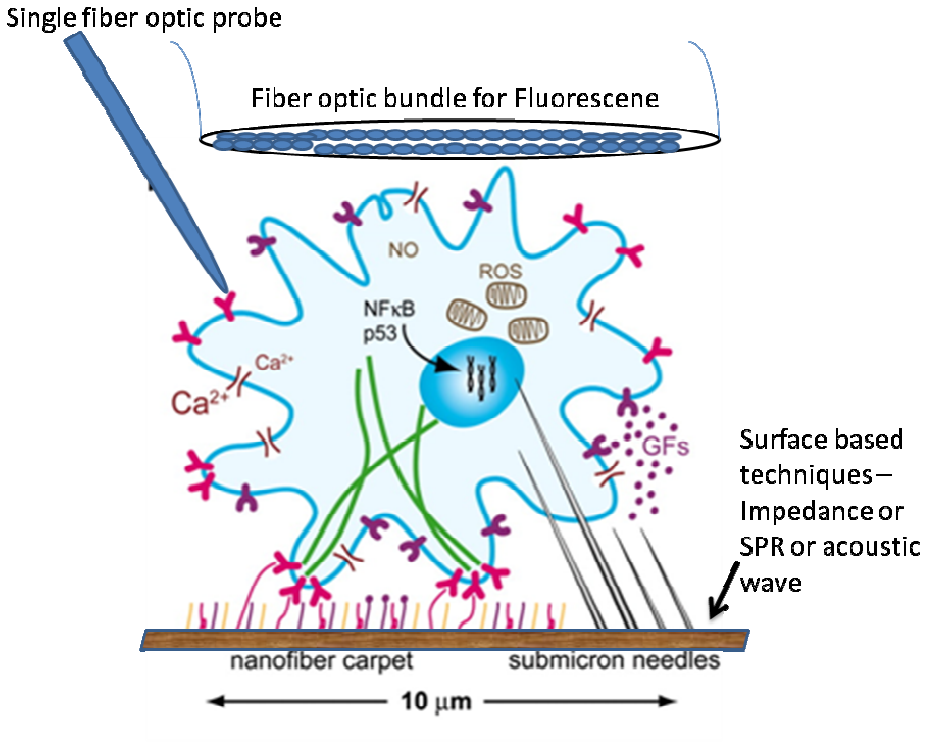

Figure 2.8: Future monitoring system (Modified from Helmke B et al 2006 [76])

2.4 Advances in nanomaterials for electrochemical based glucose biosensors

Nanomaterials have been incorporated in all three types of electrochemical biosensors discussed in the previous sections to enhance their performance. It is not possible to cover all the improvements brought about by nanomaterial incorporation, as it will be quite extensive. So we have chosen amperometric glucose biosensors as our model system to see the effects of nanomaterials on the electrode structure. Electrochemical based glucose biosensors face major challenges in terms of sensitivity, stability and selectivity when it comes to miniaturization and performing continuous measurements. To address these issues, various nanostructured materials have been explored to improve the performances of these biosensors by incorporating these nanomaterials to the

electrodes. This review examines the unique properties of these nanomaterials in the categories of metals, metal oxides, polymers and composites, and the way in which these nanomaterials enhance glucose biosensors.

2.4.1 Introduction to glucose biosensor

The history of biosensor technology begins with the design of a glucose sensor based on a Clark oxygen electrode and glucose oxidase as the enzyme to catalyze glucose oxidation in 1962 [77]. Since then there have been tremendous advances in the field of biosensors. Today glucose biosensors take up more than 85% of the commercial market for all biosensors sold worldwide [78]. Of these glucose biosensors many are used for blood glucose monitoring. Aside from blood glucose monitoring, glucose sensors also find applications in bioprocessing industry for monitoring cell cultures [79] and fermentation processes [80]. Glucose biosensors used for these purposes need to meet a different set of requirements such as functional under extreme pH and temperature conditions. The ability to continuously monitor glucose in bioprocesses is also desirable [81].

In the past few years, advances in glucose biosensors are mainly in exploiting the nascent field of nanotechnology to address critical problems facing the biosensors including poor stability, reliability and longevity [82] and low sensitivity and selectivity [83]. In this section of the review we focus on the developments made in utilizing various nanostructured materials to enhance the performances of glucose biosensors so they can also be readily used in cell culture micro-environments for monitoring.

2.4.2 A brief overview of three generations of glucose biosensors

The glucose biosensors development along the years has been separated into three generation depending on the method the electron was transferred from the enzymatic reactions to the electrode. While the very first glucose sensor measures oxygen consumption during glucose oxidation [77], the first-generation glucose biosensors detect the production of hydrogen peroxide resulted from glucose oxidation. In this case, detection of hydrogen peroxide is generally made at an anodic potential of 0.6 V with a platinum electrode. The reaction is shown below

$$GOx(FAD) + glu\cos e \rightarrow GOx(FADH_2) + gluconolactone$$

$$GOx(FADH_2) + O_2 \rightarrow GOx(FAD) + H_2O_2$$

$$H_2O_2 \rightarrow O_2 + 2H^+ + 2e^-$$

At this high anodic potential, however, other coexisting species in the blood sample such as ascorbic acid, uric acid and acetaminophen will also get oxidized, leading to unwanted interferences. To minimize these interferences, permselective membranes such as polymer coatings [84] and ionic membranes such as Nafion films [85] are used as selective filters. Another effective way to reduce these interferences is to use electrode materials having low overpotential for catalytic reduction of hydrogen peroxide. For example, platinum can be replaced by other materials like ruthenium [86], rhodium [87] and iridium [88] because they possess high catalytic activity toward reduction of hydrogen peroxide at low operating potentials. Ferric hexacyanoferrate (Prussian blue) and its analogues are often used as the electrode material since they can selectively reduce hydrogen peroxide at a low potential [89-91]. Overall, the first-generation

biosensors are highly susceptible to variation in oxygen concentration as they relied on oxygen as a cosubstrate for the generation of hydrogen peroxide.

In the second-generation glucose biosensors, this oxygen susceptibility is minimized by using diffusional electron mediators to transfer the electrons from enzymes to electrodes. Ferrocene derivatives, tetrathiafulvalene-tetracyanoquinodimethane, quinones and ferri/ferrocyanide are commonly used as mediators [92]. The scheme of mediator is shown in the Figure 1 below.

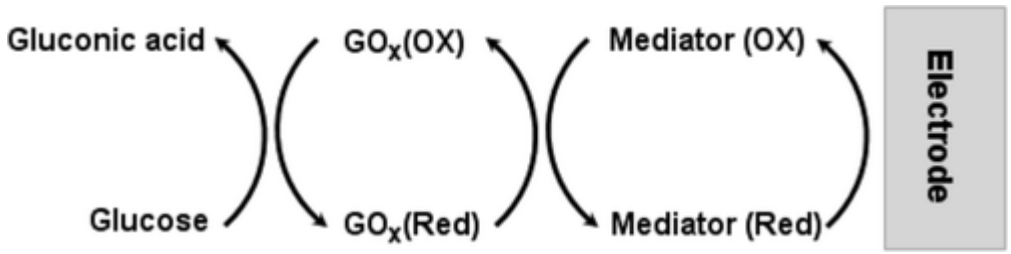

Figure 2.9: Electron transfer using mediator (Courtesy: Wang et al, 2008 [82])

An alternative method is to use an osmium complex linked to redox polymers as 'wired enzyme' electrodes [82] to shuttle electrons from enzymes to electrodes [93,94].

The third-generation glucose biosensors seek direct electron transfer (DET) between the redox center (the co-factor of the enzyme that can undergo redox reactions) of glucose oxidase and electrodes (Figure 2.9). According to the Marcus theory [95], the ability for DET depends on the structural rigidity of the redox species and the potential difference as well as the distance between neighboring redox centers. Since the distance from a redox center to an electrode surface is often relatively large and that the protein shell usually shields the redox center, electron transfer by a tunneling mechanism seldom occurs spontaneously. Thus to facilitate DET from enzymes to the electrode, not only the

distance between the redox centers and the electrode needs to be as short as possible but also the orientation of the enzymes needs to be properly aligned with respect to the electrode surface [96]. In the case of flavin adenine dinucleotide (FAD)—the redox center of the glucose oxidase enzyme which is located deep inside the protein structure—few study reports qausi-reversible voltammograms of FAD/$FADH_2$ redox activity, indicative of DET from glucose oxidase to the electrode [97]. The DET behavior can be examined directly by running cyclic and linear voltammetry to electrodes at different scan rates [98]. It should be noted that in the case of glucose detection, many studies which report DET between glucose oxidase and the electrode actually require the involvement of oxygen [99] and/or mediators [100]. True DET in glucose detection in de-aerated solution without a mediator is still not commonly pursued [101].

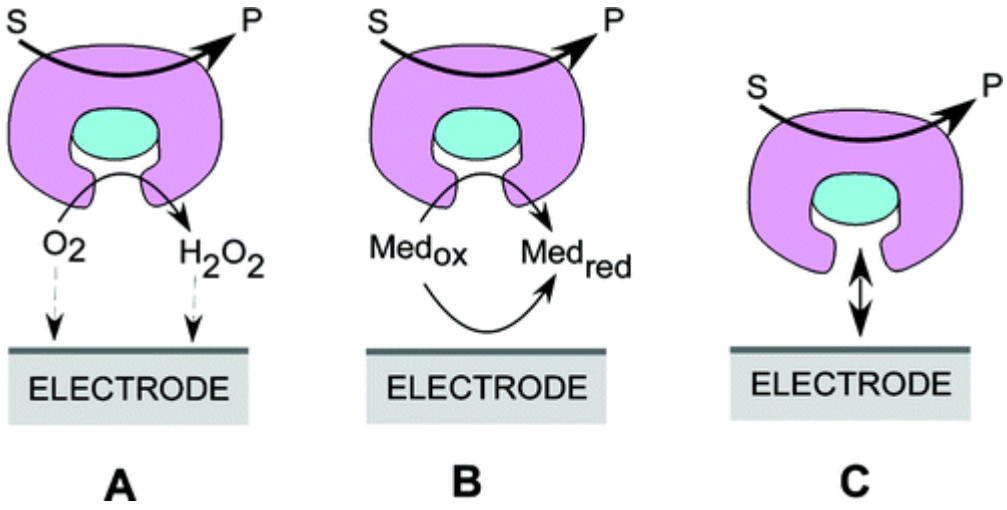

Figure 2.10: Mechanisms of direct electron transfer (Courtesy: [82])

Although glucose oxidase is one of the most stable enzymes, it loses activity during storage and when exposed to environments having pH of below 2 or above 8 and temperatures above 40^{o}C, or containing ionic detergents [102]. This concern over enzyme

stability stirs a drive to develop another important class of glucose biosensors in which glucose oxidation is directly performed at the electrode surface nonenzymatically. So far, metals such as platinum [103], gold [104,105] and nickel [106] have been used to directly oxidize glucose. Other materials like metal oxides [107] and alloys [108] have also been tried. Of these nonenzymatic approaches, direct electro-oxidation of glucose with platinum electrodes has been studied extensively [109-111]. Main challenges are found to be slow glucose oxidation kinetics, electrode poisoning by adsorbed intermediates and chloride ions at Pt electrodes, and poor sensitivity. A detailed review on nonenzymatic glucose biosensors can be found in the literature [112].

2.4.3 Nanomaterials in glucose biosensors

Nanomaterials are known as materials that have sizes in the range from single nanometers to a few hundreds of nanometers in at least one dimension. Nanomaterials can be classified according to their basic structures as 0D (clusters and particles), 1D (nanotubes and nanowires), and 2D (nanoplates and films) [113]. Common nanomaterials include carbon based materials (e.g., fullerenes, carbon nanotubes and graphenes), metal, metal oxides, polymers and composites. Nanomaterials possess unique physical and chemical properties that are different from their bulk counterparts such as high surface-to-volume ratio, high catalytic activity, improved absorption for enzyme immobilization, and enhanced electron transfer capability [114]. The ability to tailor materials at nanoscale has brought many advances in recent years to the development of many electrochemical based biosensors, especially the glucose biosensors.

The performances of biosensors are often examined according to their 1) calibration characteristics such as sensitivity, linear concentration range and detection limit, 2) selectivity and reliability, 3) response time and 4) reproducibility, stability and lifetime [4]. The sensitivity of a glucose sensor is usually determined through a linear regression of the measured current values with respect to glucose concentration. From this analysis, enzymatic kinetic parameters such as Michaelis Menton constants, K_m and I_{max}, can be determined using the Lineweaver Burk reciprocal approach. When nanomaterials are incorporated to the electrodes of glucose biosensors, increases in sensitivity and I_{max} values and decreases in K_m values are often observed due to possibly increased enzyme loading at nano modified electrode surfaces.

Nanomaterials have also been explored to increase the selectivity of glucose biosensors. For example, nanomaterials with a higher catalytic efficiency and lower overpotential for hydrogen peroxide reduction can help lower the operating potential of the glucose biosensors [115], thus minimizing the interferences from nonspecific species. Use of polymeric materials in nanocomposites as permselective filter can also help reduce interferences [116,117].

Nanomaterials can prolong the stability and lifespan of enzyme-based glucose biosensors by stabilizing enzymes in immobilization. Common methods such as covalent attachments [118] and polymeric entrapment [28] have been used to immobilize enzymes. But the unique properties of nanomaterials such as high surface area, high surface energy, and high porosity make direct adsorption of the enzymes onto electrode surfaces possible [119]. Nanoporous cavities are found to stabilize the enzymes by

reducing the unfolding of the enzyme proteins [120]. Nanomaterials with charged surfaces are found to make enzyme extremely stable through electrostatic absorption [121]. In some cases, nanomaterials are used in the glucose biosensors solely for their ability to retain the native activity of glucose oxidase after immobilization [122].

Nanomaterials are also promising in facilitating DET from FAD (the redox center of glucose oxidase) by offering physical dimensions matching that of enzymes. Nancomposite materials have been effectively used in achieving direct electron transfer [123]. Nanomaterials can also be made catalytically active for direct glucose oxidation through composite structuring with proper constituent components. The high surface area of nanomaterials has been used to overcome the sluggish kinetics of direct glucose oxidation. Some materials have shown catalytic activity toward glucose oxidation only in nanostructured form.

2.4.4 Future perspective

What we have dealt here is a model enzyme biosensor system (glucose biosensor) and use of nanomaterials from this system can also be extrapolated to other enzyme based biosensor systems. The current trend in accurate cell culture analysis system is having biosensors that are rapid responding, stable, and reliable, and able to make continuous measurements.

2.5 Summary of information gathered from the background information

1) There is lot of applications if we can effective monitoring cell cultures
2) Electrochemical biosensors provide an simple and efficient way of monitoring cell cultures

    a. Several examples are already present in literature for use in cell culture monitoring

3) Amperometric biosensors with enzymatic electrodes will be best for continuous monitoring
4) Amperometric biosensors presently have of drawbacks like lower sensitivity, selectivity and stability when used for continuous monitoring
5) Nanomaterial based electrodes if exploited properly present elegant solutions to improve on the drawback of amperometric biosensors.

CHAPTER 3

PROPOSED IDEA AND OBJECTIVES

3.1 Proposed idea

From the background information it is clear that there is a need for an effective amperometric biosensor that can be used for monitoring cell culture. So we wanted to chiefly develop a microfluidic based electrochemical biosensor that can measure changes from cell culture. This biosensor should have electrodes that can be very sensitive and specific to the analyte of interest. It should also give reliable and stable long term measurements in the medium like Minimum Essential Media (MEM) solution in which the cells are grown. So the proposed ideas and hypothesis were

1) Use of 3D gold nanopillars for increasing the sensitivity
2) Improve the enzyme immobilization methods for 3D nanopillars for achieving highly specific and sensitive biosensor.
3) Utilize nanomaterial – enzyme interactions for increasing the biosensor stability
4) Incorporate the 3D nanopillars based electrodes in microfluidic channel for performing continuous measurements
5) Have electrode modifications to reduce interference

3.2 Significance of the device

The proposed device will find application in the fields of cell physiology, cell biology and toxicology as they will meet the requirement of continuous real time measurements in in-vitro conditions and also providing controlled environment for cell cultures.

3.3 Proposed biosensor design and its working principle

Figure 3.1 shows of the proposed microfluidic biosensor we want to develop. All the electrodes shown in the schematic were to be incorporated with 3D gold nanopillars.

1) The first electrode will be the anti-interference electrode that can consume interfering species.
2) The second electrode will be the enzyme electrode were the enzyme layer was immobilized
3) The third will be the working electrode on which a potential was applied to perform amperometric measurements
4) The Counter electrode will complete the electrical circuit.

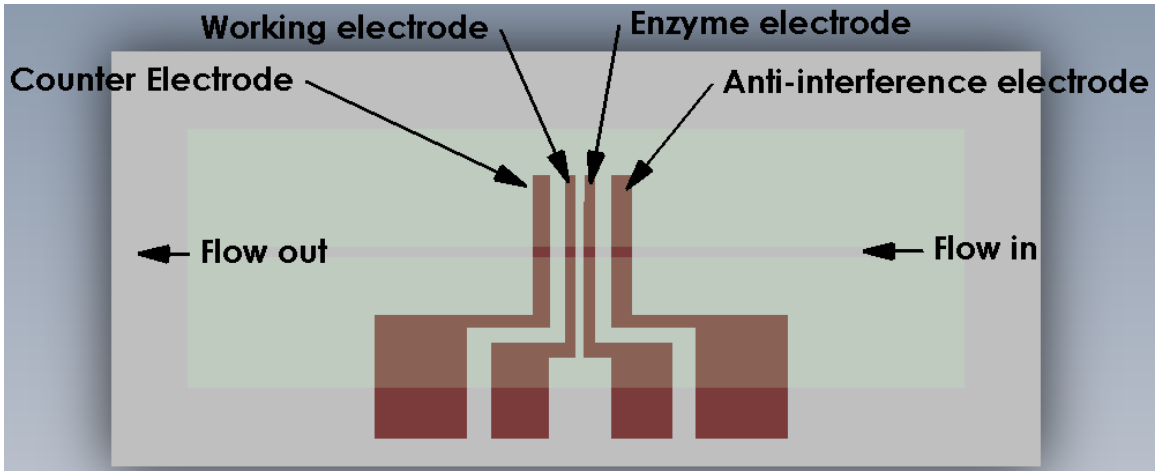

Figure 3.1: Schematics of the proposed device

Figure 3.2 shows the principle of proposed microfluidic biosensor that will be used for cell culture monitoring. The device was to act as a glucose biosensor and measure the glucose consumption in cells.

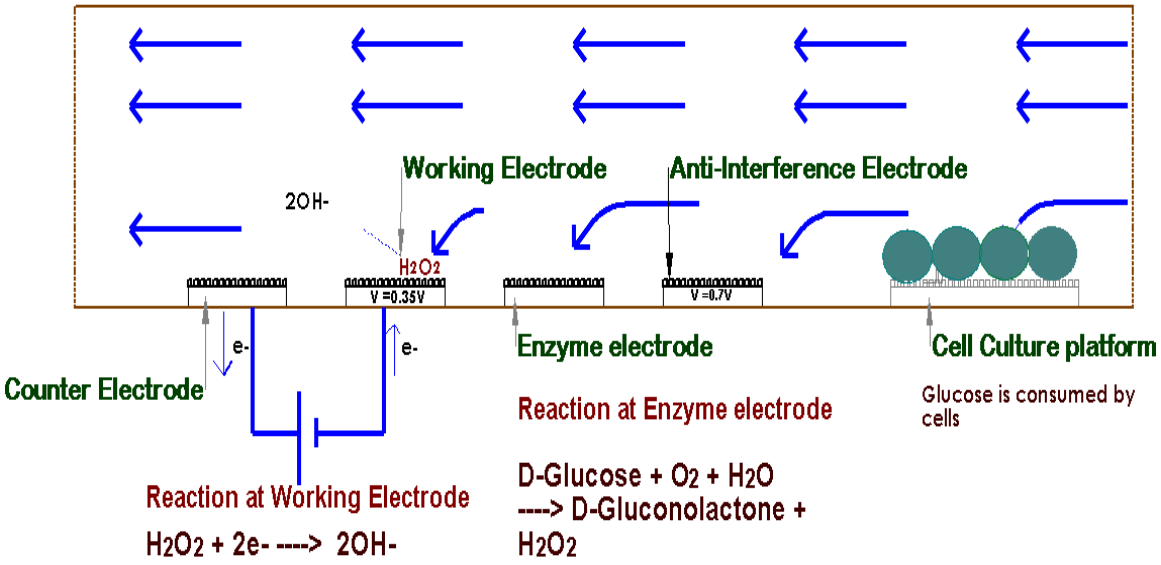

Figure 3.2: The working principle of the proposed device

3.4 Objectives

Based on the proposed device the main objectives of this work are:

1) To develop nanoporous alumina platform on glass substrates that can be used as templates for growth of 3D gold nanopillars
2) Optimize the immobilization of enzymes on 3D nanopillars
    - using polypyrrole electropolymerization or self-assembled monolayers
    - Improve the stability of enzyme immobilization process
3) Convert the 3D nanopillars as patterned electrodes for incorporation in microfluidic channels
    - Optimize the microfluidic design parameter for maximize the efficiency of the biosensor
4) Incorporation of electrode modification onto the working electrode to reduce operating potential and interference.

5) Build the biosensor with all the optimized information and study its efficacy by studying the glucose metabolic activity of the immobilized cells

The results from the work done are categorized into five sections based on these five objectives. Each section will cover the work that was accomplished to realize the respective objective.

3.5 Note on anti-interference electrode

The initial proposal of the device had the anti-interference electrodes. But preliminary results indicated that these electrodes were not able to effectively eliminate the interfering species and with potentials or surface area similar to the working electrode. Two potentiostats were needed to supply different potentials to the working and anti-interference electrodes. Area had to be increased considerably and it became unfeasible to have it in the microfluidic design. This method was also not feasible in an inter-digitated electrode setup. Therefore we dropped this electrode from the design and only had a three electrode system. So we will not further discuss about the anti-interference electrode.

SECTION I - 3D NANOPILLARS

CHAPTER 4

DEVELOPMENT OF 3D NANOPILLARS

The first objective of our study was to develop 3D nanopillars on solid supports. In this section we will have only one chapter that describes how we developed the 3D nanopillars using commercial alumina templates and also thin film alumina templates prepared in-house.

4.1 Introduction

To date, many flat or planar micro-electrodes have been used in the µ-TAS as electrochemical electrodes [124]. Although improvement in detection limits is seen, a reduction in current signal is noted owing to the small size of the micro-electrodes. To overcome this problem, a common strategy is to increase the surface area of the micro-electrode with nanostructures [125].

Nanostructures can provide large surface areas due to their high surface-to-volume ratio. But when these nanostructures are formed on a planar substrates, the overall surface-area enhancement will be limited, to a certain extent, by the size of the underlying substrate. Then the question becomes: how can one achieve a higher surface area when the size of the planar area (or the ‘real estate’) is fixed? The answer lies in a “skyscraper” metaphor, that is, to build up within a limited areal footprint [126]. Adding 3D skyscraper nanostructures onto a planar surface offers a significant increase in its overall surface area when compared with the planar surface.

In our work we developed two methods for obtaining the 3D skyscraper electrodes. The first method was based on commercial templates and the second was a thin film method exclusively developed in our lab. In this chapter we will discuss the details of both methods. Since these 3D structures were intended for biosensor applications, we limited the material to gold only in this study due to its well accepted biocompatibility.

4.2 Experimental methods

4.2.1 Formation of 200nm diameter 3D nanostructures using commercial templates

We have developed a commercial alumina template based electrodeposition technique to fabricate 3D skyscraper nanostructures [13]. In this method, a 150 nm thick gold film was first deposited onto one side of a porous anodic aluminum (PAA) disc by sputter coating. A thicker gold layer was then electrodeposited on top of the sputtered gold film to form a strong supporting base in an Orotemp24 gold plating solution (Technic Inc, Cranston, RI) under a current density of 5 mA/cm2 for two minutes in a three–electrode cell with a platinum (Pt) counter electrode and an Ag/AgCl reference electrode. This supporting base was then masked using Miccrostop solution (Pyramid plastics Inc., Hope, AK) for insulation. After that, gold nanopillars were electrodeposited through the open pores of the PAA disc from the uncoated side under an electrical current density of 5mA/cm2 at 65°C for 5 minutes. The PAA template was finally dissolved by immersing the specimen in 2M NaOH solution for 30 minutes. This procedure resulted in 3D structures having arrays of gold nanopillars standing on gold support bases. These 3D structures were cut into small pieces and used as electrodes for further studies.

Prior to immobilization procedures, the surfaces of these 3D electrodes were cleaned electrochemically by performing CV within a potential range from -0.5 to 1.5 V at a scan rate of 100 mV/s in 0.3M H_2SO_4 solution. The cleaning cycles continued until a reproducible voltammogram was obtained. After that, the electrodes were rinsed with DI water and dried with nitrogen blow. These cleaning CV's were also used to determine the roughness factor (the ratio of increase of nanostructured surface in comparison to flat electrode of similar geometrical area) [127].

4.2.2 Development of 50nm nanopillars on glass substrates

4.2.2.1 Al/Au/Ti film formation

The glass substrates used for the fabrication were first cleaned using RCA1 solution (H_20:NH_4OH:H_2O_2: 5:1:1) at 70^oC for 20minutes. Then they were etched in 0.5% HF solution for 30 seconds and finally rinsed with copious amount of water. A three-layer film consisting of Ti (5 nm), Au (20 nm) and Al (800 nm) was deposited sequentially onto the substrates using an E-beam evaporator (Kurt Lesker PVD 75). The Ti layer here serves as an adhesion layer and the Au layer is to prevent detachment of alumina layer and provide electrical conductivity during electrochemical processes.

4.2.2.2 Anodization of the top Al layer

The three-layer film formed on the glass substrate was masked with Microshield lacquer by exposing an area of 25×25 (mm). The exposed area was electropolished in a mixture of H_3PO_4:H_2SO_4:H_2O in the ratio of 2:2:1 by weight. This step not only removed any formed oxides but also reduced the surface roughness. After that, an anodization step

was applied to the top Al layer under a constant potential of 40 V in 0.3 M Oxalic acid at 4^{o}C.

To remove the barrier layer and widen the pores, the substrates were placed in 5% H_3PO_4 at 30^{o}C for 20 minutes. This step removes the alumina barrier layer, exposes underlying gold film and widens the pores.

4.2.2.3 Electrodeposition of standing nanopillars

Electrodeposition of Au was then performed through the opened pores to form Au nanopillars in an Au plating solution (Orotemp24 gold plating solution, Technic Inc, Cranston, RI) under a deposition current of 0.6 mA/cm^2. The height of the nanopillars was controlled by deposition time. In our work, 6-minute deposition yielded nanopillars of approximately 600 nm in height. The porous alumina template was then dissolved in 2 M NaOH solution to obtain vertically free standing nanopillars on the Au/Ti film coated on the glass substrate.

Prior to further processing, the standing nanopillars on substrates were cleaned by running electrochemical cyclic voltammetry (CV) in 0.1 M H_2SO_4 in a potential range from −500 mV to +1500 mV until stable CV curves were obtained for each specimen. After that specimens were rinsed in deionized water. The measured CV curves were used to determine the areas of the nanopillar modified surfaces.

4.3 Results and discussions

Adding 3D nanopillars onto a flat surface can increase the overall surface significantly. Figure 4.1 illustrates this by having vertically aligned nanopillars on a planar substrate to form a 3D structure. From Zhang G 2011 [128] calculations on surface

area increase of 3D nanopillars, it can be seen that at an aspect ratio (h/2r) of 25 and a packing density p= 50% for the nanopillars, a 51-fold increase in surface area can be achieved.

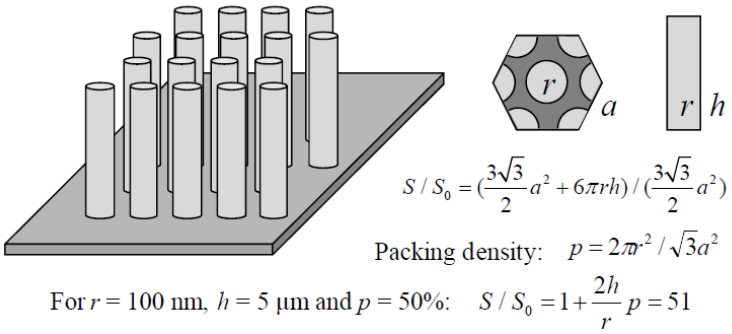

Figure 4.1: Schematic illustration for increasing the overall surface area by building 3D skyscraper structures on a limited areal footprint (Image taken from [128])

3D nanopillar electrodes have been fabricated using chemical vapour deposition methods and PVD methods. But these methods yielded nanorods that could deform because of the capillary forces generated by the nanostructure liquid interactions [129,130]). These deformations will reduce the exposed surface area in a liquid environment and making it less effective when used in aqueous based biosensor applications. So it is evident that there should be a method of nanopillar formations that can have sufficient mechanical strength to withstand the capillary forces.

So in this work we used electrodeposition techniques to deposit metal into the porous templates to obtain the mechanically stable nanostructures. We found out in our earlier work with water droplet tests that electrochemically nanostructures were mechanically very stable [128]. There was a bunching of gold nanopillars electrodes when the aspect ratio was larger than 8 – 10 (See Figure 4.2 & 4.3). But this was very different from the

nanopillars collapsing altogether as seen from PVD or CVD methods [129]. The physical conditions like surface tension, contact angle and inter-nanopillar distance and the aspect ratio will have dominating effects on the resistance of these nanopillars to capillary interaction [131].

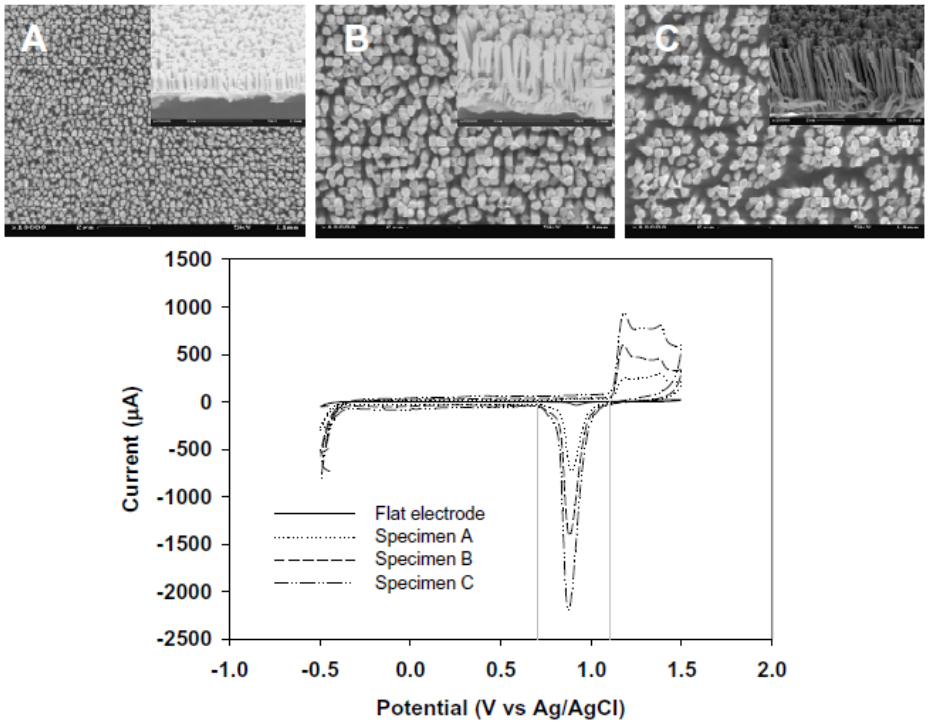

Figure 4.2: Images of 200nm nanopillars formed using commercial template method with different roughness factors (A- 20, B – 38.8, C – 63), the lower image shows the cyclic voltammograms of the three different nanopillars (Sample C has aspect ratio more than 10 and there is evidence of some bunching. The reduction peaks increase with increase in area, Images taken from [127] - results obtained from previous work in our lab).

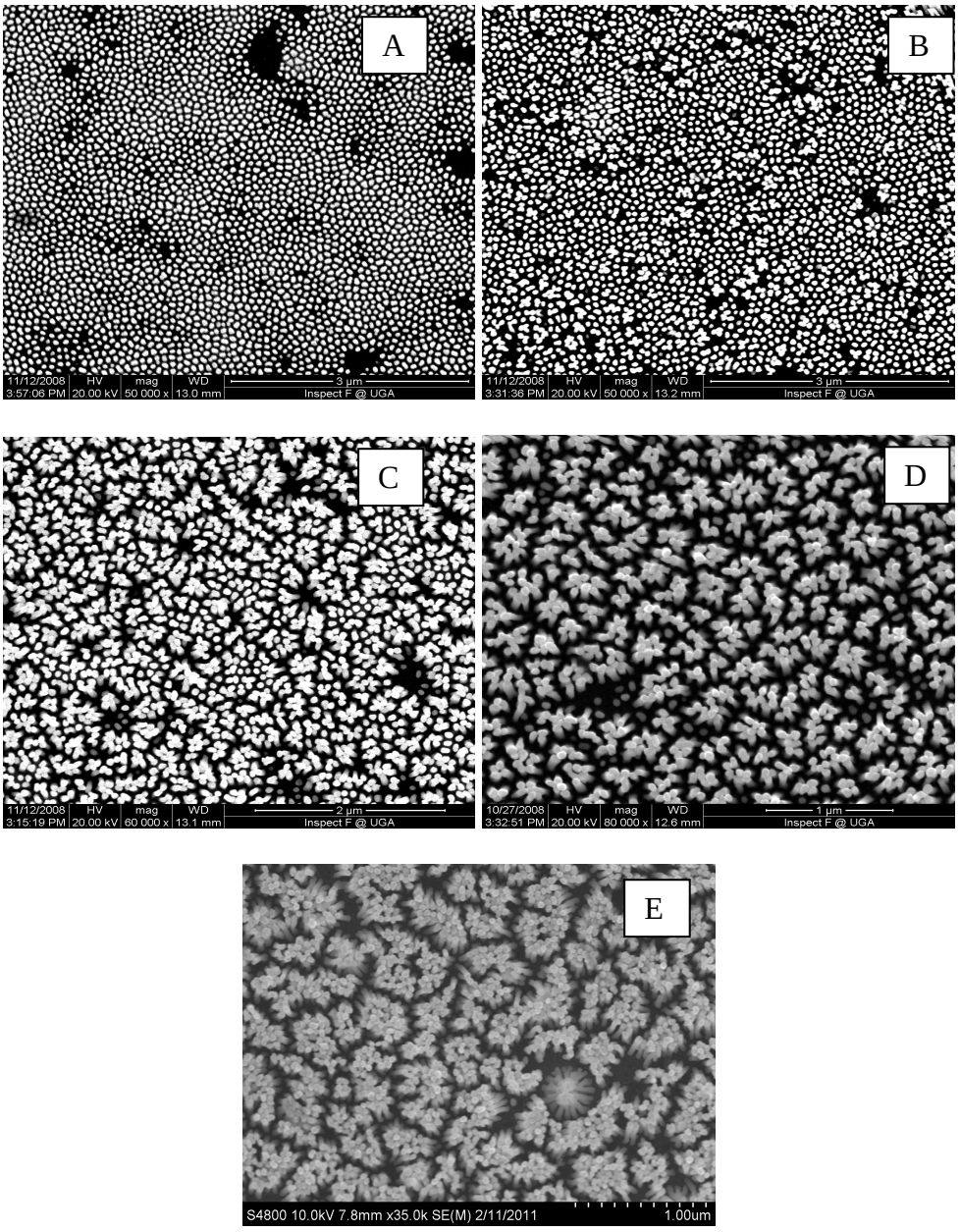

Figure 4.3: SEM images of nanopillars formed on glass substrates using thin film deposition and anodization (The images show the increasing nanopillars aspect ratios with increased deposition times: A- 1min, B – 2min, C – 3min, D- 4 mins, E-6mins deposition time. Bunching is seen significantly in Figure 4.3E where the aspect ratio is above 10)

4.3.1 50 nm diameter nanopillars formation on glass substrates

Although the surface area is drastically enhanced using the 3D nanopillars using the commercial template method, one challenge associated with these 3D skyscraper nanostructures is that it is difficult to turn them into devices through further structural processing. For this to happen, these 3D nanostructures need to be fabricated on a substrate and be processible through conventional fabrication procedures. Various methods like nanowires arrangement using dielectrophoresis [4] and polycarbonate based lithography-assisted template bonding [5] have been used to incorporate nanowires on glass or polymer substrates. But a simple, economical and highly reproducible method appears to be using porous alumina templates [6]. Although porous alumina thin films have been formed on glass or silicon substrates [7-9], their use as templates in forming standing nano structures and further processing these structures into functional devices has been rarely attempted [10]. So we developed a simple way to form three dimensional (3D) structures integrated with standing nanopillars on glass substrates.

Until now there have been different approaches to produce the anodic porous alumina structures on silicon or glass substrates. All the methods used the general procedure of depositing a thin film of aluminum on silicon or glass substrates with an underlying adhesion layer. The main difference in the methods arose from the type or number of interfacial metallic layers which was deposited before the aluminum layer. Various interfacial layers like Ti [132] , Ti/Au [133], Ti/Pt [134], Indium Tin Oxide (ITO) [135], and Ti/Cu [136] have been used on silicon or glass substrates. So the foremost problem we faced when we started nanopillar formation on glass substrates was the choice of the

suitable interfacial layer, which was necessary to obtain ordered alumina pores and providing conducting surfaces for the filling of the pores by electrodeposition. Of the various interfacial layers, a very thin layer of Ti was necessary for adhesion of other non-adherent metallic layers and also later to withstand the electrochemical oxidation experiments [137]. So the first layer was a Ti layer of 5nm thickness. In earlier studies aluminum was sometimes directly deposited over a thicker Titanium deposit to act as an adhesion and conducting layer [134]. But in our experiments it best suited for us to have another gold layer as the conducting layer because the main issue with most of the procedures mentioned in literature was the selective removal of the barrier layer. This barrier layer is a non-conducting alumina layer obstructing the pore to open into a conducting surface. The gold layer of 20 nm helped us in consistently removing the barrier layer after anodization and opening all the pores. This thickness of gold was critical since more thickness of gold resulted very high current during the end of anodization of such films. These high currents either caused highly pitted films or gradual dissolution of all the alumina. So we had to keep the thickness of the films below 20nm. We believe the higher thickness caused the intermetallic alloying of gold and alumina to form purple plaque at the gold/aluminum interface [138]. We suspect this since when thickness of the gold film was over 25 nm we could distinctly see a purple color film (when seen from the backside of the glass substrate). We could also notice a purple color when the alumina was completely etch in the anodization process.

This was crucial in forming nanopillar with uniform distribution and providing consistent surface area increase. We deposited aluminum from 800 nm to 2.5 µm and

found no problems in anodization of the aluminum film. A thicker film was necessary to get more ordered pores.

The anodization process yielded nanopores with a diameter of 40 nm. The anodization current was around 2 mA/cm^2 and was constant throughout the process until all the aluminum was anodized. When the barrier layer reached the gold layer the current started dropping rapidly as all the aluminum had been anodized. But when the anodization was prolonged this dropping current reached the lowest values and it started increasing again. This increase could have been due to breaking of some barrier layer at the bottom of the pores. . In case of stopping the anodization when the current reached its lowest value did not open all the pores even after the barrier layer removal step. Letting the current to shoot of to higher values (>50mA/cm2) dissolved all the pores completely. So we stopped the anodization when the increasing current reached around 4 mA/cm^2. This ensured all the pores were opened to the gold layer after the pore opening step. In the pore opening step the timing in phosphoric acid was optimized to 20 minutes and the resulting pore diameter after the barrier layer removal was around 50nm. This diameter was suitable of the subsequent nanopillar formation and polyprrole/enzyme deposition.

Figure 4.3A shows the SEM image of the anodized alumina film. The pore organization was not very good when compared to samples done in bulk alumina and can be partially attributed to thinner alumina film formed and the related shorter anodization time [139]. A two-step anodization was generally used to get organized pores on thin films [140]. But in our case even with a single step anodization process, the nanopillar had a consistent order and provided the same amount of increase in surface area for all batches

of samples prepared with the same electro-deposition time. The increase in area was calculated using the reduction peaks of gold in the CV obtained in 0.1 M sulfuric acid. The surface area with a roughness factor of approximately between 5 – 18 for the different nanopillar structures shown in Figure 4.3. The expected increase in surface area can also be calculated by considering a hexagonal arrangement of nanopillars (anodized alumina form hexagonal pores) with average nanopillar diameter at 50nm, inter-distance between nanopillars at 30nm and height at 600nm obtained from SEM images. The ratio of the increase in nanopillar area to that of the flat surface area can be calculated as [128] with formula shown in Figure 4.1 -

$$\frac{S}{S_o} = 1 + \frac{2h}{r} p \qquad \text{where packing density p} = \frac{2\pi r^2}{\sqrt{3}a^2}$$

S - nanopillar area, S_o - corresponsing flat electrode area

r is radius of individual nanopillar,

h is the height of the nanopillar,

a is the length of the side of the hexagonal cell

In our case when h=600 nm, r=25 nm, a=80 nm, p=0.354. So the ratio of increase in area is calculated to be S/S0=1+1200/25*0.354=18. This value also corresponds to the increase in electrochemical area found by cyclic voltammetry method in sulfuric acid.

4.4 Conclusion

Gold nanopillars electrodes were successfully formed from

a) Commercial alumina templates ,

b) Thin film alumina templates on glass substrates.

The commercial alumina template method was used whenever a hard base support was not needed. But in case of microfluidic based experiments were solid support is needed for the PDMS based microfluidic channels the thin film alumina template method optimized in our lab was used.

(Some of the material in this chapter has been adapted from the published works from Dr.Zhang's Lab - [128,141-143])

SECTION II

DEVELOPMENT OF THE ENZYME ELECTRODE

The first electrode in the microfluidic biosensor will be functionalized with enzymes (i.e glucose oxidase) for catalytically converting the analyte (i.e glucose) to a detectable electro-active species. This electrode is called the enzyme electrode. This electrode functionalization or enzyme immobilization process is a very important step because it will determine the sensitivity and stability of the biosensor. A few studies in literature have reported ways to immobilize enzymes onto order nanostructures. After an extensive literature search, we identified two methods that seem applicable to our 3D nanopillar structures based on their ability to form ultrathin layers even on complicated nanoscale geometries.

These two methods are

a) Electropolymerization studies using polypyrrole

Electropolymerization reaction happens at anodic potential when the removal of electron from the monomer initiates the polymerization reaction. This method is also extensively used to entrap the enzymes onto electrode surface during the electropolymerization reactions. By mixing the enzyme in pyrrole solution, a porous polymeric film with entrapped enzymes can be formed at the electrode surface via electrodeposition. Studies have shown that enzyme immobilized in this way has an even spatial distribution inside a porous polymer matrix due to the molecular coupling between

the pyrrole and GOx molecules. This functionalization process can be applied to electrodes with any shapes and geometries

b) Self-assembled monolayer (SAM) studies

We used alkanethiols in our studies as they can form monolayers on gold surface. In this method, one end of the alkanethiols can be attached to the gold surface through the sulfur gold bond and the other end can be modified for attaching desired biomolecules. Since these are also just a monolayer coating, the thickness is not more than 2 -3 nanometer [144].

The different studies that were conducted using these immobilization methods are

1) Optimization of polypyrrole based glucose biosensors with nanopillar array electrodes
2) The role of SAM chain length in enhancing the sensitivity of nanopillar modified electrodes for glucose detection
3) On functionalization of 3D electrodes with different nanopillar sizes (with polypyrrole and SAM immobilization techniques)
4) Influence of gold nanoparticle size on the enzyme stability in a polypyrrole/gold nanopillar electrode

The following chapters will have the detailed discussion on each of these studies.

CHAPTER FIVE

OPTIMIZATION OF POLYPYRROLE BASED GLUCOSE BIOSENSORS WITH NANOPILLAR ARRAY ELECTRODES

5.1 Introduction

Electrochemical polymerization is one of the simple and attractive techniques for immobilizing enzymes on electrodes [145]. It gives control over the enzyme loading and enzyme layer thickness. It is mostly a one step process avoiding denaturing of bio-molecules and gives control over properties and thickness of the polymer films by controlling the choice of the monomer and the electrolysis charge [146]. The process also avoids manual deposition and aids in miniaturized biosensor development [147]. Polypyrrole is the extensively used conducting polymer in immobilization of the enzyme glucose oxidase in electrochemical biosensors application. As polypyrrole is biocompatible it causes minimal disturbance to the working environment. It also protects electrodes from bio-fouling and interfering materials such as electro-active anions [148]. Its advantages like biocompatibility, reduced interference, and easiness to electro deposit on various surfaces making it a good candidate for glucose sensing [149]. Polypyrrole based amperometric glucose biosensor has been studied on various electrode surfaces [150,151]. The performance of this type of polypyrrole based biosensor is affected by the various electropolymerization parameters used for the immobilization of the enzyme glucose oxidase. So optimization of electropolymerization conditions of polypyrrole is necessary to obtain the best bio-sensing results. Systematic studies have been done on flat

gold surfaces and optimized conditions for deposition of polypyrrole have been obtained [152].

Electrochemical glucose biosensors based on polypyrrole have also used nanomaterials for increasing sensitivity, lowering detection limits and for better stability. Mostly the nanostructures were incorporated on the surface of the electrodes to increase the surface area. Polypyrrole-coated glucose oxidase nanoparticles have showed increased sensitivity values [153]. Carbon nanotube doped polypyrrole film also showed better activity due to surface area increase [154]. This type of disarrayed modification of surface with nanostructures can block enzyme sites and impede the substrate transport. But nanopillar and nanotube electrochemical arrays have shown better microenvironment to maintain the enzyme activity, and large surface area for enzyme–substrate contact [155]. Carbon nanotube array coated with polypyrrole has shown increased sensitivity [156]. Platinum nanofibers based polypoyrrole glucose biosensor has given the highest sensitivity values [150].

But until now no complete understanding of polyprrole or any polymer deposition on nanostructure dimensions has been achieved. Even in electrochemical deposition of polypyrrole on high surface area platinum electrodes, current density of 382μA cm^{-2} was used, which was the optimized current density for flat surfaces [150]. But optimization of polypyrrole/GODx film for obtaining maximum sensitivity on nanopillar arrays will involve the large nanopillar surface area and thickness variations during electropolymerization. The thickness of the polymer film and enzyme content affect properties like sensitivity, substrate diffusion, permselectivity and also interference

characteristics. So enhanced biosensor performance can be obtained if we optimize the polypyrrole electropolymerization parameters specifically for the nanostructure dimensions.

In this work we systematically investigated the effect of various electropolymerization parameters on the performance of the nanorod based glucose biosensor. We tried to enhance the performance of the biosensor by optimizing the nanorod roughness factor, electrodeposition current density and total charge.

5.2 Experimental methods

5.2.1 Reagent and instruments

Pyrrole, D-glucose, ascorbic acid, and Glucose oxidase (GODx), p-benzoquinone were purchased from Sigma-Aldrich. All other chemicals were of analytical grade and deionized water was used for preparation of the solutions. Glucose solution was allowed to mutarotate by preparing those 24hr before the experiments.

5.2.2 Apparatus

The conventional three-electrode system consisting of a Pt-wire counter electrode, Ag|AgCl reference electrode and the Gold nanopillar array as the working electrode was used for the Amperometric measurements. All electrochemical measurements and treatments were carried out in the 1480 MultiStat System. All potentials are reported versus the Ag|AgCl reference electrode unless indicated otherwise.

5.2.3 Nanopillar array preparation

Nanopillar array electrode (NAE) was fabricated by electrodepositing gold onto porous anodic alumina templates. The procedural details for the fabrication NAE can be

Chapter 4.2.1 .The height of the nanopillars in the NAE or the NAE roughness can be controlled by duration of electrodeposition.

All the working electrodes prepared were cleaned by performing cyclic voltammetry in 0.5M H_2SO_4. The cyclic voltammetry was performed between -500mV and 1500mV until the stable state was attained. Electrodes were then washed with deionized water. To quantify the difference in the height of the nanopillars in these NAEs, we defined a roughness ratio as the area under the reduction peak (calculated by integrating the voltammogram from 0.70 V to 1.1 V) of a NAEs electrode divided by that of the flat electrode.

5.2.4 Preparation of the enzyme electrode

The cleaned electrodes were modified with a thin layer of polypyrrole entrapped with glucose oxidase enzymes. All the polypyrrole/GODx films were prepared by galvanostatic polymerization of pyrrole in a 0.1M KCl containing 0.05M pyrrole and 0.5mg of glucose oxidase. The concentration of pyrrole and GODx has already been optimized in earlier paper [152]. So we used these concentration values for preparing the enzyme electrodes.

The electrochemical cell consisted of a single compartment three electrode system. Platinum gauze was used as the counter electrode and silver – silver chloride electrode was used as the reference electrode. The current density and time of deposition was varied to find the optimized deposit for maximum glucose sensitivity. To start with the initial values of current density and thickness were taken from earlier work on flat

electrodes [152]. Then they were varied according to the results to get the optimum values for the nanopillar electrodes.

5.2.5 Glucose Sensing

For optimization of polypyrrole/GODx electrode glucose sensing was done by evaluating the amperometric performances in a phosphate buffer solution (PBS) containing 3mM p-benzoquinone as a mediator. The polypyrrole/GODx electrode was maintained at a potential of 0.35V versus Ag/AgCl reference electrode until the background current stabilized. After the background current stabilized, calculated amount of glucose from a 1M glucose stock solution was added in the electrolyte to obtain a glucose concentration of 4mM in the electrolyte. For the amperometric measurement of glucose and other electroactive species the electrode was held at the same potential of 0.35V vs Ag/AgCl reference electrode and the steady state current was measured after the addition of glucose. The electrolyte was constantly stirred at a rate of 500rpm.

5.2.6 Kinetic analysis

After obtaining the optimized biosensor on nanopillar electrodes the typical sensing response was done to obtain the calibration curves. The addition of glucose was done increments of 2.5mM. Each addition was done after steady state current reached. All other parameters were same as the glucose sensing experiments for optimization of electrodes. The Lineweaver-Burk type-plot was used on the calibration data to find the K_m and I_{max} values.

5.2.7 Experiments and criteria for optimization of parameters

Our main intention was to obtain the highest glucose sensitivity by evaluating the various parameters like nanopillar height, current density of deposition and total current passed at different levels. So the main criterion for choosing the optimum level of each parameter was the value of the parameter which yielded the highest glucose current response in the amperometric evaluation.

We first did the optimization of the nanopillar height. With increase in nanopillar height the electrochemical surface area changes. Sensitivity of the glucose biosensor depends on the height of the nanopillars as the surface area changes. So it was first necessary to optimize the nanopillar height to obtain maximum performance. We controlled the height of nanopillars by varying the roughness factors. The roughness values were calculated as mentioned earlier.

To measure the effect of roughness factor only, we kept the current density and total current passed constant. The experiment was repeated for two set of current density ($100\mu A/cm^2$ & $191\mu A/cm^2$) to confirm that the observed phenomenon is consistent even when current densities changed. The total amount of current passed was fixed at $150mC/cm^2$ which meant that we controlled the time of deposition correspondingly. The thickness change with nanopillar height was considered to be negligible.

After the optimization of the nanopillar array height, the current density of deposition was varied and the glucose response was measured. Initially we chose the current densities to be of 100, 191, 382, and $573\mu A/cm^2$ similar to the current densities used in the optimization on flat gold electrodes. The total amount of current passed was still kept constant at $150mC/cm^2$. Experiments were further done using lower current densities till

$10\mu A/cm^2$ to optimize the current density for the nanopillars which was different from the flat electrodes. The time of electropolymerization for lower current densities below $50\mu A/cm^2$ was reduced by decreasing the total charge to $75mC/cm^2$. This was done as shorter time periods yielded more consistent results .The current densities were applied in accordance with the geometrical area of the electrode surface and not the calculated electrochemical area.

Finally the total charge of deposition was optimized. The optimized values of nanopillar height and current density of deposition obtained from the two earlier experiments were kept constant in these set of experiments. We varied the total current passed from $50mC/cm^2$ to $600mC/cm^2$ and measured the glucose sensitivity changes. The optimum values were obtained from the results of all these experiments.

In these set of experiments not only the glucose response was done but also the response of interference species ascorbic acid was done. This is because besides glucose sensitivity, a main criterion for glucose biosensors is selectivity. Ascorbic acid, Uric acid and acetaminophen are the common electroactive species coexisting in glucose samples. They tend to reduce the overall selectivity and accuracy of the sensor [157]. We chose ascorbic acid to test the selectivity as done in earlier studies [158]. So for the optimized electrode the current response for the interference species like ascorbic acid should also be the least. We did the ascorbic acid response only in the total current passed experiments because ascorbic acid response was mostly limited by the polypyrrole layer thickness.

5.3 Results and discussions

5.3.1 Effect of Nanorod height on the response of the enzyme electrode

Figure 5.1 shows the cyclic voltametric response of the gold nanopillar electrodes for various roughness factors used in the experiments. These CV curves were used for finding the roughness factors by comparing them with the surface area of flat electrode. Figure 5.1 also shows the changes in glucose sensitivity to that of nanopillar roughness values. The sensitivity increased with increase in nanopillar height and saturation values after a roughness factor of 57. This phenomenon was observed with both the current densities used in the experiments. The roughness factor of 15 and 60 corresponded to individual nanopillar height of 1 micron and 6 microns. The current saturation occurring at higher nanorod height can be attributed to diffusion of the glucose not reaching the bottom of the nanorods. The glucose concentration was found to reduce at the bottom space in between two nanorods in a previous work [159]. In the same work $K_4Fe(CN)_6$ with higher reaction rate was found to not reach the bottom and the surface area was not effectively used. Similarly at glucose reaction rates we assume that after a certain height they would also not effectively use all the nanorod surface area. So the saturation can be attributed to nanorods with larger heights not using the increase in surface area fully.

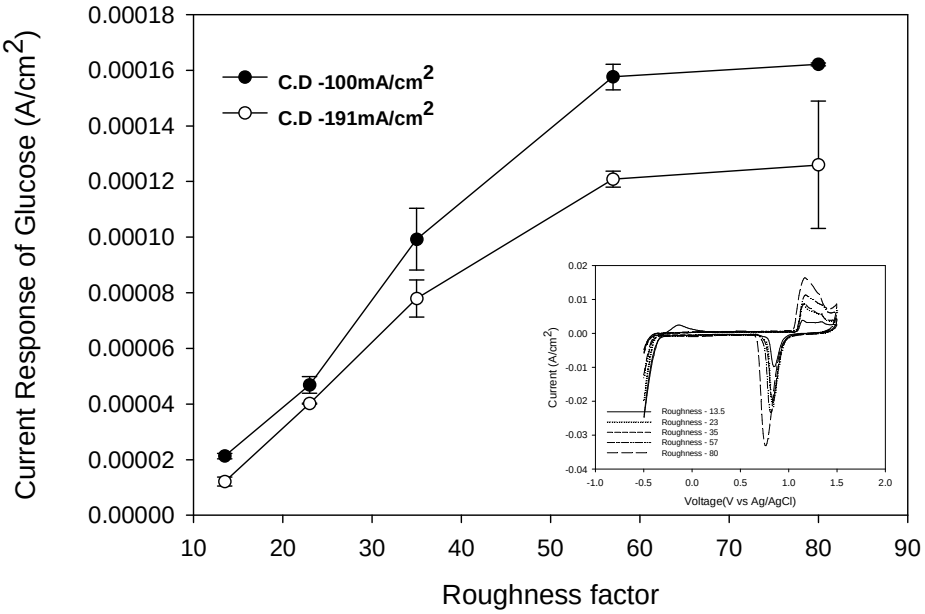

Figure 5.1: Effect of the roughness factor on glucose current response for applied current densities of 100μA/cm^2 and 191μA/cm^2

As the saturation of sensitivity occurred at higher roughness factors the optimized roughness factor was taken to be around 60 for electropolymerization of polypyrrole on gold nanopillar array electrode.

5.3.2 Effect of current density of deposition on the response of the enzyme electrode

The results of the glucose sensitivity variation with current density can be seen from figures 5.2A and 5.2B. The maximum glucose sensitivity is obtained at 50μA/cm^2. It is different from the optimum value obtained for flat gold electrodes.

In figure 5.2A the current densities are similar to the current densities used in the flat electrodes. But at high current density of 573μA/cm^2 yielded dark deposits and the SEM images showed the deposits were masking the nanopillars in many areas as seen in SEM image in Figure 5.3-D. So we did not apply current density higher than 382μA/cm^2. We

also reduced the current density up to 10μA/cm^2 to consider the current density variations in individual nanopillar which were different from that of flat electrodes. In these experiments we had the total charge as 75mC/cm^2 just to have lesser deposition time and more obtaining more consistent results. This was reasonable as even in this different total charge the optimum current density was again at the same value and exhibited similar trend. These results are shown in figure 5.2B. The optimum current density is 50μA/cm^2 as indicated by the maximum current response observed.

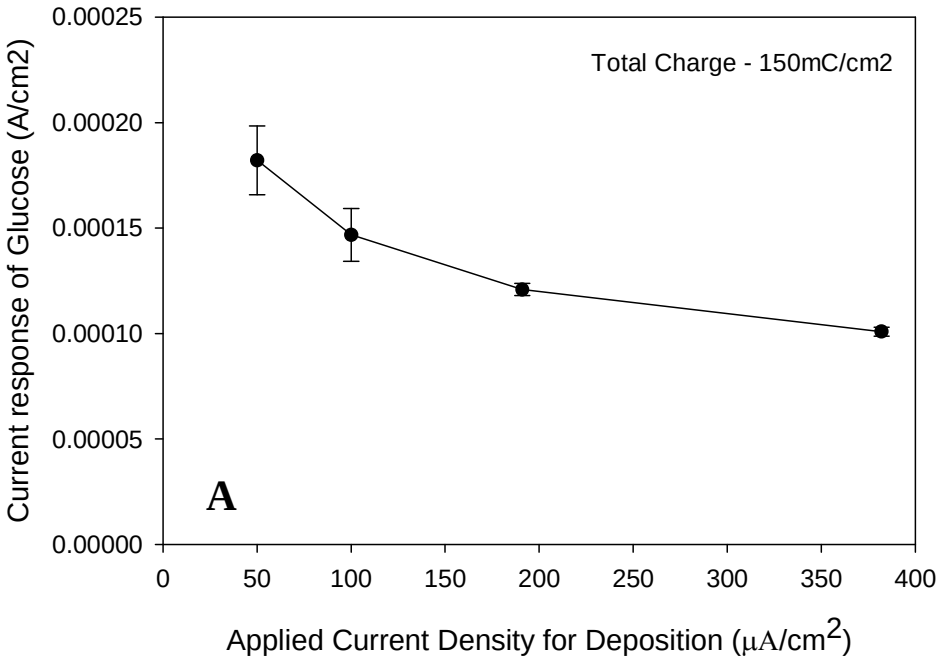

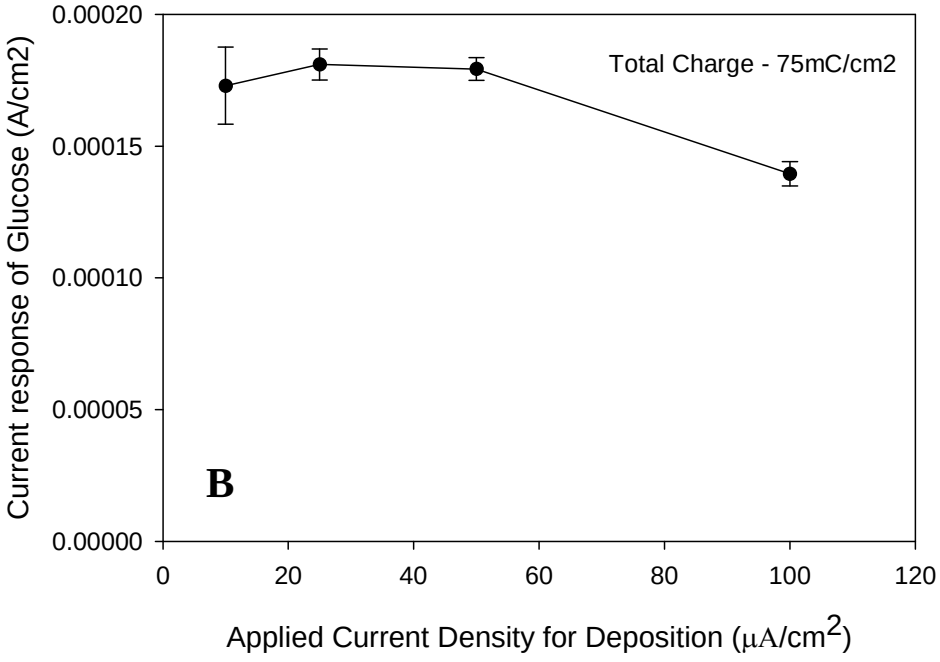

Figure 5.2: Effect of current densities on the glucose current response. (Figure 5.2 (A): Initially done with current densities similar to flat electrodes, Figure 5.2 (B): Current densities below 50μA/cm2 were tested to find the saturation current density)

The reason for the difference is because of the local thickness variations at the nanopillar electrodes as seen in the SEM images (Figures 5.3A-B) and the total increased surface area. The local thickness variation can be seen from the SEM Figure 5.3B. The thickness of deposit at the end of the electrode is visibly higher when deposited at higher current densities.

The thickness variation can be related to the current density variations locally on individual nanopillars. The current distribution on individual nanopillars can be compared to the current distribution in the high aspect ratio trenches where the bottom of the trenches has lesser current density than the top [160]. They also get filled up at the top openings and not the bottom when high current densities are applied. This is generally avoided in normal cathodic electrodeposition by using additives or applying pulsed current.

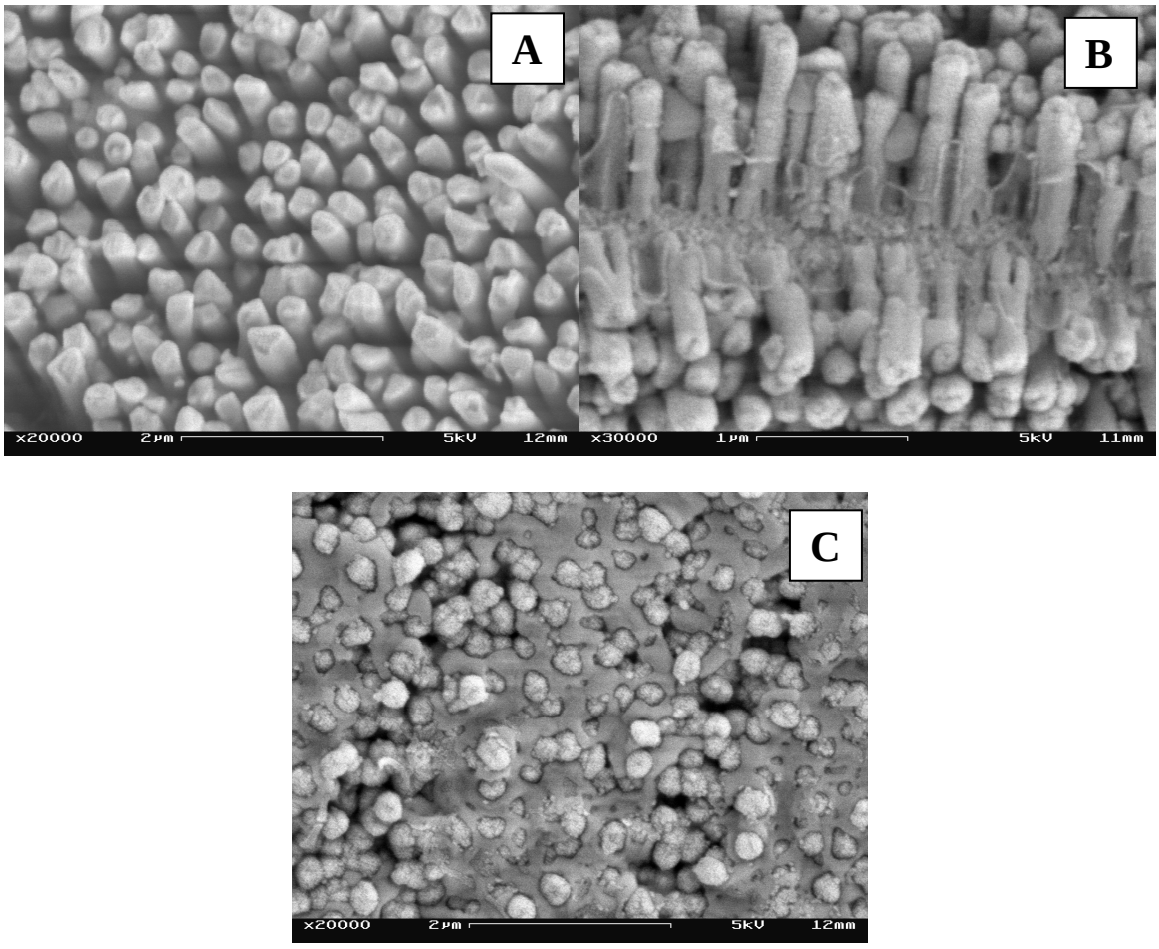

Figure 5.3: SEM images of nanopillars coated with polypyrrole/GODx (Figure 5.3 (A) Nanopillars coated with polypyrrole/GODx at applied current density of 50µA/cm^2 and total current of 150mC/cm^2, Figure 5.3 (B) Nanopillars coated with polypyrrole at applied current density of 100µA/cm^2 and total charge of 150mC/cm^2, Figure 5.3 (C) Nanopillars getting filled at the top with polypyrrole when the applied current density was 573µA/cm^2 and total charge)

5.3.3 Effect of total charge passed on the response of the enzyme electrode

The polypyrrole thickness is a major factor in glucose sensitivity as it acts as a diffusion barrier to glucose [157,161]. Generally increase in polypyrrole film thickness decreases the sensitivity of the glucose biosensor [152]. Theoretical studies show that when the film was thicker resulted in larger diffusion barrier for all the substrates and the current was mass transport controlled [162,163]. Thinner film were limited by the amount of enzyme and consequently due to enzyme reaction kinetics. Therefore optimum film thickness is critical in the performance of the polypyrrole based enzyme electrode.

As seen above the thickness of the deposit varies along the nanopillars locally. As uniform thickness is not possible on nanopillars we tried controlling the amount of deposit by passing calculated amount of current. The results are shown in figure 5.4. When the total charge passed was 150mC/cm^2 the glucose response values were maximum. From earlier work we know that the total charge of 75 mC/cm^2 corresponds to a film thickness of about 0.17µm on flat electrodes [164] . It was also found in flat electrodes that when the polypyrrole thickness is lesser than 0.1µm, the limitation of the response imposed by the diffusional constraint is minimized. As the best glucose sensing results were achieved at total charge of 150mC/cm^2, we can assume the thickness distribution was also at its optimal level. This can be seen in the results as the glucose sensitivity was lower when the total current was higher or lower than the optimum value. Going higher than the optimum total charge should be mass transport limited and going lower should be enzyme kinetically limited.

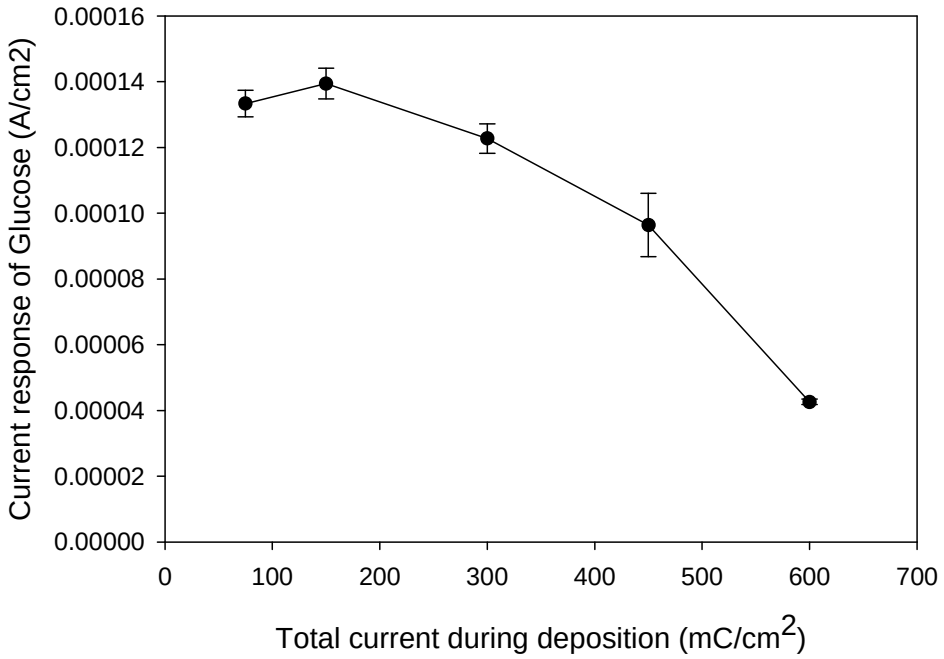

Figure 5.4: Effect of the total charge of deposition at a constant applied current density of 50µA/cm^2

Based on all the above results we concluded that the optimum conditions for preparing polypyrrole/GODx biosensor on nanopillar were nanopillar roughness factor of 60, applied current density of 50µA/cm^2, and 150mC/cm^2 of total current passed. These conditions were significantly different from the optimum conditions of flat gold electrodes. The reasons for the difference can be reasoned out as reduced thickness of polypyrrole along the nanopillars, caused by increased surface area of nanopillar array and variation in thickness of deposit locally on the nanopillars due to non-uniform current density distribution.

5.3.4 Effect of interference of ascorbic acid

Current response of ascorbic acid is shown in figure 5.5. The results showed that the interference values decreased little with increase in total current passed. The data also had

high variance that can be seen as larger error bars in the data. In the nanopillar based electrodes there is no significant fall in ascorbic acid interference contrasting to what is observed in flat electrodes with increasing thickness values. This can again be explained by the low polypyrrole thickness due to high surface area and the lower thickness of the polypyrrole on the trenches of the nanopillars. As there is not much variation in the ascorbic acid interference in the parametric study, we considered optimum values discussed earlier as ideal for preparation of nanopillar based polypyrrole glucose sensors. The noise due to ascorbic acid interference will be around 5% of the original glucose signal. Other techniques to eliminate interference like overoxidized polypyrrole can be used, but interference will exist in these nanopillar based electrodes due to thickness variation of polypyrrole.

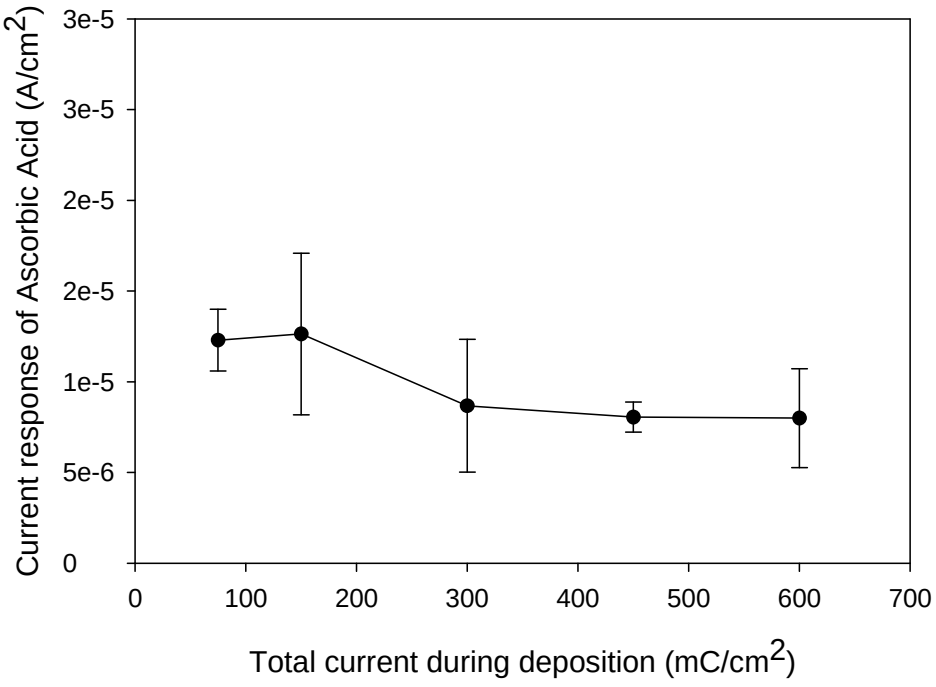

Figure 5.5: Effect of changes in total charge of deposition on Ascorbic acid Interference

5.3.5 Calibration of the optimized electrode for glucose sensing

The electrodes were prepared in the new optimized conditions and response curves were obtained for calibrating the electrode. The standard sensing response curve for successive addition of glucose with increments of 2.5mM is shown in Figure 5.6. They were further plotted for finding the K_m and I_{max} values. Figure 5.7A shows the good linear relationship between the glucose response current to the glucose concentration when plotted as a calibration plot between the glucose concentration ranges of 2.5mM to 15mM. The sensitivity obtained for glucose was 36μA/cm^2.mM. This is highest response for this system of glucose biosensor. The lower detection limit of electrode was 0.05mM which yielded a current response of 1.98μA/cm^2.

The Michelson Menton constant (K_m) and the maximum current response (I_{max}) was obtained by Lineweaver-Burk type-plot. The figure 5.7B shows the regression line corresponding to the equation:

$$\frac{1}{I_s} = \frac{1}{I_{\max}} + \left(\frac{K_m}{I_{\max}}\right)\left(\frac{1}{C}\right)$$

where I_s is the steady state current, I_{max} is the maximum current measured and C is the glucose concentration. The intercept in the graph corresponds to the $1/I_{max}$ values and Michelson Menton K_m constant can be obtained from the slope of the line. The obtained I_{max} value of 1.176 μA is high because of the large surface area which provides more enzyme substrate contact. K_m value was 46 is not similar to the K_m in the bulk soluble GOD. This indicates the diffusion and kinetic limitation are caused by the polypyrrole layer increasing the K_m value.

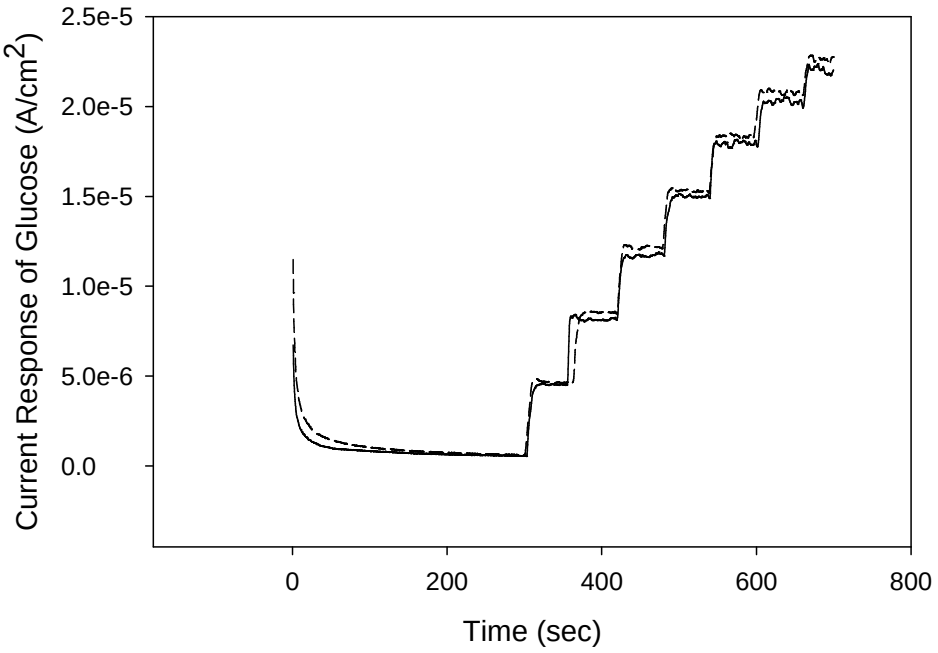

Figure 5.6: Standard current response curve with successive addition of glucose for electrodes prepared by electropolymerization on nanopillar electrodes with roughness factor of 60, at an applied current density of 50μA/cm^2 and total current of 150mC/cm^2.

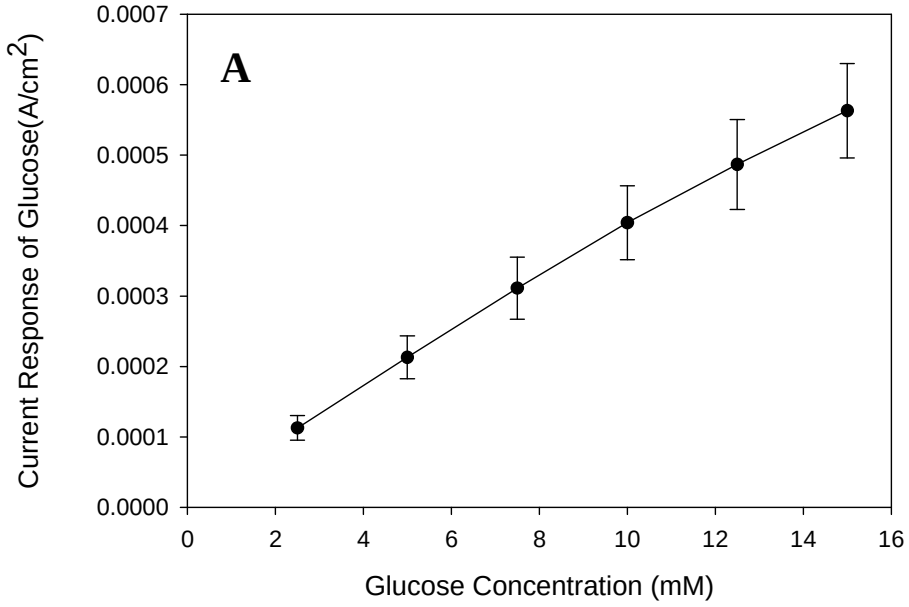

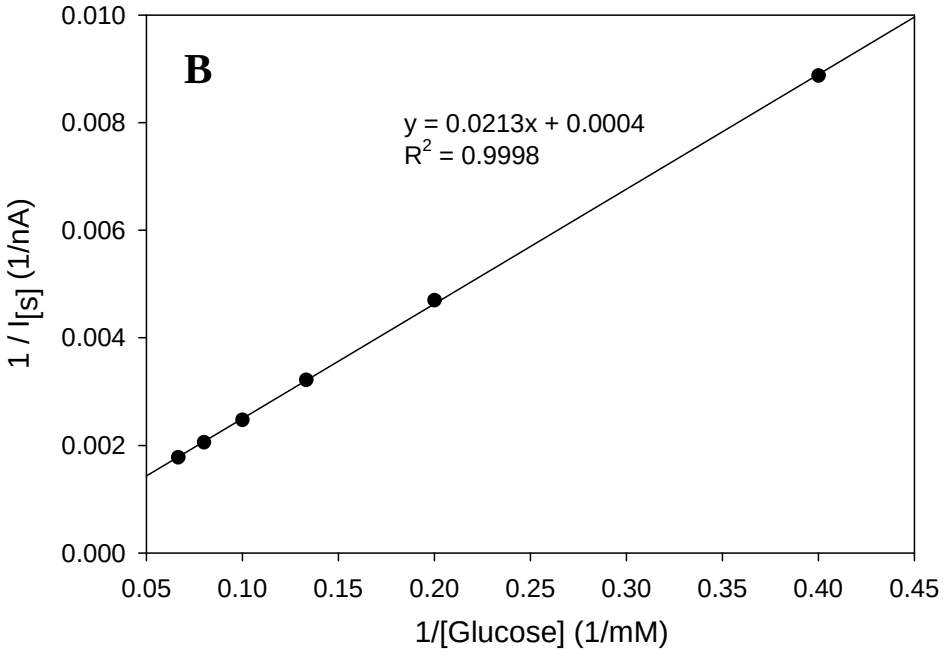

Figure 5.7: (A) Calibration plot of current response of electrode to glucose concentration (B) Lineweaver-Burk plot for determination of K_m and I_{max} values

5.4 Conclusion

The results showed that the optimum conditions for polypyrrole electro-polymerization for glucose sensing on nanopillar electrodes were different from that of flat electrode surfaces. The current density as low as $50\mu A/cm^2$ and total charge of $150mC/cm^2$ yielded the best sensitivity values for glucose detection. The variation in polypyrrole thickness over nanopillars was attributed to the changes in optimum values. We also observed a non- significant change in ascorbic acid interference values with changes in deposit properties. The optimized biosensor was analyzed for the response characteristics which yielded the K_m and I_{max} values. They were significantly better for this system of glucose biosensors. The results of this study can be extended to other electro-deposition techniques on nanopillar arrays in general. They will be significantly different from the deposition parameters on flat electrodes. The effect of interference cannot be reduced completely as done in flat electrodes until we try to get uniform polymer thickness on the nanopillars or use other techniques to eliminate interference.

(Results of this work has been published in [28,141])

CHAPTER 6

THE ROLE OF SAM CHAIN LENGTH IN ENHANCING THE SENSITIVITY OF NANOPILLAR MODIFIED ELECTRODES FOR GLUCOSE DETECTION

6.1. Introduction

Immobilization of enzymes onto electrode surfaces using self-assembled monolayers (SAM) of alkanethiols has been commonly used because SAM molecules offer easy formation of well-ordered and stable monolayers of molecules for anchoring various biosensitive molecules [165,166]. In an earlier work in our group [127], we functionalized 3D gold nanopillars with glucose oxidase (GOx) by using SAM molecules of 3-mercaptopropionic acid. These nanopillar modified electrodes exhibited a sensitivity measurement of 3.13 $\mu A \cdot mM^{-1} \cdot cm^{-2}$, which is much higher than that for a gold nanotube modified electrode (0.4 $\mu A \cdot mM^{-1} \cdot cm^{-2}$; [167]). This work was done in continuation of the previous work and to find out further how effectively SAM can be immobilized onto 3D nanopillar electrodes.

As we learned from the literature [168,169], on a flat-surface electrode SAM molecules of a longer chain length (e.g., 11-mercaptoundecanoic acid, or MUA) produced a more ordered assembly of molecules with a higher degree of surface coverage and less defects than those of a shorter chain length (e.g., 3-mercaptopropionic acid, or MPA). But MPA SAM on a flat electrode exhibited a lower electron transfer resistance than MUA SAM and gave rise to higher detection sensitivity than MUA SAM. Since the surface coverage of these SAM layers mainly depend on the surface morphology of the

electrodes [170], it is believed that the presence of the closely packed standing nanopillars in the 3D electrodes may alter the formation of the alkanethiol SAMs at the surface. This belief led us to pose a new question: which type of alkanethiol SAM, a short chain or a long chain, will help facilitate a better sensing performance for nanopillar modified electrodes.

In search of an answer to this question, two alkanethiol SAMs (i.e., the MPA and MUA) were used in this study as the anchoring molecules for the functionalization of nanopillar modified electrodes. After the SAM treatment, the electrodes were functionalized with glucose oxidase (GOx) through covalent bonds between the GOx and the respective SAMs. After that, the electrochemical property of the formed interface was characterized for assessing the quality of the SAM coverage on these electrodes by the cyclic voltammetry (CV) and electrochemical impedance spectroscopy (EIS) techniques. Finally, the sensing performance of these SAM treated and GOx functionalized nanopillar modified electrodes was evaluated for glucose detection.

6. 2. Experimental methods

6.2.1. Reagents and Materials

3-mercaptopropionic acid (MPA: HS-$(CH_2)_2$-COOH), 11-mercaptoundecanoic acid (MUA: HS-$(CH_2)_{10}$-COOH), glucose oxidase (GOx; EC 1.1.3.4 from Aspergillus Niger, 100 units/mg), *N*-hydroxysuccinimide (NHS), 2-(N-morpholino)ethanesulfonic acid (MES) and 1-ethyl-3-(3-dimethylaminopropyl) carbodiimide (EDC) were purchased from Sigma (St. Louis, MO). Porous anodic alumina templates were purchased from Whatman Inc. (Maidstone, England). Ethanol (200 Proof-absolute, anhydrous) was

purchased from Pharmco Inc. (Brookfield, CT). Other reagents of analytical grade were used without further purification and all solutions were prepared with de-ionized (DI) water.

6.2.2 Preparation of Gold Nanopillar Modified Electrodes

Gold nanopillar modified electrodes were fabricated using the commercial template method described in Chapter 4.2.1. Prior to SAM formation, the surfaces of these 3D electrodes were cleaned electrochemically by performing CV within a potential range from -0.5 to 1.5 V at a scan rate of 100 mV/s in 0.3M H_2SO_4 solution. The cleaning cycles continued until a reproducible voltammogram was obtained. After that, the electrodes were rinsed with ethanol and DI water and finally dried with nitrogen blow.

6.2.3 SAM Formation and Characterization

For SAM formation, 3D electrodes were placed in ethanol solution containing 10 mM of either the MPA or MUA molecules for 24 hours followed by washing in ethanol solution. SAM formation on these electrodes was characterized by the CV and EIS techniques at 25°C using the three-electrode cell. The CV measurements were performed by scanning the potential from -0.2 V to 0.6 V at a scan rate of 100 mV/s and the EIS measurements were performed in a frequency range from 0.1 Hz to 100 KHz with an AC signal of 10mV amplitude over the formal potential of the redox couple in 0.1 M phosphate buffered solution (PBS, pH7) containing 2 mM $Fe(CN)_6^{3-/4-}$ (ferri:ferro=1:1) mixture as the redox probe. These electrochemical experiments were performed using a potentiostat (Solartron 1480, Houston, TX) and an impedance analyzer (Solartron 1260, Houston, TX). Prior to each test run, the electrolytic solution was bubbled with nitrogen

for about 20 minutes to get rid of any dissolved oxygen, and during the test the electrolyte was blanketed with nitrogen. The obtained impedance spectra were analyzed through statistical curve-fit with an equivalent Randles circuit using ZVIEW (Scribner Associates Inc, Southern Pines, NC).

For assessing the percentage of defects in the SAM molecules, the voltammetric reduction peak associated with the uncovered area (i.e., the exposed gold oxide) of the SAM treated 3D electrode surface was evaluated. The ratio of the uncovered area of a SAM treated 3D electrode to that of a bare 3D electrode was calculated and the percentage of defects in the SAM structure determined. For these evaluations, CV measurements were obtained in 0.1 M H_2SO_4 by scanning the potential from -0.5 V to 1.5 V at a scan rate of 100 mV/s.

For quantifying the surface coverage (Γ) of the SAM molecules, the method reported in the literature [168,170,171] was used to evaluate the voltammetric reduction peak associated with SAM desorption. To do that, CV measurements were made in 0.1 M NaOH within a voltage range from -1.6 V to -0.2 V at a scan rate of 100 mV/s. From the reduction peak, the amount of charge was determined by first integrating the reduction current under the peak over time and then offsetting the value by that of a bare 3D electrode. With the formula $\Gamma=Q/nFA$ [14], in which Q is the amount of charge, n (=1) is the number of electrons involved in the reaction, F (=96485 C/mol) is the Faraday constant and A (=0.04 cm^2) is the electroactive surface area, the surface coverage of SAM molecules was determined.

6.2.4. Immobilization of Glucose Oxidase

After the SAM treatment, the surfaces of these nanopillar modified electrodes were functionalized with glucose oxidase (GOx). To do that, the carboxyl group in the formed SAMs was activated in a freshly prepared solution of 0.1 M MES acid containing 75 mM EDC and 15 mM NHS buffered at pH 4.5 for 2 hours. After washing in 0.1M PBS the electrodes were placed in 0.1 M PBS containing 1 mg/mL of the GOx with constant stirring for 2 hours. The obtained GOx functionalized electrodes were washed thoroughly with 0.1M PBS and stored at 4^{o}C in 0.1M PBS solution at pH 7.0 prior to testing.

6.2.5 Glucose Detection

For evaluating the sensing performance of these SAM treated and GOx-functionalized nanopillar modified electrodes, the amperometric currents of these 3D electrodes in response to glucose at various concentrations were measured. For the electrode reactions, when the GOx functionalized electrodes are placed in a solution containing glucose, glucose will first react with GOx to form gluconic acid and reduced-GOx. The reduced-GOx will then be converted back to its original form by reacting with p-benzoquinone, a mediator having better solubility than most other popular mediators [172]. In this reaction, the mediator gets reduced and then converted back to its original state at the electrode surface by giving away electrons. A cascade of reactions is shown schematically in the inset in figure 6.1. Amperometric measurements were made in 0.1M PBS (20 ml) containing 3mM p-benzoquinone by adding various amounts of 1M glucose using the three-electrode electrochemical cell. For all tests, a constant potential of 0.35 V was applied to the electrodes and the solution was stirred continuously for ensuring an

instant equilibrium for mass transport. During each test run, the background current was allowed to stabilize before a drop (50 µL) of 1M glucose was added to the solution, and after the amperometric current response reached a steady-state, another drop of glucose was added and the corresponding current response was measured until a new steady state was reached. In this manner, each incremental drop of glucose to the solution caused an equivalent increase in glucose concentration of 2.5 mM approximately.

6. 3 Results and discussions

6.3.1 Characterization of the Nanopillar Modified Electrodes

The roughness factor for the 3D electrodes tested in this study is approximately 45.

6.3.2. Characterization of SAM Formation

The CV curves in ferro-ferri (Figure 6.1A) that that there are more MUA molecules than MPA molecules blocking the pathways for electron transfer across the electrode-electrolyte interface for facilitating redox reactions, owing possibly to the longer chain length of the MUA molecules forming more lateral molecular bonds.

Figure 6.1B shows the impedance spectra (Nyquist plots) for SAM coated 3D electrodes. The MUA treated electrode exhibits a larger semicircle than the MPA treated electrode, suggesting a high degree of SAM coverage for the MUA than for the MPA molecules. To put this in a quantitative sense, a Randles equivalent circuit (see the upper inset in Fig.2B) consisting of a solution resistance (R_s), an electron-transfer resistance (R_{et}) and a constant phase element (CPE) capacitor was used to fit the obtained semicircular Nyquist plots to resolve the values for R_{et}. As listed in table 1, the R_{et} value obtained for the MUA treated electrode is much higher (about 27 times) than that for the

MPA treated electrode, thus confirming that the MUA molecules indeed post a higher electron transfer resistance at the electrode surface than the MPA molecules.

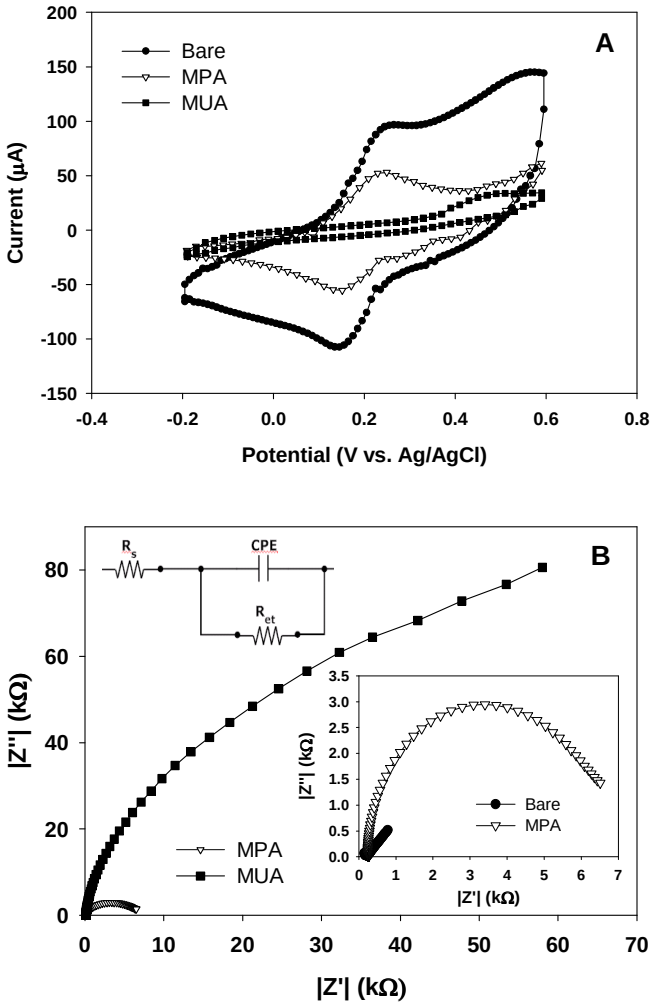

Figure. 6.1: (A) CV curves obtained for a bare, a MPA and a MUA treated electrodes evaluated with $Fe(CN)_6^{3-/4-}$ as the redox couple (B) The corresponding Nyquist plots from the impedance measurements for the same electrodes with a close-up view of the low impedance range given in the lower inset, A Randles equivalent circuit consisting of a solution resistance (Rs), an electron-transfer resistance (Ret) and a constant phase element (CPE) capacitor is given in the upper inset

Electrodes	R_{et} (ohm)		SAM	Γ (10^{-8} mol·cm^{-2})	% defect
Bare	589.5 (5.0%)		MPA	1.38±0.1	87.3
MPA	6281.0 (1.7%)		MUA	2.37±0.3	37.8
MUA	169290.0 (4.3%)				

Table 6.1: Left: the resolved R_s and R_{et} values based on the Randles circuit (fitting errors given in parenthesis), Right: the obtained values for the surface coverage and percentage of defects

The CV curves obtained from the gold-oxide reduction experiments performed in H_2SO_4 are shown in figure 6.2A. All these CV curves exhibit an Au-oxide reduction peak at around 0.78 V, indicating that all these 3D electrodes possess a certain amount of defects, or the exposed gold oxide, on the SAM treated electrode surfaces. By the ratio of the area under the reduction peak (by integrating the CV curve under the peak) of the SAM treated 3D electrode to that of the bare 3D electrode, a measure of the percentage of defects in these SAMs was obtained (see table 1): the percentage of defects is approximately 87.3% and 37.8% for the MPA and MUA SAMs, respectively. These values are high when compared with flat electrodes: 52% for the MPA and 0% for the MUA SAMs [169].

Figure 6.3B shows the CV curves obtained for evaluating the voltammetric reduction peak associated with desorption of the MPA and MUA SAM molecules. From the CV

curves, two peak currents are visible for both the MPA and MUA treated 3D electrodes. We believe that the peak current at around -0.82 V for MPA and around -1.03 V for MUA is due to the cleavage of the gold-sulfur bond. Based on these desorption peak currents, the desorption charge was determined by integrating the reduction peak from -0.8 V to -0.9 V for the MPA treated electrode and from -1.0 V to -1.2 V for the MUA treated electrode. The values for Γ were then calculated for the MUA and MPA treated electrodes as listed in table 1. Comparing with the reported values for the surface coverage of MPA (5.12×10^{-10} mol/cm^2) and MUA (8.30×10^{-10} mol/cm^2) SAMs on flat surfaces [169], the values for nanopillar modified electrodes are roughly 27 and 28 times higher respectively. This increase can be attributed to the increase in the electroactive surface area in the 3D electrodes. This increase, however, does not correspond to the actual increase in the surface area of 45 times. This phenomenon may be attributed to the high percentage of defects in the SAM structures on the nanopillar modified electrodes as well as the presence of rough surfaces at the top end of the nanopillars as seen in the SEM image. A similar observation for electrodes of rough surfaces was made by others where they attributed it to the presence of a large number of edges in the rough surfaces leading to more defects in the SAM structures [173,174].

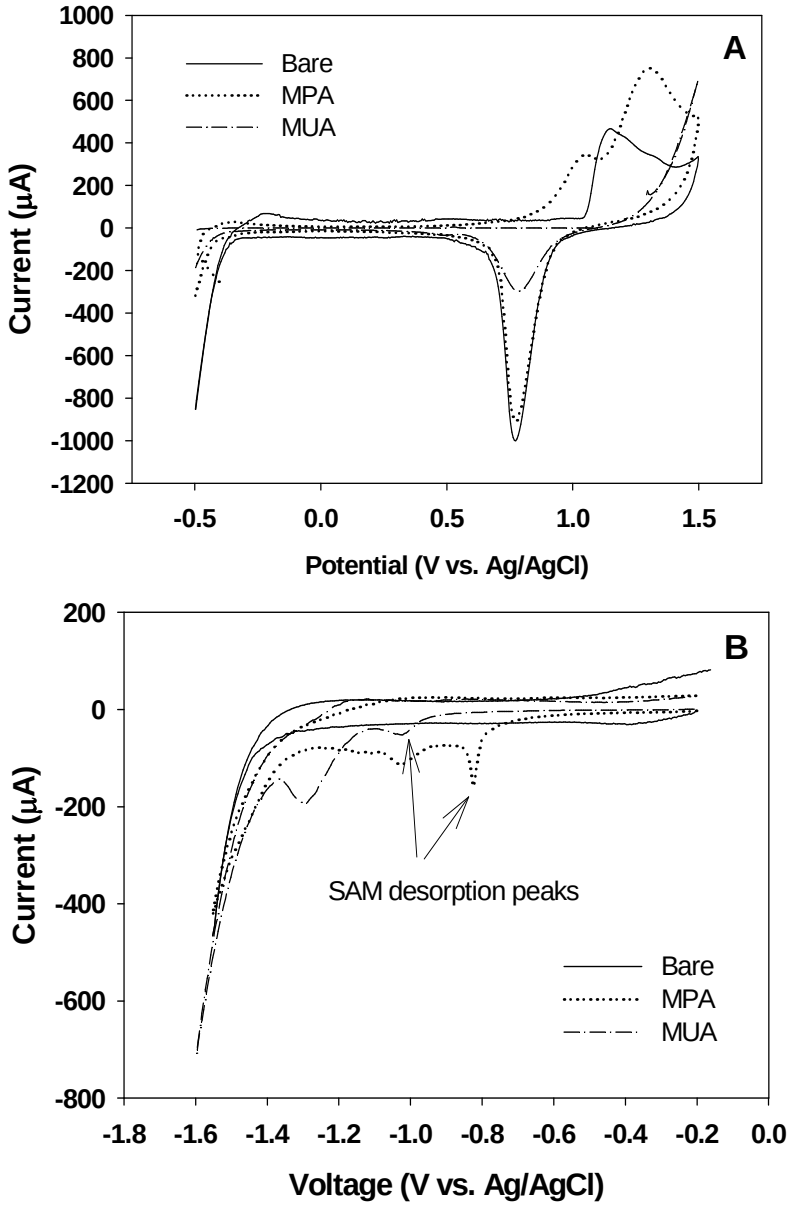

Figure 6.2: (A) CV curves obtained for the bare and MPA and MUA treated 3D electrodes in quantifying the percentage of defects in SAM molecules in electrolyte containing 0.1 M H_2SO_4 (B) CV curves obtained for the bare and MPA and MUA treated 3D electrodes in evaluating SAM desorption in electrolyte containing 0.1M NaOH

6.3.3. Amperometric Responses

Figure 6.3 shows the strip-chart measurements for the amperometric current responses of the SAM treated and GOx functionalized 3D electrodes taken as drops of glucose were added. In general, the current level for the MPA treated electrodes is much higher than the MUA treated electrodes. The detection sensitivity is found to be 2.68 $\mu A \cdot mM^{-1} \cdot cm^{-2}$ and 0.09 $\mu A \cdot mM^{-1} \cdot cm^{-2}$ for the MPA and the MUA treated 3D electrodes, respectively. The sensitivity value for the MPA treated 3D electrode (2.68 $\mu A \cdot mM^{-1} \cdot cm^{-2}$) is slightly lower than the one obtained in our earlier work (3.13 $\mu A \cdot mM^{-1} \cdot cm^{-2}$; [127]), which is as expected because the electrodes tested here had a roughness factor of 45 whereas the electrodes tested earlier had a roughness factor of 60.

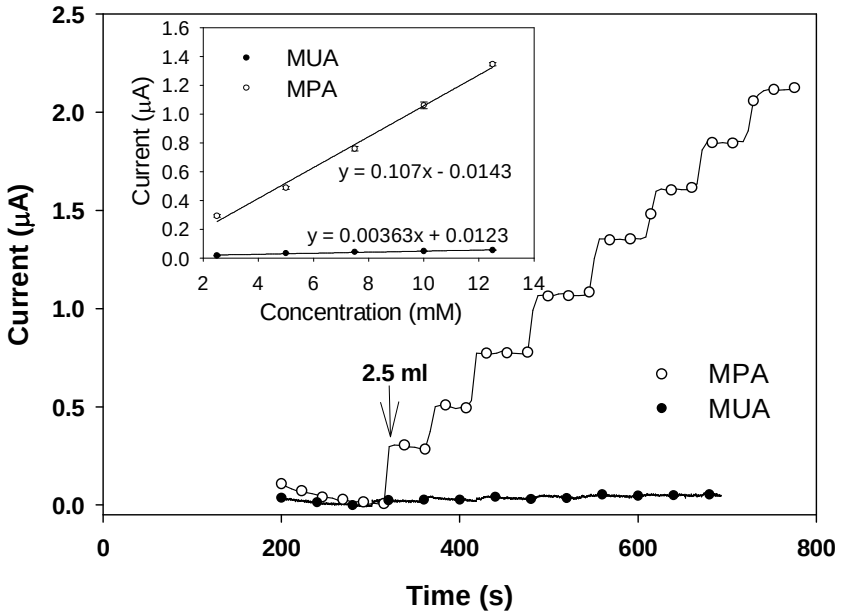

Figure 6.4: Amperometric current measurements obtained for the MPA and MUA treated 3D electrodes in response to glucose at various concentrations, the inset shows the two linear calibration curves

The results presented above indicate that the two alkanethiol SAMs (i.e., MPA and MUA) have led to a similar trend in terms of SAM surface coverage, defects, electron transfer resistance and glucose detection sensitivity for both the nanopillar modified electrodes and flat electrodes, albeit the exact values are different. To put the sensitivity values of the 3D electrodes in perspective with reference to those of flat electrodes for glucose detection, the same glucose detection studies were performed using a flat gold disc electrode with a circular area of 0.02 cm^2 (Bioanalytical Systems, West Lafayette, IN). Prior to and in between test runs, the disc electrode was polished first with a 1 μm diamond polishing sheet and then with a 50 nm alumina polishing sheet and rinsed in DI water. For the MPA and MUA treated flat electrodes, the sensitivity values were found to be 0.47 $\mu A \cdot mM^{1} \cdot cm^{-2}$ and 0.052 $\mu A \cdot mM^{1} \cdot cm^{-2}$, respectively. For the MPA treated electrodes, the presence of the nanopillars caused a 6-fold increase in detection sensitivity. Although a 6-fold increase is high, it is not higher enough with respect to the 45-fold increase in the surface area of these 3D electrodes. This disparity is certainly related to the increased amount of blockage for electron transfer from the SAM molecules covering the 3D electrode surface, but it may also suggest that the amount of GOx functionalized onto the 3D electrodes is not proportional to the available SAM surface as in the case with flat electrodes.

6.4 Conclusion

From this study we observed the same general trend in terms of SAM surface coverage, defects, electron transfer resistance, and glucose detection sensitivity when using MPA and MUA as the anchoring SAMs for the functionalization of nanopillar

modified electrodes and flat electrodes. For nanopillar modified electrodes tested here, the longer MUA produced a higher electron transfer resistance and a lower percentage of defects than the shorter MPA, but the shorter MPA led to higher sensitivity in glucose detection than the longer MUA.

(Result of this work has been published in [175])

CHAPTER 7

ON FUNCTIONALIZATION OF 3D ELECTRODES WITH DIFFERENT NANOPILLAR SIZES (WITH POLYPYRROLE AND SAM IMMOBILIZATION TECHNIQUES)

7.1 Introduction

The previous two chapters dealt with polypyrrole and SAM methods separately. In this chapter we will see discuss the influence of 3D nanostructure dimensions on both the SAM and polypyrrole immobilization methods. In this work we ask two questions: 1) How does the size of nanostructures affect enzyme immobilization? 2) How do different immobilization procedures in the presence of different nanostructures affect the underlying electron transfer and mass transport characteristics?

To answer these questions, we developed 3D nanostructures the two different nanopillar sizes (200 nm and 50 nm) as electrodes using the method described in Chapter 4.2.1 and Chapter 4.2.2, functionalized them with enzymes, and examined their glucose detection sensitivity. Again in this study (similar to the study discussed in last chapter), SAMs of two different chain lengths were used in the first functionalization method because the chain length is known to affect the sensing performance [175]. The polypyrrole electropolymerization method had been already optimized in the study discussed in Chapter 5. So we used the same optimized parameter in this study. But for the smaller 50nm diameter nanopillars optimization studies were conducted to achieve the best glucose sensing performance. Electron transfer and mass transport behavior of

the functionalized electrodes were characterized in various electrochemical experiments including the cyclic voltammetry, stripping voltammetry, impedance spectroscopy, and amperometric glucose detection.

7.2 Experimental methods

7.2.1 Integrated 3D Skyscraper Micro/Nano Structures

The 50 nm nanopillars were formed on glass substrates using the thin film alumina templates previously described in Chapter 4.2.2. 200nm gold nanopillar modified electrodes were fabricated using the template method previously described in Chapter 4.2.1. The roughness factor for both the 50 nm and 200 nm nanopillar structures was found to be approximately 18. In the following discussions we will refer to the 50 nm and 200 nm nanopillar structures as 50 nm electrodes and 200 nm electrodes, respectively.

7.2.2 Functionalization of Nanostructures

7.2.2.1 SAM/GOx Functionalized Surfaces

The SAM functionalization was similar to the details given in Chapter 6.2.3.

7.2.2.2 PPy/GOx Functionalized Surfaces

For the 200 nm electrodes, the optimized condition was at a current density of 50 $\mu A/cm^2$ and a total charge of 150 mC/cm^2, as determined in Chapter 5. For the 50 nm electrodes, an optimized condition was found by examining the outcomes of polypyrrole films of different thicknesses achieved when electrodeposition was carried out in various times (10, 20 and 35 minutes).

7.2.3 Characterization of Surface Treated 3D Electrodes

Cyclic voltammetry (CV) analysis and electrochemical impedance spectroscopy (EIS) were first performed for the SAM treated 3D electrodes as mentioned in Chapter 6.2.3. The analaysis procedure impedance values were also done according to the method mentioned in Chapter 6.2.3. For assessing the percent defect in the immobilized SAM molecules, the voltammetric reduction peak due to the exposed gold oxide on the SAM coated electrode surfaces was evaluated according to the procedure mentioned in Chapter 6.2.3. For quantifying the surface coverage (Γ) of the SAM molecules, stripping voltammetry [176] was used to evaluate the voltammetric reduction peak associated with SAM desorption. The procedure is again mention in Chapter 6.2.3.

7.2.4 Biosensing Applications

Details of this procedure are given in Chapter 6.2.4 and 6.2.5.

7.3 Results and discussions

7.3.1 3D electrodes with integrated micro/nano structures and their functionalization

For the 3D structures, we used those with standing nanopillars of two different diameters, 50 nm (shown in Fig.7.1A) and 200 nm (shown in Fig.7.1B). The height of the nanopillars was controlled such that a roughness factor (defined as the ratio of the overall surface of the 3D structure area to its projection, or ‘real estate’ area) of approximately 18 was achieved. The reason for selecting this roughness factor is that any values higher than this would result in severe bunching of the 50 nm diameter nanopillars. Because of this, we also controlled the roughness factor to about 18 for the 200 nm diameter nanopillar structures.

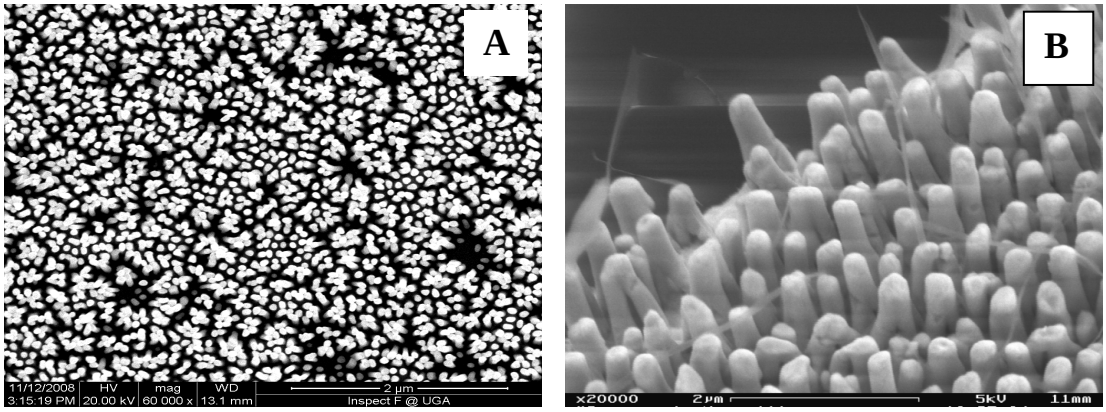

Figure 7. 1: (A) SEM image of the 50 nm 3D skyscraper nanopillar structures (B) SEM image of the 200 nm 3D skyscraper nanopillar structures

In Fig.7.2A cyclic voltammogram (CV) curves obtained for the bare and MPA or MUA treated 50 nm nanopillar structures evaluated in the presence of the redox couple $[Fe(CN)_6]^{4-}/[Fe(CN)_6]^{3-}$ are shown. In comparison between the bare and SAM treated structures, the bare one exhibits much higher redox peak currents. Between the two SAM treated structures, the MUA treated one exhibits lower redox peak currents than the MPA treated one, suggesting a higher degree of blockage for electron transfer resulting from the MUA molecules than from the MPA molecules. For both the bare and the MPA treated 3D structures the CV curves show a reversible redox event occurring at the surface with the electron transfer limited by diffusion in mass transport [127]. In contrast, the CV curves for the MUA treated structure exhibits highly irreversible redox behavior, confirming a high degree of blockage at the surface for electron transfer. These results indicate that both the MUA and MPA molecules form SAM structures covering the surface of the 3D nanopillar structures and that there are more MUA molecules than MPA molecules blocking the pathways for electron transfer across the electrode-

electrolyte interface, owing possibly to the longer chain length of the MUA molecules forming more lateral molecular bonds. Similar behavior is observed for the MPA or MUA treated 200 nm nanopillar structures as seen from results in Fig 7.2B. Fig.7.2C shows the CV results for polypyrrole treated 50 nm electrodes at various times. A large shift in the redox peaks was seen in all three cases. These peaks shifted progressively with increasing polypyrrole thickness, suggesting an increase in diffusional resistance with the increase of coating thickness.

The inset in Fig.7.2A and 7.2B shows the results for quantifying percent defects from voltammetric reduction peaks in 0.1M H_2SO_4 at around 0.78 V. The percent defect was around 97.5% and 31.7% for the 50 nm electrodes treated with MPA and MUA, respectively. In the case MUA, the percent defect for the 50 nm electrodes was lower than that for the 200 nm electrodes (37.8%), implying that MUA forms a better coating with less defect when the diameter of nanopillars was smaller. In the case of MPA, however, the percent defect for the 50 nm electrodes was higher than that for the 200 nm electrodes (87.3%). But this cannot be directly correlated as larger defects with MPA SAM, since the oxidative/reductive peaks observed in MPA modified gold electrodes can be enhanced by the oxidation of monolayer itself [177]. But this higher oxidative current which is assumed to be originating from the oxidation of the thiol hydrogen [178] is not seen in the MUA SAM. Due to these uncertainties in the origin to the oxidation/reduction currents the results from impedance method were considered more reliable for MPA and MUA SAM than the CV analysis.

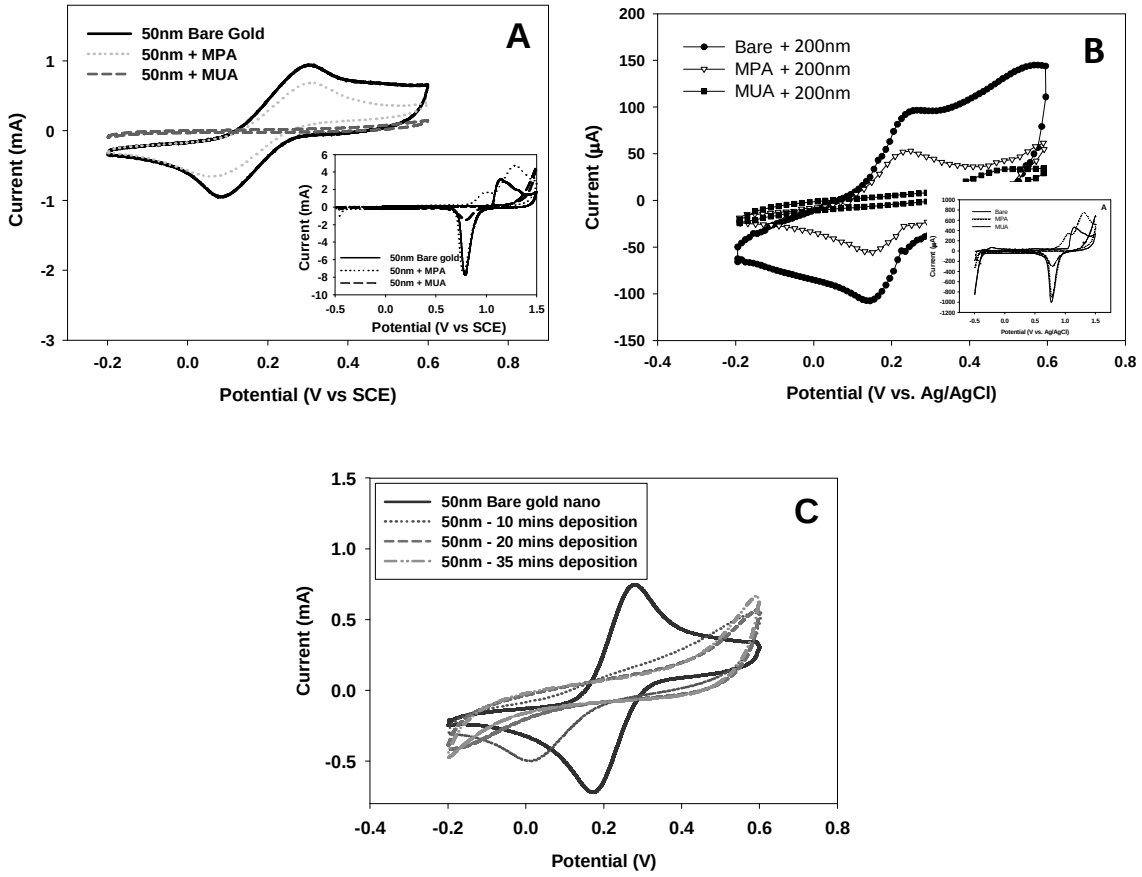

Figure 7.2: (A) Cyclic voltammogram (CV) curves obtained for 50 nm bare and MPA or MUA treated nanostructures evaluated with $Fe(CN)_6^{3-/4-}$ as the redox couple (Inset) CV curves obtained for the bare and MPA and MUA treated 50 nm 3D structures in quantifying the percent defect in SAM molecules in electrolyte containing 0.1 M H_2SO_4 (B) CV curves obtained for 200 nm bare and MPA or MUA treated nanostructures (Inset) CV curves obtained for the bare and MPA and MUA treated 200 nm 3D structures in 0.1 M H_2SO_4 (C) CV curves of bare gold, and polypyrrole deposited structures (different deposition times) evaluated in $Fe(CN)_6^{3-/4-}$

Fig.7.3A shows the corresponding impedance spectra (Nyquist plots) for the 50 nm structures. The two SAM treated structures show semicircular Nyquist plots whereas the bare one exhibits a straight line plot (see inset). Since a semicircular feature is indicative of blockage for electron transfer across the electrode/electrolyte interface, this result confirms the formation of SAM molecules at the surfaces. Moreover, the MUA treated structure exhibits a larger semicircle than the MPA treated one, suggesting a high degree of SAM coverage for the MUA than for the MPA molecules. Fig.7.3C shows the Nyquist plots obtained for the polypyrrole coated 200 nm electrodes with different film thicknesses. The curves exhibit a larger semicircle than MPA but not MUA. But the semicircle is not completely present and tends to flatted out in the lower frequency ranges indicating a significant effect from the diffusional impedance caused by the polypyrrole layer. The samples with polypyrrole coatings at different deposition times also showed an increasing trend in the semicircle radius. To put this in a quantitative sense, a Randles equivalent circuit (see the inset in Fig.7.3B) consisting of a solution resistance (Rs), an electron-transfer resistance (Ret), a constant phase element (CPE) capacitor and a Warburg diffusional impedance element was used to fit the obtained semicircular Nyquist data. CPE was used instead of the capacitor element to factor in the high roughness of the nanopillars.

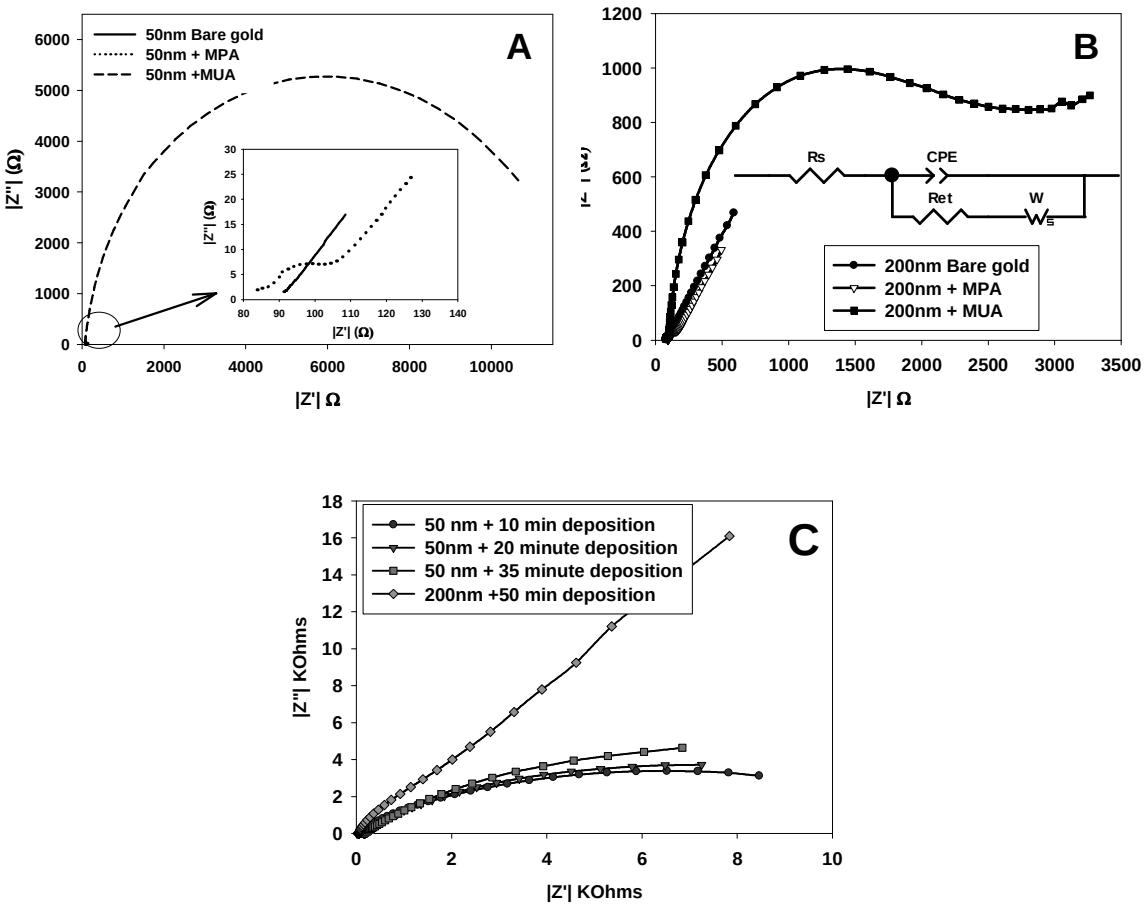

Figure 7.3: (A) The Nyquist plots from the impedance measurements for the bare, MPA and MUA immobilized electrodes on 50 nm with a close-up view of the low impedance range given in the lower inset (B) Nyquist plots from the impedance measurements for the bare, MPA and MUA immobilized electrodes on 200 nm electrodes Equivalent circuit elements used is shown in the inset: Solution resistance (R_s), Electron-transfer resistance (R_{et}) and Constant Phase Element (CPE), Warburg diffusional impedance (W) (C) Nyquist plots from the impedance measurements for polypyrrole electrodeposited at different time duration on the 50 nm electrodes and fully deposited 200 nm electrode

Table 1 lists the values for the electron-transfer resistance (R_{et}) and the Warburg diffusional impedance (W) obtained. The ratio of the values (after / before deposition) is used for comparison purpose to avoid sample to sample variation. Of the two SAM cases for the 50 nm and 200 nm electrodes, the MUA case exhibits a high electron transfer resistance arising from a higher degree of coverage. For the polypyrrole cases of the 50 nm electrodes deposited for 10 and 20 minutes, the changing ratio in R_{et} is similar to that of all the MPA cases. But the W values in all the polypyrrole cases are much higher. The changing ratios for R_{et} and W are approximately 20 and 25 respectively when the polypyrrole deposition is carried out for 35 minute. Results between the 50 nm and 200 nm electrodes show that the 50 nm electrodes had an increased ratio of change of R_{et} and W is case of MUA SAM when compared to the 200 nm electrodes. This higher degree of coverage can be because of the increased MUA SAM adsorption onto the smaller diameter electrodes. But in case of MPA SAM R_{et} and W change is not statistically different between the 50 nm and 200 nm electrodes, even when 50 nm electrodes has slightly higher average values than 200 nm electrodes .

50 nm electrodes		Before deposition (Ω)	After deposition (Ω)	Average change of Ratio
MPA	R_{et}	15 ± 4.8	26.96 ± 3.5	1.79
	W	105 ± 15	335.6 ± 100	3.19
MUA	R_{et}	17.82 ± 7	11635±2000	652.92
	W	214.6 ± 65	negligible	~
Polypyrrole				
Deposited in 10 min	R_{et}	42 ± 11	155 ± 15	3.69
	W	60720 ± 1000	93210 ± 5200	1.54
Deposited in 20 min	R_{et}	15 ± 2.8	65.5 ± 45	4.37
	W	369 ± 42	11900 ± 300	32.25
Deposited in 35 min	R_{et}	18.29 ± 1	349.9 ± 200	18.68
	W	297 ± 17	16969 ± 300	57.13
200 nm electrodes				
MPA	R_{et}	30 ± 2	59 ± 6	1.69
	W	647 ± 100	925 ± 300	1.43
MUA	R_{et}	62 ± 4	2366 ± 300	38.1
	W	2135 ± 400	1622 ± 1200	0.75
Polypyrrole 50 minutes	R_{et}	372 ± 20	9200 ± 1000	24.73
	W	315 ± 30	54500 ± 5000	173

Table 7.1: R_{et} and W values based on the respective equivalent circuits for MPA, MUA and polypyrrole (different deposition times) treated electrodes

Fig.4 shows the CV curves obtained for evaluating the voltammetric reduction peak associated with desorption of MPA and MUA molecules from 50 nm and 200 nm electrodes. From the CV curves, two current peaks are visible for both the MPA and

MUA treated 3D electrodes. The peak at around -0.82 V for MPA and around -1.03 V for MUA is due to the cleavage of the gold-sulfur bond [175,177]. The values for Γ were then calculated for the MUA and MPA treated electrodes as listed in inset Table 2. When compared with flat electrodes [13] the amount of MPA and MUA on the 50 nm electrodes was 17 times and 18 times higher, respectively. This increase in the amount of SAM is proportional to the roughness factor of 18. But in case of 200 nm diameter nanostructures, the amount of SAM immobilized was only 12 -13 times higher although the increase in area was about 18 times. So the general trend of all the electrochemical characterization studies suggests a more effective immobilization of SAM on the smaller diameter 3D electrodes.

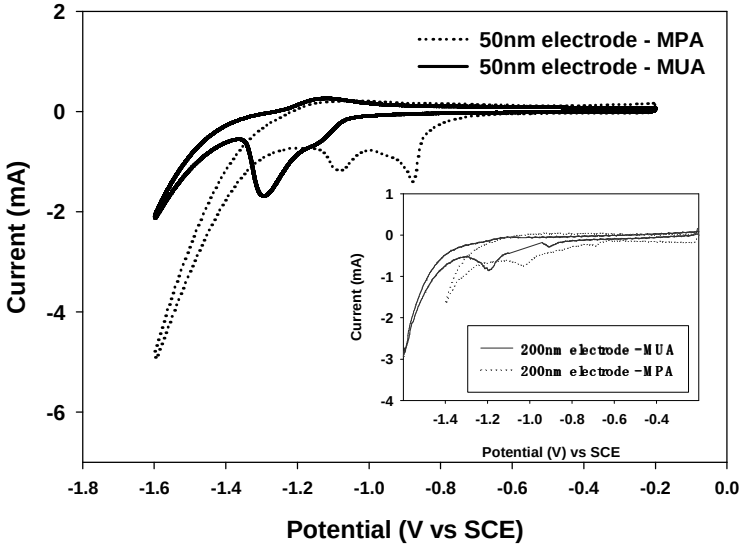

Figure 7.4: CV curves obtained for the MPA and MUA immobilized 50 nm 3D electrodes in evaluating SAM desorption in electrolyte containing 0.1M NaOH (Inset shows 200 nm nanopillar results)

	% defects for 50 nm electrodes	% defect on 200 nm electrodes	Γ for 50 nm ($mol \cdot cm^{-2}$) x 10^{-9}	Γ for 200 nm ($mol \cdot cm^{-2}$) x 10^{-9}
MPA	97.5	87.3	8.9 ± 0.17	7.1
MUA	31.7	37.8	15.1 ± 2	11.8

Table 7.2: Percent defect and surface coverage values of MPA and MUA on 50 nm and 200 nm electrodes

Figure 7.5A shows the amperometric current responses to glucose for the 200 nm electrodes. The polypyrrole immobilization method had the highest sensitivity in the 200 nm electrodes. Figures 7.5C & 5D show the amperometric current responses to glucose and the linear calibration curves for the 50 nm electrodes functionalized with MPA/GOx, MUA/GOx and PPy/GOx (35 min), respectively. Of the three immobilization methods on 50 nm electrodes, the polypyrrole electrode again showed the highest current response (6.34 $\mu A \cdot cm^{-2} \cdot mM^{-1}$). But this value is lower than the value for the 200 nm electrodes (8.4 $\mu A \cdot cm^{-2} \cdot mM^{-1}$). This difference may be attributed to the polypyrrole deposition parameters. To obtain an optimal detection outcome for the 50 nm electrodes, the current density and total charge for the electro-deposition of PPy/GOx were lowered to 35 $\mu A/cm^2$ and 85 mC/cm^2, respectively, as compared with those for the 200 nm electrode, namely, 50 $\mu A/cm^2$ and 150 mC/cm^2, respectively [28]. This was necessary in order to avoid clogging the inter-pillar space with polypyrrole (occurred at a current density of 50 $\mu A/cm^2$ for the 50 nm electrodes). A reduced total charge in the case of 50 nm electrodes also meant a lesser amount of GOx immobilization at the surface. All these contributed to

the reduction of detection sensitivity of the PPy/GOx treated 50 nm electrodes. Fig. 5B shows that in the cases where polypyrrole deposition was done in 10 and 20 minutes (on the 50 nm electrodes) the detection sensitivity was much lower than in the case of 35 minutes deposition.

The sensitivity for the MPA/GOx treated 50 nm electrodes (6.32 $\mu A \cdot mM^{-1} \cdot cm^{-2}$) was higher than the sensitivity obtained for the MPA/GOx treated 200 nm electrodes (4.8 $\mu A \cdot mM^{-1} \cdot cm^{-2}$). A similar trend is also seen for the MUA/GOx treated electrodes (2.59 $\mu A \cdot mM^{-1} \cdot cm^{-2}$ for 50 nm electrodes as opposed to 1.85 $\mu A \cdot mM^{1} \cdot cm^{-2}$ for 200 nm electrodes). In general, we observed that MUA (with a longer chain) provides better coverage, lesser defects and lower sensitivity than MPA (with a shorter chain). The current responses from the all the SAM treated electrodes exhibited small sample-to-sample variation (indicated by small error bars; Fig 6).

Putting the impedance values (Table 1) and the sensitivity values (Figure 7.6) together, we found that the polypyrrole (35 minutes) case had higher electron transfer and diffusion resistances than the MPA case although the former exhibited higher detection sensitivity. One possible explanation for this could be attributed to that the enzymes trapped in the polypyrrole matrix were much more active than those tethered to the SAMs.

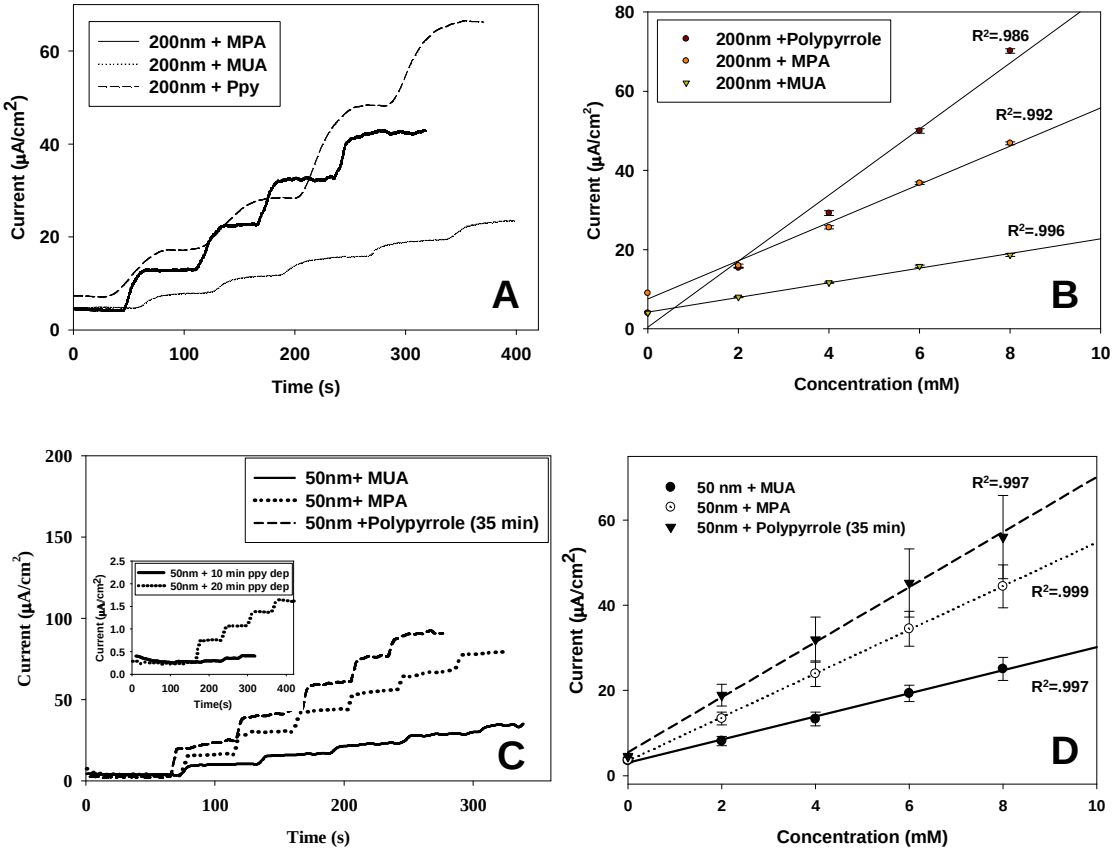

Figure 7.5: (A) Amperometric results of MPA and MUA and polypyrrole treated 200 nm electrodes (B) Linear calibration curves of the immobilization procedures in 200 nm electrodes (C) Amperometric results of MPA, MUA and polypyrrole coated at 35 minutes on 50 nm electrodes (Inset) Amperometric results of polypyrrole coated at 10 and 20 minutes on 50 nm electrodes (D) Linear calibration curves of the immobilization procedures in 50 nm electrodes

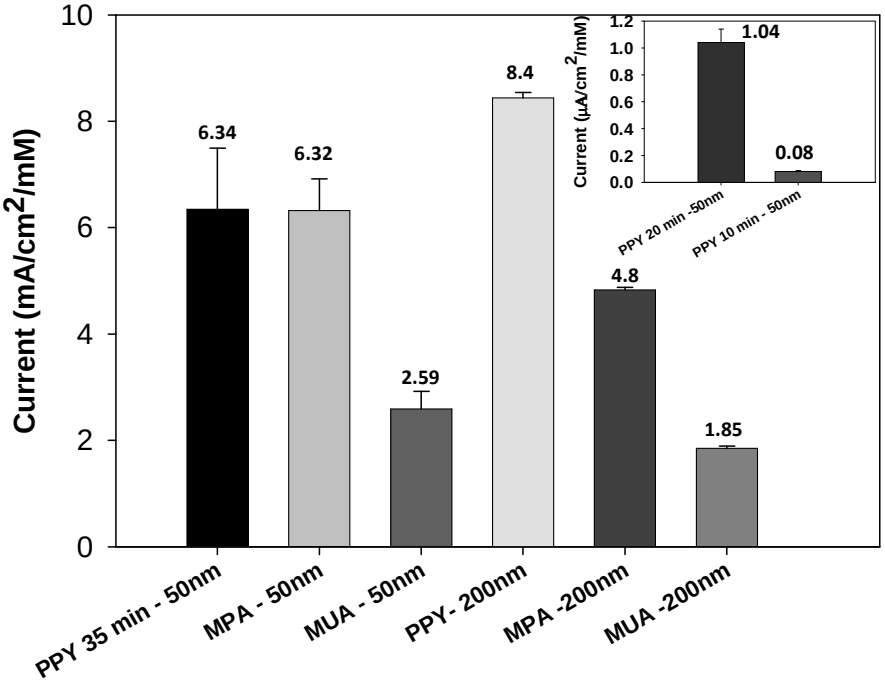

Figure 7.6: Comparison of glucose sensitivity of the different immobilization methods in the 50 nm and 200 nm electrodes respectively

7.4 Conclusion

This work has provided some insights into how the size of nanostructures affects the functionalization (with enzymes) of 3D electrodes consisting of standing nanopillars. Clearly, 3D electrodes with different nanopillar diameters require different functionalization strategies. For an alkanthiol SAM based strategy, SAMs are formed more efficiently on the 50 nm electrodes than on the 200 nm electrodes, which in turn results in higher glucose detection sensitivity values (for both the MPA and MUA SAMs) for the 50 nm electrodes. For a polypyrrole based strategy, the optimized electro-deposition procedure (for entrapping glucose oxidase enzymes) in 3D electrodes leads to

lower detection sensitivity values for the 50 nm electrodes than for the 200 nm electrodes. Put it in another way, of the two functionalization strategies evaluated, the polypyrrole method provides better glucose detection performances with larger nanopillar electrodes, but with smaller nanopillar electrodes the MPA SAM and polypyrrole methods produce similar glucose detection performances.

CHAPTER 8

USE OF NANOPARTICLES FOR BETTER ENZYME STABILITY AND THE SIZE EFFECT OF NANOPARTICLES

8.1 Introduction

The polypyrrole coating in the previous methods was not more than 20 nm and this caused the electrochemical biosensors to lose it activity within 3 weeks of preparation either by leaching or denaturation. The enzyme layers formed on the SAM coatings were even more unstable than the polypyrrole coatings. It is therefore very important to improve the stability of the enzyme layer such that a biosensor can make continuous long term measurements. One idea was to exploit the nanoparticle/enzyme interaction to make more stable environment for the enzymes. Thus we examined how gold nanoparticles of different sizes, when incorporated into the pyrrole/enzyme mixture prior to electropolymerization, can enhance the stability of the enzyme electrode in a 3D nanopillar biosensor.

Gold nanoparticles (GNPs) have been extensively used in electrochemical biosensors to functionalized enzymes to electrode surfaces, mediate electrochemical reactions as redox catalysts and amplify signals in electrochemical immunoassays [179].They have also been used in biosensors to enhance the activity of glucose oxidase [180] and improve the stability of glucose oxidase at higher temperatures [181]. In this work we are more interested in the stability provide by the GNPs in electrochemical biosensors. Proteins in general have shown enhanced stability when adsorbed on carbon nanoparticles or gold

nanoparticles. Unfavorable interactions between adjacent proteins contribute to their deactivation in harsh environments and lower protein surface interaction due to the curvature is thought to be the reason why proteins are more stable with nanoparticles or nanotubes [182].

It is also well known that the size of the GNPs has a significant effect on its interactions with proteins [183,184]. It was found that a reduction in size of the GNPs increased the activity of glucose oxidase [7]. But there has been no study to examine the effect of the GNPs' size on the stability of a glucose biosensor. In this study we investigated this by preparing GNPs of 3 different sizes (2 - 4 nm, 8 -10 nm and 25 – 30 nm). Electrochemical characterization techniques and UV-vis spectroscopic measurements were performed to understand how the GNP/enzyme and GNP/pyrrole interactions helped enhance the stability of the glucose biosensor. These studies were first performed in 3-electrode beaker setup and then confirmed in the microfluidic biosensor setup.

8.2 Experimental methods

8.2.1 Reagents and solutions

Pyrrole, D-glucose, glucose oxidase (GOx)- Type X, sodium citrate, potassium borohydride, (Tetrakis(hydroxymethyl)phosphonium chloride), Chitosan (100,000 Da) and p-benzoquinone of analytical grade were purchased from Sigma-Aldrich (St Louis, MO, USA). All solutions were prepared using deionized water. Glucose solution was allowed to mutarotate for 24 h prior to experiments.

8.2.2 Preparation of Gold nanoparticles(GNPs)

8.2.2.1 Tetrakis(hydroxymethyl)phosphonium chloride based reduction method

Small gold nanoparticles (2−4 nm in diameter) in aqueous solution were prepared by the reduction of chloroauric acid with (Tetrakis(hydroxymethyl)phosphonium chloride) THPC as detailed in the literature [185]. In brief 200µL of THPC (12µL/ml) and 100µl 0.6M NaOH was added to 20ml of water and mixed for 15 minutes. 400µL of 1wt% HAuCl4 was added after 15 min and was left to react for another 15 minutes. Final solution turned brown in color.

8.2.2.2 Citrate/ KBH_4 reduction (8- 10nm)

1 ml of 1% HAuCl4 aqueous solution and 1 ml of 1% trisodium citrate was added to 100 ml DI water under vigorous stirring for 1 minute. 0.11% KBH_4 solution was added after 1 minute under vigorous stirring for 10 minutes until the solution color changed to dark red.

8.2.2.3 Chitosan method [186]

1ml of 1% $HAuCl_4$ was mixed with 100ml of 0.05 % chitosan in 1% acetic acid. The mixture heated to 70 °C under constant stirring for 2 hours until the solution turned red.

8.2.2.4 Sodium citrate reduction [187]

40 – 45 nm gold nanoparticles were prepared using the sodium citrate as the reducing agent. In this method 20 mL of 1.0 mM $HAuCl_4$ was brought to a boil and then a 2 mL of a 1% solution of trisodium citrate dehydrate was quickly added. The mixture was heated for 10 minutes until the solution turned to wine red color.

8.2.3 TEM images

A 50-µL portion of gold nanoparticle sample solution was dropped on a copper grid (Electron Microscopy Sciences). The grid was then drained dry with a tissue paper and dried overnight in a desiccator. The samples were examined using a high-resolution transmission electron microscope (STEM-Hitachi HD2000).

8.2.4 Preparation of Nanostructure electrodes

3D nanostructured electrodes with nanopillars of 50 nm in diameter were prepared and cleaned using the methods mentioned in Chapter 4.2.2.

8.2.5 Electrode functionalization with enzyme/gold nanoparticles

The electrochemically cleaned 3D nanopillars on the glass substrates were functionalized using Glucose oxidase (GOx) / Polypyrrole/ GNPs. To do that, electro-polymerization of a pyrrole with GOx and GNPs was performed under at a current density of 35 $\mu A/cm^2$ for 35 minutes in 0.1 M KCl solution containing 0.05 M pyrrole, 0.5 $mgml^{-1}$ GOx [28]. The amount of the GNP solution added varied from 3µL/ml to 6µL/ml. The pH was maintained at 7.2 and this was the pH that was maintained in other characterization experiments.

For microfluidic biosensor the polypyrrole deposition was done with a setup mentioned in Chapter 8.2.3. The most effective gold nanoparticle size and concentration from the external beaker setup studies was used for the microfluidic studies.

The electrodes prepared were characterized using amperometric glucose measurements to check the for the enzyme stability. Rest of the characterization techniques were done to see check the nature of interactions between GNP – polypyrrole and GNP-enzyme.

8.2.6 Amperometric measurements

Amperometric measurements were made similar to the method described in Chapter 5.2.5. Each incremental was equivalent to 2.5mM increase in glucose concentration. The amperometric measurements were done on the 1day, 3 day and 12 days and 120 days after functionalization of the nanopillars with polypyrrole and the different size GNPs.

8.2.7 Electrochemical characterization methods

Cyclic voltammetry (CV) measurements was done on the electrodes functionalized with the enzyme and nanoparticles in a solution of 0.1M PBS , 3mM benzoquinone and 1mM glucose between a potential range of -0.4 V to 0.4 V and at a scan rate of 50 mV/s. Electrochemical Impedance Spectroscopic (EIS) studies were performed in a frequency range from 0.1 Hz to 100 KHz with an AC signal of amplitude of 10mV (vs. Ag/AgCl) in the same electrolyte solution.

8.2.8 UV-vis spectroscopy and Zeta potential

The UV-vis measurements were conducted in the Biotek Instrument Incorporation – Synergy 4 analyzer, by placing the GNPs / GOx solution in 24 well plates. UV-vis absorbance measurements were collected between wavelengths of 400nm to 800nm, with a resolution of 1 nm, for the GNPs and GNPs with enzymes. For the absorbance measurements the concentration of the GOx was 1 mg/ml and GNPs concentration varied from 85µM to 450µM (half the original concentration of the as such prepared GNPs). For the fluorescence measurements the excitation wavelength of enzyme was 270 nm and the emission spectra were recorded from 300 to 500 nm. The concentration of GOx was .005mg/ml and the GNPs concentration varied from 3µL/ml to 6µL/ml. Zeta-potential

were measured using the Brookhaven Instrument Corporation (Holtsville, NY, USA) – ZetaPlus zeta potential analyzer. 10 µL for the gold nanoparticles stock solution was added into the cuvettes having 2ml water. 10 µL of 1mg/ml GOx was further added to see the shift in zeta potential.

8.3 Results and discussions

Figure 8.1 shows the TEM images of the various nanoparticles prepared using the different methods. From the images the average diameter of the GNPs prepared using the THPC based reduction methods was 2 – 4nm, potassium borohydride based reduction method was 8 – 10 nm, Chitosan based reduction method was 25 – 30nm, and sodium citrate based reduction method was 40 – 45 nm. The average roughness of the gold nanopillars used in this study was around 15.

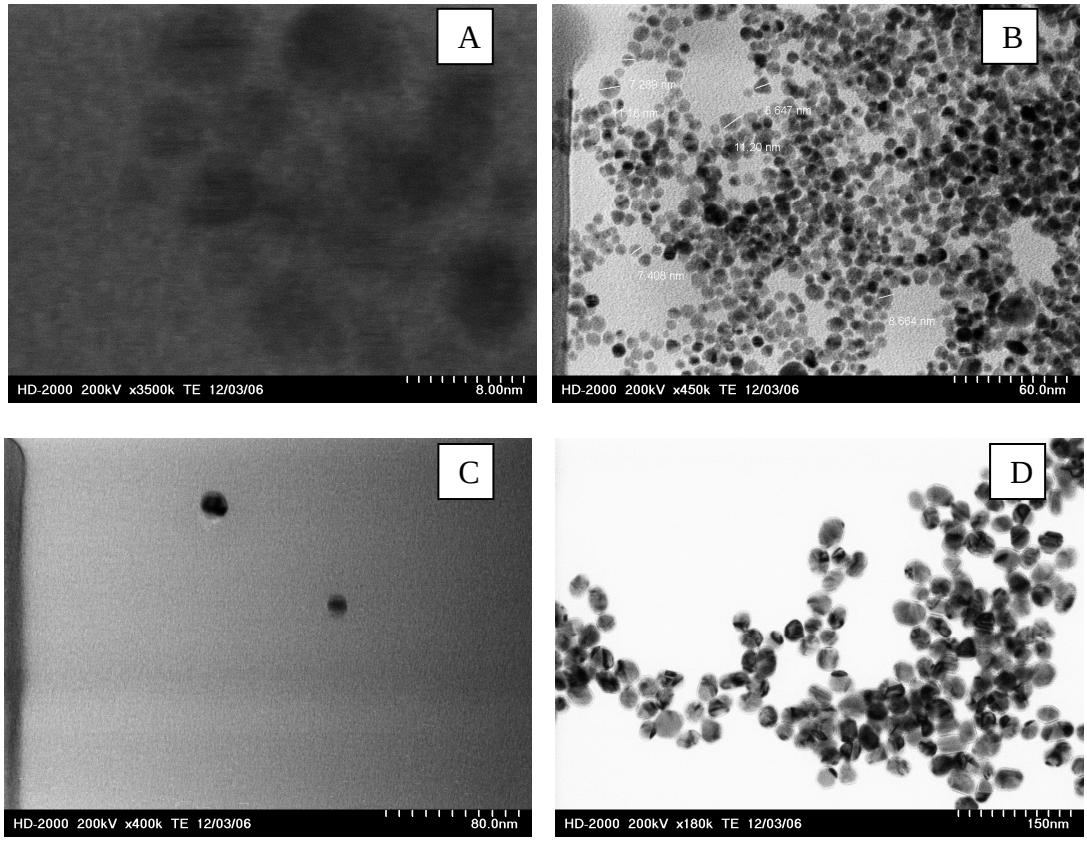

Figure 8.1: TEM images of GNPs from THPC (A), KBH_4 (B), Chitosan (C), Sodium citrate (D) reduction methods

Earlier results without any GNPs gave a sensitivity value of 6 μA/mM/cm^2 in glucose detection. It is thus desirable not to lower this sensitivity value when GNPs are added. Assuming that the $HAuCl_4$ initially present were totally reduced in all these methods, we would estimate a concentration of GNPs approximately 0.324 mM, 0.17 mM, 0.17 mM and 0.9 mM for the THPC, KBH_4, Chitosan and Sodium citrate methods, respectively. In this study we found that a certain amount of dilution of the GNP concentration is necessary in order to achieve better detection sensitivity, and dilution of GNPs < 120 times will reduce the sensitivity value drastically. Thus, in our study, only 60 μL of the

GNPS prepared by the THPC method (0.324mM) was added, and 120 µL of the GNPs prepared by of the KBH_4 and Chitosan methods was added. Since the concentration of the as-prepared GNPs for the former method (0.324 mM) is about twice that for the latter method (0.17mM), this dilution will result in a comparable amount of GNPs in the electrolyte.

The sodium citrate based methods yielded nanoparticles with diameters of 40 – 45 nm, almost the same as the interpillar spacing (~40 nm). Since the polypyrrole coating deposited had a thickness in the range of 20 – 30 nm, we believe that these large nanoparticles would not be entrapped in the polypyrrole matrix. Therefore we did not use them for glucose sensitivity studies.

8.3.1 Amperometric results

Figure 8.2 shows the amperometric response to the stepwise addition of 2.5mM of glucose and their corresponding sensitivity calibration curves for various GNP-incorporated electrodes on different days. The case of 25-30 nm GNPs showed the least sensitivity of 0.876 µA/mM/cm^2 (note that varying the GNP concentration did improve sensitivity). Overall, there was a steady trend in the loss of sensitivity over time. On the 120th day a loss of almost 70% in sensitivity was seen when compared with the first day. In the case of 8-10 nm GNPs, an increasing trend in sensitivity was seen on the 3rd and 12th day in comparison with the first day (Day 1: 5.44 µA/mM/cm^2, Day 12: 8.61 µA/mM/cm^2). But on the 120th day, the sensitivity dropped to 5.37 µA/mM/cm^2, a 38% drop from that of Day 12. The case of 2 -4 nm GNPs gave the best performance in terms of stability. These electrodes reached the peak sensitivity on Day 12 (8.87 µA/mM/cm^2)

and lost about 23% percent of its peak sensitivity on Day 120 (6.78 μA/mM/cm^2). But in comparison with the sensitivity value on Day 1 (5.67 μA/mM/cm^2), the value on Day 120 was still higher by 20 %. Figure 8.3 shows the bar graph results highlighting the change in sensitivity over time for various GNP-incorporated electrodes. Clearly, these results suggest that smaller nanoparticles have a better enhancement effect to not only improve the sensitivity of the glucose biosensor but also to prolong its stability. At this moment, it is not clear what causes the increase in sensitivity in the first several days, but we speculate that it might be attributed to favorable conformational changes in the enzymes/GNP hybrid structures. Along this line of thought, the smallest nanoparticles seem to either retain the favorable conformational changes in the enzymes over a longer period of time or prevent leaching of the enzymes from the polypyrrole matrix. The following sections try to obtain some insights regarding structural conformation and enzyme activity.

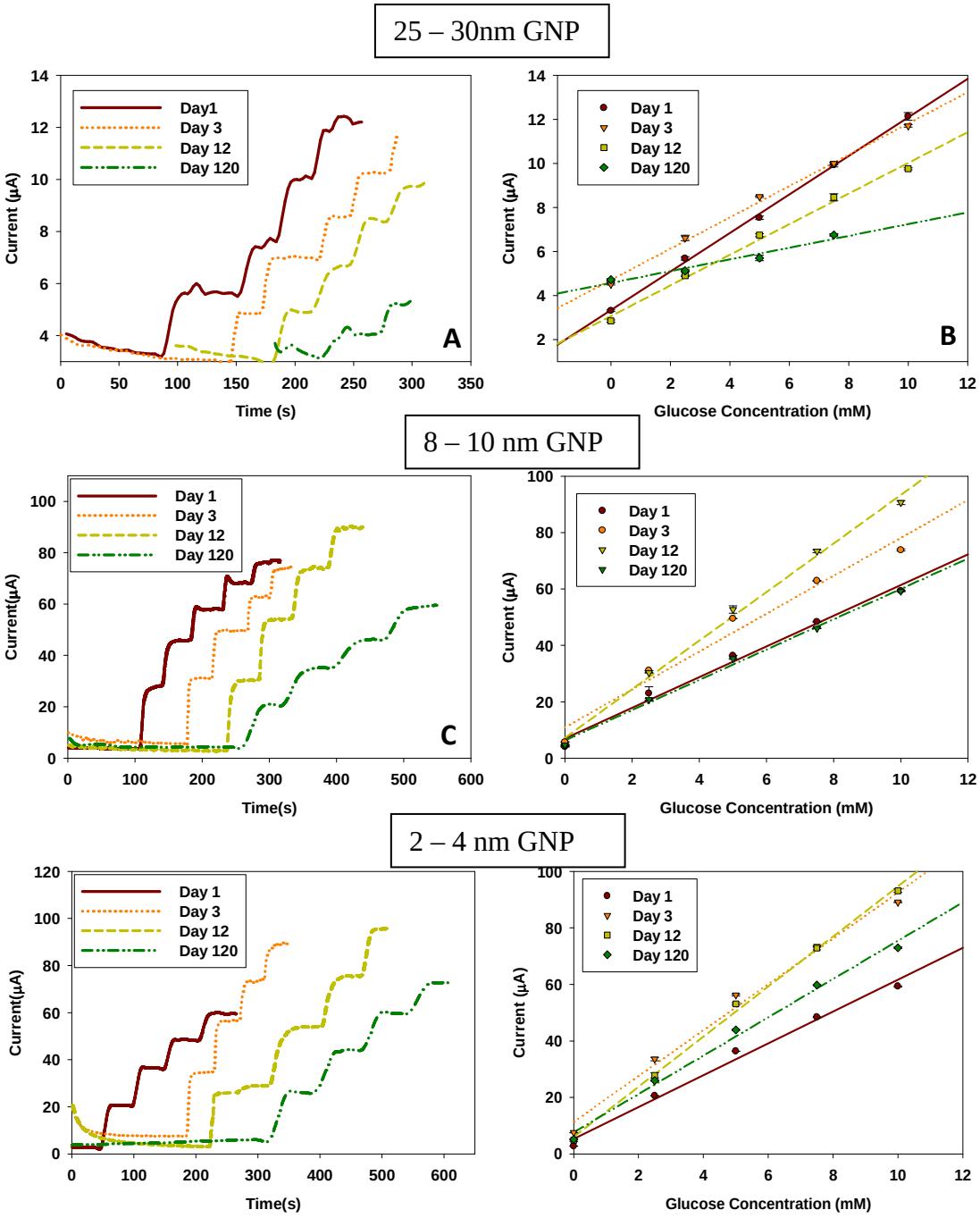

Figure 8.2: (A) Amperometric responses to stepwise additions of glucose for the polypyrrole/ Glucose oxidase/ 25 - 30 nm GNP (Chitosan) electrode (B) Calibration curve of the amperometric results for the polypyrrole/ Glucose oxidase/ 25 -30 nm electrode (C) Amperometric responses for the polypyrrole/ GOx/ 8 -10 nm GNPs (KBH_4)

electrode (D) Calibration curve of the amperometric results for the polypyrrole/ GOx/ 8 - 10 nm GNPs electrode (E) Amperometric for the polypyrrole/ GOx/ 2 - 4 nm GNP (THPC) electrode (F) Calibration curve of the amperometric results for the polypyrrole/ GOx/ 2 - 4 nm GNP electrode

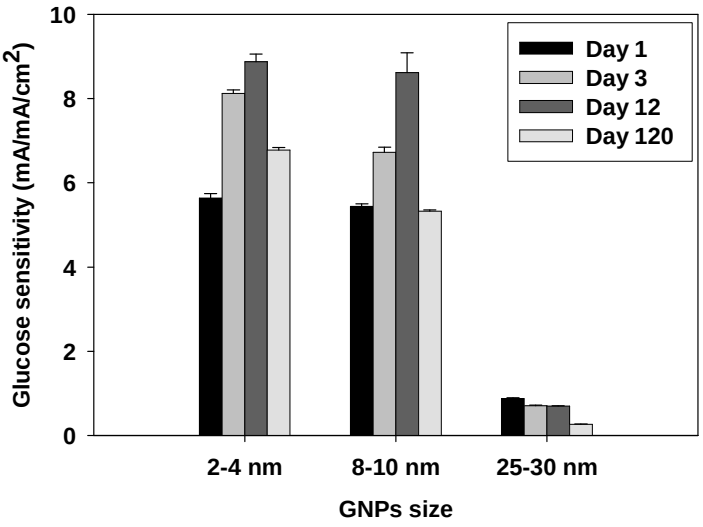

Figure 8.3: Summary of the all the sensitivity values of different GNP incorporated electrodes over a period of 120 days

8.3.2 CV and EIS measurements

Interactions of GNPs with polypyrrole can enhance the electrochemical properties of coated electrodes. We tried to do CV and EIS measurements on the GNP/PPy/ Glucose Oxidase incorporated electrodes to see if there was evidence of enhanced electrochemical properties. The CV measurements were done in a solution of 0.1M PBS containing 3mM benzoquinone and 1mM glucose to measure the oxidation and reduction peaks of the hydroquinone produced in the presence of glucose and benzoquinone respectively. As seen from Figure 8.4A, the 2-4 nm GNP-incorporated electrodes had the highest

oxidation peak current (0.76mA) followed by the 8-10 nm case (0.69mA) and the 25–30 nm case (0.34mA). The increase trend in this oxidative peak current of benzoquinone with decreasing GNP size is similar to that in the amperometric current responses. These results are consistent since the amount of hydroquinone generated depends mostly on the active enzyme sites for glucose oxidation. For the reductive peak of benzoquinone, the 8-10nm and 25–30 nm cases had similar peak values (-0.74mA), whereas the 2–4 nm case showed a higher reduction peak (-0.92 mA). Since the concentration of benzoquinone is the same in all these cases, the change in current can occur only if there is more active surface area for the reduction reaction. This implies that the 2-4 nm GNPs incorporated in the polypyrrole can also enhance the reactions. Similar results were also evident from the EIS experiments shown in Figure 8.4B.

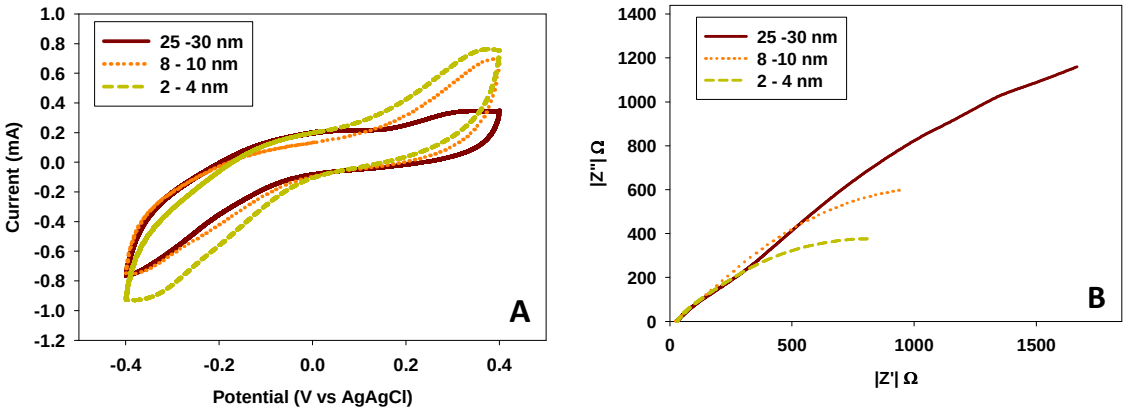

Figure 8.4: (A) CV of polypyrrole/ glucose Oxidase/ GNP electrode in 0.1M PBS, 3mM benzoquinone and 1mM glucose (B) Nyquist Plots of the electrochemical impedance results of polypyrrole/ glucose Oxidase/ GNP electrode in 0.1M PBS, 3mM benzoquinone and 1mM glucose

8.3.3 Zeta potential

The surface charge changes of the gold nanoparticles when they interact with enzymes can be examined by studying the Zeta potential changes. This can be used to understand the type of interactions between the GNPs and enzymes. In order to obtain this information, the surface charge (zeta potential) of the GNPs before and after enzyme additions was measured and the results are seen in Figure 8.5. The GNPs in water were mostly negatively charged and the chitosan based GNP was the most positive as they can be covered with the cationic chitosan [188]. Upon addition of enzyme, surface charge of the GNPs increased (became less negative). The most change was seen in the chitosan reduced GNPs and the least change was in 2 – 4 nm GNPs .Even though at the neutral pH the surface charge of glucose oxidase molecules are negative (pI: 4.2), there are changes in zeta potential in the positive direction indicating the interactions are complex and similar to the earlier results of BSA on citrate stabilized GNPs [189].

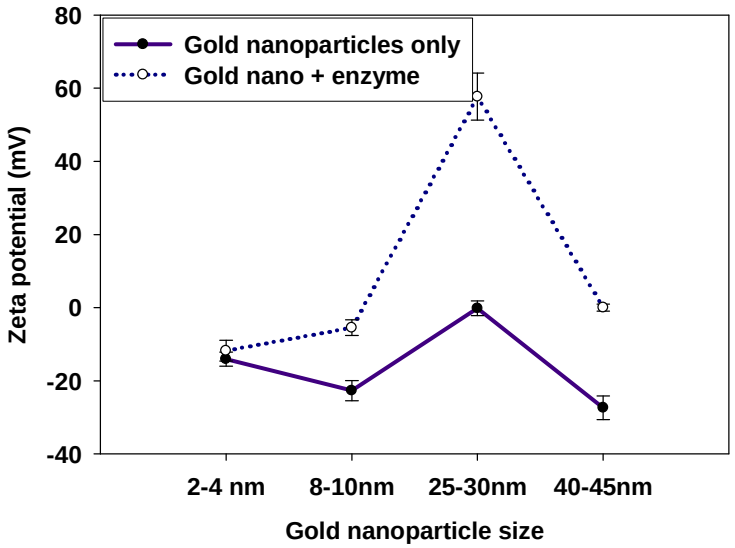

Figure 8.5: Zeta potential of the GNPs and GNP- enzyme mixture

8.3.4 UV – Vis absorbance spectroscopy

In UV-vis absorbance studies we were looking for the surface plasmon resonance (SPR) peaks shifts of GNPs when they interact with enzymes. Figure 8.6 shows the UV – Vis absorbance between 400nm to 700nm. The surface plasmon resonance (SPR) of the GNPs peak is around 520nm. The exact peak locations are size dependent because of the mean free path of the electrons is reduces as the size of the GNPs reduces [190]. 2 -4 nm gold nanoparticles are too small to have the distinct surface plasmon absorption peak as seen in Figure 8.6A [185]. After the addition of glucose oxidase the red shift (shifts towards larger wavelengths) in the peaks is observed in case of 8- 10nm, 25 – 30nm and 40 -45 nm GNPs. This shift is larger when the nanoparticle is smaller. The red shift of the spectrum peak results from changes in the local refractive index around the nanoparticles because of the enzyme binding [191] and therefore it indicates a possible bioconjugation of GNP/GOx [192]. The newer peak in the case of chitosan based GNPs and enzymes can be due to the aggregation of nanoparticles (aggregation can cause peaks above 600nm) [193]. This aggregation effect can explain why the sensitivity of the chitosan based GNPs incorporated electrodes was not as high as the other samples. In case of 2 - 4nm nanoparticles there is larger blue shift (shifts to smaller wavelengths) in the resonance peak. This can happen if there is decrease in the effective refractive index around the particles and increased light scattering. But the exact reason for this phenomenon is still not clear. Overall the absorbance spectroscopy reveals the interaction of GNPs and the enzyme molecules. The entrapment of GOx in polypyrrole matrix will also involve the entrapment of GNPs and there will be possible interaction similar to the ones observed in

absorbance studies between GNPs and GOx. These interactions may be one of the main reasons for the extended life of the enzymes as the nanoscale environments are known to increase stability of proteins in general [182].

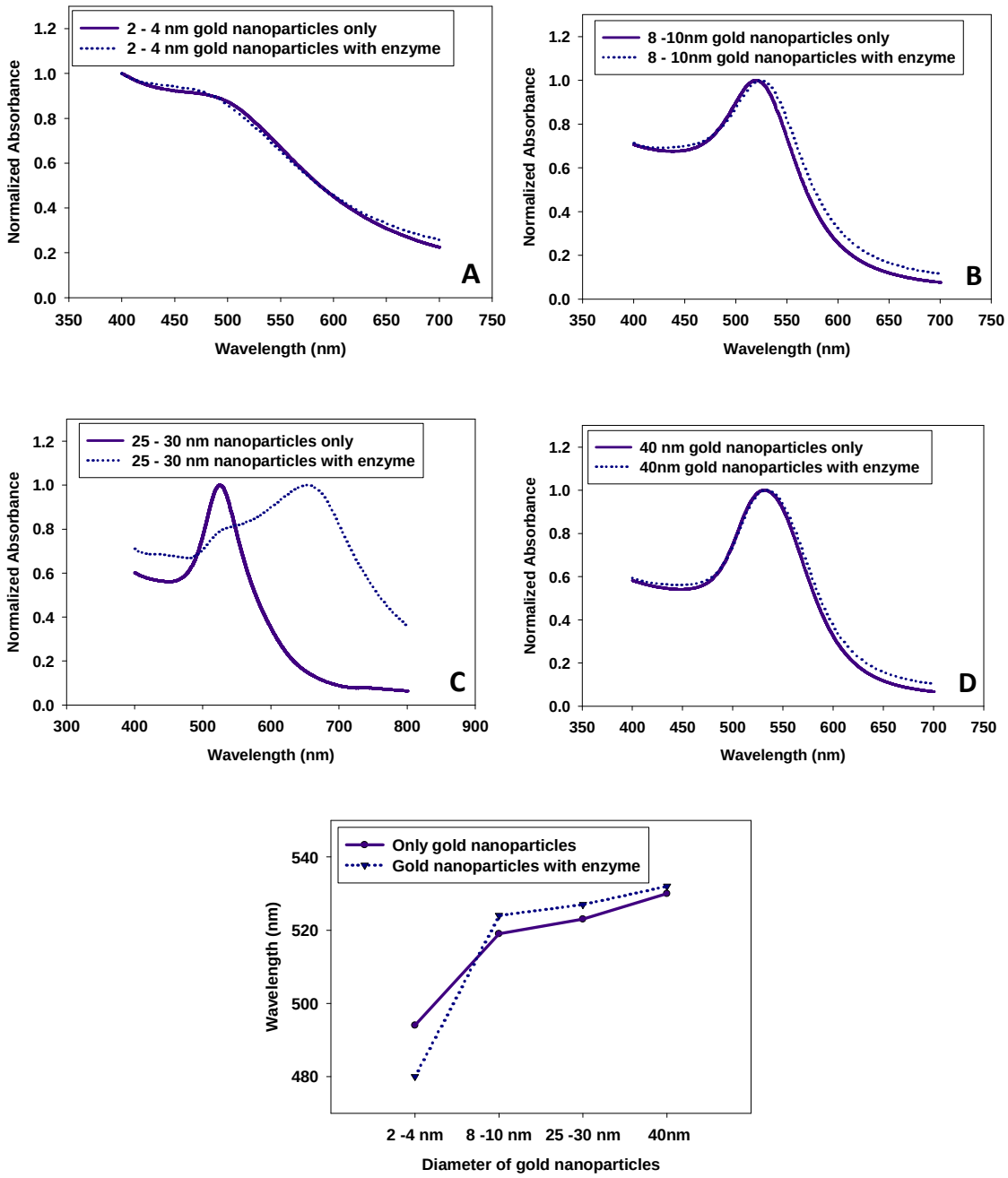

Figure 8.6: (A) Absorbance spectra of 2 – 4 nm GNPs and GNP/GOx (B) Absorbance spectra of 8 – 10 nm GNPs and GNP/GOx (C) Absorbance spectra of 25 – 30 nm (chitosan based) GNPs and GNP/GOx (D) **–** Absorbance spectra of 40 – 45 nm GNPs and GNPs/GOx (E) Peak values of absorbance of GNPs with and without enzymes

8.3.5 UV- vis fluorescene spectroscopy

Fluorescence of tryptophan residues in proteins can be used to study the interaction between GNP and proteins [194]. Interactions of tryptophan residues with GNPs are known to quench the fluorescence of tryptophan. As seen in Figure 8.7 the fluorescence intensity decreases with the addition of GNPs. It can be seen that the highest quenching occurred for the case of 2 – 4 nm NPSs. We believe that the smallest nanoparticles interacted on multiple sites of each glucose oxidase molecule, thereby quenching the fluorescence signal the most. These results also confirm the enhanced interaction of the smaller GNPs with the enzyme. These increased interactions possibly aided in the increase of the stability of the polypyrrole/ GOx/ GNP electrodes.

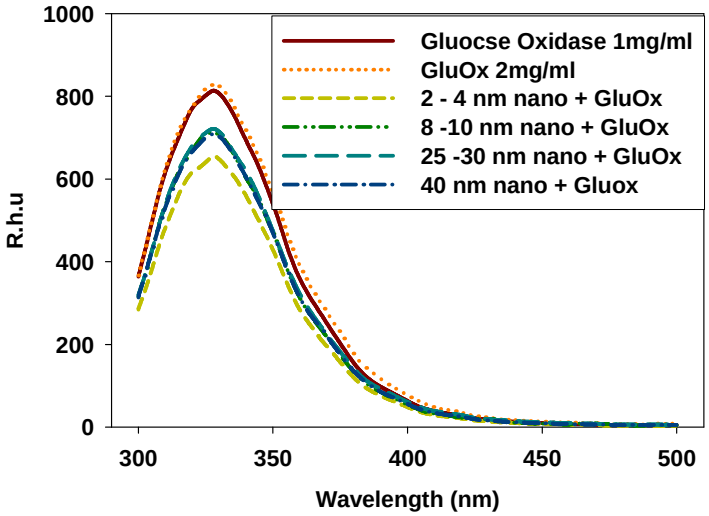

Figure 8.7: Fluorescence response of enzyme and enzyme/ GNPs to an excitation wavelength of 270nm

8.4 Conclusion

The size of the GNPs had a distinct effect on the stability of the polypyrrole entrapment based glucose biosensor. Smaller nanoparticles with diameter of 2 – 4 nm had

the least changes in glucose sensitivity over a period of 120 days. This can be attributed to the multiple interactions or contacts of the smaller nanoparticles every enzyme molecules. This was confirmed by the UV-vis spectroscopic measurements as the results indicated enhanced contact of the smaller GNPs with the enzyme. The electrochemical characterization of the deposited polypyrrole films with the smaller nanoparticles also indicated lower electron transfer resistance. This also conveys the idea that there can be interaction of gold nanoparticles and polypyrrole. So we conclude that the effective interactions of the smaller GNPs with the enzyme and polypyrrole lead to higher stability of the glucose biosensor. This study not only sheds light into gold nanoparticles enzyme interactions but also how they can be utilized in improving the stability of biomolecules in biosensors.

8.5 Highlights of the enzyme electrode studies

1) Polypyrrole electropolymerization parameters had to be modified to effectively coat the 3D gold nanopillars
2) In 200nm nanopillars, polypyrrole was better immobilization method
3) In 50nm polypyrrole and MPA SAM gave similar glucose sensing performances
4) The gold nanoparticle-enzyme co-entrapment in polypyrrole gave the best results in terms of stability
5) Since polypyrrole gave good sensing performance and also stability, this method will be the superior method for constructing the microfluidic biosensor

6) The information that SAM has enhanced adsorption in smaller diameter nanostructures will be useful in other studies like protein and DNA biosensors were SAM layers are regularly used.

SECTION III

MICROLFUIDIC GLUCOSE BIOSENSOR

All the biosensing studies discussed until now were done mainly in a 3 electrode setup in a beaker. With the method for enzyme electrode fully established, in this section we will discuss on the development of the microfluidic biosensor. Since the flow conditions in microfluidic channels are different from the beaker setup studies, we modified and optimized many of the parameters for microfluidic biosensor. These results have been discussed in the following two chapters.

Title and brief description on each of the chapter is given below

1) Enhancing the performance of a fluidic glucose biosensor with 3D electrodes

In this chapter we will discuss the patterning of the 3D electrodes and the process of formation of the PDMS based microfluidic devices. We will also discuss how the polypyrrole method became the preferred method for immobilizing enzymes in the microfluidic setup.

2) Optimizing the design of the microfluidic glucose biosensor for enhanced performance

The performance of the microfluidic glucose biosensor can also be affected by the design parameters of the microfluidic channel and other factors like flow rate. So it was essential to optimize these parameters to achieve enhanced performance of the biosensor. This work is more of an optimization study on all the other microfluidic parameters that can be helpful in improving performance of the microfluidic biosensor.

CHAPTER 9

ENHANCING THE PERFORMANCE OF A FLUIDIC GLUCOSE BIOSENSOR WITH 3D ELECTRODES

9.1 Introduction

In this chapter, the three dimensional (3D) nanopillar structures on glass substrates were used to develop a microfluidic glucose biosensor for continuous monitoring. This is done by converting the 3D electrodes into patterned electrodes through conventional photolithographic processes to form three electrochemical electrodes (i.e., Enzyme, Working and Counter electrodes) of a fluidic glucose sensor device. We introduce an effective method for preparing enzyme electrodes through electropolymerization of polypyrrole in such a fluidic channel setting.

9.2 Experimental methods

9.2.1 Formation of patterned 3D electrodes

To convert the nanopillars along with the underlying metallic film into patterned electrodes, a conventional photolithographic fabrication process was carried out. Figures 9.1A through 9.1F show the procedural steps involved. Here we used a three-electrode design to pattern the nanopillars into three electrodes to be used as enzyme electrode, working electrode and counter electrode, respectively. In this case, each of the three strip-shaped electrodes was 1 mm wide and 1 mm apart (see Figure 9.1G). To form the patterned nanopillar electrodes, a positive photoresist (PR) was spun coated on the nanopillars and after a prebake step the desired pattern was transferred in a mask aligner

(Karl Suss MJB3). After post-bake and PR development, a PR masking layer was formed on top of the nanopillars. The unmasked nanopillars and the underlying metallic layers were etched. The Au part was etched in a mixture solution containing potassium-iodide : iodine : water (4 g : 1 g : 40 ml), and the Ti part was removed in HF:H_2O_2: H_2O (1:1:50). The final product was three strip-shaped electrodes consisting of nanopillars standing on conducting Au film formed on top of the glass substrate along with their contact pads. An interdigitated electrode design with nanopillars (with five fingers - see Figure 9.2 inset) was also done using the same procedure, but with an appropriate photomask. The IDEs' individual electrodes had a width and spacing of 200 µm and this design was used to improve the detection limit.

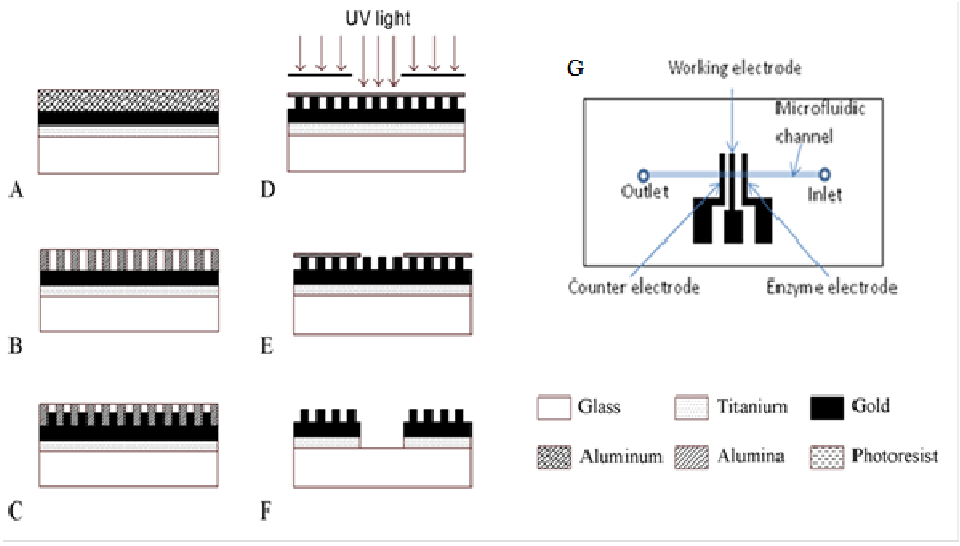

Figure 9.1: The procedural steps (A-F) used in the formation of 3D electrodes integrated with nanopillars (G) Schematic of the electrode design and position of the fluidic channel

9.2.2 Development of fluidic channel

To form a flow channel device, we placed a polydimethylsiloxane (PDMS) chamber on top of the glass substrate having the formed 3D electrodes. To make the PDMS

chamber, a mould of 15 mm long, 500 µm wide and 100 µm tall was fabricated on a glass substrate within a confined box area of 25×40 (mm) using SU-8, an epoxy based negative photoresist, through a conventional photolithography process. Two thin polymer tubes were inserted in the mold on both sides to form the inlet and outlet for the fluidic channel. A mixture of PDMS prepolymer and its curing agent in a ratio of 10:1 was prepared in a vacuum chamber. The PDMS mixture was then poured onto the mold and left for curing for 2 hours at 70 °C. The cured PDMS chamber was then separated from the glass substrate and the mould. It was rinsed with ethanol and dried in nitrogen gas. The PDMS chamber was placed over the glass substrate to house the nanopillar electrodes through a reversible bonding method. To achieve the reversible bonding, the smooth bonding surface of the PDMS and the selected area of the glass substrate (having the formed electrodes) were first wetted with ethanol and dried. After that the PDMS chamber was clamped to the glass substrate using a holding fixture made of acrylic. The reversible bond was sufficient to withstand the fluid pressure during our experiments. The area of the enzyme and working electrode (in the three electrode design) exposed in the channel after the placement of the PDMS channel was 1mm x 0.5mm each. In case of the IDE electrodes prepared it was 200 µm x 500 µm each.

9.2.3 Formation of enzyme electrode

The electrode close to the inlet (see Figure 9.1G) was converted to an enzyme electrode through an electropolymerization process with the electrode close to the outlet used as a counter electrode. The polymerization was performed in a fluidic channel setting as depicted in Figure 9.2, in which the electrolyte containing the pyrrole monomer

was flowed continuously into the fluidic channel at 5 µL/min. The electro-polymerization was carried out under an optimized galvanostatic process [28] at a current density of 50 $\mu A/cm^2$ in 0.1 M KCl containing 0.05 M of pyrrole and 0.5 mg/L of glucose oxidase (GOx) for about 40 minutes against an Ag/AgCl reference electrode. This electro-polymerization deposition process was applied to fluidic channels having nanopillar modified electrodes as well as to control channels with flat electrodes. The only difference was that in the latter, the deposition current was applied at 382 $\mu A/cm^2$ for 130 seconds according to our previously established optimal values for flat electrodes [195].

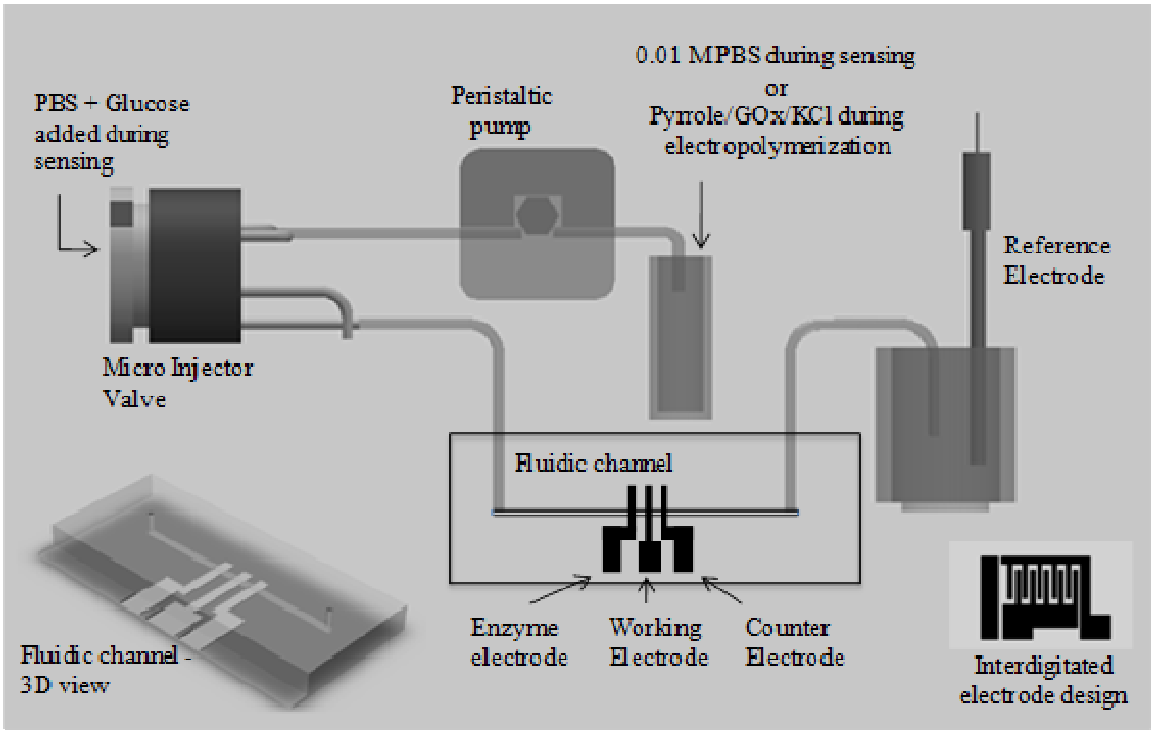

Figure 9.2: Experimental setup for electropolymerization and amperometric glucose detection. Note that during electrode functionalization, the perisaltic pump is connected to a reservior containing a mixture solution of polypyrrole, GOx and KCl; during sensing, the pump is connected to a reservior of PBS while a fixed volume of glucose in PBS is

introduced at the injector. A single set of three-electrode is shown at the low left corner and a five-finger IDEs set of three-electrode is shown at the low right corner.

9.2.4 EIS studies on polymer/enzyme layer

To assess the formed polypyrrole film on nanopillars, we performed Electrochemical Impedance Spectroscopy (EIS) measurements before and after the electro-polymerization process. All EIS measurements were done in 10 mM phosphate buffer solution (PBS) containing 5 mM $Fe(CN)_6^{3-/4-}$ and 0.15 M KCl in a frequency range from 100 mHz to 1 kHz under an AC potential with an amplitude of 50 mV (vs. Ag/AgCl). The difference in impedance due to pyrrole/GOx film deposition performed in the fluidic channel was compared with that performed in bulk solution.

9.2.5 Glucose detection

After the electro-polymerization step, all fluidic channel devices were thoroughly rinsed by passing D.I water and then 0.01 M PBS at a rate of 25 µL/min. The experimental setup was the same as the one used for the electropolymerization (Figure 9.2) except that an injector was used to introduce the analyte solution. To begin, PBS (0.01 M) containing p-benzoquinone (3 mM) as a mediator was first fed through the channel device at a constant rate of 5 µL/min while the amperometric current response was measured by holding the working electrode at 0.35 V (vs Ag/AgCl). After the current response stabilized, PBS (0.01 M) containing a known concentration of glucose and the mediator was introduced to the channel at the injector. In this setting, glucose was to be oxidized and the mediator reduced at the enzyme electrode. The reduced mediator was then oxidized at the working electrode, resulting in a current response whose value

depended on the glucsoe concentration. The experiment was repeated at various increments of glucose concentration. To compare the performance of the fluidic sensors having nanopillar modified electrodes with those having flat electrodes, the same experimental procedures were applied to fluidic devices having flat gold electrodes.

9.3 Results and discussions

9.3.1 Electrode design using photolithography

The photolithography procedure was very effective in forming the electrode structures with 3D nanopillars. Figures 9.3 show some of the structures formed on glass substrates. Almost all nanopillars remained intact after all the lithographic processes, demonstrating the robustness of the thin film alumina template method we developed to form the 3D electrodes integrated with nanopillars on glass substrates.

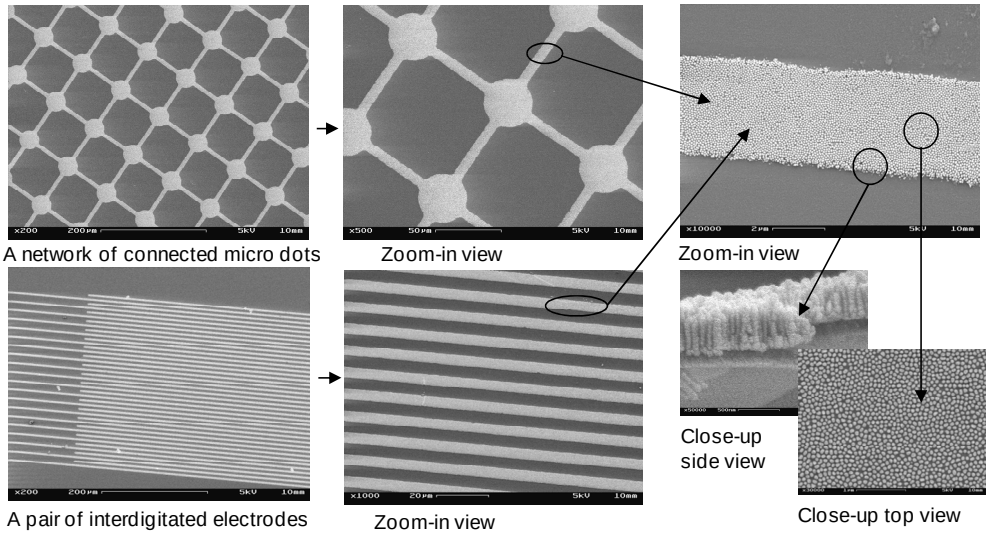

Figure 9.3: SEM images showing micro scale structures (a network of connected microdots and a pair of interdigitated electrodes) fabricated out of 3D skyscraper nanopillar structures

9.3.2 Polypyrrole/GOx deposition in fluidic channel

The direct deposition of polypyrrole/GOx onto the nanopillars in bulk solution did not yield good current responses to glucose in both flat and nanopillar electrodes (Figure 9.3D). But the deposition of polypyrrole/GOx performed in a fluidic setting showed a much enhanced current response to glucose. This improvement may be attributed to the low volume deposition in a fluidic setting with strict exclusion of oxygen [196,197]. The EIS measurements before and after polypyrrole/GOx deposition for the nanopillar electrodes are given in Figures 9.4A and 9.4B. The semicircular feature in the Nyquist plots is indicative of the blockage of electron transfer due to surface molecular deposition. A larger difference in the radius of the semicircles was seen for electrodes prepared in the fluidic channel as compared with those prepared in a bulk solution. To quantify it, a Randles Equivalent circuit (see inset in Figure 9.4A) consisting of a solution resistance (R_s), an electron-transfer resistance (R_{et}) and a constant phase element (CPE) capacitor was used to fit the obtained semicircular Nyquist plots for resolving the values for R_{et} as listed in Table-1. The change in the value of R_{et} before and after molecular deposition was about 22 fold when the deposition was done in the fluidic setting and about 10 fold when the deposition was in the bulk setting. This result showed that the deposition performed in the fluidic setting had a better coverage of the glucose oxidase molecules than did the deposition performed in a bulk solution.

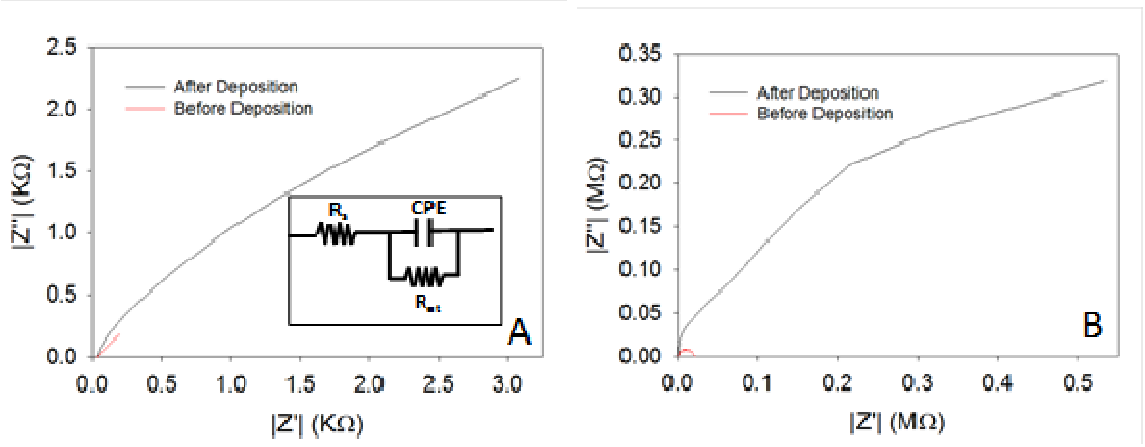

Figure 9.4: (A) Nyquist plots from the impedance measurements of nanopillar before and after polypyrrole deposition in bulk solution (Inset: A Randles equivalent circuit consisting of a solution resistance (Rs), an electron-transfer resistance (Ret) and a constant phase element (CPE) capacitor) (B) Nyquist plots from the impedance measurements of nanopillar before and after polypyrrole deposition in fluidic channel

Sample No	Deposition Procedure	R_{ET} Only gold Nanopillar (kΩ)	R_{ET} After Polypyrrole deposition (kΩ)	Increase Ratio
1	Microfluidic channel	17	376	22.1
2	Bulk deposition	0.285	2.9	10.2

Table 9.1: R_{et} values obtained by fitting the Randles Equivalent circuit

9.3.3 Results of glucose sensing experiments

When the functionalized electrode was used as the combined working and enzyme electrode, we found that the sensitivity achieved was about 30-40% of that when two separated enzyme and working electrodes were used, owing possibly to the diffusion barrier caused by the polypyrrole layer and the quick swept-away of the electroactive

species in the single electrode case. For this reason, we used separated enzyme and working electrodes in our experiments for achieving high sensing performance.

Figure 9.5 shows the current response to glucose for flat electrodes in a concentration range from 0.5 mM to 2.5 mM. From the calibration curve (Figure 9.5B) of peak current versus concentration, a sensitivity value for the flat electrodes was found to be 7.5 $\mu A/cm^2/mM$. This is much higher than other existing flat fluidic channel biosensors (e.g., 2.93 $\mu A/cm^2/mM$ [4]). To evaluate the kinetics of the enzymatic activity involved, the calibration curve was replotted as 1/I against 1/C (Figure 9.5B inset) to determine the Michaelis–Menten constant (K_m) for the enzymatic activity and the maximum current response (I_{max}). From the statistical fit to the $1/I$–$1/C$ plot, based on the Lineweaver–Burk function: $1/I = 1/I_{max} + (K_m/I_{max})\ 1/C$, the apparent K_m and I_{max} values were found to be 11.7 mM and 0.124 μA, respectively. This K_m value is much lower than the K_m values for glucose oxidase in a bulk solution (33 mM), suggesting either the glucose oxidase entrapped in the polypyrrole matrix has higher activity or a larger amount of glucose oxidase in the polypyrrole matrix participates in the reactions.

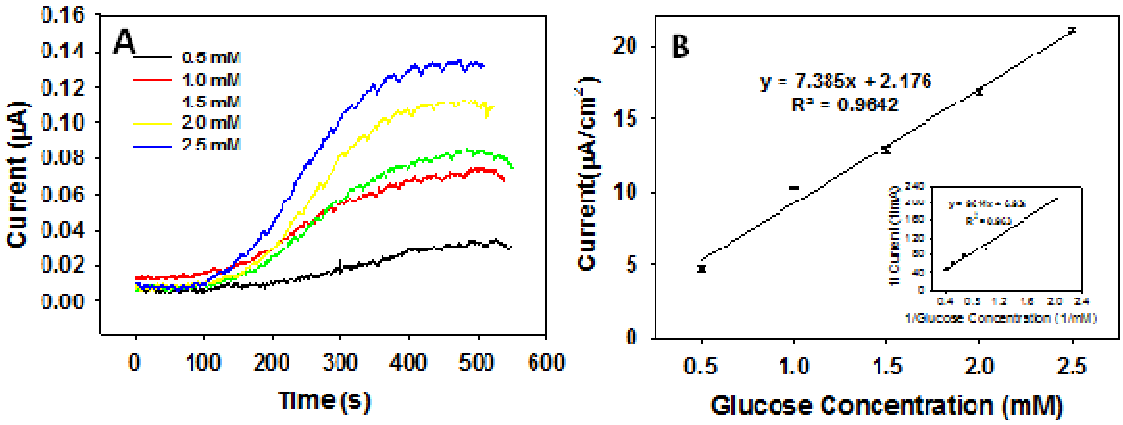

Figure 9.5: (A) Current response curves for various glucose concentrations in flat electrodes (B) Calibration plot for flat electrodes

Figure 9.6A shows the current response to glucose for the electrodes integrated with nanopillars in a linear response range of 0.5 to 2.5 mM. This range is useful for measuring glucose in hypoglycemic condition, but is low in view of the normal glucose level between 3.5 and 6.5 mM. However, it can be increased by adding a diffusion barrier to the electro-active species [4]. For example, after depositing a thin polypyrrole layer on the working electrode we expanded the linear range to 7.5 mM, albeit at the cost of losing the detection sensitivity slightly. From the calibration plot (Figure 9.6B) the sensitivity value of the nanopillar electrodes to glucose was determined to be 35.9 µA/cm^2/mM. This value is the highest ever reported for a flow based glucose sensor system. It is five times higher than that for the flat electrodes in this study. This increase can be attributed to the surface area increase provided by the skyscraper-like 3D nanopillars, allowing more surface area for enzyme immobilization and more space for efficient mass transport [142,143]. However, this current increase does not match the 18 times increase in surface

area. We speculate that the flow condition, although helping facilitate efficient mass transport, sweep away the analytes before they are detected. Thus the sensitivity may be improved when the flow rate is reduced further. The Lineweaver–Burk method was again used to determine the K_m and I_{max} values (Figure 9.6B inset) and they were 1.035 mM and 0.135 µA, respectively. The apparent activity of enzyme (K_m) is even higher in this case than the flat case, owing to the increased surface area in nanopillar electrodes for more enzyme immobilization.

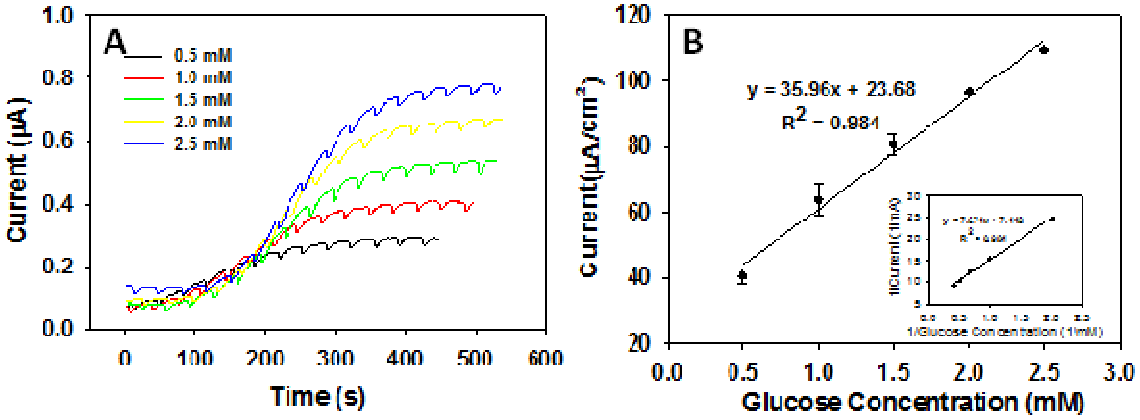

Figure 9.6: (A) Current response of electrodes with 3D nanopillars in fluidic channel (B) Calibration curve for nanopillar electrodes

9.3.4 Detection limit/ response time

The detection limit of the three electrode system biosensor was found to be approximately 15 µM with a signal to noise ratio slightly greater than 3. This detection limit is bit higher when compared with the detection limit of a microelectrode (3 µM) in a microfluidic channel [198]. We attributed this to the use of only one set of three electrodes and speculated that the detection limit could be lowered when multiple sets of

electrodes were used. To demonstrate this, we fabricated a set of interdigitated electrodes (IDEs) with five fingers, all incorporated with nanopillars (see Figure 9.2 inset). The IDEs' individual electrodes have a width and spacing of 200 µm. One branch of the IDEs was immobilized with enzyme molecules and the other branch was used as working electrode. With this IDEs design, we lowered the detection limit to 5 µM without affecting much the detection sensitivity in reference to that for the three-electrode setup. This can be seen in Figure 9.7 where the calibration curve along with the amperometric current response curves (inset-A) for the IDEs were shown in a lower range of glucose concentrations. The can be attributed to IDEs ability to capture and oxidize small amount of reactants more efficiently. Further work is going on to elucidate the cause and to achieve an even higher sensitivity and a lower detection limit (it will be discussed in a separate report).

Figure 9.6 also indicated a slow response time for the nanopillar modified electrodes (~200 s). This slow response time may be attributed to the fact that glucose molecules need to travel a long distance before entering the micro-channel for detection (see Figure 9.2), which could cause many glucose molecules to stick to the walls and the various junctions along the long pumping tube. To show this possibility, we used a shorter tube for feeding the glucose solution. To avoid using the peristaltic pump (which necessitates the need for a long pumping tube), we placed the glucose solution at a slightly elevated position above the channel device so that the glucose solution can be fed to the channel by a hydrostatic pressure. Doing this, we cut the response time to about 35 s (see inset B in Figure 9.7). This fact suggests that the overall response time can be further shortened if

the glucose through mass flow optimization. This type of setup will also reduce the amount of dead volume needed if the glucose can be introduced as close to the electrode surface.

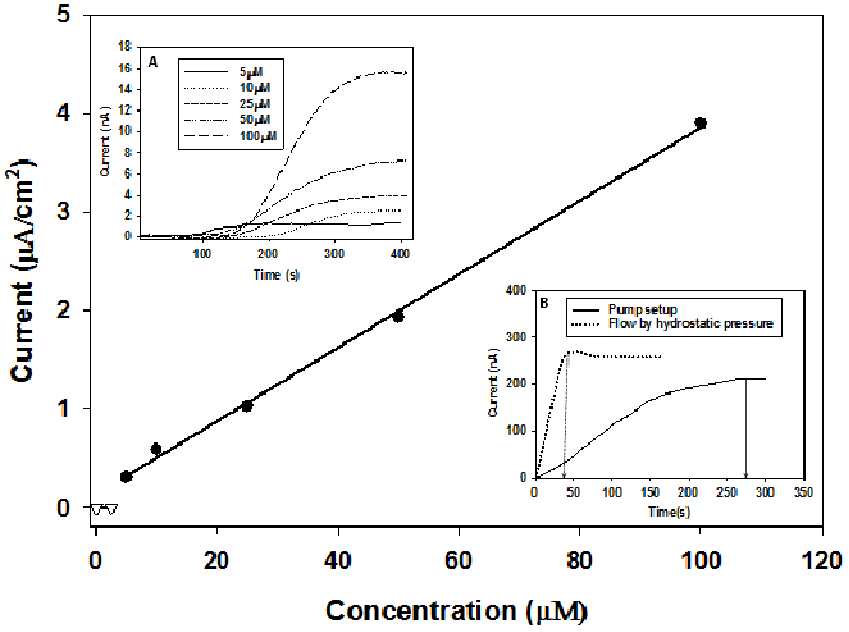

Figure 9.7: Calibration curve at a lower range of glucose concentrations for the IDEs design, Inset-A shows the current responses for the IDEs when the flow is driven by the peristaltic pump and Inset-B shows the current responses for the IDEs when the flow is driven by a hydrostatic pressure

9.4 Conclusion

We developed fluidic channel based biosensors using the 3D nanopillar modified electrodes and established an effective way to entrap enzyme in polypyrrole matrix for the functionalization of the 3D electrodes in a fluidic setting. We showed that the fluidic biosensors exhibit high sensitivity and fast response to glucose. There are many areas in which the sensor devices can be improved further. For example, the flow rate and channel

height can be adjusted; a reference electrode can be built on board using the 3D structures. The electrode and overall device design can be optimized so that the detection limit and response time can be further improved. The interference problem can be minimized by have electrode modifications like Prussian Blue that can reduce the operating voltage or have over-oxidized polypyrrole that can act as screen to interfering substances. Furthermore, the knowledge learned here regarding the use of nanostructures to enhance chemical reactions and mass transport may be applicable to other devices such as neural probes and fuel cells, among others.

This work laid the platform for building the desired microfluidic biosensor device. The polypyrrole deposition done inside the micro-channel it made it easier to immobilize the enzymes after constructing the microfluidic device. Due to this constructional convenience polypyrrole method became the preferred method after this for the development of the microfluidic biosensor. The next two studies discussed in the following chapters made polypyrrole method far more superior than the SAM methods.

(Results from this work has been published in [141])

CHAPTER 10

OPTIMIZING THE MICROFLUIDIC GLUCOSE BIOSENSOR FOR ENHANCED PERFORMANCE

10.1 Introduction

The microfluidic biosensor device discussed in Chapter 9 has overall scope of improvement in terms of sensitivity, reduction of interference and stability. This chapter discusses the optimization studies done to improve the overall performance of the microfluidic biosensor. We studied the effect of structural parameters like the channel height and width to improve the biosensor design. We studied the effect of flow rate on the current response of the biosensor to determine optimal flow conditions. A pulsed current electro-polymerization was used for improving the enzyme immobilization on 3D nanopillars. The stability of the biosensor was improved by improving the enzyme coating by co-entrapping gold nanoparticles and enzymes in polypyrrole as done in Chapter 8. To reduce interference and increase linear range, we tried coatings like overoxidized polypyrrole and Nafion on the working electrode.

10. 2 Experimental methods

10.2.1 Electrode preparation and Development of fluidic channel

Please refer to Chapter 9.2.1 and 9.2.2 for the details on electrode preparation and development of the fluidic channel. In this study we build micro-channels with different heights and widths. To obtain PDMS channels with different height, first the SU-8 molds (used for casting PDMS) were prepared with different thicknesses. The speed of the spin

coating method and viscosity of SU-8 was altered accordingly to get the required thickness of the SU-8. For example with SU 8 -2050 a spin speed of 4000 rpm yielded a 40µm thick SU-8 coating and SU-8 2025 at spin speed of 4000 yielded a thickness of 20 µm. These coatings on glass were then converted to a microchannel mold using photolithographic procedures as described in Chapter 9.2.2. To change the width of the PDMS channels, the width of the mold was changed by having the negative photomask with the desired widths. These SU-8 molds with different heights and width were then used to prepare the PDMS channels by casting a mixture of the PDMS prepolymer and curing agent (further details in Chapter 9.2.2). The channels with heights of 40µm and 20 µm were prepared. The two different widths of the channel were 500µm and 100µm.

10.2.2 Pulsed electropolymerization

Instead of a depositing polypyrrole with a constant current we used a pulsed current in this study. Studies were done to check the most optimized 'switching on time' (T_{on}) and 'switching off time' (T_{off}) of the applied pulses. T_{on} and T_{off} was varied between 100ms to 500ms to see if that affected the polypyrrole immobilization method.

10.2.3 Overoxidized Polypyrrole and Nafion coating

Polypyrrole was coated onto the working electrode using the same parameters to coat polypyrrole on enzyme electrodes (Chapter 9.2.3). The only differences were that there was no glucose oxidase in the electrolyte and the polypyrrole coating time varied between 10 minutes to 30 minutes. The overoxidized polypyrrole was obtained by oxidizing the polypyrrole coating in 0.1M NaOH potentiostatically a potential of 1.2V. The potential was applied until the current reached a steady state value. Nafion was

coated by dropping 5% Nafion solution on top of the working electrodes and drying them before attaching the PDMS channels.

10.2.4 Electropolymerization with Gold nanoparticles

Polyprrole was coated on the working electrode with procedure mention in Chapter 9.2.3. The only difference was 2 – 4 nm gold nanoparticles were added to the electrolyte along with glucose oxidase. Constant current was used in the polypyrrole deposition. These samples were tested for its stability by performing glucose testing for a period of 60 days.

10.2.5 Glucose sensing

The amperometric sensing of glucose was done as detailed in Chapter 9.2.5

10.2.6 Testing interference

Ascorbic acid was used the model interfering species. The experimental setup was similar to the glucose sensing setup detailed in Chapter 9.2.5. The only difference was that 0.5mM ascorbic acid was injected instead of the glucose.

10. 3 Results and discussions

10.3.1 Effect of channel height, channel width and flow rate

Figure 10.1 A &B shows the current response curves, of a biosensor with 40µm height and 500µm width channels, at different flow rates. Initial flat portion of the current is the background current in PBS and the increase in current response corresponds to the detection of glucose. In a typical experiment the flow speed was kept constant and 2 – 3 different glucose concentration (generally 0.5mM, 1mM and 1.5mM) each of 20 µL volume was introduced one after the other. The rise and fall of the current signal is

because of the entering and exiting of the 20 µL glucose. Each pulse of glucose was added only after the current reached the back to the background steady state values.

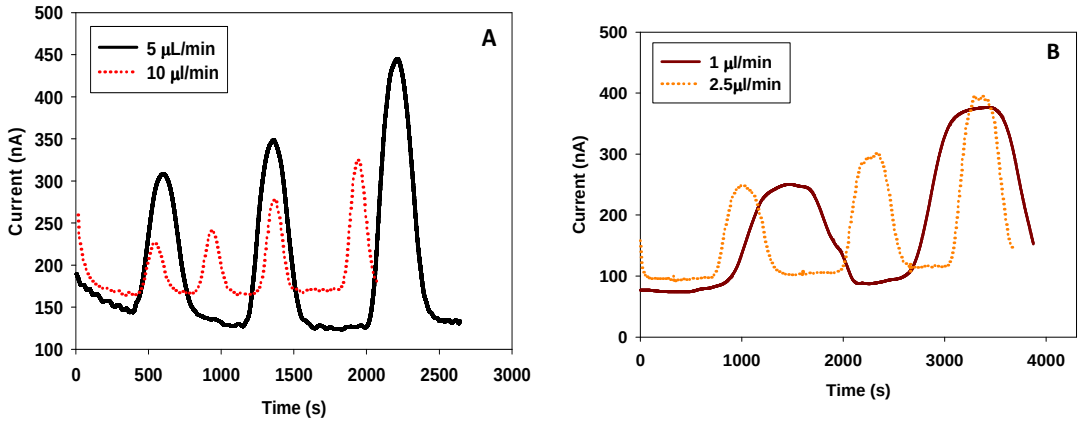

Figure 10.1: (A) & (B) Current responses of the microfluidic glucose biosensor, with 40 µm height and 500 µm width channel, when operated at different flow rates

Figure 10.2 shows the summary of the all the sensitivities calculated from different current responses (similar to current responses in Figure 10.1A&B) of the glucose biosensor with different channel height (but same channel width-500µm) operated at different flow rates. It can be inferred that there is only a small increase in sensitivity by reducing the channel height. This small change can be because there might not be a significant change in concentration of the electrochemical species close to the working electrode by changing the channel height. Since the working electrode current is a proportional to the concentration of species only close to its surface, we don't see a significant increase in sensitivity by reducing the height of the channel. Since we knew channel height did not affect the current response, only a channel with 20 µm height and 100 µm width was prepared for testing changes with the channel width. There was no

significant change in sensitivity between the 200 µm and 500 µm width channel based biosensor. The channel dimensions did not play an important factor in the design of the 3D nanopillar based biosensors. To reduce the solution resistance during electrochemical experiments we preferred the channels with 40µm height and 500µm width. This was the channel width used in rest of the experiments

By reducing the flow rate there is a very high increase in current response similar to results seen in flat electrodes [199]. At 1 µL/min the current response is approximately 70 µA/cm^2/mM and this is about 4 times higher when compared to results at 10 µL/min (~17 µA/cm^2/mM). This sensitivity is one of the highest known for any flow type biosensor. But the drawback will be the longer time needed for the glucose to reach the electrodes. Even though the response times of the 3D nanopillar electrodes are very quick (see Chapter 6), the overall response time of the fluidic biosensor will be poor if we use the slow speeds. This slow speed may not be a significant factor if instantaneous measurements are not necessary. Quicker response can be obtained if the electrodes are integrated very near to the origin of species that needs to be detected. In the case of cell culture monitoring, if the electrodes are placed very near to a microfluidic cell culture the time taken for the media solution to reach the electrodes will be very less.

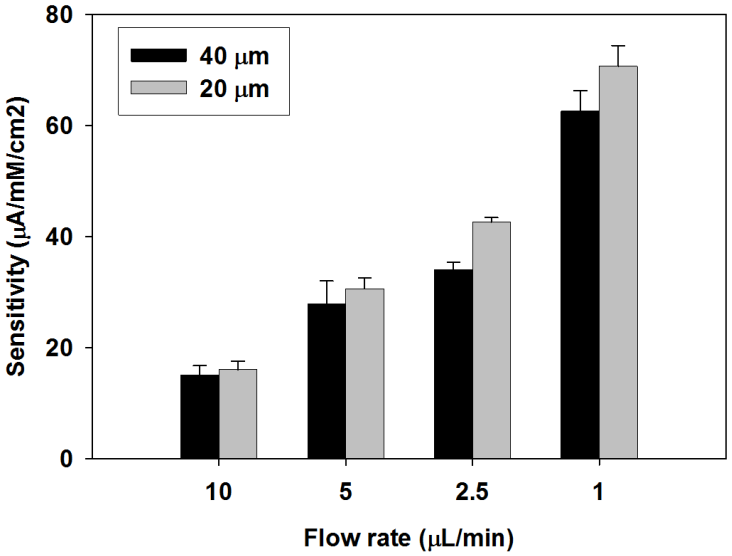

Figure 10.2: Summary of the sensitivities of the microfluidic biosensor of different channel height operated at different flow rates

10.3.2 Pulsed polymerization

Pulsed polymerization of polypyrrole has not been done until now for entrapment of enzymes. The pulsed methods are generally known to providing time for ions to replenish near the electrode surface and form better localized coatings [200]. This can be helpful in getting a more even polypyrrole coatings on the 3D nanopillars and also providing time for the larger glucose oxidase molecules to diffuse and get entrapped. The most critical factor in a pulsed deposition procedure is the T_{on} and T_{off} times. To start with we had equal time of T_{on} and T_{off}. The current response of biosensor prepared by electropolymerizing polypyrrole at different T_{on} and T_{off} is shown in Figure 10.3. As seen longer pulse widths of 500ms gave the highest response (~ 32 $\mu A/cm^2/mM$). When compared to results from the direct current deposition they were slightly better (~ 30 $\mu A/cm^2/mM$). But shorter pulsed reduced the overall biosensor sensitivity. Earlier studies

have shown that shorter pulses in the range of 100ms cause a more compact polypyrrole deposit [201]. Since entrapment of glucose oxidase needs a more porous deposit, larger pulses or the direct current is most suited for entrapment.

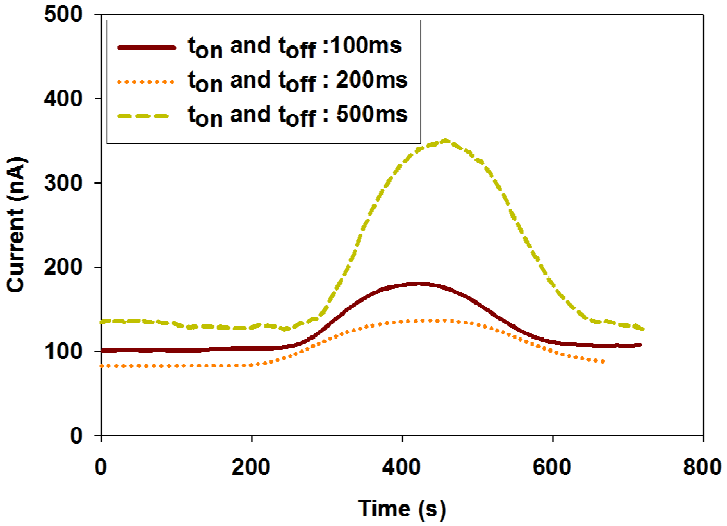

Figure 10.3: Current responses for 1mM glucose (speed 5µL/min) from biosensors prepared using pulsed electropolymerization techniques with different T_{on} and T_{off}

10.3.3 Reducing Interference

Figure 10.4 shows the response of the microfluidic biosensor for 0.5mM of ascorbic acid with the different anti-interference layers. The Figure 10.4 inset shows the response in bare 3D nanopillar electrodes. The first trials for reducing interference involved coating polypyrrole on the working electrode. The working electrode was coated with polypyrrole using the optimized parameters used in Chapter 9. The time of deposition was varied between 10 minutes to 30 minutes. The 30 minutes gave the best protection (see Figure 10. 4) but the current response signal also reduced to 75% of the bare electrode values. To improve this we used thinner polypyrrole coating (15 minute

deposition) and oxidized them into over-oxidized polypyrrole in 0.1M NaOH. Over-oxidized polypyrrole is known for its ability to act as a perm-selective membrane that can reject many of the interfering species [202]. The thinner over-oxidized polypyrrole was the most effective in reducing the interference. We were only able to coat Nafion by dropping a 5% solution of Nafion on top of the electrodes before attaching the PDMS channels. But this got mostly leached off in the flow channels. So the Nafion method was not effective in eliminating interference.

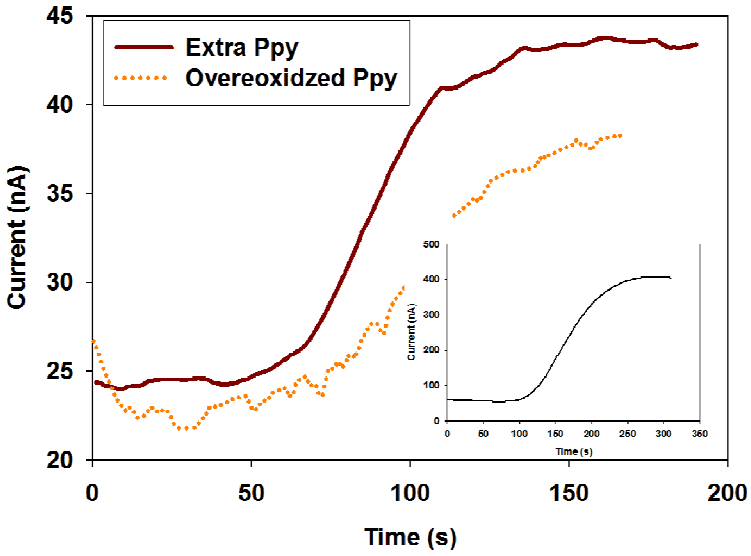

Figure 10.4: Current responses for 0.5mM of ascorbic acid with the different anti-interference layers, Inset shows the response in bare 3D nanopillar electrodes

10.3.4 Effect of GNP/polypyrrole on the microfluidic biosensor

The 2 -4 nm gold nanoparticles were used as they showed the most promising results in in Chapter 8. In case of microfluidic biosensor also there was very good improvement in stability of the glucose biosensor. There was almost no loss in activity of the biosensor after 60 days as seen in Figure 10.5.

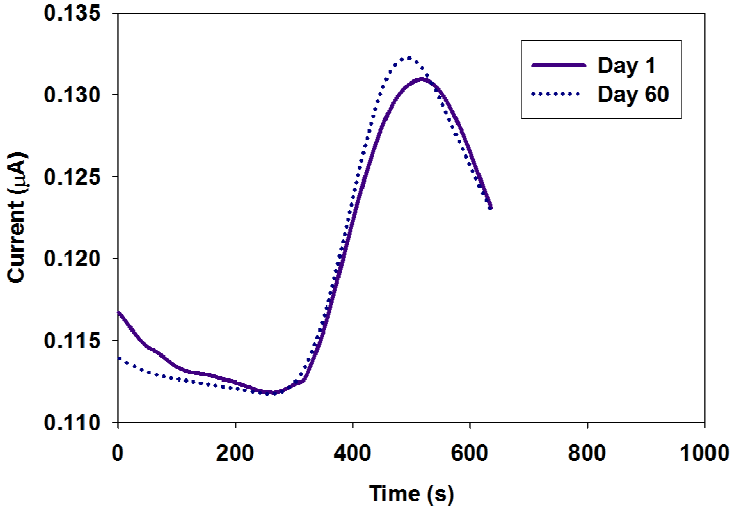

Figure 10.5: Amperometric response of the microfluidic glucose biosensor on a day after the glucose immobilization with GNPS and after 60 days

10.4 Conclusion

Channel dimensions did not have significant effect on the performance of the microfluidic biosensor with 3D nanopillars. The lower flow rates increased the sensitivity of the biosensor significantly. But the lower flow rate also made the detection much slower as the glucose took longer time to reach the electrodes. Only the larger 500ms pulsed deposition method gave good performance, but not significant enough to replace the direct current deposition done at half the time. Interference cannot be completely eliminated even using permselective coatings since the coatings are very thin. The most suitable method to eliminate interferences in these microfluidic biosensors will be modifying the electrode with materials having low hydrogen peroxide detection potential

10.5 Highlights of the microfludic biosensor studies

1) Polypyrole electropolymerization on 3D nanopillars inside microfluidic channels give a better glucose sensing performance

2) Pulsed polymerization with t_{on} : 500ms and t_{off} : 500ms gave good result, but direct deposition is much quicker
3) Height and width of the channel did not affect sensitivity of the biosensor
4) Speed of the analyte in the channel is an important factor that affects sensitivity and response time. So a proper speed must be chosen to have a quicker response time as well as higher sensitivity
5) Addition of gold nanoparticles in the polypyrrole deposit does also improve the stability of the microfluidic biosensor
6) Working electrode modifications are necessary to reduce interference and improve the linear range

SECTION IV

MODIFICATIONS OF THE WORKING ELECTRODE

The second electrode in the microfluidic channel is where the electro-active species generated at the enzyme electrode will be detected. This is called the 'working electrode' since the current changes at this electrode is important for quantifying the analyte concentration. This electrode is held at a potential where the electro-active species can readily react at the electrode surface. The electron transfer occurring during the reaction results in a current change. This current change corresponds to the concentration of electro-active species. Since the nanopillar electrodes surface area is large, the amount of current generated is also high and thereby making our biosensor highly sensitive.

Bare gold electrodes can also detect other interfering species at potentials needed to detect hydrogen peroxide. Use of mediators can reduce this working potential. As seen in the previous microfluidic studies overoxidized polypyrrole and a combination of mediator can reduce the effect of interfering species. In all the previous studies benzoquinone was used as the mediator. But all these diffusional mediators are not compatible with cell cultures as they have to be mixed in the media solution. Exposure to these mediators can be fatal for the cells. So we need electrode modifications on the 3D gold nanopillars that can either detect hydrogen peroxide directly at lower potentials or act as solid state redox mediators. So in this section the gold electrodes will be modified with materials that can improve the selectivity and avoid the use of diffusional mediators.

The choice of materials was based on its specificity to oxidize or reduce hydrogen peroxide. More specificity will results in reduced interference. Two materials chosen in this study were

a) Prussian Blue and

b) Poly Neutral Red

These materials were chosen as they are inexpensive and easy to deposit electrode modifications. Prussian Blue has high specificity for hydrogen peroxide detection. But this electrode modification is highly unstable in neutral pHs. If this material has to be used in a neutral pH cell culture media, its stability has to be improved. So we studied all the methods available to improve Prussian Blue stability in neutral pH conditions. We have summarized the results of these studies in Chapter 11.

The second material – polyneutral red is much more stable in neutral pHs. It can reduce hydrogen peroxide and also act as a solid state redox mediator that can transfer the electrons from the glucose oxidase molecules to the electrode. So we wanted to evaluate which of its property will be best for our microfluidic device. In chapter 12 we will discuss how an effective polyneutral red coating can be obtained on 3D nanopillars and the best mechanism by which we can detect glucose.

Of these two electrode modifications the better performing material will be chosen to build the final microfluidic biosensor for detecting glucose changes in media solution.

CHAPTER 11

EVALUATION OF METHODS USED TO IMPROVE THE STABILITY OF PRUSSIAN BLUE AND ITS ANALOGUES IN NEUTRAL MEDIA DURING HYDROGEN PEROXIDE REDUCTION

11.1 Introduction

Prussian Blue (PB) or Ferri ferrocyanide ($Fe(III)_4[Fe(II)(CN)_6]_3$) is a coordination compound with the Iron(III) atom coordinated to the nitrogen and the iron (II) atom coordinated to the carbon atoms. Prussian blue is known for selectively and electrocatalytically reducing hydrogen peroxide [90]. Since hydrogen peroxide is the byproduct of the oxidase based enzymes, PB offers a low-cost and effective solution for amperometric measurements. The main advantage of reducing hydrogen peroxide using PB is that the operating voltage can be set very low (i.e., 0V vs Ag-AgCl) [91]. At such a low operating potential it is less likely that non-specific species will interfere with intended measurements.

One problem with Prussian Blue, however, is its instability as a hydrogen peroxide transducer. In neutral media, the reduction of hydrogen peroxide produces hydroxyl ions $H_2O_2 + 2e^- \longrightarrow 2OH^-$. This reduction increases the pH and in turn solubilizes PB on the electrode surface [203]. So the stability of PB is always an issue when used for hydrogen peroxide reduction. Many attempts have been made to address this problem by coating a protective film of wither polyaniline, polypyrrole, poly (3,4-ethylene-dioxythiophene) (PEDOT) [204], Nafion [205] or chitosan [206] on Prussian blue.

Nanocomposites of polypyrrole and Prussian blue have been shown to improve the stability of PB [207] since polypyrrole helps prevent Prussian blue from decomposition at the presence of OH^- ions. A recent study also showed that the hybrid films of Prussian blue and polyaniline were stable at a higher pH condition [208]. The stability of Prussian blue can also be improved by forming nanocomposites with CNTs [209]. Besides Prussian blue, other metal hexacyanoferrate materials and mixed-metal hexacyanoferrate such as copper hexacyanoferrate (CuHCF) [210] and copper-palladium hexacyanoferrate (CuPd HCF) [211] have been demonstrated as electrodes for glucose detection.

One concern for these available protection methods is that the stability tests for these PB modified electrodes are often performed in solution either with a pH of less than 6 or with higher buffer concentration. Moreover, these tests have so far not been done for continuous long term measurements. This means that these protection methods have not been tested in culture media. So the question we ask is: will the protection methods still be effective in culture media like environment such as 1 mM buffer solution at pH of 7.2?

Very little information is present in the literature on mechanism by which these protection methods improve the stability of PB. Based on the possible routes in which these protection methods function as discussed in the literature, we hypothesize that the protection mechanism is either by shielding the PB (as in case of conducting polymers) or by acting as a buffer layer neutralizing the OH^- ions.

In this study we first evaluated several different metal hexacyanoferrates such as PB, CuHCF and CuPd HCF and their stability at neutral pH. Of these hexacyanoferrates, the one showing the best stability was further analyzed for its protective effectiveness.

Besides these individual species, hybrid materials of hexaxyanoferrate and conducting polymer (i.e polypyrrole, polyaniline and PEDOT) were also tested. We chose chitosan and Polyethylenimine (PEI) as the materials for protecting metal hexacyanoferrate nanoparticles by its buffering action. Chitosan and PEI were chosen for that the positive surface charges of both these cationic polymers can balance off the negatively charged OH^- ions. We prepared the hexacyanoferrates in the form of nanoparticles in order to offer a high surface area for this purpose. Furthermore, we coated metal hexacyanoferrates on top of a self-assembled monolayer as an additional step to improve the stability of metal hexacyanoferrates [212]. Figure 11.1 shows the different protection schemes we tested in this study. Most of the procedures used to prepare the metal hexacyanoferrates were modified from existing methods to suit our unique 3D nanopillar structures, but some (e.g., chitosan protected PB, PEI coated PB) were tested for the first time. The stability of the materials prepared were evaluated using cyclic voltammetric and amperometric measurements with and without the presence of hydrogen peroxide.

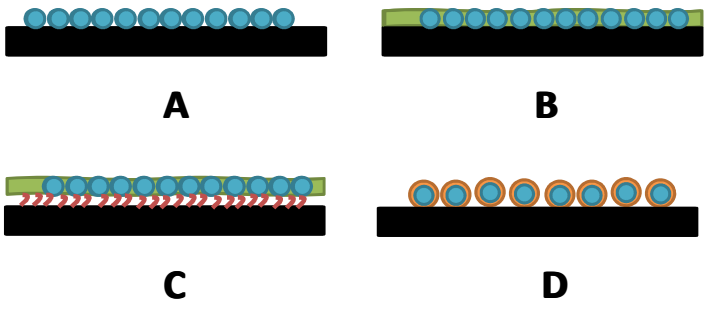

A – Prussian Blue analogues nanoparticles only on electrode
B – Co-deposit of Prussian blue analogue and conducting polymer
C – Prussian blue analogue deposit on SAM layer
D – Each Prussian blue nanoparticles protected with polymer coating

Figure 11.1: Schematic of the different protection method tested in this study

11.2 Experimental methods

11.2.1 Chemicals

Pyrrole, Aniline, 3,4-ethylenedioxythiophene (EDOT), chitosan and Polyethylenimine (PEI) were purchased from Sigma-Aldrich (St Louis, MO, USA). Potassium ferrocyanide, Potassium ferricyanide, Copper (II) Chloride, Palladium chloride, Nickel Chloride, Hydrochloric acid, Phosphoric acid and Potassium hydroxide was purchased from Fisher scientific.

11.2.2 Electrochemical setup

A conventional three-electrode electrochemical cell consisting of a Pt-wire counter electrode and an Ag/AgCl reference electrode was used for the electrochemical processes, and a Princeton VersaSTAT MC electrochemical system (Oak Ridge, TN, USA) was used for electrochemical measurements.

11.2.3 Preparation of Nanostructure electrodes

3D electrodes with 50 nm nanopillars were formed on glass substrates using the thin film alumina templates previously described in Chapter 4.2.2.

11.2.4 Electrochemical deposition of PB

Electrochemical deposition of PB was carried out in a solution of 2.5 mM $K_3Fe(CN)_6$, 2.5mM $FeCl_3$, 0.1M HCl, and 0.1M KCl at a potential of 0.4mA/cm^2 . The electrodeposition was done through anodized alumina pores to obtain PB nanopillars. To obtain a thin layer of PB onto 3D gold nanopillars, a pulsed current of 0.4 mA/cm^2 was applied with t_{on}: 100 ms and t_{off}: 400 ms in the same electrolyte solution. After

electrodeposition the samples were activated in 0.1M KCl and 0.1M HCl by performing cyclic voltammetry between −0.1 V to 0.4 V at a sweep rate of 50 mV/s.

11.2.5 Electrochemical deposition of Polymers on PB

Polypyrrole and PB was electrodeposited from an electrolyte containing 0.1M KCl, 0.05M pyrrole and 10mM $K_3Fe(CN)_6$ by cyclic voltammetry performed at a scan rate of 50mV/s and a potential range of -0.3V to 0.7V .

11.2.6 Chemical deposition of PB and its analoques

PB nanoparticles were coated onto 3D gold nanopillars using a chemical deposition process containing Potassium ferrocyanide [213,214]. In this method the 3D nanopillar electrodes were dipped sequentially into solutions of

1) 0.1M KCl / 10mM $K_4Fe(CN)_6$ (pH adjusted to 3 with HCl)

2) 0.1M KCl / 10mM $FeCl_3.6H_2O$ (pH adjusted to 3 with KOH) and

3) 0.1M KCL (pH 3.0)

The samples are immersed for 1 minute in each of the solutions which were constantly stirred. This dipping process is repeated three times. The coated samples were heat treated at 100°C for 1 hour after the deposition process. CuHCF was also deposited onto 3D gold nanopillars through a similar dipping method except that the second dipping solution was changed to 0.1M KCl/ 10mM $CuCl_2$ with a pH of 3. In the case of CU-Pd HCF the second dipping solution was a mixture of 5mM $CuCl_2$ and 5mM $PdCl_2$.

11.2.7 Chemical deposition of PB/polymer

Interfacial chemical deposition of PB and analogues along with conducting polymers was done similar to the method described earlier [215]. The 3D nanopillar samples were dipped sequentially into solutions of

1) 0.1M KCl/0.05M Pyrrole or EDOT or aniline

2) 0.1M KCl / 10mM $K_4Fe(CN)_6$ (pH adjusted to 1.5 with HCl)

3) 0.1M KCl / 10mM $FeCl_3.6H_2O$ (pH adjusted to 1.5)

For preparing copper hexacyanoferrate based films the second solution was replaced with 0.1M KCl/ 10mM $CuCl_2$. In case of CU-Pd HCF the second dipping solution was a mixture of 5mM $CuCl_2$ and 5mM $PdCl_2$. The solutions were mildly stirred and the dipping time in each of solution was 1 minute.

11.2.8 Formation of SAM coated 3D electrodes for PB deposition

To coat cysteamine SAM, the 3D nanostructures were immersed in ethanol solution containing 2.5 mM cysteamine SAM for 24 hours. After that, the nanostructures were removed and rinsed thoroughly in ethanol and then water. Several different types of PB and their analogues were coated on top of the SAM coated 3D electrodes.

11.2.9 Chitosan based PB/CuHCF nanoparticle synthesis

PB nanoparticles were prepared by mixing 1mM $K_3Fe(CN)_6$ solution (in 0.1% HCl) and 1mM Chitosan solution (in 0.1% HCl) in dark at 60°C for 3 hours, based on the method described by Ding et al [216]. Extra chitosan was added to increase the concentration of chitosan by 0.5% in the PB nanoparticle solution. Chitosan with nanoparticles was deposited on the gold nanopillars by applying a potential of -1V for 2 minutes [217]. Chitosan protected CuHCF nanoparticles were prepared by mixing 1mM

$CuCl_2$ and 1mM $K_3Fe(CN)_6$ in 1mM chitosan solution, similar to the method used in preparing chitosan coated PB nanoparticles [218].

11.2.10 PEI coated PB nanoparticles on ITO electrodes

Coating of PEI onto PB nanoparticles was done using the method detailed by Zhai et al [219]. Starting with a solution of 10mM $FeCl_3$, 10mM $K_3Fe(CN)_6$, and 0.1M KCl at a pH 1.12, 3 mL of solution containing 0.125 g of PEI was added and refluxed for 30 minutes until PB nanoparticles were formed. Since the PEI was positively charged, we electrostatically adsorbed the PEI coated PB onto sheets of flat Indium Tin Oxide (ITO) carrying negative surface charges and used them as electrodes (sheet resistance of 5 – 10 Ω/cm^2). To do so, ITO sheets were dipped into the solution containing the PEI coated PB for 30 minutes followed by washing in copious amount of water.

11.2.11 Electrochemical characterization

Cyclic voltammetry (CV) analyses were performed for the PB deposited 3D electrodes in a three-electrode electrochemical cell in 10mM phosphate buffer solution (PBS) with a pH 7.2. After that, similar CV analyses were performed in a solution of 10mM PBS and 1mM H_2O_2. Most of the CV measurements were performed by scanning the potential from -0.2 V to 0.5 V at a scan rate of 50 mV/s. In some cases (e.g., for assessing PB deposits on the surface of the 3D electrodes and examining the reaction processes) CVs were measured by changing the scan rates from 10 mV/s to 100 mV/s in 10mM PBS.

Amperometric measurements were made in 10mM PBS (pH 7.2) with a certain amount of hydrogen peroxide at a constant electrode potential of -100 mV (vs. Ag-AgCl

reference). During the amperometric experiment, the solution was stirred constantly for ensuring instant equilibrium for mass transport. In each test run, the background current was allowed to stabilize before a 10µl of 1M H_2O_2 was added to 20ml of PBS. After the amperometric current response reached a steady-state, another drop of glucose was added and the corresponding current response was measured until a new steady state was reached. Each incremental drop of H_2O_2 increased the H_2O_2 concentration of approximately 0.5 mM.

SEM images of the PB coated samples were obtained from S-4800 Field Emission Scanning Electron Microscope (Hitachi). Energy dispersive x-ray analysis (EDAX) was used to determine the chemical composition of the PB coated electrodes.

11.3 Results and discussions

Figure 11.2A shows an SEM image of a 3D gold nanostructure formed on glass substrates. The height of the nanopillars was controlled to give rise to an increase in surface area of about 15 times with respect to the projected area. Figure 11.2B shows an SEM image of a PB coated 3D nanostructure, Figure 11.2C shows an SEM image of a PB PB nanoparticle coated 3D nanostructures, and Figure 11.2D shows an SEM image of a PB /polypyrrole co-coated 3D nanostructure. In these experiments, we also tried to coat additional layers of the protective films but found that the extra coating did not yield any improvement in terms of stability. So all the results discussed here are for thin coatings that just cover the gold nanopillars without compromising much the increased surface area.

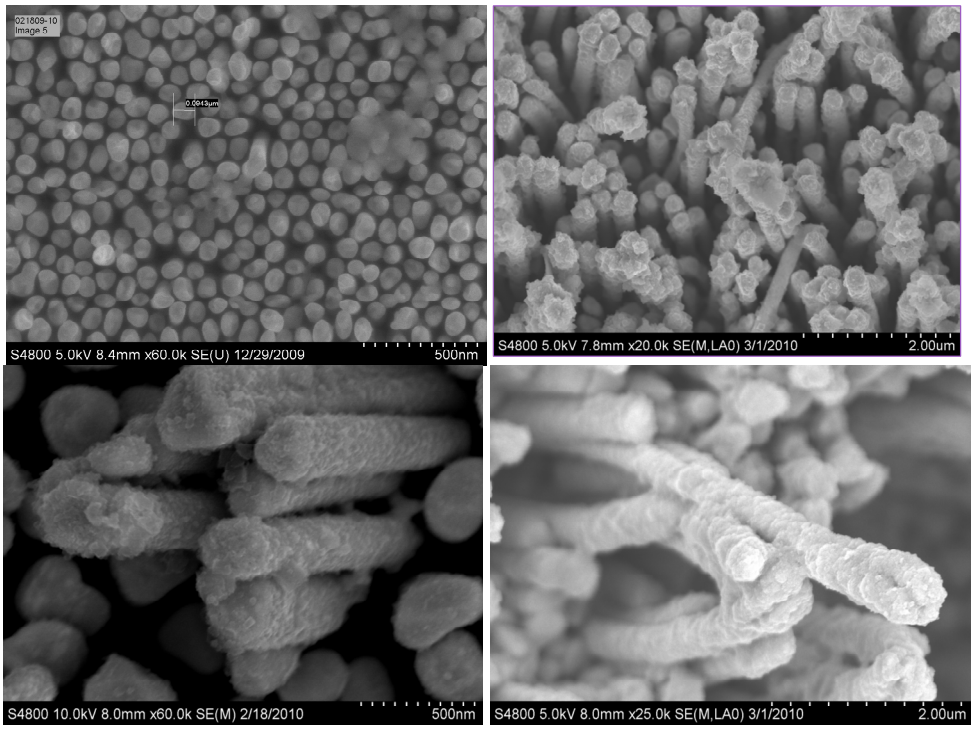

Figure 11.2: (A) 3D gold nanopillars on glass templates (B) PB electrodeposited on gold nanopillars (C) PB nanoparticles coated on gold nanopillars using chemical deposition method (D) PB/polypyrrole codeposited by chemical deposition method

11.3.1 Stability of PB only (Electrochemical and Chemical deposition)

We first examined if the electrochemically or chemically deposited PB was stable in PBS at pH 6. Electrochemically deposition was done on the gold nanopillars and also inside porous alumina templates. The alumina templates were dissolved in mixture of 6% wt phosphoric acid and 1.8% chromic acid leaving 3D PB nanopillar structures. Of all the Prussian blue and its analogues tried in this study, the 3D electrodes coated with PB alone showed the largest linear range of response for hydrogen peroxide. Figure 11.3A shows the amperometric response of the PB nanopillars. However, a servere reduction in both

the oxidation and reduction peaks can be seen in Figure 11.3B for the PB coated nanopillars. Since in this case only the loss of material can account for the reduction in the peaks, this fact suggests that a large amount of PB may leach out from the nanopillars during tests.

On the other hand, PB deposited chemically on gold nanostructures had better stability, especially after heat treatment at 100°C for 1 hour. Figure 11.3C shows some measured CV curves in PBS (pH 6) at several scan rates. Since anodic or cathodic peak current was linearly proportional to the scan rate, it can be concluded that the electron transfer process was a kinetic controlled process rather than a diffusion controlled process. The amperometric currents measured in PBS (pH 6) show that the chemically deposited PB was stable at this lower pH, albeit with a smaller linear range (Figure 11.3D). But at pH 7.2, the PB lost its activity very fast as it can be seen in the CVs curves in Figure 11.3E, where CV curves of consecutive cycles are shown. A reduction in redox peak current with increasing cycles suggests again a loss of PB. Even without addition of H_2O_2 the electrode lost its activity and this loss was further accelerated when 1mM of H_2O_2 was added to the solution. These results point to the fact that at pH 6 chemically deposited PB is much more stable than electrochemically deposited PB. But unprotect PB - either electrochemically deposited or chemically deposited, has poor stability in neutral pHs.

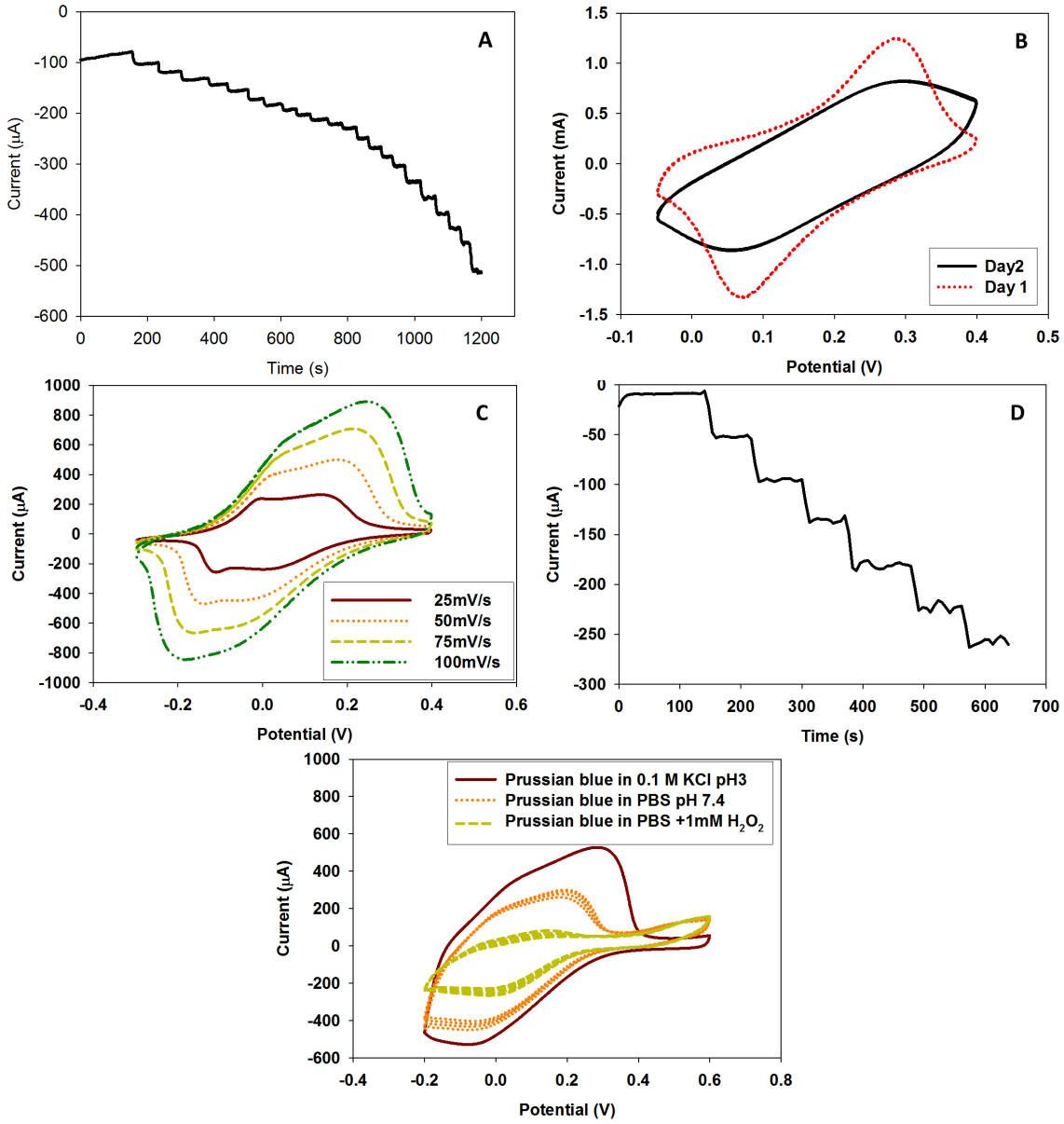

Figure 11.3: (A) Amperometric measurement of electrochemically deposited PB nanorods. (B) Stability of the nanorods studies using CV in PBS (pH-6) (C) CVs at different scan rate for the chemically deposited PB nanoparticles. (D) Amperometric measurements of the chemically deposited PB nanoparticles (E) Stability of chemically deposited PB nanoparticles in PBS at neutral buffer and with H_2O_2

11.3.2 Stability of Copper, Copper/Palladium analogues

The copper analogue of PB is copper hexacyanoferrate (CuHCF) and it is known to have higher stability than PB [203]. The CV (Figure 11.4 A) and amperometric (Figure 11.5A) measurements of CuHCF in 10mM PBS at pH of 7.2 show only a small amount of loss in activity in neutral pHs. The current peak of the 10^{th} cycle drops approximately 15% compared with the peak of the first cycle. Similarly the drift in amperometric current response is very small. Similarly, mixed metal hexacyanoferrate such as the Copper/Palladium hexacyanoferrate (Cu-Pd HCF) also showed a high stability at neutral pH [211]. These results showed that at neutral pH, CuHCF and Cu-Pd HCF had much better stability than PB, even in the presence of H_2O_2. But a decrease in stability is observed as the concentration of hydrogen peroxide increases.

11.3.3 Stability of conducting polymer/ PB analogues

We first examined the stability of electrochemically co-deposited PB/polymer, and found that this approach did not yield any better stability for PB (in PBS at pH 7.2; Figure 11.4 B); the stability was similar to that of directly deposited PB. Since it was clearly seen that the any electrochemical deposition have inferior stability when compared to the chemical deposition method, we proceeded to test the rest of the protection method using chemical deposition methods.

Figures 11.4C to Figure 11.4F show the CV results of chemically co-deposited CuHCF or CU-Pd HCF with conducting polymers like polyaniline, polypyrrole, or PEDOT. The stability of these materials in PBS was found to be fairly good. Almost no change in the CV peak currents was seen after 10 cycles. In the presence of 1 mM H_2O_2,

however, the decrease in peak currents was less than 15% in all the cases. Compared with unprotected CuHCF, the change in the peak current after addition of H_2O_2 was higher in the case of polymer protected samples. This can be attributed to the presence of the conducting polymers that may enhance the electron transfer between CuHCF and electrode surface. Amperometric results of these samples are given in Figures 11.4A and 5B. The most stable readings were for the polypyrrole/CuHCF hybrid samples. Cu-Pd HCF hybrid samples had higher sensitivity as seen in the unprotected samples. The results for the PEDOT hybrid material are not much different from unprotected hexacyanoferrate samples, owing that the low solubility of PEDOT might have reduced the effective incorporation of the polymer. In summary, the CuHCF conducting polymer hybrid materials did improve the stability in PBS at pH 7.2, although a less loss in stability was achieved for repeated runs.

While it is still not clear how conducting polymers protect the PB analogues from dissolving into solution when the local pH increases due to hydrogen peroxide reduction , we speculate that the polymers may form a physical barrier to prevent the material from dissolution. Further work is necessary to elucidate the protection mechanism such that the stability of these protective methods can be improved.

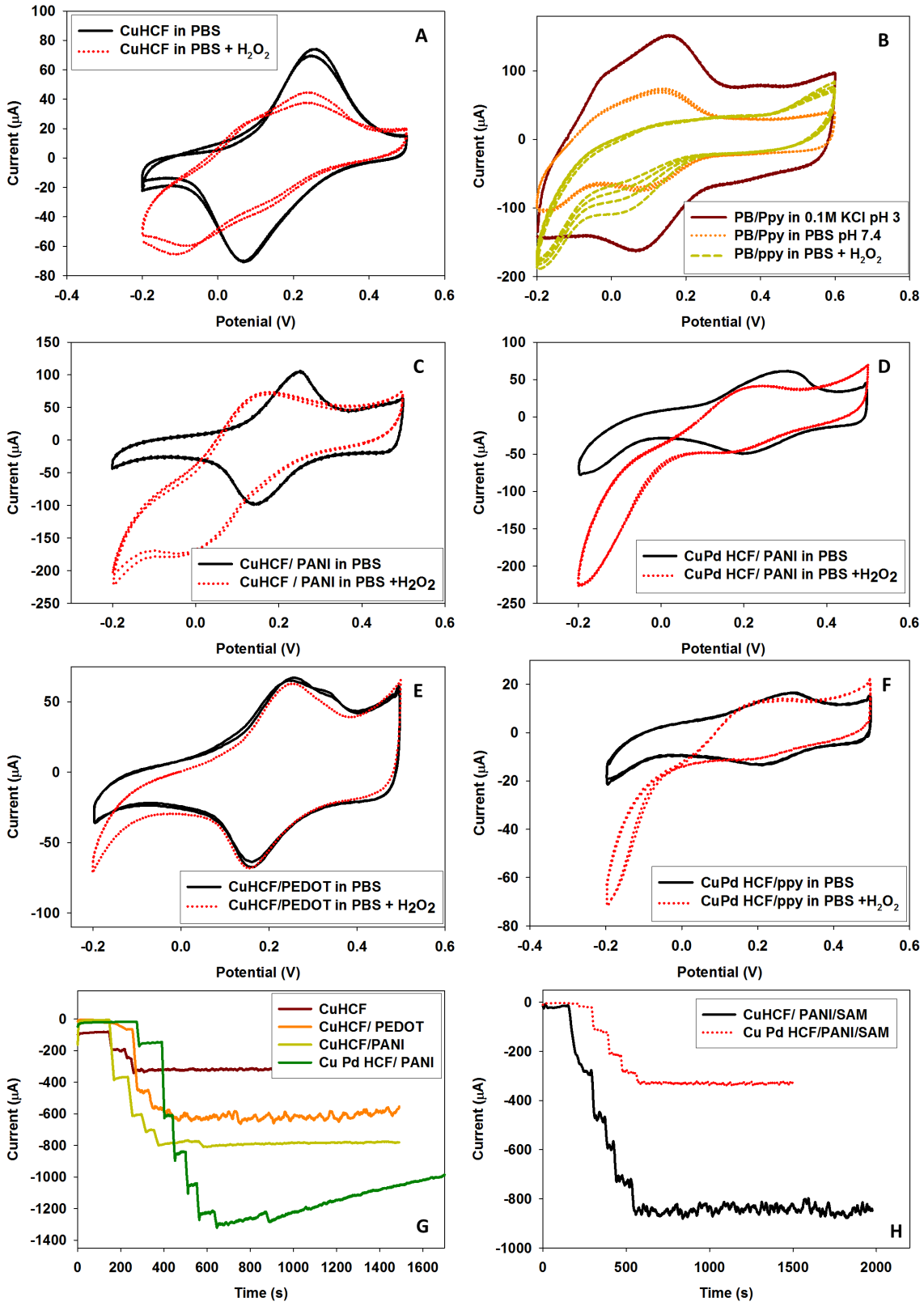
A
CuHCF in PBS
CuHCF in PBS + H2O2
Current (µA)
Potenial (V)
B
PB/Ppy in 0.1M KCl pH 3
PB/Ppy in PBS pH 7.4
PB/ppy in PBS + H2O2
Current (µA)
Potential (V)
C
CuHCF/ PANI in PBS
CuHCF / PANI in PBS +H2O2
Current (µA)
Potential (V)
D
CuPd HCF/ PANI in PBS
CuPd HCF/ PANI in PBS +H2O2
Current (µA)
Potential (V)
E
CuHCF/PEDOT in PBS
CuHCF/PEDOT in PBS + H2O2
Current (µA)
Potential (V)
F
CuPd HCF/ppy in PBS
CuPd HCF/ppy in PBS +H2O2
Current (µA)
Potential (V)
G
CuHCF
CuHCF/ PEDOT
CuHCF/PANI
Cu Pd HCF/ PANI
Current (µA)
Time (s)
H
CuHCF/ PANI/SAM
Cu Pd HCF/PANI/SAM
Current (µA)
Time (s)

Figure 11.4: CVs of (A) CuHCF , (B) PB/PPy, (C) CuHCF/PANI, (D) Cu-Pd HCF/PANI, (E) CuHCF/PEDOT, (F) CuHCF/PPy in PBS (pH7.2) and H_2O_2, Amperometric response for hydrogen peroxide of (G) All CuPD HCF/CuHCF/ polymer hybrids except CuHCF/PPy and (H) CuHCF/PPy

Now let us have a look of how effective the formation of hybrid materials using the chemical deposition method. Figure 11.5 shows the characterization of the Polypyrrole/CuHCF coated electrodes using cyclic voltammetry at different scan rates. The linear relationship between the peak current and the scan rate suggests a kinetics limited electrochemical process, thus confirming that the Polypyrrole/CuHCF hybrids have been effective formed on the surface of the gold nanopillar electrodes. Similar CV results are observed with the other hybrid materials. SEM images (Figure 11.6A) and EDAX results (Figure 11.6B) support these arguments as the electrodes are seen to have a smooth coating on top of gold nanopillars and the coated hybrid material consists of multiple chemical compositions.

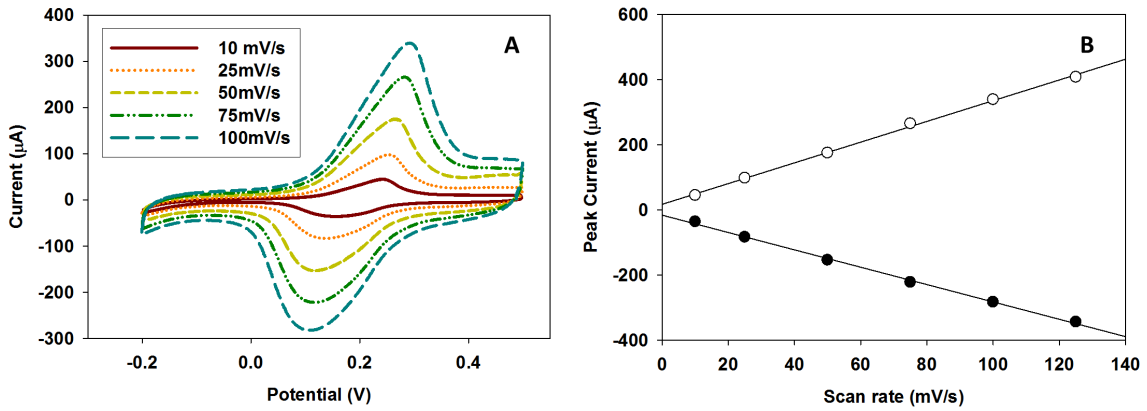

Figure 11.5: (A) CV of CuHCF/PPy in PBS at different scan rates (B) The peaks current from the CVs vs scan rates for the CuHCF/PPy sample

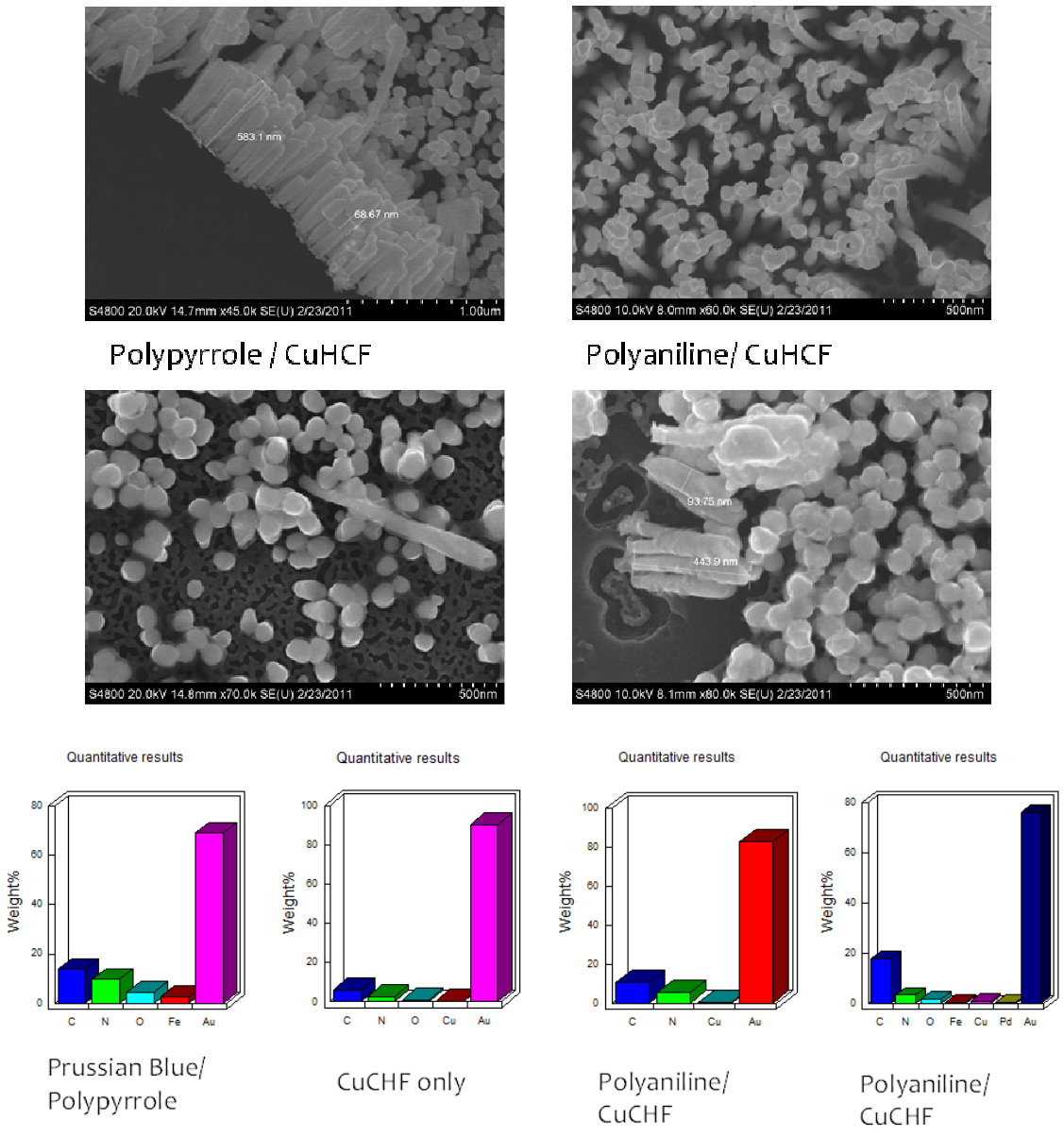

Figure 11.6: SEM images of CuHCF/PPy and CuHCF/PANI coated nanopillars and EDX elemental analysis of the various deposits

11.3.4 Stability of PB analogues on self-assembled monolayers (SAM)

SAM layers have been shown earlier to improve the stability of metal hexacyanoferrates when coated on top of them, especially SAMs with amine groups which are known to possess positive charges [212]. Following this idea, we used cysteamine SAM to provide the amine terminated ends for better CuHCF deposition. Figure 11.7 shows the deposition of CuHCF/polyaniline hybrid onto cysteamine SAM treated gold 3D electrodes. Clearly, the change in peak currents between cycles during CV experiments (Figure 11.7A) in PBS in the presence of H_2O_2 was very small (<5%). The amperometric results also showed very stable results, albeit with a lot of noise. The change in peak current with addition of hydrogen peroxide was also relatively small. The response time of the amperometric current was fast when compared with that for the case without SAM. Both these can be due to the diffusional resistance from the closely packed SAM layers. CuPd HCF samples had an odd amperometric response: more current change is seen at the second addition of 1mM of H_2O_2 than the first addition, implying a non-linear current response when the Cu-Pd HCF hybrid material is coated on top of the SAM layer. It is thus clear that even though the SAM coating improved the stability of CuHCF hybrid materials, the diffusional resistance of SAM to electron transfer may negate the overall benefit.

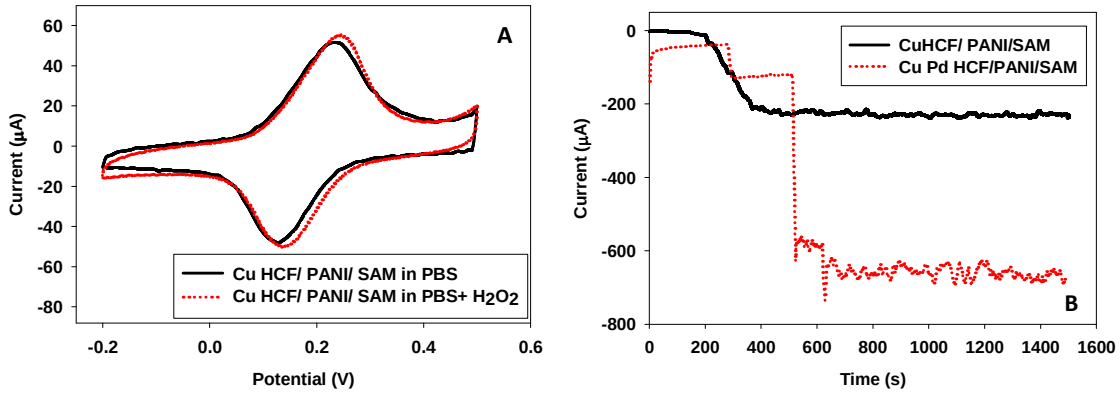

Figure 11.7: (A) CV of SAM/CuHCF/PANI done in PBS (pH7.2) and in presence of H_2O_2 (B) Amperometric responses of SAM/CuHCF/PANI and SAM/Cu-Pd HCF/PANI

11.3.5 Stability of PB nanoparticles covered by protective film

In this method, individual PB or CuHCF nanoparticles were prepared with a coating of chitosan or PEI. Chitosan, a polysaccharide, was chosen because it is known to protect PB [212] due to the presence of amine groups, making it a polycationic polymer. This cationic nature enables it to act as buffer to regulate the pH around the PB nanoparticles. Under this hypothesis, the performance of the PB coated chitosan deposited onto gold nanopillars was tested using the CV and amperometric studies. As seen from CV results (Figure 11.8A) the amount of PB deposited using this method is relatively small when compared with the previous methods. But the amperometric results were relatively higher in the presence of H_2O_2. We believe there is also reduction of hydrogen peroxide by the exposed gold nanopillars [220]. The Prussian blue formed by this method was not very stable (as seen from the drift in amperometric results) contrary to our earlier hypothesis. This may be attributed to the fact that at a pKa value of 6.5, the amount protonated amines available in chitosan is much less than that at neutral pH.

PEI is a cationic polymer having primary, secondary and tertiary amines with a pKa value around 9, 8 and 6-7, respectively. So PEI is bound to have more cationic species that can act as a buffer at neutral pHs. Thus PEI coated PB nanoparticles with positive surface charges were coated electrostatically onto negatively charged flat ITO substrates. Figure 11.8B (what about 8A, 8C?) shows a CV curve where a more pronounced oxidation peak is present possibly due to the positive surface charges. The amperometric results (Figure 11.8D) showed a drift and loss of signal in the presence of hydrogen peroxide, possibly due to the still large size of the PB nanoparticles which is estimated to be 50 nm [219]. We thus speculate that smaller PB nanoparticles may provide better buffering effect and thus a better stability.

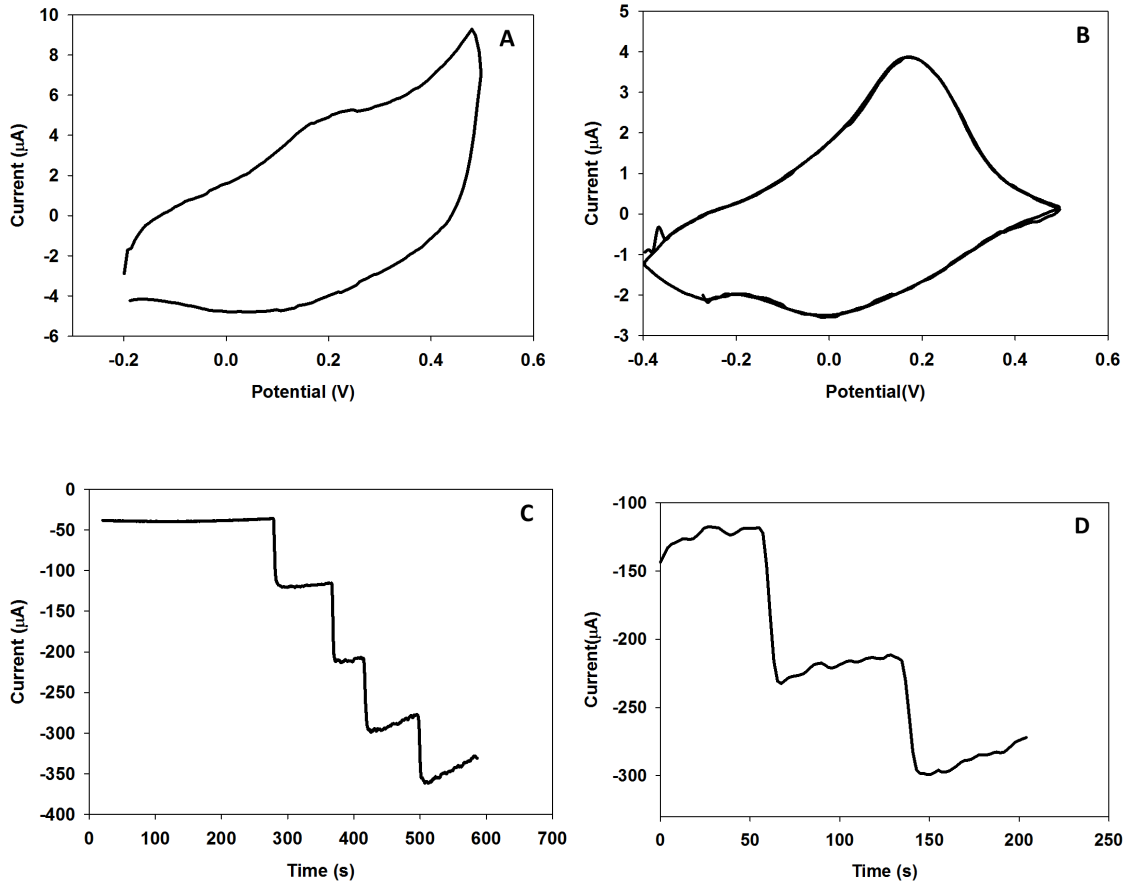

Figure 11.8: (A) CV of chitosan coated PB done in PBS (pH7.2) (B) CV of PEI coated PB done in PBS (pH7.2) (C) Amperometric responses of chitosan coated PB for hydrogen peroxide (D) Amperometric responses of PEI coated PB for hydrogen peroxide

11.3.6 Stability in cell culture media

Figure 11.8 shows the stability of CuHCF/polypyrrole and CuHCF/aniline/SAM in cell culture media. In cell media, these materials which showed higher stability in 10mM PBS at pH 7.2 exhibited very poor stability. Without the presence of hydrogen peroxide, the stability was poor, and with the presence of hydrogen peroxide the stability became

even worse. In actual culture media, all these protection methods fail to deliver acceptable outcomes.

11.4 Conclusion

Of the different PB and anaologues tested in this study CuHCF was a more stable electrode material for hydrogen peroxide reduction in neutral buffer solution. Of the different protection methods used, co-deposition of conducting polymer- CuHCF yielded better stability. Presence of SAM on electrode surface also improved the CuHCF stability, but a loss of signal and linearity occurred due to the SAM layer. Other protective coatings such as chitosan and PEI (based on their surface charges to act as buffer) did not show any desirable stability. Even the most stable methods in neutral buffer solutions were not able to replicate their stability in cell culture media. The existing methods that are available to increase the stability of PB and its analogues during hydrogen peroxide reduction do not show satisfactory performance.

CHAPTER 12

DEVELOPMENT OF POLYNEUTRAL RED BASED ELECTRODES FOR MONITORING GLUCOSE IN CELL CULTURE MEDIA

12.1 Introduction

The second approach used for electrode modification was polyneutral red (PNR). The monomer neutral red is a phenazine dye (N^8,N^8,3-trimethylphenazine-2,8,-diamine) with redox properties. The polyphenazines are interesting polymers because of their tendency to act as conducting polymers and at the same time as a redox mediator [221]. There have already been various reports using PNR as a redox mediator in electrochemical biosensors [222-224]. It is also used for detecting hydrogen peroxide along with horseradish peroxidase HRP enzyme [225]. PNR and PEDOT were co-deposited on carbon electrodes and used for hydrogen peroxide detection [226]. Since they have properties similar to conducting polymers they have also been demonstrated to entrap enzymes [225,227].

With the existing knowledge on PNR materials, it is clear that it can be used either as a hydrogen peroxide sensor or as a redox mediator. In this study we intended to investigate whether PNR coatings on 3D nanopillar electrodes are more effective as a hydrogen peroxide transducer or as a direct redox mediator (See Figure 11.3 for both the transducing mechanisms). We deposited PNR on 3D gold nanopillar electrodes in an electrochemical procedure tailored for our 3D nanostructures in a microfluidic setup. PNR and PNR/PEDOT polymers coated on the 3D electrodes were tested for hydrogen

peroxide transduction. For investigating the redox mediating capability, glucose oxidase was immobilized using the entrapment method during electro-polymerization.

12.2 Experimental methods

12.2.1 Electropolymerization of PEDOT

The electropolymerization of neutral red was carried out by means of the cyclic voltammetry in a solution consisting of 1 – 5mM neutral red, 0.1M KNO_3 and 25mM (KH_2PO_4/K_2HPO_4) phosphate buffer with a pH of 6 [224] . The potential range was varied between -1V to 1V at a scan rate of 50mV/s.

12.2.2 Electropolymerization of PEDOT/PNR

The electropolymerization of the co-polymer was performed by using the reported process [226] with modifications. PNR and PEDOT was copolymerized using cyclic voltammetry in solution containing 0.5 mM neutral red, 5mM EDOT, 0.1M KNO_3 and 25mM (KH_2PO_4/K_2HPO_4) phosphate buffer with a pH of 6. During preparation of the electrolyte solution the EDOT took almost 2 hours to fully dissolve in the electrolyte while the solution was de-aerated continuously with nitrogen gas. The potential range for cyclic voltammetry was varied between -1.2V to 1V at a scan rate of 50mV/s.

11.2.3 Electropolymerization with Glucose Oxidase

Electropolymerization of PNR and PNR/PEDOT copolymer was carried out in the presence of glucose oxidase. The same electrolytes as in two previous methods with addition of 1mg/ml glucose oxidase were used.

11.2.4 Electrochemical characterization

Cyclic voltammetry (CV) analyses were performed for the PNR deposited 3D electrodes in a three-electrode electrochemical cell in 1 mM phosphate buffer solution (PBS) at pH 7.2 or 1X Minimum Essential Medium (MEM) solution. All the CV measurements were performed by scanning the potential from -1 V to 0.5 V at a scan rate of 50 mV/s. Amperometric measurements were made in 1 mM PBS (pH 7.2) and the MEM media solution at a constant electrode potential of -400 mV (vs. Ag-AgCl reference). Hydrogen peroxide and glucose concentration in the solution was incremented by 0.5mM and 1mM respectively.

11.2.5 Microfluidic measurements

Electropolymerization was conducted inside microchannels similar to the procedure used for polypyrrole in Chapter 7. PNR was also deposited on 3D nanopillar electrodes outside the channel and then the mold of PDMS channels were mounted to complete the device. To mount the PDMS mold, PDMS curing agent was first spin coated [228] on a glass slide at speeds of 6000 rpm, and binding surface of the PDMS mold is stamped on the spun-coated curing agent. After that the PDMS mold is quickly removed and placed onto the chip containing the 3D electrodes. The completed device is conditioned at 100 °C for 1 hr before further use. Because of the heating at 100 °C, it was necessary to know if the heating process had any negative effect on the PNR. This was done by performing CVs in PBS before and after the heat treatment with the loss of redox peaks due to heating quantified.

Amperometric measurements were also taken in the microfluidic channel using methods described in Chapter 7. Initially the microfluidic device was used to perform

hydrogen peroxide measurements. Then for testing glucose, the enzyme electrode was created by depositing glucose oxidase using electropolymerization of polypyrrole as mentioned in Chapter. The PNR coated electrode was used as the working electrode.

12.3 Results and discussions

12.3.1 PNR deposit

Polyneutral red (PNR) can be obtained by electropolymerization of neutral red. The polymerization reaction starts initially with the formation of the cationic radical by electrochemical oxidation. The number of radicals formed during oxidation controls the structure of the polymer obtained. Therefore the electropolymerization of neutral red depends on the applied potential and also the pH of the electrolyte [229].

Electropolymerization of PNR has been mainly done by performing cyclic voltammograms between -1V to 1V (vs Ag-AgCl) in an electrolyte containing neutral red monomer and nitrate ion based supporting electrolyte [224]. Nitrate ions are known to form better films at more neutral pHs [230]. So in this study also we used potassium nitrate as the supporting electrolyte. The oxidation of neutral red starts at an anodic potential of 0.7V and shifts to more positive potentials with increasing cyclic voltammetric scans [231] . The electropolymerization of PNR on the 3D nanopillars were done by performing the CV scans -0.9V to 0.75V (vs Ag-AgCl). Because a higher anodic potential would lead to more deposition completely masking the surfaces of 3D nanopillars, we set the upper bound for the anodic potential in CVs to 0.75 V (vs Ag/AgCl). Figure 12.1A shows some typical CV cycle curves during electropolymerization of neutral red on 3D nanopillars. The redox peaks around −0.7 and

−0.4 V, due to neutral red leuco–neutral red reduction–oxidation, increase as the number of CV cycles increases, indicateing the growth of the PNR film [231].

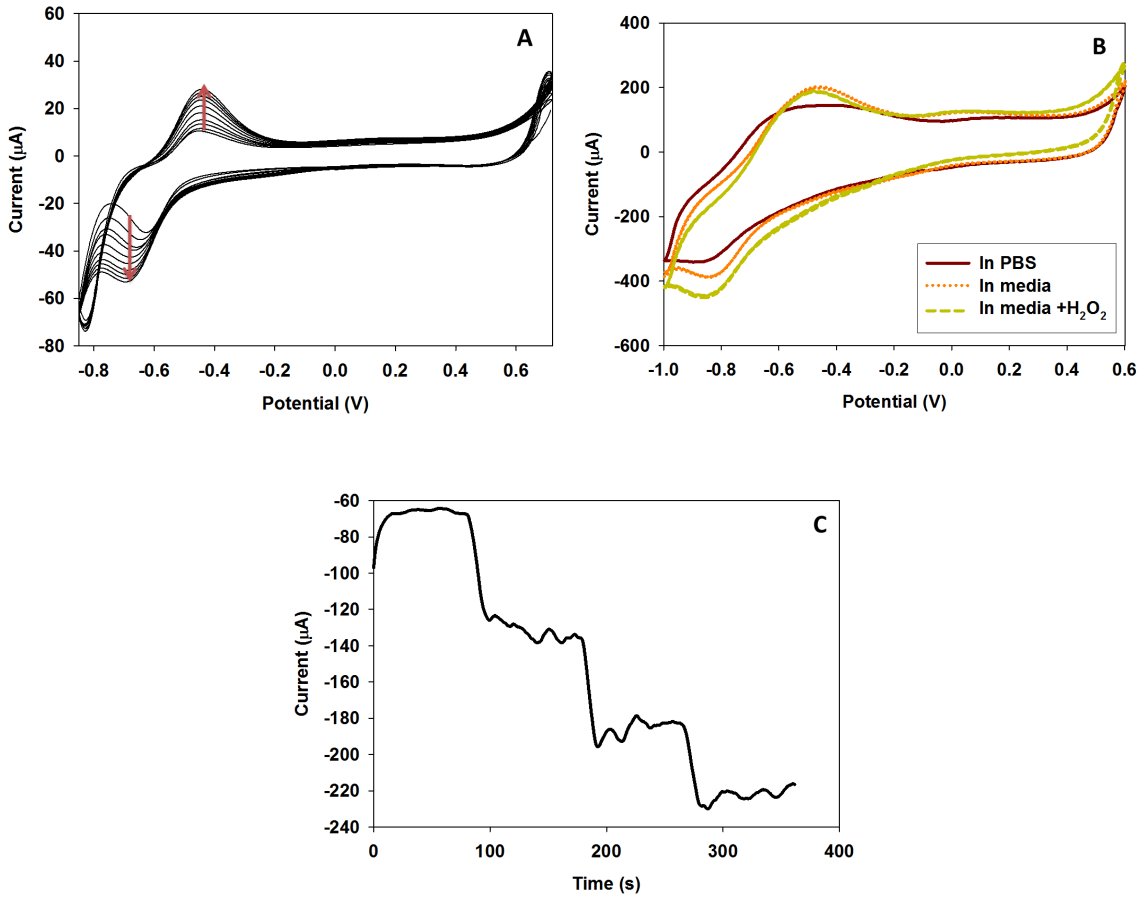

Figure 12.1: (A) CV deposition of PNR in 0.1M KNO_3, 5mM Neutral Red and 25mM phosphate buffer with a pH of 6 (B) Amperometric measurements for hydrogen peroxide (0.5mM additions) in media solution (C) CVs in 1 mM PBS at pH of 7.2 and Minimum Essential Media (MEM) solution

After successful deposition of PNR, the 3D nanopillar electrodes were tested for their stability in phosphate buffer solution and minimum essential medium (MEM). The MEM solution mainly contains 1mM sodium phosphate buffer salts, NaCl, $CaCl_2$, and

$MgSO_4$. The CV responses of the PNR coated gold nanopillars are seen in Figure 12.1B B) CVs in 1 mM PBS at pH of 7.2 and Minimum Essential Media (MEM) solution. Expect for the first 2 -3 cycles the rest of CV cycles showed relative good reproducibility, indicating that PNR was very stable in neutral PBS and MEM. The reduction current increased as hydrogen peroxide was added to the MEM solution (Figure 12.1B in media + H_2O_2 curve). While the results (Figure 12.1B in H_2O_2 shows the 1^{st} and 5^{th} CV cycle with small changes) did show changes with repeated CV cycles, the changes were very small compared with the case of Prussian Blue. Figure 12.1C show the amperometric measurements made in the MEM solution by adding 0.5mM of hydrogen peroxide incrementally. The current response led to a detection sensitivity value as high as 400 $\mu A/cm^2/mM$ (need a calibration curve here), although much noise and poor stability were visible in the current response (Figure 12.1C). A major difference between PNR and PB cases is that the repeat results (5 repeats) of the PNR case showed almost no decrease in sensitivity in the presence of hydrogen peroxide. In contrast, the sensitivity of the PB case decreased continuously in each subsequent measurement.

12.3.2 PNR/ PEDOT deposit

PNR/PEDOT deposits have already been shown as good electrode materials for hydrogen peroxide sensing [226]. Here we set out to examine how they would fare on the 3D gold nanopillar structures. To obtain a better co-deposition of PEDOT, the concentration of neutral red was reduced by a tenth (as compared with the case of PNR only). Figure 12.2A shows the CV curves during deposition of PNR/PEDOT polymers with the potential range set from -1.1 V to 0.75 V. We kept the same anodic potential

limit as the one in the PNR case but extended the cathodic potential limit to -1.1 V in order to accommodate the redox peaks because we anticipated an increase in the separation of redox peaks due to presence of the PEDOT in the deposit causing heightened diffusion resistance (mainly the counter ions). Figure 12.2B shows the CV response curves in MEM solution with and without hydrogen peroxide. Since the ratio of the peak currents between the cases with and without hydrogen peroxide is much higher than that obtained in the PNR alone case, the PNR/PEDOT co-deposit was considered better an electrode material for hydrogen peroxide reduction.

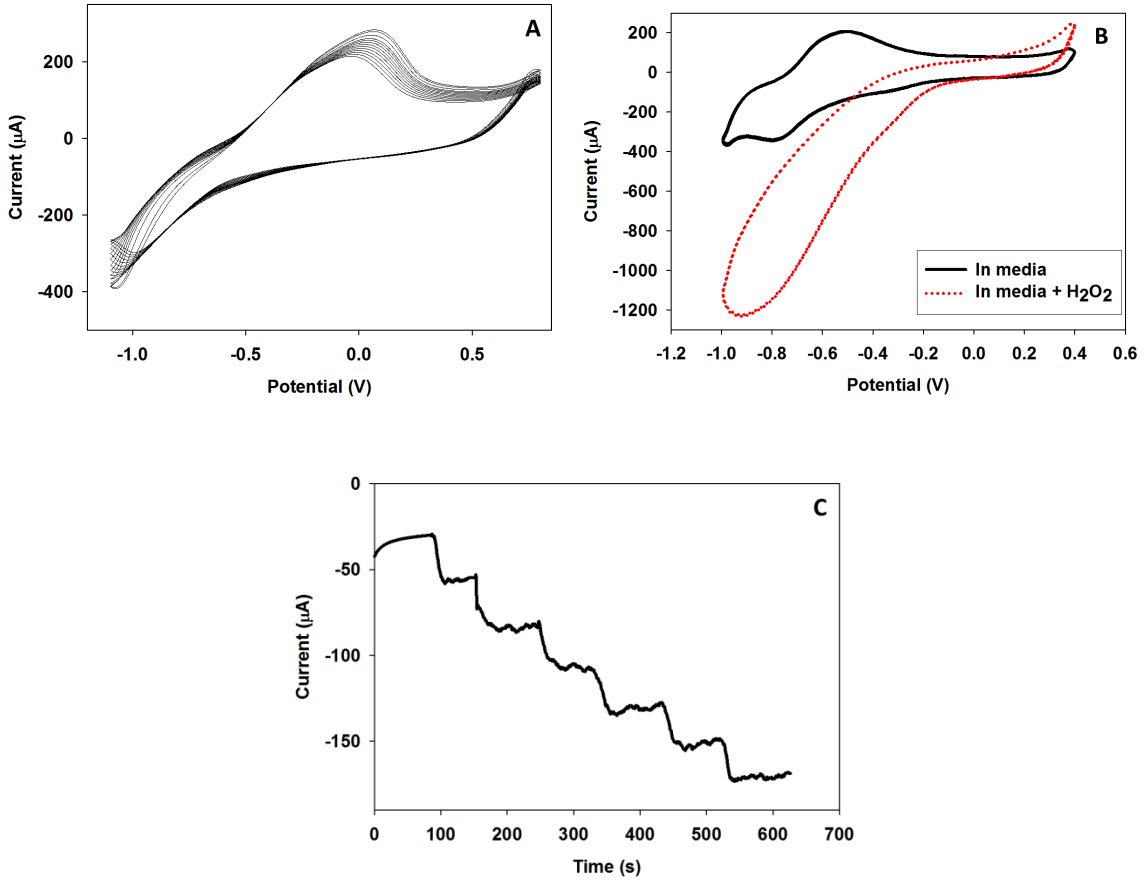

Figure 12.2: (A) CV deposition of PNR/PEDOT in 0.1 M KNO_3, 0.5 mM Neutral Red, 5 mM EDOT and 25 mM phosphate buffer with a pH of 6 (B) CVs of the PNR/PEDOT in Minimum Essential Media (MEM) solution and with addition of 1 mM hydrogen peroxide (C) Amperometric measurements for hydrogen peroxide (0.5mM additions) in media solution (The area of sample used in 2C is $1/5^{th}$ of the sample area used in Figure 12.2 A &B)

12.3.3 PNR and PNR/PEDOT for glucose oxidase entrapment

Although conducting polymers are often used to entrap enzymes for the development of enzymatic biosensors as was discussed in previous chapters, PNR is not one of these

often used conducting polymers. Particularly glucose oxidase has never been entrapped into PNR. However, if this is possible, there will no need to detect hydrogen peroxide, because PNR can by itself act as a mediator as illustrated in Figure 12.3A. Using this mechanism we will see current increases due to the oxidation of PNR, in contrast to the H_2O_2 mechanism (Figure 12.3B) where we will see current decrease due to reduction of PNR. To date, only FAD molecules [227] and HRP enzyme molecule [225] have been entrapped in PNR and both have been used for hydrogen peroxide detection. So in this part of work, we set out to demonstrate, for the first time, the entrapment of glucose oxidase using PNR. We believe that if successful, especially if the glucose oxidase entrapped in PNR had good linear response range and high sensitivity in glucose detection, we can drastically simplify the detection mechanism by using a two-electrode microfluidic system in which the enzyme and working electrodes are merged into one.

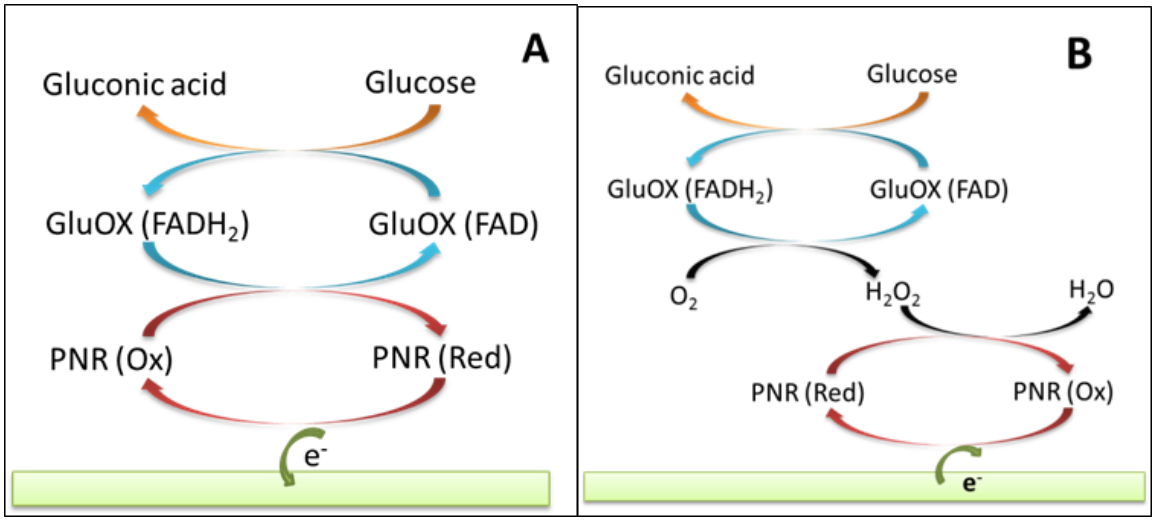

Figure 12.3: (A) Schematic of mechanism of redox mediation by PNR (B) Mechanism of hydrogen peroxide reduction

Figure 12.4A shows the CVs with which PNR was deposited along with glucose oxidase. This figure shows an example case at high potential range (-1 V to 1V). Other potential ranges for the CVs (similar to the PNR and PNR/PEDOT cases) were also used. To control the thickness of deposition, about 6 - 8 CV cycles were carried out for the high potential case, and about 30 CV cycles were done for the low potential case (e.g., with a upper limit of 0.75V). Figure 12.4B shows the amperometric response to glucose for the PNR/glucose oxidase electrode deposited at the low oxidation potentials. Trial 1 and Trial 2 represented two different samples of almost the same geometrical area operated amperometrically at -0.4V, but the results differed significantly, owing possibly to the different amounts of enzyme entrapped in the polymer. Since the electrodes were controlled at -0.4 V, the resulted currents were primarily originated from reduction reactions. We thus suspect that hydrogen peroxide reduction occurs in these cases, as illustrated in Figure 12.3B.

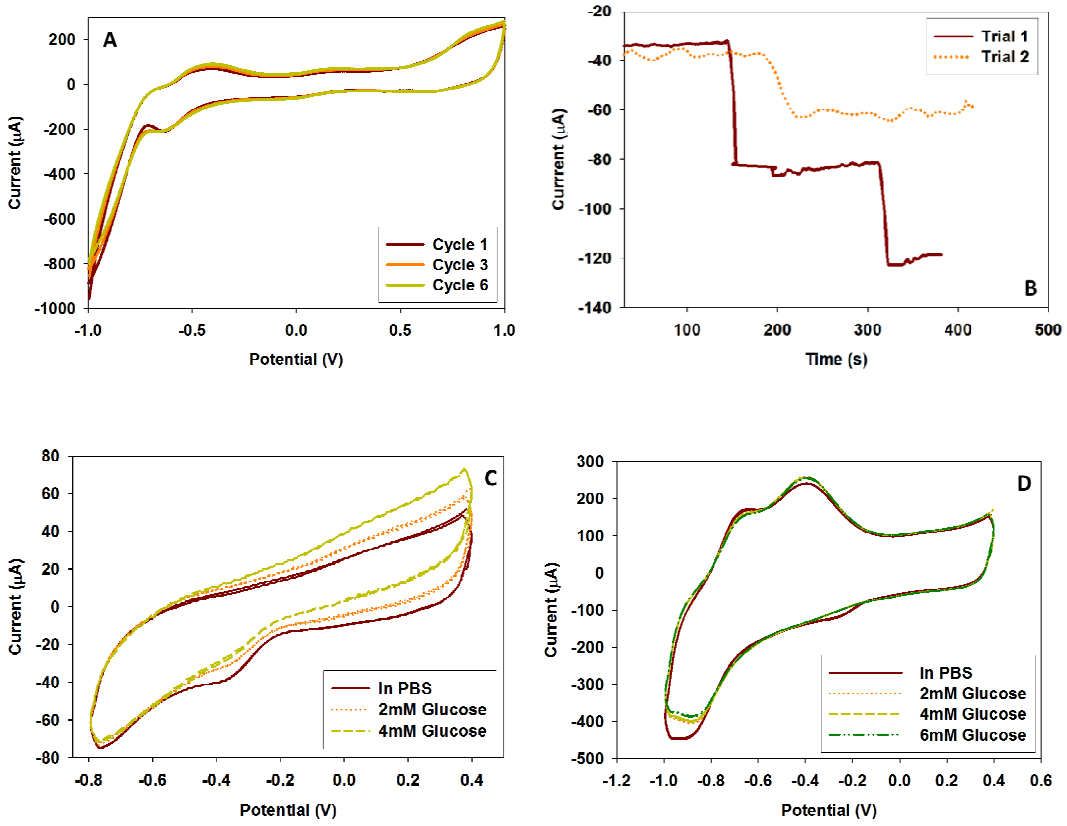

Figure 12.4: (A) CV deposition of PNR in 0.1M KNO_3, 0.5mM Neutral Red, 5mM EDOT and 25mM phosphate buffer with a pH of 6 in presence of 1mg/ml glucose oxidase (B) Amperometric measurements of glucose (1mM additions) in phosphate buffer (C) & (D) CVs of PNR/PEDOT with entrapped glucose oxidase in 1mM PBS and with additions of glucose

Figures 12.4C and 12.4D show the results from two electrodes coated with PNR/PEDOT and glucose oxidase. A decrease in the reduction peak around -0.4V with increasing glucose concentration is seen. This implies that the reaction mechanism can be similar to the one shown in Figure 12.3A in which oxidation reaction taking place at the electrode surface which in turn causes a decrease in the reduction peak at -0.4V. The

amount of active glucose oxidase entrapped seemed to variy with samples. This can be seen from Figure 12.4D, where current saturation occurs at a glucose concentration of 2mM. Even though glucose oxidase was successfully entrapped in PNR and PNR/PEDOT, we noted a lack of consistency in glucose sensitivity and considerable amount of noise in the signal. Therefore this entrapment method was not used in any of the further experiments.

12.3.4 Microfluidic experiments

Based on the previous experiments and results, we believe that the PNR/PEDOT could be a better material for hydrogen peroxide detection. To verify this in a microfluidic environment, we first deposited PNR onto the 3D nanostructures and then mounted the PDMS channel to form the microfluidic device. Due to need for heat treatment for mounting the PDMS channel, we examined stability of PNR. Figure 12.5 shows the CVs of PNR/PEDOT coatings before and after the heat treatment. Only a slight change in the CV curves is seen, thus we believe the deposition of PNR in this manner is effective.

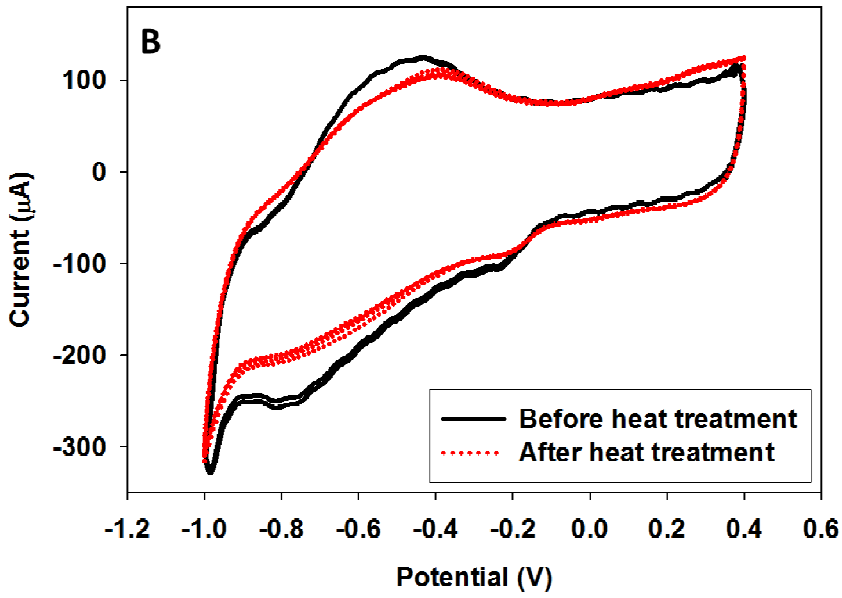

Figure 12.5 CV of PNR/PEDOT before and after heat treatment at 100°C

Figure 12.6 shows the obtained amperometric current response in which the operating potentials was around -0.5V vs Ag-AgCl. A slight higher potential was applied in the microfluidic setup when compared to external amperometric conditions (-0.4V) to compensate the resistive losses in the microfluidic channel. This compensatory resistance was calculated each time using the Princeton VersaStat VMC instrument and software. On average an over potential of 100 mV is enough to compensate the resistive loss. Figure 12.6B and 12.6C show the glucose response in the microfluidic device when the enzyme electrode was prepared using the gold nanoparticle method (Chapter 8) and PNR/PEDOT coated 3D nanopillars as the working electrode. The glucose sensitivity of the device was around 5.2 μA/ mM /cm^2 based on the area of the electrode used.

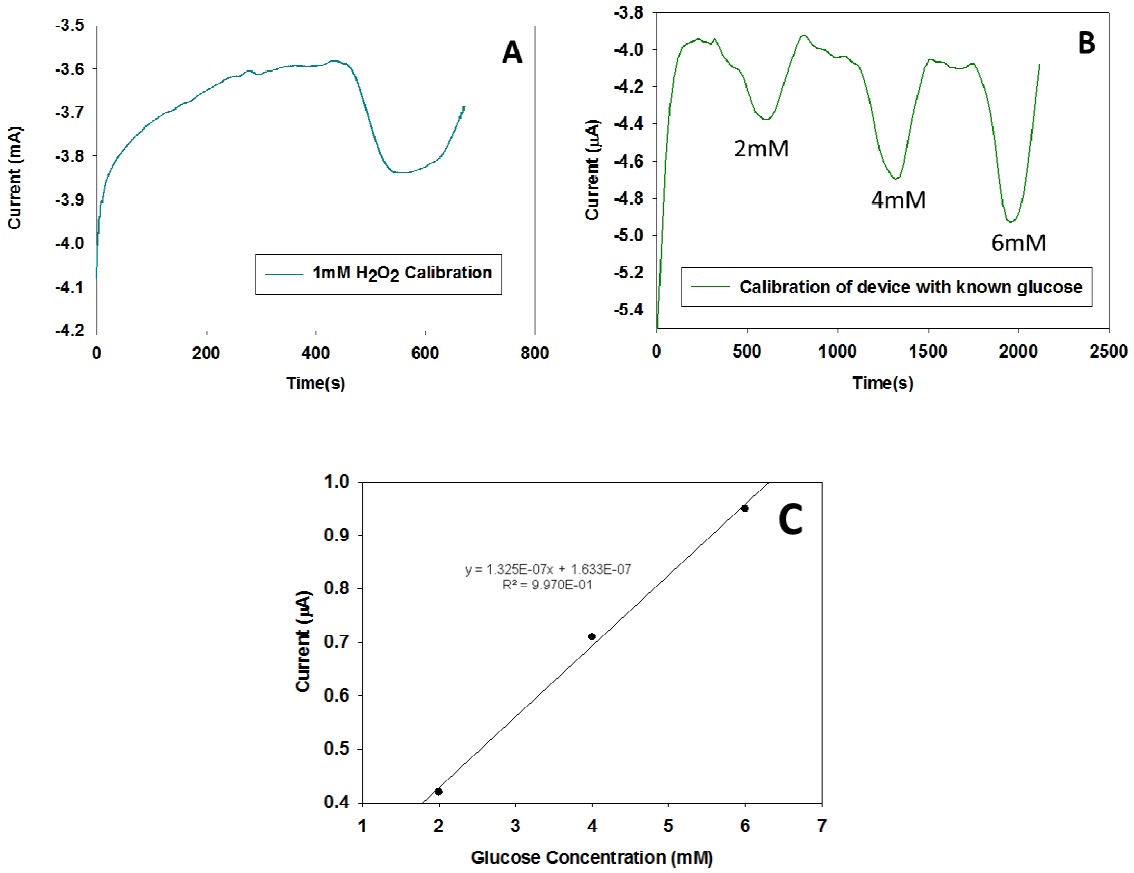

Figure 12.6: (A) Amperometric measurements of (0.5mM) hydrogen peroxide in phosphate buffer (B) Amperometric measurements of glucose (1mM additions) in 1mM phosphate buffer (C) Calibration curve for the glucose measurements

12.4 Conclusion

We found that PNR/PEDOT seems to be a better candidate for hydrogen peroxide detection based on its sensitivity and stability. We also demonstrated for the first time entrapment of glucose oxidase in PNR and PNR/ PEDOT polymers for glucose detection purpose. However this entrapment method was not as promising due to the inconsistency in the obtained sensitivity values. A poor linear range and high noise in the current

responses were also associated with this entrapment method. Of all the electrode modification methods tested above, the PNR/PEDOT method produced much better performance in hydrogen peroxide detection, thus it was used to modify the working electrode in the microfluidic channel. The amperometric results for the microfluidic channel also produced a reasonably good sensitivity of 5.2 μA/ mM /cm^2 for glucose detection.

12.5 Highlights of the working electrode studies

a. None of the protection methods for Prussian Blue and its analogues gave satisfactory stability in cell culture media. So this material was considered not appropriate for multiple measurements.
b. Polyneutral Red was more stable in cell culture media and the hydrogen reduction mechanism was a more preferred method for glucose detection
c. Redox mediation of Polyneutral red had smaller sensitivity and linear range and was a not preferable method.
d. Polyneutral Red was preferred for working electrode modification for cell culture monitoring.

SECTION V

CHAPTER 13

MONITORING CELL CULTURE USING MICROFLUIDIC BIOSENSOR

13.1 Introduction

Until now we have discussed studies that were performed for making a sensitive, stable and reliable 3D nanopillar electrode based biosensor for monitoring changes in cell culture media. From these various studies, the best results were taken to build the microfluidic biosensor that can monitor cell culture. The following list gives the optimized parameters used in the development of the biosensor

1) 3D nanopillars were patterned as 3 electrodes or IDEs
2) Height of the channel was 40 µm and width was 500 µm.
3) Polypyrrole electropolymerization was done in presence of glucose oxidase and 2 -4 nm gold nanoparticle inside microfluidic channel
4) The working electrode was coated with PNR/PEDOT before attaching the microchannel
5) PDMS curing agent was used as the adhesive to seal the PDMS and glass substrate with the 3D nanopillar electrodes
6) The flow rate for amperometric studies was maintained between 1 -5 µL/min

13.2 Experimental methods

13.1 Electrode preparation: Refer to Chapter 4.2.2

13.2 PDMS Channel preparation: Refer to Chapter 9.2.2

13.3 Working electrode modification: Refer to Chapter 12.2.2

13.4 PDMS channel bonding: Refer to Chapter 12.2.5

13.5 Polypyrrole/ GNP/Glucose oxidase coating for enzyme electrode: Refer to Chapter10.2

13.6 Amperometric measurements: Refer to chapter 9.2.5

13.7 Cell Culture experiments:

Cells used for glucose consumption studies were 3T3 fibroblasts. 500 mL of basal media, Dulbecco's modified Eagle medium (DMEM) with 50 mL fetal bovine serum and 5 ml Penicillin Streptomycin (all from Mediatech Cellgro, Manassas, VA) was used as the cell culture media. For the experiments in T-75 flasks and microfluidic cell culture the 3T3 mouse fibroblasts were maintained in culture under established conditions of 5% CO_2 at 37°C.

For measuring glucose changes in T-75 flasks the 3T3 fibroblasts were seeded into Tissue culture-flasks and cultured for 3 days. A volume of 15 ml culture medium was supplied initially. At regulars intervals (12 hrs or 24 hrs) an aliquot (500 µL) of the medium was taken out for testing. This reduction in volume was taken into account when considering the overall change in glucose consumption.

Two types of microfluidic experiments were performed. In the first type of experiments, PDMS camber had a height of 150 µm and a bottom surface area of 1.5 cm^2 was fabricated as the fluidic channel and bonded to a glass slide using oxygen plasma technique. An inlet and an outlet were made using sterilized needles. The PDMS- needle interface was sealed with RTV sealant to prevent any leakage. The device was then

sterilized with 2 hours of autoclave at 100°C and 2 hours of UV irradiation. The microfluidic chamber was first incubated in the medium supplemented with bovine fetal serum for 1 hr. Then the cells were injected and let to stay there for an hour before perfusion of the DMEM solution was done. This method yielded successful cell cultures, but it was never possible to maintain a sterile environment for integrating the microfluidic biosensor.

In the second type of experiments, 3T3 cells were grown in a 12-well plate. PDMS was molded (with inlet and outlet) into a cylindrical shape to fit one of the chambers in the 12 well plates. After growing the cells in the 12-well plate for 1 day and making sure the cells were completely adherent, the molded PDMS was placed on one of 12-well plates as close to the surface as possible without destroying the cells. With this experiment we did not have control of the height of the chamber, but it was practically easier to make measurements with this setup.

13.3 Results and discussions

13.3.1Theoretical calculations of glucose consumption in 3T3 cell culture

The consumption of HEPG cells has been already measured using a planar glucose biosensor [232]. They measured and found that HEPG cells had a high glucose consumption of 1.5mg/day from a $1cm^2$ area. In this experiment the authors expected glucose concentrations to change in a range of 1.4–2.8mM at a flow rate of 30µL/min [232]. From literature it can be found that consumption of glucose by the 3T3 cells was much lesser. It can vary between 0.1 – 0.15 mg/day/cm^2 after 3 days of cell culture [233], when the initial cell density was $3x10^4$ cells/ cm^2. In our case the number of cells will be

an order of magnitude higher. But if we go by conservative values and consider them in our case, the glucose consumption will be 0.1 mg/day/cm^2. If we have a flow rate at 5 µL/min, the theoretical consumption rate is calculated as:

Glucose consumption per minute = 6.94 $x10^{-5}$ mg/min/cm^2

At a flow rate of 5µL/min the amount of glucose available is 5x 10^{-3} mg/min based on the initial concentration of glucose. For an initial concentration of glucose 5.6 mM or 1000 mg/L in the medium, the amount of change in glucose after 1 min = (0 .005mg - 6.94 $x10^{-5}$mg) = 0.00493 mg. This amount of change, when expressed in glucose concentration change in mM, is (0.00493/5$x10^{-6}$)/180 = 5.47 mM.

There will be a change of 0.12 mM in glucose concentration. This can be improved if the flow rate is reduced even further (1 µL/min will have a change of 0.6mM). Since the detection limit of our biosensor is below 0.1mM we can definite measure these changes. These calculations are the most conservative values. The real changes can be even higher.

In case of T75 flasks the total surface area for cell to grow is 7.5 cm^2. Glucose consumption per day from that area considering the conservative consumption rate of 0.1 mg/day/cm^2 is 0.75 mg/day.

Volume of media solution = 15ml

Initial amount of glucose is 15mg

Change in glucose amount per day = 15 – 0.75 mg = 14.25mg

Theoretical change in concentration per day = 0.28 mM

So the microfluidic biosensor can measure even the changes in the T-75 flask with great accuracy if measurements are done three to four times at regular intervals. Theoretically,

glucose concentration changes in the T-flasks and microfluidic cell cultures can be monitored using the microfluidic biosensor.

13.3.2 Results of testing in T-flask

Figure 13.1 shows the experimental setup used to measure the glucose in the medium obtained from T-flasks. An aliquot of the medium was injected into the sample injector. A minimum volume of 50 – 100 µL was needed to be injected into the injector. This was the reason 500 µL of sample was taken out to perfom multiple measurements. The solution that was injected from the syringe pump was either the DMEM solution with 1g/L glucose or without any glucose. If there was glucose we were looking at the hydrogen peroxide reduction current to reduce to lesser negative values (it will be seen as an increase in the graph). If there is no glucose in the media from the syringe pump then the increase current will increase more negatively. Both these methods were tried to check the glucose concentrations.

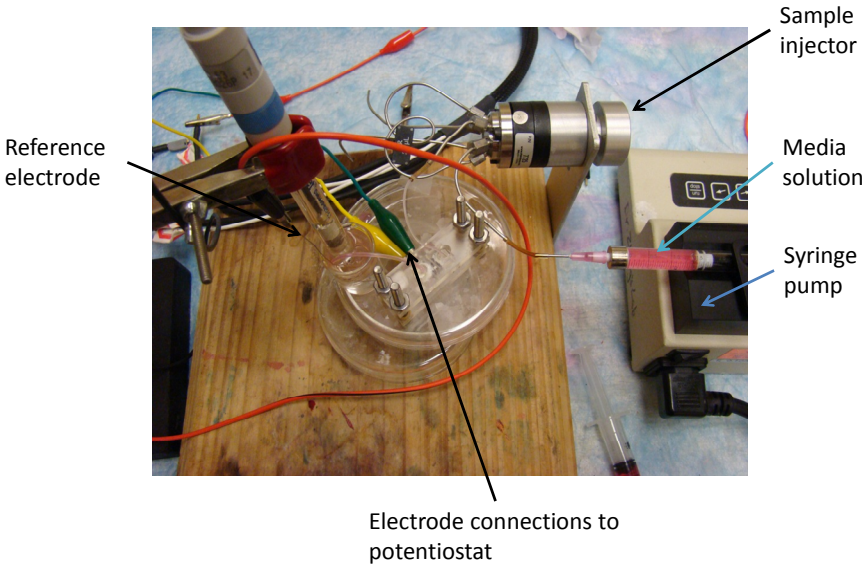

Figure 13.1: Experimental setup for measuring the samples obtained from T-flasks

Figure 13.2 A and B shows the measurements done with a base line as the media with 5.6 mM glucose concentration. The lowering of level shows that the amount of glucose level was lesser than the highest amount of 5.6mM. Figure 13.3 shows the changes in glucose concentration calculated from the calibration curves of the devices. As seen there is not much change within 4 hours. But samples from different days show different levels of glucose.

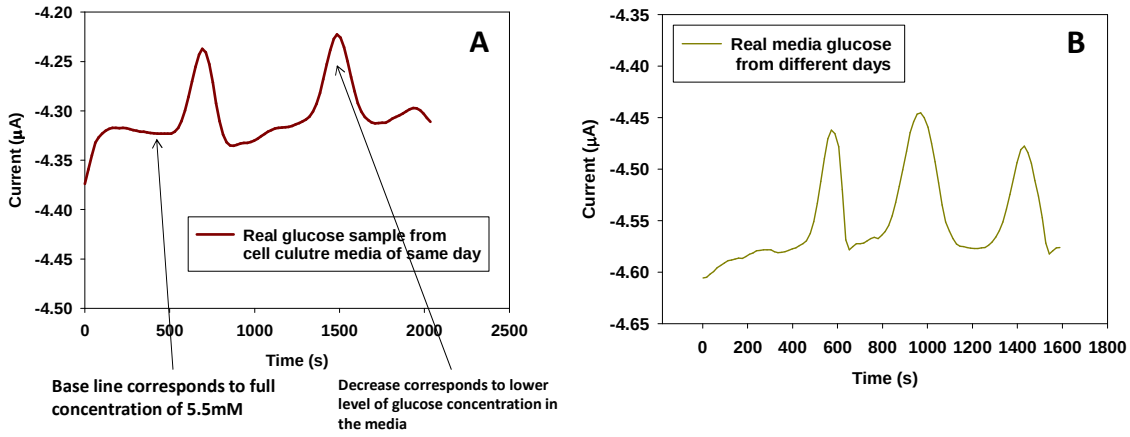

Figure 13.2 A & B: Samples from the 3T3 cells grown in T-75 flasks tested for their glucose content

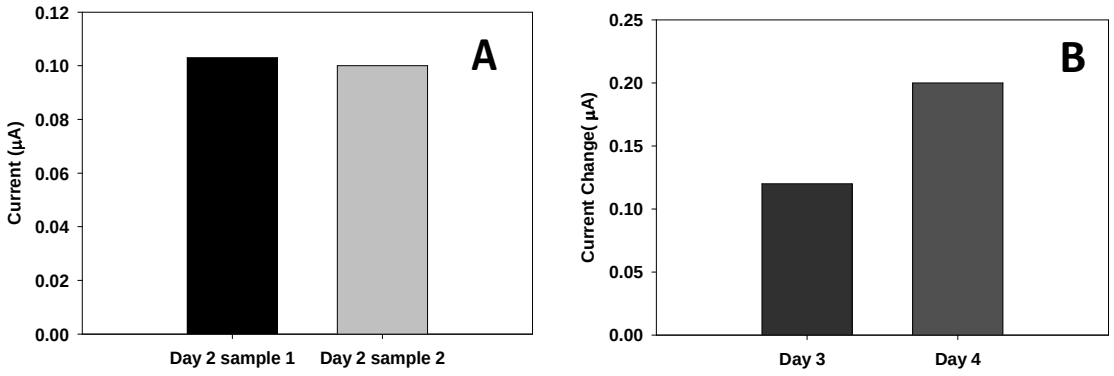

Figure 13.3: (A) Changes in glucose concentration when samples were collected with 4 hours difference (B) Changes in glucose consumption on 2 different days

The previous results confirm that the sensor was reliable to measure the glucose concentration changes. Further experiments were conducted with media solution without glucose as the base line. Since the base line has no glucose the following results will show increase in current in the negative direction. The base lines were more stable using this procedure. Figure 13.4A summarizes all the glucose values obtained from the calibrated values (Figure 13.4B). The initial cell concentration was 200,000 and 500,000 cells/cm^2 respectively. The glucose consumption of the 200,000 cell culture system was 1.7mM after 1 day and 3.3mM after 3 days. In case of 500,000 cell culture system, the first day consumption was 2.7mM and the after 3day consumption was 4.1mM. The first day consumption was higher than the next 2 days. After 3 days the cells were fully confluent and had multiple layers. This might explain the non-linear consumption, as there can diffusion limitations for all cells to consume the glucose.

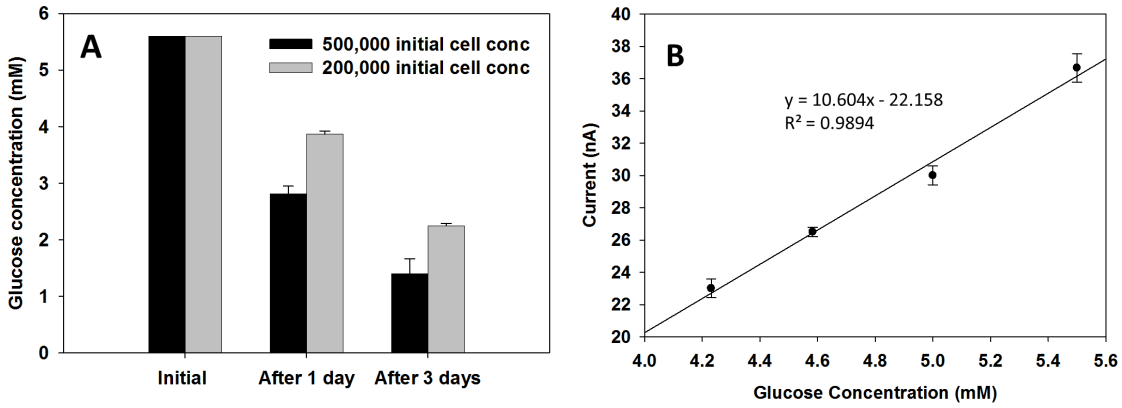

Figure 13.4: (A) Average glucose consumption of the 200,000 and 500,000 cells/cm^2 cell cultures (B) The calibration curve from which the current values from the biosensor responses was converted to glucose concentration values

13.3.3 Verification of the biosensor values

The values from the microfluidic biosensor were compared with the values of the YSI (YSI Incorporated, Yellow Springs, Ohio, USA) glucose analyzer. The same samples that were tested in the microfluidic biosensor were tested with the YSI glucose analyzer for the glucose concentrations. Figure 13.6 A shows that the values from the microfluidic biosensor are accurate when compared to the YSI measurements, except for one outlier value. We also compared the glucose measurement values from a Hemocue glucose analyzer results with the YSI glucose analyzer. These results show that the measurements don't match properly (Figure 13.5 B). Since the YSI glucose analyzer was more accurate when standard media solutions were tested, we believe that it is more accurate than the Hemocue glucose analyzer. From these verification results we can assume that the microfluidic biosensor developed is as accurate as an YSI glucose analyzer.

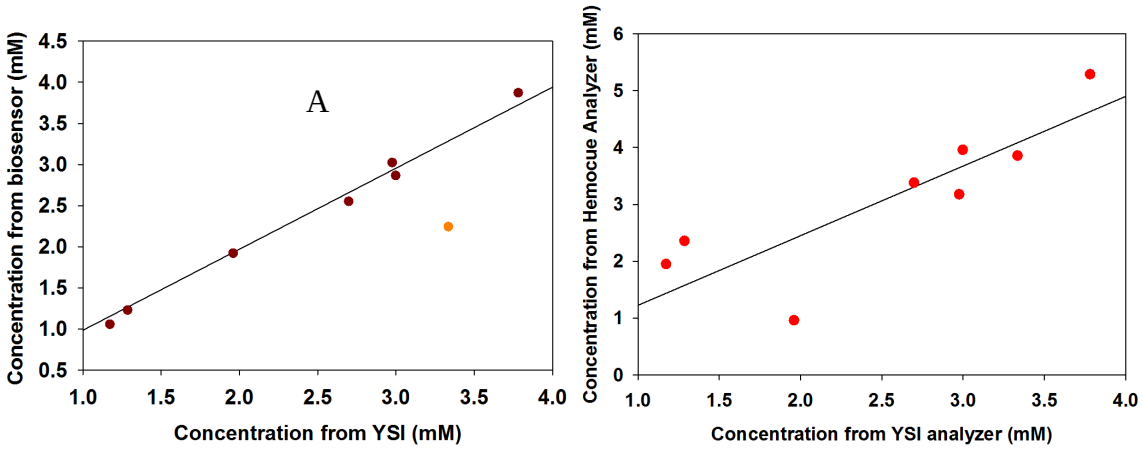

Figure 13.5: (A) Microfluidic biosensor results compared to an YSI glucose analyzer (B) Hemocue glucose analyzer results compared to an YSI glucose analyzer

13.3.4 Microfluidic cell culture experiments

Figure 13.6 shows the successful culturing of 3T3 cells inside the microfluidic channel. But no successful glucose measurements were done due to non-sterile conditions and bubble entrapment in the microfluidic biosensor.

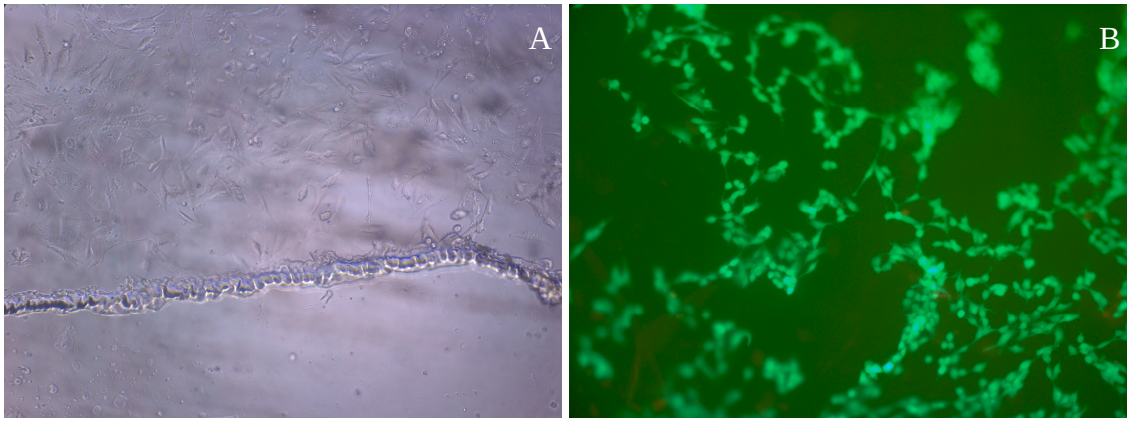

Figure 13.6: (A) Cells inside the microfluidic chamber (B) Live dead analysis of the cell in the microfluidic chamber

The more successful results in microfluidic conditions were obtained by growing cell culture in a 12 well plates. PDMS molds were prepared in the same dimensions as one of the wells in the culture plate. After the cells were cultured for 2 days the media from the well with cells was completely removed. Teflon taped PDMS mold was placed as close to the cell culture. A 500 µ spacer was placed in the bottom of the well. So the final height of channel was 500 µm approximately. Media solution was continuously perfused continuously at 10 µL/min. The outlet was connected to the microfluidic biosensor and current changes were measured. Figure 13.7 - A and B show the details of this setup.

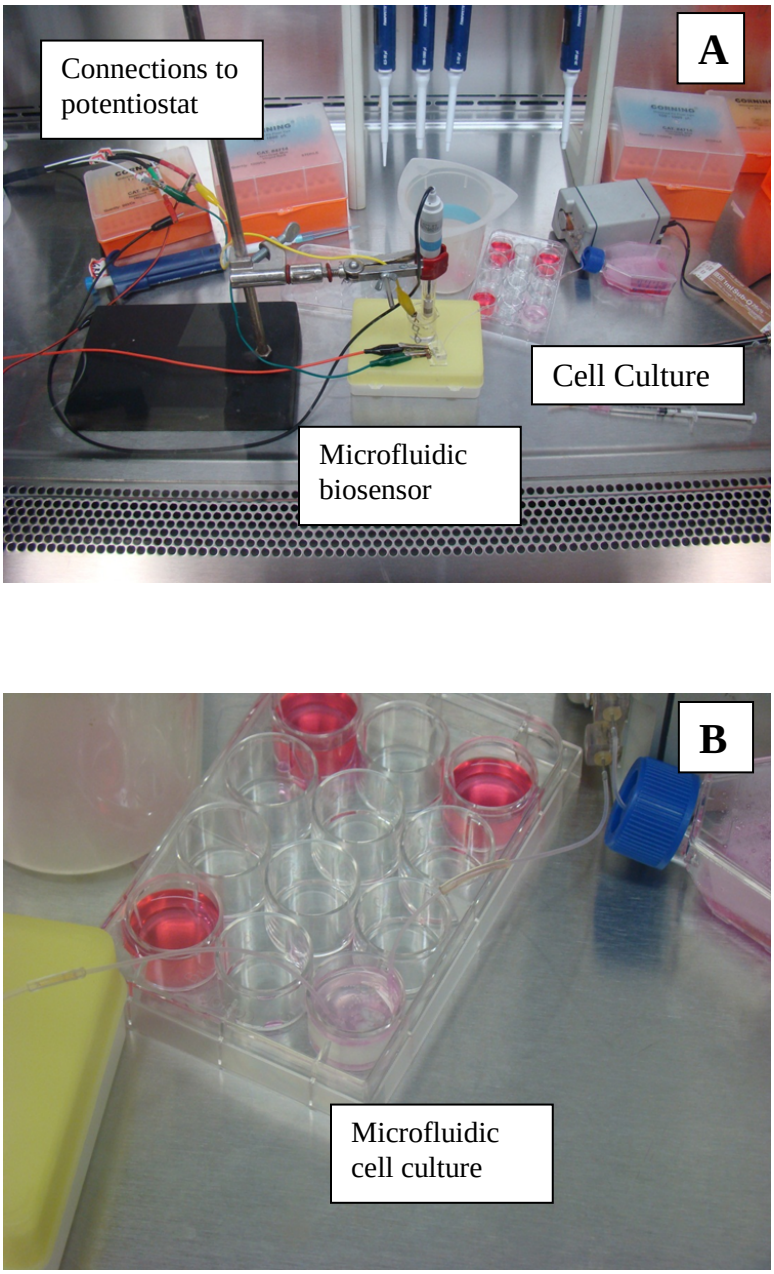

Figure 13.7: (A) and (B) - Images of the microfluidic cell culture and the biosensor

Figure 13.8 shows the current response of the microfluidic biosensor when attached to a microfluidic cell culture. The change in current is around 3.5 nA when compared to current response of initial glucose concentration (5.6 mM). So that will correspond to

0.31mM change in glucose concentration. This value corresponds to the theoretical values when considering the higher initial number of cells and the area (~ 3 cm^2).

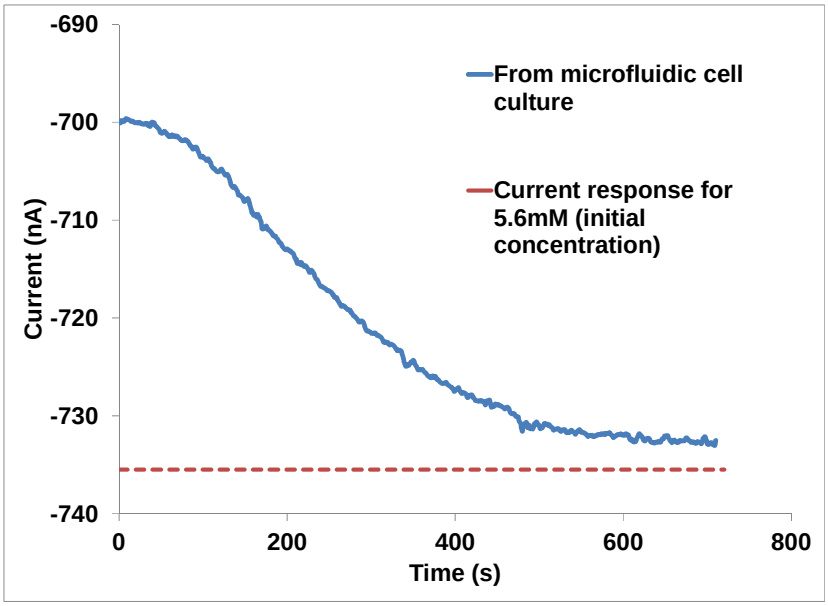

Figure 13.8: Current response for the media from microfluidic cell culture

13.4 Conclusion

The microfluidic biosensor was successfully demonstrated for monitoring glucose changes in the cell cultures. The biosensor was stable and produced repeatable readings. This study can be further extended to measure other species that can be enzymatically converted to electrochemically detectable species. This 3D nanopillar biosensor can serve as an effective platform for developing and monitoring many more metabolic species to understand the cell mechanisms.

CHAPTER 14

CONCLUSIONS AND FUTURE WORK

- The microfluidic biosensor was successfully demonstrated for monitoring microfluidic based cell culture.
- The development of a microfluidic biosensor will bring technical know-how toward constructing continuous glucose monitoring devices
- The methods used to develop 3D electrodes incorporated with nanopillars can be used for other applications such as neural probes, fuel cells, solar cells etc.
- The knowledge obtained from the immobilization of enzymes onto nanostructures shed some new insight into nanomaterial/biomolecule interactions
- Scope of improvement in the biosensor
    - Further reduce interferences with more protection on the working electrode
    - Incorporation of solid state reference electrode inside the microfluidic channels.
    - Integrate the electrodes with the microfluidic cell culture to provide more sterile conditions and easy operation (see Figure 14.1)
    - Integrate more different enzymes and oxygen sensing electrodes in parallel flow channels for monitoring multianalytes

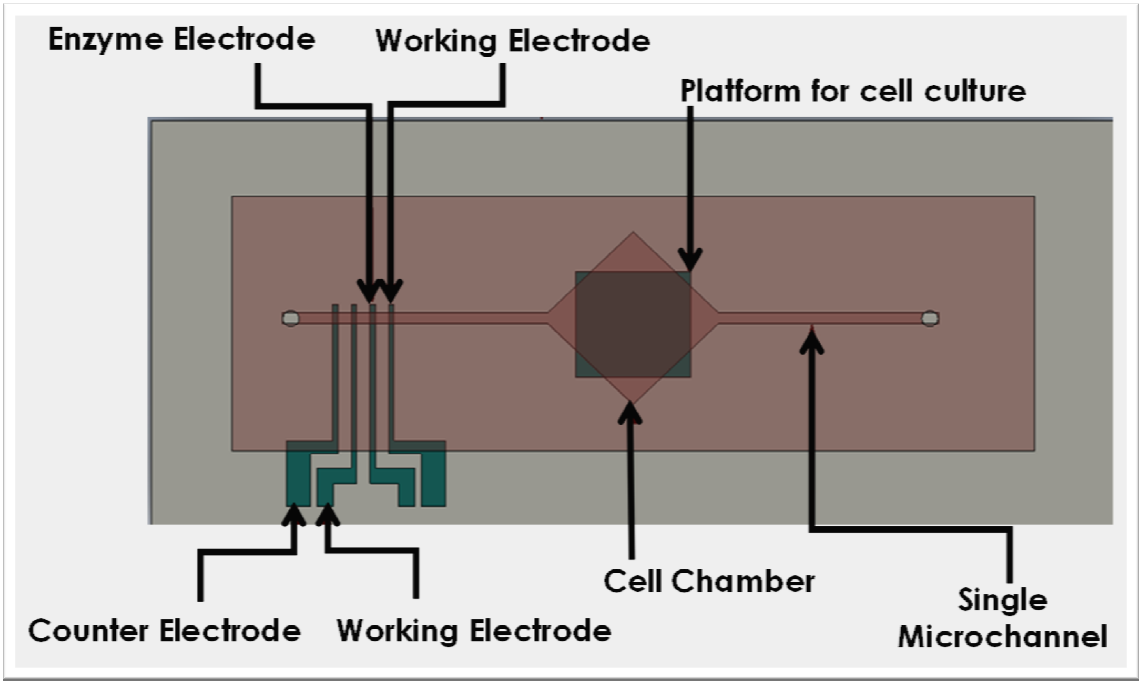

Figure 14.1: Schematic of an integrated electrode and cell culture platform

REFERENCES

[1] Ciosek P, Zawadzki K, Å□opaciÅ„ska J, Skolimowski M, Bembnowicz P, Golonka L, et al. Monitoring of cell cultures with LTCC microelectrode array. Analytical and Bioanalytical Chemistry 2009 04/01;393(8):2029-2038.

[2] Wolf B, Brischwein M, Grothe H, Stepper C, Ressler J, Weyh T. Lab-on-a-Chip Systems for Cellular Assays. BioMEMS 2006:269-307.

[3] Borges R, Camacho M, Gillis KD. Measuring secretion in chromaffin cells using electrophysiological and electrochemical methods. Acta Physiologica 2008;192(2):173-184.

[4] Thévenot D, Toth K, Durst R, Wilson G. Electrochemical Biosensors: Recommended Definitions and Classification*. Anal Lett 2001 03;34(5):635.

[5] Girard PP, Cavalcanti-Adam E, Kemkemer R, Spatz JP. Cellular chemomechanics at interfaces: sensing, integration and response. Soft Matter 2007;3(3):307-326.

[6] J.P. Wikswo, A. Prokop, F. Baudenbacher, D. Cliffel, B. Csukas, M. Velkovsky. Engineering challenges of bioNEMS: the integration of microfluidics, micro- and nanodevices, models and external control for systems biology. Nanobiotechnology, IEE Proceedings - 2006;153(4):81-101.

[7] Yeon JH, Park JK. Microfluidic cell culture systems for cellular analysis. Biochip J 2007;1(1):17-27.

[8] Kim L, Toh Y, Voldman J, Yu H. A practical guide to microfluidic perfusion culture of adherent mammalian cells. Lab Chip 2007;7(6):681-694.

[9] Tanaka Y, Sato K, Shimizu T, Yamato M, Okano T, Kitamori T. Biological cells on microchips: New technologies and applications. Biosensors and Bioelectronics 2007 11/30;23(4):449-458.

[10] Yi C, Li C, Ji S, Yang M. Microfluidics technology for manipulation and analysis of biological cells. Anal Chim Acta 2006 2/23;560(1-2):1-23.

[11] Yi C, Zhang Q, Li C, Yang J, Zhao J, Yang M. Optical and electrochemical detection techniques for cell-based microfluidic systems. Analytical and Bioanalytical Chemistry 2006 03/01;384(6):1259-1268.

[12] Wang J. Electrochemical detection for microscale analytical systems: a review. Talanta 2002 2/11;56(2):223-231.

[13] Lacher NA, Garrison KE, Martin RS, Lunte SM. Microchip capillary electrophoresis/ electrochemistry. Electrophoresis 2001;22(12):2526-2536.

[14] Gooding J. Electrochemical DNA Hybridization Biosensors. Electroanalysis 2002;14(17):1149-1156.

[15] Yotter RA, Lee LA, Wilson DM. Sensor technologies for monitoring metabolic activity in single cells-part I: optical methods. Sensors Journal, IEEE 2004;4(4):395-411.

[16] Chudy M, Grabowska I, Ciosek P, Filipowicz-Szymanska A, Stadnik D, Wyzkiewicz I, et al. Miniaturized tools and devices for bioanalytical applications: an overview. Analytical and Bioanalytical Chemistry 2009 10/01;395(3):647-668.

[17] Dale N, Hatz S, Tian F, Llaudet E. Listening to the brain: microelectrode biosensors for neurochemicals. Trends Biotechnol 2005 8;23(8):420-428.

[18] Gao Y, Bhattacharya S, Chen X, Barizuddin S, Gangopadhyay S, Gillis KD. A microfluidic cell trap device for automated measurement of quantal catecholamine release from cells. Lab Chip 2009;9(23):3442-3446.

[19] Perry M, Li Q, Kennedy RT. Review of recent advances in analytical techniques for the determination of neurotransmitters. Anal Chim Acta 2009 10/19;653(1):1-22.

[20] Yun Y, Eteshola E, Bhattacharya A, Dong Z, Shim J, Conforti L, et al. Tiny Medicine: Nanomaterial-Based Biosensors. Sensors 2009;9(11):9275-9299.

[21] Lim M, Ye H, Panoskaltsis N, Drakakis EM, Yue X, Cass AEG, et al. Intelligent bioprocessing for haemotopoietic cell cultures using monitoring and design of experiments. Biotechnol Adv 2007 8;25(4):353-368.

[22] The Helmholtz Centre for Environmental Research.
Biosensors - Development and Application.

[23] Yu D, Blankert B, Viré J, Kauffmann J. Biosensors in Drug Discovery and Drug Analysis. Anal Lett 2005;38(11):1687.

[24] Wightman RM. Probing Cellular Chemistry in Biological Systems with Microelectrodes. Science 2006 March 17;311(5767):1570-1574.

[25] Allen J. Bard and Larry R. Faulkner, Electrochemical Methods: Fundamentals and Applications, New York: Wiley, 2001.

[26] Pohanka M, Skladal P. Electrochemical biosensors-principles and applications. J Appl Biomed 2008;6(2):57-64.

[27] Ronkainen NJ, Halsall HB, Heineman WR. Electrochemical biosensors. Chem Soc Rev 2010;39(5):1747-1763.

[28] Gangadharan R, Anandan V, Zhang G. Optimizing the functionalization process for nanopillar enhanced electrodes with GOx/PPY for glucose detection. Nanotechnology 2008;19(39):395501.

[29] Leszczyszyn D, Jankowski J, Viveros O, Diliberto E,Jr, Near J, Wightman R. Nicotinic receptor-mediated catecholamine secretion from individual chromaffin cells. Chemical evidence for exocytosis. J Biol Chem 1990 September 5;265(25):14736-14737.

[30] House JL, Anderson EM, Ward WK. Immobilization techniques to avoid enzyme loss from oxidase-based biosensors: a one-year study. 2007.

[31] Ding L, Du D, Zhang X, Ju H. Trends in Cell-Based Electrochemical Biosensors. Curr Med Chem 2008 12/21;15(30):3160-3170.

[32] Wu C, Luk H, Lin YT, Yuan C. A Clark-type oxygen chip for in situ estimation of the respiratory activity of adhering cells. Talanta 2010 4/15;81(1-2):228-234.

[33] Torisawa Y, Shiku H, Yasukawa T, Nishizawa M, Matsue T. Multi-channel 3-D cell culture device integrated on a silicon chip for anticancer drug sensitivity test. Biomaterials 2005 5;26(14):2165-2172.

[34] Li MW, Spence DM, Martin RS. A Microchip-Based System for Immobilizing PC 12 Cells and Amperometrically Detecting Catecholamines Released After Stimulation with Calcium. Electroanalysis 2005;17(13):1171-1180.

[35] Chen P, Xu B, Tokranova N, Feng X, Castracane J, Gillis KD. Amperometric Detection of Quantal Catecholamine Secretion from Individual Cells on Micromachined Silicon Chips. Anal Chem 2003 02/01;75(3):518-524.

[36] Hafez I, Kisler K, Berberian K, Dernick G, Valero V, Yong MG, et al. Electrochemical imaging of fusion pore openings by electrochemical detector arrays. Proc Natl Acad Sci U S A 2005 September 27;102(39):13879-13884.

[37] Cheng H, Huang W, Chen R, Wang Z, Cheng J. Carbon fiber nanoelectrodes applied to microchip electrophoresis amperometric detection of neurotransmitter dopamine in rat pheochromocytoma (PC12) cells. Electrophoresis 2007;28(10):1579-1586.

[38] Cui H, Ye J, Chen Y, Chong S, Sheu F. Microelectrode Array Biochip:â€‰ Tool for In Vitro Drug Screening Based on the Detection of a Drug Effect on Dopamine Release from PC12 Cells. Anal Chem 2006 09/01;78(18):6347-6355.

[39] Spence DM, Torrence NJ, Kovarik ML, Martin RS. Amperometric determination of nitric oxide derived from pulmonary artery endothelial cells immobilized in a microchip channel. Analyst 2004;129(11):995-1000.

[40] Amatore C, Arbault S, Chen Y, Crozatier C, Tapsoba I. Electrochemical detection in a microfluidic device of oxidative stress generated by macrophage cells. Lab Chip 2007;7(2):233-238.

[41] Arbault S, Sojic N, Bruce D, Amatore C, Sarasin A, Vuillaume M. Oxidative stress in cancer prone xeroderma pigmentosum fibroblasts. Real-time and single cell monitoring of superoxide and nitric oxide production with microelectrodes. Carcinogenesis 2004 April 1;25(4):509-515.

[42] von Woedtke T, JÃ¼lich W, Alhitari N, Abel P, Hanschke R. Biosensor-controlled perfusion culture to estimate the viability of cells. Medical and Biological Engineering and Computing 2002 11/12;40(6):704-711.

[43] Kauri LM, Jung S, Kennedy RT. Direct measurement of glucose gradients and mass transport within islets of Langerhans. Biochem Biophys Res Commun 2003 5/2;304(2):371-377.

[44] Cai X, Klauke N, Glidle A, Cobbold P, Smith GL, Cooper JM. Ultra-Low-Volume, Real-Time Measurements of Lactate from the Single Heart Cell Using Microsystems Technology. Anal Chem 2002 02/01;74(4):908-914.

[45] Mao L, Xu F, Xu Q, Jin L. Miniaturized Amperometric Biosensor Based on Xanthine Oxidase for Monitoring Hypoxanthine in Cell Culture Media. Anal Biochem 2001 5/1;292(1):94-101.

[46] Wahl F, Obrenovitch TP, Hardy AM, Plotkine M, Boulu R, Symon L. Extracellular Glutamate During Focal Cerebral Ischaemia in Rats: Time Course and Calcium Dependency. J Neurochem 1994;63(3):1003-1011.

[47] Niwa O, Kurita R, Horiuchi T, Torimitsu K. Continuous Monitoring of L-Glutamate Released from Cultured Rat Nerve Cells with a Microfabricated On-Line Sensor at a Slow Flow Rate. Electroanalysis 1999;11(5):356-361.

[48] Niwa O, Kurita R, Liu Z, Horiuchi T, Torimitsu K. Subnanoliter Volume Wall-Jet Cells Combined with Interdigitated Microarray Electrode and Enzyme Modified Planar Microelectrode. Anal Chem 2000 03/01;72(5):949-955.

[49] Kurita R, Tabei H, Hayashi K, Horiuchi T, Torimitsu K, Niwa O. Improvement in signal reliability when measuring -glutamate released from cultured cells using multi-channel microfabricated sensors. Anal Chim Acta 2001 8/24;441(2):165-174.

[50] Hayashi K, Kurita R, Horiuchi T, Niwa O. Selective detection of -glutamate using a microfluidic device integrated with an enzyme-modified pre-reactor and an electrochemical detector. Biosensors and Bioelectronics 2003 9;18(10):1249-1255.

[51] Castillo J, Blöchl A, Dennison S, Schuhmann W, Csöregi E. Glutamate detection from nerve cells using a planar electrodes array integrated in a microtiter plate. Biosensors and Bioelectronics 2005 4/15;20(10):2116-2119.

[52] Castillo J, Isik S, Blöchl A, Pereira-Rodrigues N, Bedioui F, Csöregi E, et al. Simultaneous detection of the release of glutamate and nitric oxide from adherently growing cells using an array of glutamate and nitric oxide selective electrodes. Biosensors and Bioelectronics 2005 2/15;20(8):1559-1565.

[53] Isik S, Castillo J, Blöchl A, Csöregi E, Schuhmann W. Simultaneous detection of l-glutamate and nitric oxide from adherently growing cells at known distance using disk shaped dual electrodes. Bioelectrochemistry 2007 1;70(1):173-179.

[54] Kurita R, Hayashi K, Horiuchi T, Niwa O, Maeyama K, Tanizawa K. Differential measurement with a microfluidic device for the highly selective continuous measurement of histamine released from rat basophilic leukemia cells (RBL-2H3). Lab Chip 2002;2(1):34-38.

[55] Iwaki S, Ogasawara M, Kurita R, Niwa O, Tanizawa K, Ohashi Y, et al. Real-Time Monitoring of Histamine Released from Rat Basophilic Leukemia (RBL-2H3) Cells with a Histamine Microsensor Using Recombinant Histamine Oxidase. Anal Biochem 2002 5/15;304(2):236-243.

[56] Dale N. Delayed production of adenosine underlies temporal modulation of swimming in frog embryo. J Physiol (Lond) 1998;511(1):265-272.

[57] Llaudet E, Botting NP, Crayston JA, Dale N. A three-enzyme microelectrode sensor for detecting purine release from central nervous system. Biosensors and Bioelectronics 2003 1;18(1):43-52.

[58] Wall M, Eason R, Dale N. Biosensor measurement of purine release from cerebellar cultures and slices. Purinergic Signalling 2010:1-10.

[59] Llaudet E, Hatz S, Droniou M, Dale N. Microelectrode Biosensor for Real-Time Measurement of ATP in Biological Tissue. Anal Chem 2005 05/01;77(10):3267-3273.

[60] Zare RN, Kim S. Microfluidic Platforms for Single-Cell Analysis. Annu Rev Biomed Eng 2010 07/01;12(1):187-201.

[61] Kim J, Johnson M, Hill P, Gale BK. Microfluidic sample preparation: cell lysis and nucleic acid purification. Integr Biol 2009;1(10):574-586.

[62] Mata D, Bejarano D, Botero ML, Lozano P, Constantí M, Katakis I. Screen-printed integrated microsystem for the electrochemical detection of pathogens. Electrochim Acta 2009;55(14):4261-4266.

[63] Sun P, Laforge FO, Abeyweera TP, Rotenberg SA, Carpino J, Mirkin MV. Nanoelectrochemistry of mammalian cells. Proceedings of the National Academy of Sciences 2008 January 15;105(2):443-448.

[64] Yum K, Wang N, Yu M. Nanoneedle: A multifunctional tool for biological studies in living cells. Nanoscale 2010;2(3):363-372.

[65] Ayliffe HE, Frazier AB, Rabbitt RD. Electric impedance spectroscopy using microchannels with integrated metal electrodes. Microelectromechanical Systems, Journal of 1999;8(1):50-57.

[66] Han A, Frazier AB. Ion channel characterization using single cell impedance spectroscopy. Lab Chip 2006;6(11):1412-1414.

[67] Han K, Han A, Frazier AB. Microsystems for isolation and electrophysiological analysis of breast cancer cells from blood. Biosensors and Bioelectronics 2006 4/15;21(10):1907-1914.

[68] Yeon JH, Park J. Cytotoxicity test based on electrochemical impedance measurement of HepG2 cultured in microfabricated cell chip. Analytical Biochemistry 2005 6/15;341(2):308-315.

[69] Brischwein M, Motrescu ER, Cabala E, Otto AM, Grothe H, Wolf B. Functional cellular assays with multiparametric silicon sensor chips. Lab Chip 2003;3(4):234-240.

[70] Otto AM, Brischwein M, Niendorf A, Henning T, Motrescu E, Wolf B. Microphysiological testing for chemosensitivity of living tumor cells with multiparametric microsensor chips. Cancer Detect Prev 2003;27(4):291-296.

[71] Warsinke A. Electrochemical Biochips for Protein Analysis. Biosensing for the 21st Century 2008:155.

[72] Velasco M, Missailidis S. New trends in aptamer-based electrochemical biosensors. Gene Therapy and Molecular Biology 2009;13(1):1-10.

[73] Mir M, Jenkins ATA, Katakis I. Ultrasensitive detection based on an aptamer beacon electron transfer chain. Electrochemistry Communications 2008 10;10(10):1533-1536.

[74] Bang GS, Cho S, Kim B. A novel electrochemical detection method for aptamer biosensors. Biosensors and Bioelectronics 2005 12/15;21(6):863-870.

[75] Bogomolova A, Komarova E, Reber K, Gerasimov T, Yavuz O, Bhatt S, et al. Challenges of Electrochemical Impedance Spectroscopy in Protein Biosensing. Anal Chem 2009 05/15;81(10):3944-3949.

[76] Helmke BP, Minerick AR. Designing a nano-interface in a microfluidic chip to probe living cells: Challenges and perspectives. 2006 April 25;103(17):6419-6424.

[77] Clark LC,Jr., Lyons C. ELECTRODE SYSTEMS FOR CONTINUOUS MONITORING IN CARDIOVASCULAR SURGERY. Ann N Y Acad Sci 1962;102(Automated and Semi-Automated Systems in Clinical Chemistry):29-45.

[78] Newman JD, Turner APF. Home blood glucose biosensors: a commercial perspective. Biosensors and Bioelectronics 2005 6/15;20(12):2435-2453.

[79] Male KB, Gartu PO, Kamen AA, Luong JHT. On-line monitoring of glucose in mammalian cell culture using a flow injection analysis (FIA) mediated biosensor. Biotechnol Bioeng 1997;55(3):497-504.

[80] MAO X, WU J, YING Y. Application of Electrochemical Biosensors in Fermentation. Chinese Journal of Analytical Chemistry 2008 12;36(12):1749-1755.

[81] Xu Y, Sun J(, Mathew G, Jeevarajan AS, Anderson MM. Continuous glucose monitoring and control in a rotating wall perfused bioreactor. Biotechnol Bioeng 2004;87(4):473-477.

[82] Wang J. Electrochemical Glucose Biosensors. Chem Rev 2008 02/01;108(2):814-825.

[83] Grieshaber D, MacKenzie R, Vörös J, Reimhult E. Electrochemical Biosensors - Sensor Principles and Architectures. Sensors 2008;8(3):1400-1458.

[84] Sasso SV, Pierce RJ, Walla R, Yacynych AM. Electropolymerized 1,2-diaminobenzene as a means to prevent interferences and fouling and to stabilize immobilized enzyme in electrochemical biosensors. Anal Chem 1990 06/01;62(11):1111-1117.

[85] Harrison DJ, Turner RFB, Baltes HP. Characterization of perfluorosulfonic acid polymer coated enzyme electrodes and a miniaturized integrated potentiostat for glucose analysis in whole blood. Anal Chem 1988 10/01;60(19):2002-2007.

[86] Wang J, Naser N, Angnes L, Wu H, Chen L. Metal-dispersed carbon paste electrodes. Anal Chem 1992 06/01;64(11):1285-1288.

[87] Wang J, Liu J, Chen L, Lu F. Highly Selective Membrane-Free, Mediator-Free Glucose Biosensor. Anal Chem 1994 11/01;66(21):3600-3603.

[88] Wang J, Rivas G, Chicharro M. Iridium-dispersed carbon paste enzyme electrodes. Electroanalysis 1996;8(5):434-437.

[89] Karyakin AA, Gitelmacher OV, Karyakina EE. A High-Sensitive Glucose Amperometric Biosensor Based on Prussian Blue Modified Electrodes. Anal Lett 1994;27(15):2861.

[90] Karyakin AA, Karyakina EE. Prussian Blue-based ‘artificial peroxidase' as a transducer for hydrogen peroxide detection. Application to biosensors. Sensors Actuators B: Chem 1999 9/7;57(1-3):268-273.

[91] Karyakin AA. Prussian blue and its analogues: electrochemistry and analytical applications. Electroanalysis 2001;13(10):813-819.

[92] Chaubey A, Malhotra BD. Mediated biosensors. Biosensors and Bioelectronics 2002 6/26;17(6-7):441-456.

[93] Heller A. Electrical connection of enzyme redox centers to electrodes. J Phys Chem 1992 04/01;96(9):3579-3587.

[94] Degani Y, Heller A. Electrical communication between redox centers of glucose oxidase and electrodes via electrostatically and covalently bound redox polymers. J Am Chem Soc 1989 03/01;111(6):2357-2358.

[95] Marcus RA, Sutin N. Electron transfers in chemistry and biology. Biochimica et Biophysica Acta (BBA) - Reviews on Bioenergetics 1985 8/1;811(3):265-322.

[96] Freire RS, Pessoa CA, Mello LD, Kubota LT. Direct electron transfer: an approach for electrochemical biosensors with higher selectivity and sensitivity. Journal of the Brazilian Chemical Society 2003;14(2):230-243.

[97] Wu Y, Hu S. Biosensors based on direct electron transfer in redox proteins. Microchimica Acta 2007 06/01;159(1):1-17.

[98] Laviron E. General expression of the linear potential sweep voltammogram in the case of diffusionless electrochemical systems. J Electroanal Chem 1979 7/25;101(1):19-28.

[99] Zhang Y, Shen Y, Han D, Wang Z, Song J, Li F, et al. Carbon nanotubes and glucose oxidase bionanocomposite bridged by ionic liquid-like unit: Preparation and electrochemical properties. Biosensors and Bioelectronics 2007 10/31;23(3):438-443.

[100] Liu X, Shi L, Niu W, Li H, Xu G. Amperometric glucose biosensor based on single-walled carbon nanohorns. Biosensors and Bioelectronics 2008 7/15;23(12):1887-1890.

[101] Wang Z, Liu S, Wu P, Cai C. Detection of Glucose Based on Direct Electron Transfer Reaction of Glucose Oxidase Immobilized on Highly Ordered Polyaniline Nanotubes. Anal Chem 2009 02/15;81(4):1638-1645.

[102] Wilson R, Turner APF. Glucose oxidase: an ideal enzyme. Biosensors and Bioelectronics 1992;7(3):165-185.

[103] Park S, Chung TD, Kim HC. Nonenzymatic Glucose Detection Using Mesoporous Platinum. Anal Chem 2003 07/01;75(13):3046-3049.

[104] Hsiao MW, Adzic RR, Yeager EB. The effects of adsorbed anions on the oxidation of D-glucose on gold single crystal electrodes. Electrochim Acta 1992 2;37(2):357-363.

[105] Li Y, Song Y, Yang C, Xia X. Hydrogen bubble dynamic template synthesis of porous gold for nonenzymatic electrochemical detection of glucose. Electrochemistry Communications 2007 5;9(5):981-988.

[106] Schick K, Magearu V, Huber C. Amperometric nonenzymatic determination of serum glucose by means of a nickel-catalyst electrode. Clin Chem 1978 March 1;24(3):448-450.

[107] Xie Y, Huber CO. Electrocatalysis and amperometric detection using an electrode made of copper oxide and carbon paste. Anal Chem 1991 09/01;63(17):1714-1719.

[108] Sun Y, Buck H, Mallouk TE. Combinatorial Discovery of Alloy Electrocatalysts for Amperometric Glucose Sensors. Anal Chem 2001 04/01;73(7):1599-1604.

[109] Lei H, Wu B, Cha C, Kita H. Electro-oxidation of glucose on platinum in alkaline solution and selective oxidation in the presence of additives. J Electroanal Chem 1995 2/7;382(1-2):103-110.

[110] Vassilyev YB, Khazova OA, Nikolaeva NN. Kinetics and mechanism of glucose electrooxidation on different electrode-catalysts: Part I. Adsorption and oxidation on platinum. J Electroanal Chem 1985 12/10;196(1):105-125.

[111] Ernst S, Heitbaum J, Hamann CH. The electrooxidation of glucose in phosphate buffer solutions : Part I. Reactivity and kinetics below 350 mV/RHE. J Electroanal Chem 1979 7;100:173-183.

[112] Park S, Boo H, Chung TD. Electrochemical non-enzymatic glucose sensors. Anal Chim Acta 2006 1/18;556(1):46-57.

[113] Pokropivny VV, Skorokhod VV. Classification of nanostructures by dimensionality and concept of surface forms engineering in nanomaterial science. Materials Science and Engineering: C 2007 9;27(5-8):990-993.

[114] Schmid G, Decker M, Ernst H, Fuchs H, Grünwald W, Grunwald A, et al. Small dimensions and material properties. A Definition of Nanotechnology 2003.

[115] Liu G, Lin Y. Amperometric glucose biosensor based on self-assembling glucose oxidase on carbon nanotubes. Electrochemistry Communications 2006 2;8(2):251-256.

[116] Zeng J, Wei W, Liu X, Wang Y, Luo G. A simple method to fabricate a Prussian Blue nanoparticles/carbon nanotubes/poly(1,2-diaminobenzene) based glucose biosensor. Microchimica Acta 2008 01/01;160(1):261-267.

[117] Li J, Lin X. Glucose biosensor based on immobilization of glucose oxidase in poly(o-aminophenol) film on polypyrrole-Pt nanocomposite modified glassy carbon electrode. Biosensors and Bioelectronics 2007 6/15;22(12):2898-2905.

[118] Zhang S, Wang N, Niu Y, Sun C. Immobilization of glucose oxidase on gold nanoparticles modified Au electrode for the construction of biosensor. Sensors Actuators B: Chem 2005 9/14;109(2):367-374.

[119] Vamvakaki V, Chaniotakis NA. Immobilization of enzymes into nanocavities for the improvement of biosensor stability. Biosensors and Bioelectronics 2007 5/15;22(11):2650-2655.

[120] Zhou H, Dill KA. Stabilization of Proteins in Confined Spacesâ€ . Biochemistry (N Y) 2001 09/01;40(38):11289-11293.

[121] Sun XW, Wang JX, Wei A. Zinc oxide nanostructured biosensor for glucose detection. J Mater Sci Technol 2008;24(4).

[122] Shan D, Zhu M, Xue H, Cosnier S. Development of amperometric biosensor for glucose based on a novel attractive enzyme immobilization matrix: Calcium carbonate nanoparticles. Biosensors and Bioelectronics 2007 3/15;22(8):1612-1617.

[123] Liu Y, Feng X, Shen J, Zhu J, Hou W. Fabrication of a Novel Glucose Biosensor Based on a Highly Electroactive Polystyrene/Polyaniline/Au Nanocomposite. The Journal of Physical Chemistry B 2008 07/01;112(30):9237-9242.

[124] Xu X, Zhang S, Chen H, Kong J. Integration of electrochemistry in micro-total analysis systems for biochemical assays: Recent developments. Talanta 2009 11/15;80(1):8-18.

[125] - Pumera M, - Escarpa A. - Nanomaterials as electrochemical detectors in microfluidics and CE: Fundamentals, designs, and applications. - ELECTROPHORESIS - 2009;- 30(- 19):- 3315-- 3323.

[126] Dunn B, Long JW, Rolison DR. Rethinking multifunction in three dimensions for miniaturizing electrical energy storage. Electrochemical Society Interface 2008:49.

[127] Anandan V, Yang X, Kim E, Rao Y, Zhang G. Role of reaction kinetics and mass transport in glucose sensing with nanopillar array electrodes. Journal of Biological Engineering 2007;1(1):5.

[128] Zhang G. Design and Fabrication of 3D Skyscraper Nanostructures and Their Applciations in Biosensors, in New Perspectives in Biosensors Technology and Applications. ; 2011. p. 269-290.

[129] Fan J-, Dyer D, Zhang G, Zhao Y-. Nanocarpet Effect: Pattern Formation during the Wetting of Vertically Aligned Nanorod Arrays. Nano Lett 2004 11/01; 2012/03;4(11):2133-2138.

[130] Lau KKS, Bico J, Teo KBK, Chhowalla M, Amaratunga GAJ, Milne WI, et al. Superhydrophobic Carbon Nanotube Forests. Nano Lett 2003 12/01; 2012/03;3(12):1701-1705.

[131] Zhang G. Design and Fabrication of 3D Skyscraper Nanostructures and Their Applications in Biosensors. 2011.

[132] Zhao G, Xu C, Li H. Highly ordered cobalt-manganese oxide (CMO) nanowire array thin film on Ti/Si substrate as an electrode for electrochemical capacitor. Journal of Power Sources 2007 1/1;163(2):1132-1136.

[133] BALAKRISHNAN S, KRIPESH V, CHONG SERCHOONG. Fabrication of Self-Organized Metal Nanowire Array using Porous Alumina Template for Off-Chip Interconnects. International Journal of Nanoscience 2006;5(4; 4):453-458.

[134] Rabin O, Herz PR, Lin Y-, Akinwande AI, Cronin SB, Dresselhaus MS. Formation of Thick Porous Anodic Alumina Films and Nanowire Arrays on Silicon Wafers and Glass. Advanced Functional Materials 2003;13(8):631-638.

[135] Chu SZ, Wada K, Inoue S, Todoroki S. Fabrication and characteristics of nanostructures on glass by Al anodization and electrodeposition. Electrochimica Acta 2003 9/30;48(20-22):3147-3153.

[136] Sharma G, Chong SC, Ebin L, Hui C, Gan CL, Kripesh V. Fabrication of patterned and non-patterned metallic nanowire arrays on silicon substrate. Thin Solid Films 2007 2/26;515(7-8):3315-3322.

[137] Hoogvliet JC, van Bennekom WP. Gold thin-film electrodes: an EQCM study of the influence of chromium and titanium adhesion layers on the response. Electrochimica Acta 2001 11/1;47(4):599-611.

[138] Chen G. On the Physics of Purple-Plague Formation, and the Observation of Purple Plague in Ultrasonically-Joined Gold-Aluminum Bonds. Parts, Materials and Packaging, IEEE Transactions on 1967;3(4):149-153.

[139] Masuda H, Fukuda K. Ordered Metal Nanohole Arrays Made by a Two-Step Replication of Honeycomb Structures of Anodic Alumina. Science 1995 June 9;268(5216):1466-1468.

[140] Bwana N. Synthesis of highly ordered nanopores on alumina by two-step anodization process. Journal of Nanoparticle Research 2008 02/01;10(2):313-319.

[141] Gangadharan R, Anandan V, Zhang A, Drwiega JC, Zhang G. Enhancing the performance of a fluidic glucose biosensor with 3D electrodes. Sensors Actuators B: Chem 2011 12/15;160(1):991-998.

[142] Anandan V, Rao Y, Zhang G. Nanopillar arrays with superior mechanical strength and optimal spacing for high sensitivity biosensors. Proceedings of Nanotech 2005:217–220.

[143] Anandan V, Rao Y, Zhang G. Nanopillar array structures for high performance electrochemical sensing. International journal of nanomedicine 2006;1:73-79.

[144] Ehler TT, Malmberg N, Noe LJ. Characterization of Self-Assembled Alkanethiol Monolayers on Silver and Gold Using Surface Plasmon Spectroscopy. J Phys Chem B 1997 02/01; 2012/04;101(8):1268-1272.

[145] Barlett PN, Cooper JM. A review of the immobilization of enzymes in electropolymerized films. J Electroanal Chem 1993 12/30;362(1–2):1-12.

[146] Cosnier S. Biomolecule immobilization on electrode surfaces by entrapment or attachment to electrochemically polymerized films. A review. Biosensors and Bioelectronics 1999 5/31;14(5):443-456.

[147] Schuhmann W, Kranz C, Huber J, Wohlschläger H. Conducting polymer-based amperometric enzyme electrodes. Towards the development of miniaturized reagentless biosensors. Synth Met 1993 11/23;61(1–2):31-35.

[148] Ramanaviciene A. Application of Polypyrrole for the Creation of Immunosensors. - Critical Reviews in Analytical Chemistry 2002(- 3):245.

[149] Ramanavičius A, Ramanavičienė A, Malinauskas A. Electrochemical sensors based on conducting polymer—polypyrrole. Electrochim Acta 2006 8/25;51(27):6025-6037.

[150] Wang J, Nosang M, Minhee Y, Harold M. Glucose oxidase entrapped in polypyrrole on high-surface-area Pt electrodes: a model platform for sensitive electroenzymatic biosensors. J Electroanal Chem 2005;575:139-146.

[151] Chen C, Jiang Y, Kan J. A noninterference polypyrrole glucose biosensor. Biosensors and Bioelectronics 2006 12/15;22(5):639-643.

[152] Uang YM, Chow TC. Criteria for Designing a Polypyrrole Glucose Biosensor by Galvanostatic Electropolymerization. Electroanalysis 2002;14:1564-1570.

[153] Ramanavičius A, Kaušaitė A, Ramanavičienė A. Polypyrrole-coated glucose oxidase nanoparticles for biosensor design. Sensors Actuators B: Chem 2005 11/11;111-112:532-539.

[154] Wang J, Musameh M. Carbon-nanotubes doped polypyrrole glucose biosensor. Anal Chim Acta 2005 5/10;539(1–2):209-213.

[155] Yang M, Qu F, Lu Y, He Y, Shen G, Yu R. Platinum nanowire nanoelectrode array for the fabrication of biosensors. Biomaterials 2006 12;27(35):5944-5950.

[156] Gao M, Gordon LD. Biosensors Based on Aligned Carbon Nanotubes Coated with Inherently Conducting Polymers. Electroanalysis 2001;15:1089-1094.

[157] Cho J, Shin M, Kim H. Electrochemical adsorption of glucose oxidase onto polypyrrole film for the construction of a glucose biosensor. Sensors Actuators B: Chem 1996 1/15;30(2):137-141.

[158] Uang Y, Chou T. Fabrication of glucose oxidase/polypyrrole biosensor by galvanostatic method in various pH aqueous solutions. Biosensors and Bioelectronics 2003 11/30;19(3):141-147.

[159] Anandan V,. Role of reaction kinetics and mass transport in glucose sensing with nanopillar array electrodes. Journal of Biological Engineering 2007;1:5.

[160] Georgiadou M, Veyret D, Sani RL, Alkire RC. Simulation of Shape Evolution during Electrodeposition of Copper in the Presence of Additive. J Electrochem Soc 2001 January 2001;148(1):C54-C58.

[161] Hämmerle M, Schuhmann W, Schmidt H-. Amperometric polypyrrole enzyme electrodes: effect of permeability and enzyme location. Sensors Actuators B: Chem 1992 1;6(1–3):106-112.

[162] Lichtenberger J, Fromherz P. A Cell-Semiconductor Synapse: Transistor Recording of Vesicle Release in Chromaffin Cells. Biophys J 2007 3/15;92(6):2262-2268.

[163] Gros P, Bergel A. Improved model of a polypyrrole glucose oxidase modified electrode. J Electroanal Chem 1995 4/18;386(1–2):65-73.

[164] Fortier G, Brassard E, Bélanger D. Optimization of a polypyrrole glucose oxidase biosensor. Biosensors and Bioelectronics 1990;5(6):473-490.

[165] Lee S, Anandan V, Zhang G. Electrochemical fabrication and evaluation of highly sensitive nanorod-modified electrodes for a biotin/avidin system. Biosensors and Bioelectronics 2008 2/28;23(7):1117-1124.

[166] Chaki NK, Vijayamohanan K. Self-assembled monolayers as a tunable platform for biosensor applications. Biosensors and Bioelectronics 2002 1;17(1–2):1-12.

[167] Delvaux M, Demoustier-Champagne S. Immobilisation of glucose oxidase within metallic nanotubes arrays for application to enzyme biosensors. Biosens Bioelectron 2003;18:943-951.

[168] Ding S, Chang B, Wu C, Lai M, Chang H. Impedance spectral studies of self-assembly of alkanethiols with different chain lengths using different immobilization strategies on Au electrodes. Anal Chim Acta 2005 12/4;554(1-2):43-51.

[169] Campuzano S, Gálvez R, Pedrero M, de Villena FJM, Pingarrón JM. Preparation, characterization and application of alkanethiol self-assembled monolayers modified with tetrathiafulvalene and glucose oxidase at a gold disk electrode. J Electroanal Chem 2002 5/17;526(1-2):92-100.

[170] Losic D, Gooding JJ, Shapter JG, Hibbert DB, Short K. The influence of the underlying gold substrate on glucose oxidase electrodes fabricated using self-assembled monolayers. Electroanalysis 2001;13:1385-1393.

[171] Sawaguchi T, Sato Y, Mizutani F. In situ STM imaging of individual molecules in two-component self-assembled monolayers of 3-mercaptopropionic acid and 1-decanethiol on Au(111). J Electroanal Chem 2001 1/19;496(1-2):50-60.

[172] Cooper JC, Hall EAH. Catalytic reduction of benzoquinone at polyaniline and polyaniline/enzyme films. Electroanalysis 1993;5(5-6):385-397.

[173] Losic D, Shapter JG, Gooding JJ. Influence of Surface Topography on Alkanethiol SAMs Assembled from Solution and by Microcontact Printing. Langmuir 2001 05/01; 2012/03;17(11):3307-3316.

[174] Graaf H, Baune M, Wang C, Urisu T. Influence of Substrate Roughness on the Formation
 of Aliphatic Self-Assembled Monolayers (SAMs) on Silicon(100). Japanese Journal of Applied Physics 2002;41(- Part 1, No. 6B):- 4390.

[175] Anandan V, Gangadharan R, Zhang G. Role of SAM Chain Length in Enhancing the Sensitivity of Nanopillar Modified Electrodes for Glucose Detection. Sensors 2009;9(3):1295-1305.

[176] Walczak MM, Popenoe DD, Deinhammer RS, Lamp BD, Chung C, Porter MD. Reductive desorption of alkanethiolate monolayers at gold: a measure of surface coverage. Langmuir 1991 11/01;7(11):2687-2693.

[177] Campuzano S, Pedrero M, Montemayor C, Fatás E, Pingarrón JM. Characterization of alkanethiol-self-assembled monolayers-modified gold electrodes by electrochemical impedance spectroscopy. J Electroanal Chem 2006 1/1;586(1):112-121.

[178] Widrig CA, Chung C, Porter MD. The electrochemical desorption of n-alkanethiol monolayers from polycrystalline Au and Ag electrodes. Journal of Electroanalytical Chemistry and Interfacial Electrochemistry 1991 7/25;310(1-2):335-359.

[179] Guo S, Wang E. Synthesis and electrochemical applications of gold nanoparticles. Anal Chim Acta 2007 8/29;598(2):181-192.

[180] Pandey P, Singh SP, Arya SK, Gupta V, Datta M, Singh S, et al. Application of Thiolated Gold Nanoparticles for the Enhancement of Glucose Oxidase Activity. Langmuir 2007 03/01; 2012/03;23(6):3333-3337.

[181] Li D, He Q, Cui Y, Duan L, Li J. Immobilization of glucose oxidase onto gold nanoparticles with enhanced thermostability. Biochem Biophys Res Commun 2007 4/6;355(2):488-493.

[182] - Increasing Protein Stability through Control of the Nanoscale Environment. - Langmuir (- 13):- 5833.

[183] - Effect of Colloidal Gold Size on the Conformational Changes of Adsorbed Cytochrome c:□ Probing by Circular Dichroism, UV−Visible, and Infrared Spectroscopy. - Biomacromolecules (- 1):- 46.

[184] Jiang X, Jiang J, Jin Y, Wang E, Dong S. Effect of Colloidal Gold Size on the Conformational Changes of Adsorbed Cytochrome c:â€‰ Probing by Circular Dichroism, UVâˆ'Visible, and Infrared Spectroscopy. Biomacromolecules 2005 01/01; 2012/03;6(1):46-53.

[185] Duff D. A new hydrosol of gold clusters. 1. Formation and particle size variation. - Langmuir 1993(- 9):- 2301.

[186] Huang H. Synthesis of Chitosan-Stabilized Gold Nanoparticles in the Absence/Presence of Tripolyphosphate. - Biomacromolecules 2004,(- 6):- 2340.

[187] - Turkevich J, - Stevenson PC, - Hillier J. - A study of the nucleation and growth processes in the synthesis of colloidal gold. - Discuss Faraday Soc (-):- 55.

[188] Bhumkar D, Joshi H, Sastry M, Pokharkar V. Chitosan Reduced Gold Nanoparticles as Novel Carriers for Transmucosal Delivery of Insulin. Pharmaceutical Research 2007;24(8):1415-1426.

[189] Brewer SH, Glomm WR, Johnson MC, Knag MK, Franzen S. Probing BSA Binding to Citrate-Coated Gold Nanoparticles and Surfaces. Langmuir 2005 09/01; 2012/03;21(20):9303-9307.

[190] Haiss W, Thanh NTK, Aveyard J, Fernig DG. Determination of Size and Concentration of Gold Nanoparticles from UVâˆ'Vis Spectra. Anal Chem 2007 06/01; 2012/03;79(11):4215-4221.

[191] Fujiwara K, Watarai H, Itoh H, Nakahama E, Ogawa N. Measurement of antibody binding to protein immobilized on gold nanoparticles by localized surface plasmon spectroscopy. Analytical and Bioanalytical Chemistry 2006;386(3):639-644.

[192] Shang L, Wang Y, Jiang J, Dong S. pH-Dependent Protein Conformational Changes in Albumin:Gold Nanoparticle Bioconjugates:â€‰ A Spectroscopic Study. Langmuir 2007 02/01; 2012/03;23(5):2714-2721.

[193] Shipway AN, Lahav M, Gabai R, Willner I. Investigations into the Electrostatically Induced Aggregation of Au Nanoparticlesâ€ . Langmuir 2000 11/01; 2012/03;16(23):8789-8795.

[194] Ao L, Gao F, Pan B, Cui D, Gu H. Interaction between Gold Nanoparticles and Bovine Serum Albumin or Sheep Antirabbit Immunoglobulin G. Chinese Journal of Chemistry 2006;24(2):253-256.

[195] Uang Y, Chou T. Criteria for Designing a Polypyrrole Glucose Biosensor by Galvanostatic Electropolymerization. Electroanalysis 2002;14(22):1564-1570.

[196] Nien P, Huang M, Chang F, Ho K. Integrating an Enzyme-Entrapped Conducting Polymer Electrode and a Prereactor in a Microfluidic System for Sensing Glucose. Electroanalysis 2008;20(6):635-642.

[197] Habermüller K, Schuhmann W. A Low-Volume Electrochemical Cell for the Deposition of Conducting Polymers and Entrapment of Enzymes. Electroanalysis 1998;10(18):1281-1284.

[198] Kurita R, Hayashi K, Fan X, Yamamoto K, Kato T, Niwa O. Microfluidic device integrated with pre-reactor and dual enzyme-modified microelectrodes for monitoring in vivo glucose and lactate. Sensors and Actuators B: Chemical 2002 12/10;87(2):296-303.

[199] Hashimoto M, Upadhyay S, Suzuki H. Dependence of the response of an amperometric biosensor formed in a micro flow channel on structural and conditional parameters. Biosensors and Bioelectronics 2006 6/15;21(12):2224-2231.

[200] Schuhmann W, Kranz C, Wohlschläger H, Strohmeier J. Pulse technique for the electrochemical deposition of polymer films on electrode surfaces. Biosensors and Bioelectronics 1997 12/30;12(12):1157-1167.

[201] Sharma RK, Rastogi AC, Desu SB. Pulse polymerized polypyrrole electrodes for high energy density electrochemical supercapacitor. Electrochemistry Communications 2008 2;10(2):268-272.

[202] Centonze D, Guerrieri A, Malitesta C, Palmisano F, Zambonin PG. Interference-free glucose sensor based on glucose-oxidase immobilized in an overoxidized non-conducting polypyrrole film. Fresenius' Journal of Analytical Chemistry 1992;342(9):729-733.

[203] Garjonyte R, Malinauskas A. Operational stability of amperometric hydrogen peroxide sensors, based on ferrous and copper hexacyanoferrates. Sensors Actuators B: Chem 1999 7/1;56(1–2):93-97.

[204] Chiu J, Yu C, Yen M, Chen L. Glucose sensing electrodes based on a poly(3,4-ethylenedioxythiophene)/Prussian blue bilayer and multi-walled carbon nanotubes. Biosensors and Bioelectronics 2009 3/15;24(7):2015-2020.

[205] de Mattos IL, da Cunha Areias MC. Automated determination of glucose in soluble coffee using Prussian Blue–glucose oxidase–Nafion® modified electrode. Talanta 2005 6/15;66(5):1281-1286.

[206] Xue M, Xu Q, Zhou M, Zhu J. In situ immobilization of glucose oxidase in chitosan–gold nanoparticle hybrid film on Prussian Blue modified electrode for high-sensitivity glucose detection. Electrochemistry Communications 2006 9;8(9):1468-1474.

[207] Miao Y, Liu J. Assembly and electroanalytical performance of Prussian blue/polypyrrole composite nanoparticles synthesized by the reverse micelle method. Science and Technology of Advanced Materials 2009;10(2):025001.

[208] Zou Y, Sun L, Xu F. Biosensor based on polyaniline–Prussian Blue/multi-walled carbon nanotubes hybrid composites. Biosensors and Bioelectronics 2007 5/15;22(11):2669-2674.

[209] Li Z, Chen J, Li W, Chen K, Nie L, Yao S. Improved electrochemical properties of prussian blue by multi-walled carbon nanotubes. J Electroanal Chem 2007 5/1;603(1):59-66.

[210] Fiorito PA, Brett CMA, Córdoba de Torresi SI. Polypyrrole/copper hexacyanoferrate hybrid as redox mediator for glucose biosensors. Talanta 2006 4/15;69(2):403-408.

[211] Guadagnini L, Giorgetti M, Tarterini F, Tonelli D. Electrocatalytic Performances of Pure and Mixed Hexacyanoferrates of Cu and Pd for the Reduction of Hydrogen Peroxide. Electroanalysis 2010;22(15):1695-1701.

[212] Ji X, Ren J, Ni R, Liu X. A stable and controllable Prussian blue layer electrodeposited on self-assembled monolayers for constructing highly sensitive glucose biosensor. Analyst 2010;135(8):2092-2098.

[213] Liu Y, Chu Z, Jin W. A sensitivity-controlled hydrogen peroxide sensor based on self-assembled Prussian Blue modified electrode. Electrochemistry Communications 2009 2;11(2):484-487.

[214] Demiri S, Najdoski M, Velevska J. A simple chemical method for deposition of electrochromic Prussian blue thin films. Mater Res Bull 2011 12;46(12):2484-2488.

[215] Borisova A, Karyakina E, Cosnier S, Karyakin A. Current-Free Deposition of Prussian Blue with Organic Polymers: Towards Improved Stability and Mass Production of the Advanced Hydrogen Peroxide Transducer. Electroanalysis 2009;21(3-5):409-414.

[216] Ding Y, Hu Y, Gu G, Xia X. Controllable Synthesis and Formation Mechanism Investigation of Prussian Blue Nanocrystals by Using the Polysaccharide Hydrolysis Method. J Phys Chem C 2009 08/20; 2011/12;113(33):14838-14843.

[217] Zhang W, Wang L, Zhang N, Wang G, Fang B. Functionalization of Single-Walled Carbon Nanotubes with Cubic Prussian Blue and Its Application for Amperometric Sensing. Electroanalysis 2009;21(21):2325-2330.

[218] Zhang Q, Zhang L, Li J. Fabrication and electrochemical study of monodisperse and size controlled Prussian blue nanoparticles protected by biocompatible polymer. Electrochim Acta 2008 2/25;53(7):3050-3055.

[219] Zhai J, Zhai Y, Wang L, Dong S. Rapid Synthesis of Polyethylenimine-Protected Prussian Blue Nanocubes through a Thermal Process. Inorg Chem 2008 08/01; 2012/03;47(16):7071-7073.

[220] Meng F, Yan X, Liu J, Gu J, Zou Z. Nanoporous gold as non-enzymatic sensor for hydrogen peroxide. Electrochim Acta 2011 4/30;56(12):4657-4662.

[221] Pauliukaite R, Ghica ME, Barsan MM, Brett CMA. Phenazines and Polyphenazines in Electrochemical Sensors and Biosensors. Anal Lett 2010 07/06; 2012/03;43(10-11):1588-1608.

[222] Emilia Ghica M, Brett CMA. Development and Applications of a Bienzymatic Amperometric Glycerol Biosensor Based on a Poly(Neutral Red) Modified Carbon Film Electrode. Anal Lett 2006 07/01; 2012/03;39(8):1527-1542.

[223] Broncová G, Shishkanova T, Krondak M, Volf R, Král V. Optimalization of Poly(neutral red) Coated-wire Electrode for Determination of Citrate in Soft Drinks. Sensors 2008;8(2):594-606.

[224] Ghica M, Brett C?. Development of Novel Glucose and Pyruvate Biosensors at Poly(Neutral Red) Modified Carbon Film Electrodes. Application to Natural Samples. Electroanalysis 2006;18(8):748-756.

[225] Qu F, Yang M, Jiang J, Feng K, Shen G, Yu R. Novel poly (neutral red) nanowires as a sensitive electrochemical biosensing platform for hydrogen peroxide determination. Electrochemistry Communications 2007 10;9(10):2596-2600.

[226] Gonçalves AR, Ghica ME, Brett CMA. Preparation and characterisation of poly(3,4-ethylenedioxythiophene) and poly(3,4-ethylenedioxythiophene)/poly(neutral red) modified carbon film electrodes, and application as sensors for hydrogen peroxide. Electrochim Acta 2011 4/1;56(10):3685-3692.

[227] - Lin KC, - Lin YC, - Chen SM. - Electrocatalytic reaction of hydrogen peroxide and NADH based on poly(neutral red) and FAD hybrid film. - Analyst (- 1):- 186.

[228] Björn Samel and M Kamruzzaman Chowdhury,and G. The fabrication of microfluidic structures by means of full-wafer adhesive bonding using a poly(dimethylsiloxane) catalyst. J Micromech Microengineering 2007;17(8):1710.

[229] Karyakin AA, Karyakina EE, Schmidt H. Electropolymerized Azines: A New Group of Electroactive Polymers. Electroanalysis 1999;11(3):149-155.

[230] Benito D, Gabrielli C, García-Jareño JJ, Keddam M, Perrot H, Vicente F. Study by EQCM on the voltammetric electrogeneration of poly(neutral red). The effect of the pH and the nature of cations and anions on the electrochemistry of the films. Electrochim Acta 2003 11/30;48(27):4039-4048.

[231] Pauliukaite R, Ghica M, Barsan M, Brett C. Characterisation of poly(neutral red) modified carbon film electrodes; application as a redox mediator for biosensors. Journal of Solid State Electrochemistry 2007;11(7):899-908.

[232] Pereira Rodrigues N, Sakai Y, Fujii T. Cell-based microfluidic biochip for the electrochemical real-time monitoring of glucose and oxygen. Sensors Actuators B: Chem 2008 6/16;132(2):608-613.

[233] Leclerc E, Furukawa KS, Miyata F, Sakai Y, Ushida T, Fujii T. Fabrication of microstructures in photosensitive biodegradable polymers for tissue engineering applications. Biomaterials 2004 8;25(19):4683-4690.